Developing Pre-Vascularized Modular Microenvironments for Ischemic Applications

by

Ana Ysabel Rioja

A dissertation submitted in partial fulfillment
of the requirements for the degree of
Doctor of Philosophy
(Biomedical Engineering)
in the University of Michigan
2017

Doctoral Committee:

Professor Andrew J. Putnam, Co-chair
Professor Jan P. Stegemann, Co-chair
Professor Jacques Nör
Assistant Professor Ariella Shikanov

Ana Y. Rioja

arioja@umich.edu

ORCID iD: 0000-0003-0246-2578

DEDICATION

To my parents: Jesus Rioja and Ruby Sanchez

For all the love and sacrifices you have made for me and Paola

ACKNOWLEDGEMENTS

First of all, I would like to thank my thesis advisers, Professors Andrew J. Putnam and Jan P. Stegemann. Thank you for believing in me, for all your support and guidance, for teaching me not to give up on my goals and to push forward no matter what situation I am faced with. To my other committee members, thank you for all your support – for taking time to meet with me and provide me with great feedback that has strengthened my dissertation.

I would also like to thank the former and current members of the Cell Signaling in Engineered Tissues (CSET) group. Dr. Bita Carrion, Dr. Jacob Ceccarelli, Dr. Isaac Janson, Dr. Marina Vigen, Dr. Rahul Singh, and Dr. Jeff Beamish – Thank you for all your advice; it was nice to get to know you during my PhD and to receive tips on how to be successful in graduate school. To Dr. Yen Peng Kong – I will always be thankful for all the help and guidance you gave me throughout my years at the University of Michigan. I don't think I would have accomplished as much without your advice.

I want to acknowledge the former and current members of the Cell-Matrix Interactions & Tissue Engineering (CMITE) group. In particular, Dr. Ethan Daley, Dr. Paul Turner, Adeline Hong, and Brandan Walters. I really enjoyed our conversations and working with each and every one of you. Ethan – it was a pleasure to write a paper with you and I am happy to have learn a lot from you.

To my undergrad Julia, I appreciate all the experimental help you gave me. I wish you the best in graduate school and your future career. I also want to thank Jonathan Bezenah for helping

me quantifying data, Dr. Anu David for giving me very useful advice on histology staining, and Dr. Gopinath Tiruchinapally for helping me with the NMR data collection and analysis. To Aresha Martinez, Esmeralda Hernandez-Hamed, Diana Olvera, Karlo Malaga, James Buquet, and all the other friends I made in Michigan: Thank you for being my support system and family while I was here. I will never forget all the adventures we had while pursuing our doctoral degrees. To Dr. Yvonne Davis, Mr. Bernard Batson and Mr. Michael Oratowski – thank you for believing in me. You knew I would become a scientist before I did.

Paola, my sister, thank you for supporting me and reminding me that we can do anything. I know that you will be successful no matter what path you take. To my boyfriend, Kyle Huston, thank you for being there with me every step of the way towards our Ph.D. goal. I will never forget how supportive you have been with me. To conclude, I would like to thank my parents Jesus and Ruby, for everything you have done for me. I wouldn't be where I am today without all your sacrifice and love. You taught me that I can be successful no matter what we are faced with. I wouldn't be where I am today if it wasn't for the two of you. I will always be grateful to you and God for who I am.

TABLE OF CONTENTS

LIST OF FIGURES

LIST OF TABLES

LIST OF APPENDICES

LIST OF ABBREVIATIONS

(Symbols, Numerical Order, Alphabetical Order)

°C	Celsius
2D	Two-dimensional
3D	Three-dimensional
α-SMA	Alpha-smooth muscle actin
ATF	Adipose tissue fragments
AG	Agarose
ANOVA	Analysis of variance
ARF	Acoustic radiation force
BAEC	Bovine aortic endothelial cells
BCEC	Bovine capillary endothelial cells
bFGF	Basic fibroblast growth factor
BMMNCs	Bone marrow derived mononuclear cells
CAM	Chorioallantoic membrane
CLI	Critical limb ischemia
COL	Collagen
COL-FIB	Collagen-fibrin
D_2O	Deuterium oxide
DAPI	4′,6- diamidino-2-phenylindole
DLL4	Delta-like-4 ligand
DMEM	Dulbecco's modified eagle medium
DPBS	Dulbecco's phosphate-buffered saline
DUE	Dual-mode ultrasound elastography
EC	Endothelial cells
ECM	Extracellular matrix
EGM-2	Endothelial growth medium

EMG	Electromyography
EPCs	Endothelial progenitor cells
ES	Embryonic stem cells
FBS	Fetal bovine serum
FDA	Food and Drug Administration
FGN	Fibrinogen
FIB	Fibrin
FU	Fibrin degradation units
FUS	Focused ultrasound
G’	Shear modulus
HA	Hydroxyapatite
HC	High concentration
HGF	Hepatocyte growth factor
HIF	Hypoxia inducible factor
H&E	Hematoxylin and eosin
HUVECs	Human umbilical vein endothelial cells
iPS	Induced pluripotent stem cells
LC	Low concentration
LDPI	Laser Doppler perfusion imaging
M199	Medium 199
MnSOD	Manganese superoxide dismutase
MFD	Microfluidic devices
MSCs	Mesenchymal stem cells
MVECs	Microvascular endothelial cells
NAOH	Sodium hydroxide
NHLFs	Normal human lung fibroblasts
NIH	National Institutes of Health
NMR	Nuclear Magnetic Reasonance
PAD	Peripheral arterial disease
FDA	Food and Drug Administration
FGF	Fibroblast growth factor

PBS	Phosphate buffer saline
PDMS	Polydimethylsiloxane
PEG	Polyethylene glycol
PGA	Polyglycolic acid
PRF	Pulse repetition frequency
RF	Radio frequency
RPM	Revolutions per minute
SEM	Standard error of the mean
SFEGM-2	Serum free endothelial growth medium
SUSI	Spectral ultrasound imaging
TBS-T	Tris-buffered saline
TGF-β	Transforming growth factor beta
UEA-I	Ulex europaeus agglutinin I
PPM	Parts per million
VEGF	Vascular endothelial growth factor
VEGF-A	Vascular endothelial growth factor A
VEGFR2	Vascular endothelial growth factor receptor 2
vSMCs	Vascular smooth muscle cells
Z-fix	Zinc-buffered formalin solution

ABSTRACT

Critical limb ischemia (CLI), the end-stage of lower limb peripheral arterial disease, is characterized by a lack of oxygen/nutrient supply and subsequent tissue death. CLI patients with comorbidities are often ineligible for open bypass surgery. As an alternative approach, we developed pre-vascularized microbeads to jump-start inosculation with host vasculature after minimally invasive delivery and quickly restore blood flow to the ischemic tissue.

Endothelial cells and fibroblasts were encapsulated in two microbead types – fibrin (FIB) and collagen-fibrin (COL-FIB) – and embedded immediately in FIB hydrogels to determine which initiated endothelial sprout formation to a greater extent. Cell viability in both microbead types was high (≥75%). Two weeks after embedding, cells in FIB microbeads produced a higher network length than those in COL-FIB microbeads. Cells pre-cultured in FIB microbeads for three days prior to embedding in larger hydrogels exhibited the most extensive endothelial tube area coverage *in vitro*.

Fibrin microbead formulations were also evaluated for their ability to initiate vessel formation *in vivo* by injection into subcutaneous pockets on the dorsal surface of immuno-compromised mice. Implants containing microbeads pre-cultured for 3 days had greater vessel coverage, higher total number of vessels, and less implant compaction at D3, and more mature vessels at D7 *in situ*, compared to other conditions. The improved distribution of mature vessels generated by the implants containing pre-cultured microbeads was attributed to the preservation of implant volume, which was confirmed with ultrasound imaging of model implants *in vitro*. Furthermore, implants containing pre-cultured microbeads displayed lower bulk elastic moduli

compared to controls, but higher local stiffness near the microbeads, suggesting the distribution of cells within the implants plays a role in construct compaction and volume maintenance. Collectively, these findings show cellular microbeads pre-cultured for 3 days *in vitro* are more effectively able to nucleate vascularization *in vivo*.

FIB microbead aggregation increased with pre-culture time. Agarose-based microbeads reduced aggregation and provided the most distributed endothelial network post-embedding when made with hydroxyapatite and fibrinogen. These microbeads supported pre-culture, which helped to increase the network length post-embedding. Overall, this work demonstrates the therapeutic potential of vascularized microbeads for ischemic pathologies.

CHAPTER 1

Introduction

1.1 Clinical Motivation

Peripheral arterial disease (PAD) is caused by the obstruction of blood due to plaque formation in the arterial wall [1]. Plaque formation is initiated by the accumulation of lipoproteins, particularly of low-density lipoprotein (LDL), which causes an inflammatory response and the recruitment of macrophages which in turn leads to LDL modification and storage. Subsequent steps include the recruitment and death of smooth muscle cells (SMCs) and other inflammatory cells, the replacement and expansion of collagen matrix secreted by SMCs, and plaque calcification. [2] This blockage prevents or reduces the normal blood flow through the body, limiting the oxygen and nutrient diffusion downstream of the affected regions. Cells and tissues residing in these ischemic regions – lacking oxygen and nutrients – often die and lose functionality, causing additional problems including ischemic ulcers and gangrene. [1]

The most frequent and main symptom in patients who suffer from lower extremity PAD is intermittent claudication (IC) [1]. IC is pain and/or cramping in the legs and especially calf muscles while exercising. This pain is likely to go away with rest within a 10-minute frame [3]. Perhaps because the pain subsides so quickly, 10 to 50% of patients with IC do not seek medical attention for this symptom [3]. In addition, 75 to 80% of PAD patients do not present clinical intermittent claudication [3].

Non-invasive techniques such as ankle-brachial systolic pressure index (ABI), are often utilized to test for PAD in patients who have higher risks of suffering from this disease, but don't present IC [3]. Risk factors are based on age, gender, smoking, sex, ethnicity, and diabetes [3-5]. Patients who suffer from PAD also have higher risks of suffering a heart attack, stroke, or death due to other cardiovascular diseases, independent of whether patients display any PAD symptoms [5].

As lower limb PAD progresses and worsens, it reaches its end stage, known as critical limb ischemia (CLI) [6]. CLI patients feel pain while moving and resting [7]. It is estimated that about 18 million Americans suffer from PAD, and 2 million of these patients also develop critical limb ischemia (CLI) [8, 9]. The Sage research and consulting group reported that "in 2007, there were approximately 2.8 million people in Western Europe who suffered from CLI", and they have predicted that about 3.4 million people in that region will have this disease by 2020 [10]. In addition, the president of the Sage group acknowledged that "because of the global epidemic of diabetes and the fact that diabetics represent 60% to 80% of CLI patients, we believe that critical limb ischemia represents a major and significantly underestimated worldwide problem" [10]. Other studies have also shown that diabetics have double the chance of developing IC while their probability of developing PAD is three to four times higher than other patients [3].

As of now, approximately 20% of patients who suffer from chronic CLI will die after one year of their diagnosis; this mortality rate has been found to stay constant in long term studies [3]. Patients who are inoperable or whose reconstructions were unsuccessful are often part of pharmacotherapy trials. Unfortunately, 40% of these patients will lose a lower limb while 20% will die within 6 months [3]. For this reason, multiple therapies and technologies are being investigated and utilized to develop solutions/preventions to this disease.

1.2 Treatments

The management of a patient with PAD depends on the severity of the disease. If the disease is not limiting the patient's lifestyle (mild to moderate symptoms) then it can be managed with exercise and pharmaceutical therapy. On the other hand, if the disease is more severe, an arteriograph or arteriogram, is performed to assess the ischemic wound size and determine the surgical treatment. Arteriography (or angiography) is a technique that uses a contrast dye to facilitate vessel imaging which can be done with x-rays or magnetic resonance imaging [11].

1.2.1 Pharmaceutical Therapies

Pharmaceutical therapies use different drugs to reduce cholesterol and lipid accumulation in the circulation, thereby reducing the formation of atherosclerotic plaques and maintaining vessel patency. Physical therapy may be combined with drug therapy to prevent further vessel damage. Vasodilators are drugs that augment the blood flow in peripheral vessels of humans with normal health, but they are ineffective at treating CLI [12]. Some vasodilators like tolazoline, reserpine, guanethidine, and methyldopa affect the sympathetic nervous system, while papaverine, niacin, isoxsuprine, and cyclandelate are categorized as direct-acting drugs. None of these vasodilators have been shown to have any benefits when employed in clinical studies of obstructive vascular diseases [12]. A 1959 blood flow study found that vasodilators were not useful for CLI treatment; instead of increasing blood flow in ischemic regions, they decreased blood flow no matter how they were administered to the patient (oral dose or intravenous injection) [13].

Other drugs such as naftidrofuryl (serotonin/neurotransmitter antagonist), buflomedil (adrenolytic agent/adrenaline inhibitor), and cilostazol (phosphodiesterase inhibitor) have

improved patients' walking distances and lifestyles. Although these agents provide positive effects, they are more beneficial for patients with acute limb ischemia. [1]

1.2.2 Surgical Interventions

Surgery is more likely to be performed in patients with severe PAD – that is, with CLI. The type of surgical intervention is determined based on the location and severity of the occlusive area. When lesions are small and localized within a specific area, they can be treated with endovascular interventions such as percutaneous transluminal angioplasty; however, bypass surgery or other re-vascularization surgeries must be done when dealing with more severe critical ischemic areas. [1, 14]

Percutaneous transluminal angioplasty was introduced in 1964 by Dotter and Judkins as a replacement for open surgical procedures. This technique employs catheterization and arteriography. [15] In brief, a balloon catheter (tube) is inserted into an artery using angiography to track its location through the vessel in real time. The physician moves the balloon close to the plaque, prior to inflating it. Once it's inflated, the balloon will dilate the vessel, dislodge (or compress) the plaque, and thereby relieve the blockage. [16] Even though this technique prevents amputations and continues to be improved with catheter/balloon modifications, it has not been demonstrated to provide better outcomes when compared to open surgery [1, 14].

Re-vascularization interventions are performed on 50-90% of CLI patients [3]. Bypass surgery is an open surgical technique that create new vessels from existing ones. Surgeons surgically create a new blood flow channel to bypass the obstructive area which allows blood flow to return. Depending on the severity of the surgery, patients will take 4 weeks to 12 weeks to return to their regular work schedule [17].

Unfortunately, patients who undergo open surgery have a risk of needing additional interventions due to hematomas or ineffective grafts. In addition, if the vein quality is poor (e.g vein is too calcified), surgeons may be unable to perform distal anastomosis in the patient and are unlikely to determine this problem prior to starting the surgery. Patients with successful surgeries, however, are less likely to have a future amputation or death. [14]

1.3 Vascular Development/Vascularization

The cardiovascular system is the first organ system that is functional during human development [18]. This system is responsible for supplying oxygen and nutrients to the tissues while removing waste to sustain cells and tissues within the body. The arteries and veins comprise the cardiovascular system [19]. The arteries carry oxygenated blood away from the heart. The blood is then carried into smaller arteries, arterioles (80 to 100 μm) and eventually to capillaries (10 to 15 μm) [20]. The venous system carries the deoxygenated blood from the capillaries back to the heart via the large venules and veins. [18]

Blood vessels have an inner lining (endothelium) made up of endothelial cells (ECs). Mural cells cover the endothelium and provide structural support to vessels [18, 19, 21, 22]. They also have important roles in vessel functionality, blood vessel maturation, and the angiogenesis process. Mural cell density irregularity and improper attachment to the endothelium can lead to vessel deformities and multiple vascular diseases.

Mural cells stabilize and participate in endothelial vessel formation [18]. These mural cells are divided into two groups: pericytes and vascular smooth muscle cells. Capillaries and smaller vessels are covered by pericytes, whereas larger vessels like arteries and veins are surrounded by vascular smooth muscle cells [18, 23]. The larger vessels contain different layers: the tunica intima,

tunica media, and tunica adventitia. These layers are made with endothelial cells, vascular smooth muscle cells, and/or extracellular matrix secreted by the vascular smooth muscle cells. The thickness of the vessel walls is dependent on the vessel type. [18, 19, 21, 22] Pericyte recruitment and differentiation are driven by many growth factors such as platelet-derived growth factors (PDGF) and transforming growth factor-β (TGF-β) [21]. These will be discussed in more detail in the angiogenic factor delivery section (section 1.4.1).

Vascular assembly of endothelial cells usually occurs through one of two complementary processes: vasculogenesis and angiogenesis. Vasculogenesis involves the de novo formation of vessels from non-existing ones by differentiation and proliferation of EC, while angiogenesis is defined as the formation of new interconnected vessels from pre-existing ones by network modification [24]. These two processes are key to vascularization and will be discussed in more detail in Chapter 2.

Once vessel formation and remodeling occur, vessels begin to mature. Mural cells provide key molecular signals to maintain vessel integrity, allowing blood vessels to withstand different blood pressures depending on the vessel type and their location in the body. Endothelial cells residing in the arteries withstand higher shear stresses as the blood is carried from the heart into the body. More supporting cells are recruited to arterial vessels to provide arterial wall strength and distribute the force of the blood flow. [18, 25]

1.4 Regenerative Medicine Strategies for Re-vascularization

As previously mentioned, lack of oxygen prevents cells residing in tissues from performing their regular function and, in the case of CLI, can eventually result in amputation due to tissue death/necrosis. For this reason, new therapeutic approaches exploiting principles of tissue

engineering are being developed to treat ischemic conditions and prevent tissue death and organ failure. Approaches such as angiogenic factor delivery, *in vivo* pre-vascularization, and *in vitro* pre-vascularization have all shown some potential to re-vascularize ischemic regions.

1.4.1 Angiogenic Factor Delivery

Growth factors are important in the vascular development process and have been explored therapeutically with the goal of re-vascularizing ischemic regions. Vascular endothelial growth factor (VEGF) is the most commonly used growth factor in studies examining angiogenic factor delivery. VEGF increases vessel formation, ensures viability of immature blood vessels, facilitates recruitment of pericytes, accelerates pericyte coverage of vessels, recruits endothelial cells, and promotes their proliferation. [24, 26] However, vessel regression occurs less than a month after VEGF delivery, and high VEGF concentrations have been found to provide abnormal vessel formation [27]. In addition, VEGF dosage and delivery time/ frequency must be very controlled for proper vessel formation to occur [28, 29].

Transforming growth factor-β (TGF-β) aids vascular development by inducing pericyte adhesion and differentiation [30]. It also inhibits the proliferation of both mural and endothelial cells and increases the secretion of elastin from many cells such as smooth muscle cells and fibroblasts [18, 30-32]. The platelet-derived growth factor subunit B (PDGF-B) is secreted by endothelial cells to recruit mural cells and induce their proliferation for vessel maturation [18, 25, 33].

Basic fibroblasts growth factor (bFGF) is a mitogenic cationic polypeptide known for stimulating endothelial cells, vascular smooth muscle cells, and other cells [34, 35]. bFGF is found in adrenal glands, bovine and human brains, retinas, kidney, and other tissues [35]. This mitogen

produces plasminogen (plasmin pre-cursor) activators, and is responsible for inducing EC invasion, migration, proliferation, and sprout formation [36]. A study showed that bFGF is a self-stimulating growth factor since ECs not only express it, but also produce it and secrete it to induce their own proliferation [37].

Expression of bFGF in serum has been to be higher in cancer patients than normal patients [38]. In addition, patients responding to cancer treatment tend to have lower levels of hepatocyte growth factor [38]. Hepatocyte growth factor (HGF) has a role in vessel formation and EC invasion, which has been linked to tight junction disruption [38]. It also stimulates EC growth and wound healing repair [39].

Many growth factors and their combinations have been explored for angiogenic delivery with the goal of creating vessels within an ischemic region and facilitating vessel maturation. Although these aforementioned growth factors as well as others are important in vascular development and have the potential to improve blood perfusion [20], appropriate dosages must be employed to form mature and organized vessels to improve blood perfusion without causing negative side effects such as vessel leakage. In addition, controlling growth factor release temporally is very complex since growth factors must be delivered in a specific order to mimic the natural vessel development process [20, 40, 41]. Due to the complexity of vascular development as well as the limitations of growth factor delivery, human clinical trials for ischemic conditions have had limited success with this technique [24, 41-43].

1.4.2 Pre-vascularization

Tissue engineering, also known as regenerative medicine, focuses on developing techniques that can prevent diseases and/or replace organs/tissues damaged due to illnesses. This

field includes many areas, such as cells and materials [44]. Cells have been reprogrammed to differentiate into different lineages depending on the tissue being investigated. Scaffolds can be modified chemically, mechanically, and/or biologically with the introduction of multiple materials including proteins and growth factors. [44] Additional tissue engineering background is discussed in Chapter 2.

One major hurdle in vascularization techniques is cell survival after *in vivo* implantation, since it takes multiple days for new vasculature to reach the cells within the implant and deliver the necessary oxygen and nutrients for their viability [22, 45]. For this reason, pre-vascularization techniques focus on developing scaffolds containing vasculature to improve cell viability and reduce re-vascularization time within an ischemic region.

In Vitro Pre-vascularization

The scaffold matrix developed for vascular tissue engineering must be biocompatible to minimize an inflammatory response in the host which can ultimately lead to additional problems rather than provide solutions. It must also permit the infiltration of cells (endothelial sprout infiltration), and support cell adhesion and proliferation to allow vessel formation to occur (biomimetic characteristics). [20, 46-48]

Different endothelial cells including human umbilical vein endothelial cells (HUVECs), endothelial progenitor cells (EPCs), and microvascular endothelial cells (MVECs) are co-cultured with mural cells such as normal human lung fibroblasts (NHLFs) and mesenchymal stem cells (MSCs) in three-dimensional (3D) matrices to develop vascularized tissues prior to implantation [49-52]. A common material employed to develop *in vitro* vascularized tissues is fibrin. Fibrin is the primary constituent of the provisional matrix that forms during wound healing. This protein is

often used in vascularization studies because of its ability to stimulate the ingrowth of new vessels. [51, 53-55]

Pre-vascularized *in vitro* tissues can accelerate both inosculation between the host and the implant vasculature [52, 56] and also vessel maturation in the implant [57]. This pre-vascularization not only provides better vascularization in situ, but it also improves viability of cells residing in the *in vitro* implants [58]. Although there are multiple benefits for employing this *in vitro* pre-vascularization technique, blood perfusion in the implant does not necessarily occur instantaneously since the implant is typically not connected to the host vasculature micro surgically during implantation [59].

In Vivo Pre-vascularization

In this technique, acellular porous scaffolds are designed to allow host vessel infiltration and formation to occur within their matrices. To do so, these scaffolds are injected or implanted *in vivo*. Once the scaffold is perfused *in situ*, it can be transplanted in another region reducing blood perfusion time in the new implanted area [60]. This approach to develop new tissues has been studied for bone formation applications [61].

Arteriovenous (AV) loops can also be used for *in vivo* pre-vascularization, tissue replacement, transfer, and/or reconstruction [46, 62]. AV loops are made surgically by connecting a vein and artery using a graft [62]. This loop is then placed within a circular groove of a designed acellular scaffold to promote vascularization. The AV loop and scaffold can then be placed in a chamber, and then removed at different time points to access vascularization within implant. [63]

One of the most common *in vivo* pre-vascularization tissues are bone flaps. They are made by implanting bone segments near blood vessels such as epigastric vascular bundle [64] and

saphenous vessel bundle [65]. The vessels vascularize the implant region, are then removed by the surgeon and placed in the ischemic region [59, 66]. Tanaka et al. investigated the differences between arteriovenous shunt loop and arteriovenous bundles and determined that even though the AV loops had more potential in vascularizing an implant, the arteriovenous bundle could also vascularize the implant and was a simpler vascular carrier for skin flaps [67].

In vivo pre-vascularization of scaffolds has shown potential for ischemic re-vascularization. However, fats, donor cells, pathogens, and other toxic agents must be removed if scaffolds are transplanted from a donor to a patient suffering from ischemia (allograft) to prevent a negative inflammatory response. In addition, hematomas and infections can occur after the scaffolds are implanted in situ. Although these negative effects don't cause deaths, hematomas yield a lower blood vessel density when compared to scaffolds with successful vascular carriers (i.e. AV loops) interventions. [63] Once the vascularized *in vivo* implant is excised, the implant must then be placed in the ischemic region and connected to the host vasculature with microsurgery, providing immediate vascularization in the ischemic region [59].

Unfortunately, complex surgical procedures limit the feasibility of pre-vascularization techniques as therapeutic solutions. Therefore, we propose a technique that has the potential to vascularize tissue by combining positive aspects of these existing techniques while overcoming some of their major surgical limitations.

1.5 Hypothesis

The long-term goal of this project is to develop a new therapy that will restore blood flow to damaged tissue by creating pre-vascularized tissue modules containing human endothelial cells (ECs) and supporting stromal cells that act like pericytes, to jump-start inosculation with the host

vasculature after being injected in a minimally invasive manner. This dissertation aims both to develop pre-vascularized microbeads containing human umbilical vein endothelial cells (HUVECs) co-cultured with normal human lung fibroblasts (NHLFs), and also to demonstrate the microbeads' ability to improve blood perfusion in a subcutaneous animal model. Previous *in vivo* studies have shown that pre-vascularized macro tissues have the potential to vascularize ischemic regions faster than the delivery of cells with or without an additional matrix (macro tissues) [68-70]. ***We hypothesize that pre-vascularized microbeads, delivered in a minimally invasive manner, will form microvasculature in vivo at a faster rate than fresh EC- fibroblast co-cultures embedded in microbeads (control microbeads) and pure fibrin matrices (cellular hydrogels).***

1.6 Specific Aims

The following aims outline how the overall project will be accomplished:

Aim 1: Develop microbeads that can be delivered in a minimally invasive manner and are capable of supporting endothelial sprout formation within a model matrix. Prior to starting any pre-vascularization studies, it is necessary to first design efficient way(s) to create control (fresh ECs-NHLFs) microbeads. Quantification of sprout formation within and from control microbeads will be done to analyze the effects of microbead size, cell density, and microtissue matrix.

Aim 2: Investigate the effects of microbead pre-culture on the formation of vessel network *in vitro* and in a subcutaneous model *in vivo*. Design and apply an *in vitro* platform to compare the degree of vessel formation (vascularization) between control and pre-vascularized microbeads. This aim will also assess the capability of the proposed vasculogenic therapy in an *in vivo* environment. Laser Doppler Perfusion Imaging (LDPI) will be employed to quantify blood

perfusion occurring from the implanted constructs. The microbead pre-culture time that will be used in subcutaneous studies will be determined by embedding pre-cultured microbeads in fibrin hydrogels for one week. Fluorescent images of the hydrogels will then be taken to quantify the endothelial tube area coverage within the fibrin hydrogel. HUVECs will be stained with Ulex Europaeus Agglutinin I (UEA I) prior to measuring tube area coverage.

Aim 3: Investigate alternative microbead formulations that enhance endothelial vessel distribution. This aim will explore a combination of materials to improve microbead injectability and handling by augmenting microbead sphericity, providing a higher microbead production yield by limiting their adhesion and aggregation, and supplying a more homogenous network distribution in an "ischemic-like region".

By evaluating the capability of the pre-vascularized microbeads to inosculate with host vasculature, these aims will allow us to investigate the re-vascularization potential of the proposed minimally-invasive technique. The proposed technique may not only stimulate inosculation post-implantation, but it may also minimize negative post-surgical side-effects that may arise from open surgery vascularization techniques.

1.7 Preliminary Studies

Previous *in vitro* [49, 51] and *in vivo* [53, 71] studies published by the Putnam lab have demonstrated that network formation occurs when co-culture of HUVECs and stromal cells (e.g. mesenchymal stem cells, fibroblasts, etc.) are embedded in natural materials, such as fibrin. Although fibrin promotes vasculogenesis, it is mechanically weak and had not been employed alone in the microbead development process established in the Stegemann lab [55]. Therefore, type-I collagen, the most abundant extracellular protein in the body, was incorporated in the

microbead recipe to enhance the microbead mechanical properties and determine if its addition was beneficial for vascular microbead development (see chapter 3). The collagen-fibrin microbead processing protocol was adjusted based on previous work done by the Stegemann lab on collagen-fibrin matrices [72], collagen-agarose microbeads [73], and chitosan-fibrin microbead processing [55].

1.8 Translational Potential

The long-term goal of this line of regenerative medicine research is to develop a new therapy that will restore blood flow to damaged tissue by creating pre-vascularized tissue modules to jump-start inosculation with the host vasculature after being injected in a minimally invasive manner. Therefore, we recognize that the simpler the final therapy is, the higher the probability that it will be approved by the US Food and Drug Administration (FDA). Products composed of acellular biomaterials are more commercially successful in regenerative medicine than products composed of biomaterials and cells [74, 75].

While scaffolds' regulatory path to the clinic is comparatively straightforward, development of cell-based treatments requires consideration of cell culture effectiveness, the most relevant animal model, and the future clinical trials. These clinical trials depend on the FDA categorization of the final product (e.g. drug, medical device) [74]. Complexity increases as cells are introduced to the biomaterial. For this reason, there are no FDA-approved cell-based regenerative biomaterials currently employed clinically in the cardiovascular area. [74, 75]

Prestwich et al. [75] stated that biotech companies prefer developing cell products in approved materials even if a new cell-biomaterial approach is more likely to be clinically effective. We employed FDA-approved biomaterials along with HUVECs and NHLFs in our study.

Acellular microbeads in a fibrin precursor were also used to demonstrate that cells are needed for the final therapeutic approach.

1.9 Scope of Thesis

Chapter 1 motivates the dissertation, describes the background of previous work, current treatments employed to address CLI, the overall hypothesis of this work, and the aims addressing the hypothesis. Chapter 2 defines the vascularization processes: vasculogenesis, angiogenesis, arteriogenesis, and inosculation; and it introduces the tissue engineering field and its strategies to study vasculogenesis, angiogenesis, and re-vascularization. Chapter 3 was published in 2016 in Acta Biomaterialia following peer review, and it addresses aim 1 by first developing control microbeads (fresh HUVECs-NHLFs) that support endothelial sprouting. Endothelial cells and fibroblasts were encapsulated in two different microbead materials – pure fibrin and 40-60 wt.% collagen-fibrin – to determine matrix effects on endothelial sprouting and network formation. HUVEC-NHLF microbeads were characterized *in vitro* in terms of cell density, cell viability, and cell proliferation to find any differences between these two matrices.

Chapter 4 (aim 2) presents pure fibrin microbead pre-culture *in vitro* studies and mouse subcutaneous studies. This chapter addresses aim 2 by evaluating endothelial vessel formation and inosculation to host vasculature from four different constructs: (1) control (fresh ECs-NHLFs) microbeads, (2) pre-cultured microbeads, (3) cells, and (4) acellular microbeads. These implants were injected with fibrin subcutaneously in the backs of mice. The goal of this study was to determine if there was value in pre-culturing microtissues prior to injecting them in the subcutaneous mouse model. Vessel density, vessel area, and total number of vessels were also quantified in this chapter. Chapter 5 addresses aim 3 by demonstrating how the microbead matrix

and pre-culture not only affects endothelial vessel distribution, but also affects microbead production yield, viability of encapsulated cells, and distribution homogeneity. This chapter was accepted for publication this year in the Acta Biomaterialia journal. The overall summary, future work, and preliminary studies for future work can be found in Chapter 6. The appendices contain the experimental protocols that will facilitate future reproducibility of the main experimental work.

1.10 References

1. Ouriel, K., *Peripheral arterial disease.* Lancet, 2001. **358**(9289): p. 1257-64.

2. Bentzon, J.F., et al., *Mechanisms of plaque formation and rupture.* Circulation research, 2014. **114**(12): p. 1852-1866.

3. Norgren, L., et al., *Inter-Society Consensus for the Management of Peripheral Arterial Disease (TASC II).* Journal of Vascular Surgery, 2007. **45**(1, Supplement): p. S5-S67.

4. Criqui, M.H., et al., *Ethnicity and peripheral arterial disease: the San Diego Population Study.* Circulation, 2005. **112**(17): p. 2703-7.

5. Weitz, J.I., et al., *Diagnosis and treatment of chronic arterial insufficiency of the lower extremities: a critical review.* Circulation, 1996. **94**(11): p. 3026-49.

6. Varu, V.N., M.E. Hogg, and M.R. Kibbe, *Critical limb ischemia.* J Vasc Surg, 2010. **51**(1): p. 230-41.

7. Falluji, N. and D. Mukherjee, *Critical and acute limb ischemia: an overview.* Angiology, 2014. **65**(2): p. 137-46.

8. Sanguily, J., et al., *Reducing Amputation Rates in Critical Limb Ischemia Patients Via a Limb Salvage Program: A Retrospective Analysis.* Vascular Disease Management, 2016. **13**(5): p. E112.

9. Yost, M., *Critical Limb Ischemia Volume I: United States Epidemiology, 2010.* Atlanta: The Sage Group, 2010.

10. Atlanta, G.S.G., *THE SAGE GROUP Reports that in 2007 Approximately 2.8 Million People in Western Europe Suffered from Critical Limb Ischemia [press release]*. 2008.

11. Meissner, O.A., et al., *Critical Limb Ischemia: Hybrid MR Angiography Compared with DSA.* Radiology, 2005. **235**(1): p. 308-318.

12. Coffman, J.D., *Vasodilator drugs in peripheral vascular disease.* New England Journal of Medicine, 1979. **300**(13): p. 713-717.

13. Gillespie, J.A., *THE CASE AGAINST VASODILATOR DRUGS IN OCCLUSIVE VASCULAR DISEASE OF THE LEGS.* The Lancet, 1959. **274**(7110): p. 995-997.

14. Bradbury, A., et al., *Bypass versus angioplasty in severe ischaemia of the leg (BASIL): multicentre, randomised controlled trial.* Lancet, 2005. **366**(9501): p. 1925-1934.

15. DOTTER, C.T. and M.P. JUDKINS, *Transluminal Treatment of Arteriosclerotic Obstruction.* Description of a New Technic and a Preliminary Report of Its Application, 1964. **30**(5): p. 654-670.

16. Steele, P.M., et al., *Balloon angioplasty. Natural history of the pathophysiological response to injury in a pig model.* Circulation Research, 1985. **57**(1): p. 105-112.

17. Mullany, C.J., *Coronary artery bypass surgery.* Circulation, 2003. **107**(3): p. e21-e22.

18. Udan, R.S., J.C. Culver, and M.E. Dickinson, *Understanding vascular development.* Wiley Interdisciplinary Reviews-Developmental Biology, 2013. **2**(3): p. 327-346.

19. Eichmann, A., et al., *Vascular development: from precursor cells to branched arterial and venous networks.* International Journal of Developmental Biology, 2003. **49**(2-3): p. 259-267.

20. Kannan, R.Y., et al., *The roles of tissue engineering and vascularisation in the development of micro-vascular networks: a review.* Biomaterials, 2005. **26**(14): p. 1857-1875.

21. Gaengel, K., et al., *Endothelial-mural cell signaling in vascular development and angiogenesis.* Arterioscler Thromb Vasc Biol, 2009. **29**(5): p. 630-8.

22. Rivron, N.C., et al., *Engineering vascularised tissues in vitro.* Eur Cell Mater, 2008. **15**: p. 27-40.

23. Owens, G.K., *Regulation of differentiation of vascular smooth muscle cells.* Physiological reviews, 1995. **75**(3): p. 487-517.

24. Yancopoulos, G.D., et al., *Vascular-specific growth factors and blood vessel formation.* Nature, 2000. **407**(6801): p. 242-8.

25. Mitsumata, M., et al., *Fluid shear stress stimulates platelet-derived growth factor expression in endothelial cells.* American Journal of Physiology - Heart and Circulatory Physiology, 1993. **265**(1): p. H3-H8.

26. Benjamin, L.E., I. Hemo, and E. Keshet, *A plasticity window for blood vessel remodelling is defined by pericyte coverage of the preformed endothelial network and is regulated by PDGF-B and VEGF*. Development, 1998. **125**(9): p. 1591-1598.

27. Davies, N., et al., *The dosage dependence of VEGF stimulation on scaffold neovascularisation.* Biomaterials, 2008. **29**(26): p. 3531-3538.

28. Ozawa, C.R., et al., *Microenvironmental VEGF concentration, not total dose, determines a threshold between normal and aberrant angiogenesis.* The Journal of clinical investigation, 2004. **113**(4): p. 516-527.

29. Dor, Y., et al., *Conditional switching of VEGF provides new insights into adult neovascularization and pro-angiogenic therapy.* The EMBO journal, 2002. **21**(8): p. 1939-1947.

30. Winkler, E.A., R.D. Bell, and B.V. Zlokovic, *Central nervous system pericytes in health and disease*. Nature neuroscience, 2011. **14**(11): p. 1398-1405.

31. Hirai, M., et al., *Latent TGF-β-binding protein 2 binds to DANCE/fibulin-5 and regulates elastic fiber assembly.* The EMBO Journal, 2007. **26**(14): p. 3283-3295.

32. Marigo, V., et al., *Identification of a TGF-β Responsive Element in the Human Elastin Promoter*. Biochemical and Biophysical Research Communications, 1994. **199**(2): p. 1049-1056.

33. Keck, P.J., et al., *Vascular permeability factor, an endothelial cell mitogen related to PDGF*. Science, 1989. **246**(4935): p. 1309-12.

34. Klagsbrun, M. and P.A. D'Amore, *Regulators of angiogenesis.* Annu Rev Physiol, 1991. **53**: p. 217-39.

35. Esch, F., et al., *Primary structure of bovine pituitary basic fibroblast growth factor (FGF) and comparison with the amino-terminal sequence of bovine brain acidic FGF*. Proceedings of the National Academy of Sciences, 1985. **82**(19): p. 6507-6511.

36. Montesano, R., et al., *Basic fibroblast growth factor induces angiogenesis in vitro.* Proceedings of the National Academy of Sciences, 1986. **83**(19): p. 7297-7301.

37. Schweigerer, L., et al., *Capillary endothelial cells express basic fibroblast growth factor, a mitogen that promotes their own growth.* Nature, 1987. **325**(6101): p. 257-259.

38. Sezer, O., et al., *Serum levels of the angiogenic cytokines basic fibroblast growth factor (bFGF), vascular endothelial growth factor (VEGF) and hepatocyte growth factor (HGF) in multiple myeloma.* European journal of haematology, 2001. **66**(2): p. 83-88.

39. Bussolino, F., et al., *Hepatocyte growth factor is a potent angiogenic factor which stimulates endothelial cell motility and growth.* The Journal of cell biology, 1992. **119**(3): p. 629-641.

40. Sun, Q., et al., *Sustained release of multiple growth factors from injectable polymeric system as a novel therapeutic approach towards angiogenesis.* Pharm Res, 2010. **27**(2): p. 264-71.

41. Mikos, A.G., et al., *Engineering complex tissues.* Tissue engineering, 2006. **12**(12): p. 3307-3339.

42. Henry, T., et al., *Results of intracoronary recombinant human vascular endothelial growth factor (rhVEGF) administration trial.* Journal of the American College of Cardiology, 1998. **31**: p. 65.

43. Powell, R.J., et al., *Safety and efficacy of patient specific intramuscular injection of HGF plasmid gene therapy on limb perfusion and wound healing in patients with ischemic lower extremity ulceration: results of the HGF-0205 trial.* Journal of vascular surgery, 2010. **52**(6): p. 1525-1530.

44. Khademhosseini, A. and R. Langer, *A decade of progress in tissue engineering.* Nature protocols, 2016. **11**(10): p. 1775-1781.

45. Griffith, L.G. and G. Naughton, *Tissue engineering--current challenges and expanding opportunities.* Science, 2002. **295**(5557): p. 1009-1014.

46. Kneser, U., et al., *Tissue engineering of bone: the reconstructive surgeon's point of view.* Journal of cellular and molecular medicine, 2006. **10**(1): p. 7-19.

47. Sugiura, T., A.Y. Lee, and T. Shinoka, *Tissue Engineering in Vascular Medicine.* Frontiers, 2017. **4**: p. 3-35.

48. Laschke, M. and M. Menger, *Vascularization in tissue engineering: angiogenesis versus inosculation.* European Surgical Research, 2012. **48**(2): p. 85-92.

49. Ghajar, C.M., et al., *Mesenchymal stem cells enhance angiogenesis in mechanically viable prevascularized tissues via early matrix metalloproteinase upregulation.* Tissue Eng, 2006. **12**(10): p. 2875-88.

50. Ghajar, C.M., et al., *The effect of matrix density on the regulation of 3-D capillary morphogenesis.* Biophys J, 2008. **94**(5): p. 1930-41.

51. Rao, R.R., et al., *Matrix composition regulates three-dimensional network formation by endothelial cells and mesenchymal stem cells in collagen/fibrin materials.* Angiogenesis, 2012. **15**(2): p. 253-64.

52. Chen, X., et al., *Prevascularization of a fibrin-based tissue construct accelerates the formation of functional anastomosis with host vasculature.* Tissue Eng Part A, 2009. **15**(6): p. 1363-71.

53. Grainger, S.J., et al., *Stromal cell identity influences the in vivo functionality of engineered capillary networks formed by co-delivery of endothelial cells and stromal cells.* Tissue Eng Part A, 2013. **19**(9-10): p. 1209-22.

54. Griffith, C.K., et al., *Diffusion limits of an in vitro thick prevascularized tissue.* Tissue Eng, 2005. **11**(1-2): p. 257-66.

55. Chen, Z., L. Wang, and J.P. Stegemann, *Phase-separated chitosan-fibrin microbeads for cell delivery.* J Microencapsul, 2011. **28**(5): p. 344-52.

56. Tremblay, P.L., et al., *Inosculation of tissue-engineered capillaries with the host's vasculature in a reconstructed skin transplanted on mice.* American journal of transplantation, 2005. **5**(5): p. 1002-1010.

57. Rouwkema, J., J.D. Boer, and C.A.V. Blitterswijk, *Endothelial cells assemble into a 3-dimensional prevascular network in a bone tissue engineering construct.* Tissue engineering, 2006. **12**(9): p. 2685-2693.

58. Levenberg, S., et al., *Engineering vascularized skeletal muscle tissue.* Nature biotechnology, 2005. **23**(7): p. 879.

59. Rouwkema, J., N.C. Rivron, and C.A. van Blitterswijk, *Vascularization in tissue engineering.* Trends in biotechnology, 2008. **26**(8): p. 434-441.

60. Kang, K.-T., P. Allen, and J. Bischoff, *Bioengineered human vascular networks transplanted into secondary mice reconnect with the host vasculature and re-establish perfusion.* Blood, 2011. **118**(25): p. 6718-6721.

61. Stevens, M.M., et al., *In vivo engineering of organs: The bone bioreactor.* Proceedings of the National Academy of Sciences of the United States of America, 2005. **102**(32): p. 11450-11455.

62. Lind, B., et al., *Arteriovenous loop grafts for free tissue transfer.* Vascular and endovascular surgery, 2012. **46**(1): p. 30-33.

63. Kneser, U., et al., *Engineering of vascularized transplantable bone tissues: induction of axial vascularization in an osteoconductive matrix using an arteriovenous loop.* Tissue engineering, 2006. **12**(7): p. 1721-1731.

64. Gill, D.R., et al., *The prefabrication of a bone graft in a rat model.* The Journal of hand surgery, 1998. **23**(2): p. 312-321.

65. Hokugo, A., et al., *Prefabrication of vascularized bone graft using guided bone regeneration.* Tissue Engineering, 2004. **10**(7-8): p. 978-986.

66. Lee, J.-H., C.P. Cornelius, and N. Schwenzer, *Neo-osseous flaps using demineralized allogeneic bone in a rat model.* Annals of plastic surgery, 2000. **44**(2): p. 195-204.

67. Tanaka, Y., et al., *Tissue engineering skin flaps: which vascular carrier, arteriovenous shunt loop or arteriovenous bundle, has more potential for angiogenesis and tissue generation?* Plastic and reconstructive surgery, 2003. **112**(6): p. 1636-1644.

68. Riemenschneider, S.B., et al., *Inosculation and perfusion of pre-vascularized tissue patches containing aligned human microvessels after myocardial infarction.* Biomaterials, 2016. **97**: p. 51-61.

69. Halkos, M.E., et al., *Intravenous infusion of mesenchymal stem cells enhances regional perfusion and improves ventricular function in a porcine model of myocardial infarction.* Basic Research in Cardiology, 2008. **103**(6): p. 525-536.

70. Nakamuta, J.S., et al., *Cell therapy attenuates cardiac dysfunction post myocardial infarction: effect of timing, routes of injection and a fibrin scaffold.* PLoS One, 2009. **4**(6): p. e6005.

71. Kniazeva, E., S. Kachgal, and A.J. Putnam, *Effects of extracellular matrix density and mesenchymal stem cells on neovascularization in vivo.* Tissue Eng Part A, 2011. **17**(7-8): p. 905-14.

72. Rowe, S.L. and J.P. Stegemann, *Microstructure and mechanics of collagen-fibrin matrices polymerized using ancrod snake venom enzyme.* J Biomech Eng, 2009. **131**(6): p. 061012.

73. Batorsky, A., et al., *Encapsulation of adult human mesenchymal stem cells within collagen-agarose microenvironments.* Biotechnol Bioeng, 2005. **92**(4): p. 492-500.

74. Pashuck, E.T. and M.M. Stevens, *Designing regenerative biomaterial therapies for the clinic.* Sci Transl Med, 2012. **4**(160): p. 160sr4.

75. Prestwich, G.D., et al., *What is the greatest regulatory challenge in the translation of biomaterials to the clinic?* Sci Transl Med, 2012. **4**(160): p. 160cm14.

CHAPTER 2

Vascularization Strategies in Tissue Engineering

Chapter 2 will describe the vascular processes: vasculogenesis, angiogenesis, arteriogenesis, and inosculation. The three main components used in tissue engineering applications are cells, materials, and growth factors; and these components as applied in vascular tissue engineering will also be described. This chapter also lists different *in vitro* and *in vivo* models used in the vascular tissue engineering field to understand and develop vascular tissues in the body.

2.1 Vasculogenesis

Vasculogenesis is the process of de novo formation of blood vessels. This process encompasses endothelial cell (EC) differentiation, proliferation, migration, and organization into a primary capillary plexus [1-4]. During early development, progenitor cells residing in the middle layer of the embryo known as the mesoderm begin to differentiate into endothelial and hemopoietic (blood) cells by the initiation of fibroblast-derived growth factors [2, 5, 6]. Endothelial and hemopoietic progenitor cells begin their differentiation close to each other in areas known as blood islands. These islands have hemopoietic progenitor cells in their core with angioblasts (endothelial progenitor cells) located on the periphery [3].

The two progenitor cells can differentiate on their own or in association with each other, depending on the anatomical region of vascular development [3]. Vesicle formation occurs from these islands and vascular channel formation occurs as vesicles merge, while angioblasts differentiate into endothelial cells [7]. Angioblasts won't stain with certain endothelial cell markers until complete endothelial cell differentiation has occurred and they are able to form lumens [3]. Some of these endothelial cell markers include vascular endothelial growth factor receptors and vascular endothelial cadherin [2].

In addition to vessel formation, extracellular matrix (ECM) is deposited in the endothelial vessel outer walls, and the lumen forms, leading to formation of basement membrane and blood flow (vessel maturation) [3]. Although EC proliferation is very common during embryogenesis, EC proliferation rate decreases significantly during adulthood [3, 8]. Since EC comprise the inner layer of the vessels and they are involved in multiple vascular processes in the body, they are often studied in the tissue engineering field and will be discussed in more detail throughout this chapter.

2.2 Angiogenesis

Angiogenesis is a multifaceted biological process where new vessels form from existing ones [9]. There are two types of angiogenesis: sprouting angiogenesis and intussusceptive (also known as non-sprouting or splitting) angiogenesis [6]. Sprouting angiogenesis is the most common type of angiogenesis and occurs when new sprouts are formed from existing parent vessels. The key publications that introduced this process were Hertig in 1935 and Folkman in 1971 [10]. Sprouting angiogenesis is triggered by a local angiogenic stimulus that activates neighboring endothelial cells that make up the inner vessels [11]. This EC activation leads to a cascade of

events including vessel dilation, higher vessel permeability, and basement membrane degradation of the parent vessel [12].

Many factors can trigger angiogenesis including the reduction or complete lack of oxygen within a region in the body, an inflammatory response, changes in the extracellular matrix, growth factors, and/or mechanical or intercellular stimuli [13]. As the endothelial cells are triggered, they begin to migrate, proliferate and/or differentiate in order to form new vessels and return the tissue to homeostasis. [14]

Cells in the body use different pathways to communicate with each other for proper tissue/body functionality. Notch signaling is involved in various processes, including angiogenesis, that depend on the activation of a notch cell receptor with a ligand. There are four Notch receptors (Notch 1-4) and two types of notch ligands, the Delta and Serrate families, that are classified based on their structures. Delta-like-4 (DLL4) is part of the Delta family and has been shown to play an important role in vascular development. [15]

Vascular endothelial growth factor A (VEGF-A) binds to the EC VEGF receptor 2 (VEGFR2). The endothelial cell which is most activated by VEGF-A, known as the tip cell, forms filopodia or cytoplasmic projections that extend toward the angiogenic stimulus that releases VEGF-A [16]. The formation of the tip cell(s) caused by VEGF-A release leads to the DLL4-Notch 1 signaling; the EC neighboring the tip cell will have their Notch 1 receptor activated by DLL4. This Notch activation suppresses the VEGF response in cells next to a tip cell, preventing the formation of multiple tip cells from a single parent vessel [17, 18].

As the non-proliferating leading tip cell migrates, the proliferating endothelial cells follow and fill up the gap between the tip cell and their two original neighboring cells that still reside in the parent vessel. These proliferative cells identified as stalk cells are in charge of elongating the

newly formed sprout. The VEGF-A spatial distribution alters the tip cell migration while VEGF-A concentration modifies the proliferation of the stalk cells. [16] Since stalk cells are not part of the original parent vessel, no lumen exists in the sprout elongation area. [12, 16]

Studies have shown that EC proliferation and migration occur near the tip cell and that EC migration from the parent vessel decreases EC-EC interaction. This disruption in the cell-cell contact causes an increase in vessel permeability [13, 19]. Although both migration and proliferation occur during this process, EC proliferation is not necessary for EC sprouting to occur, but it is necessary for further vessel growth [20].

Lumen formation occurs in the formed sprouts (tubulogenesis), and once two tip cells find each other and connect (inosculation), a new capillary/vessel is formed [12]. During the angiogenesis process, the basement membrane of the parent vessels are degraded with proteolytic enzymes in the regions where the tip cells and stalk cells formed the new sprouts. Therefore, after the new capillary/vessel is formed, a new basement membrane is synthesized and pericytes and vascular smooth muscle cells are recruited to stabilize the vessel. [21]

Intussusceptive angiogenesis also known as non-sprouting or splitting angiogenesis is a relatively newly discovered process that describes how a pre-existing vessel splits into two. The pre-existing vessel increases its size due to continuous insertion of small trans-capillary tissue pillars (capillary wall) into its lumen, changing their morphology and forming a new capillary network inside of the original vessel [22, 23].

2.3 Arteriogenesis

Arteriogenesis is the third of the three processes responsible for vascularization in the body. This process was named by a group of scientists in 1996, and describes the process of an arteriole

maturing into an artery [24]. As a major vessel becomes obstructed, proliferation and remodeling of pre-existing collateral arterial vessels occur in order to increase their lumen size and provide better blood perfusion to ischemic tissues. [10, 13]

A pressure gradient created by blood obstruction in a region in the body causes blood velocity to increase and higher blood shear stress inside the vessels. As this occurs, the endothelium becomes activated and a cascade of events causes cells such as endothelial and vascular smooth muscle cells to take part of vascular remodeling in this arteriogenesis process. [10]

While angiogenesis is initiated by transcription factors known as hypoxia inducible factors (HIF) that are activated in regions with not enough oxygen supply (hypoxic regions) [25], arteriogenesis is triggered by inflammation and shear stress. Unlike angiogenesis, arteriogenesis can occur in areas where oxygen levels are normal and this process can last from days to weeks [10]. After the angiogenesis process occurs, blood flow can increase by a factor of 1.5 to 1.7; while in arteriogenesis the increase in blood can be as high as 10 to 20 times more [24]. The arteriogenesis process also relies on multiple growth factors in addition to VEGF and other cells that are triggered during the inflammatory process [24].

2.4 Inosculation

Inosculation is the process that describes the connection between vessels. Plastic surgeons use this process to connect the host vasculature with blood vessels located within the implanted graft for instantaneous blood flow to occur [26]. Skin grafts [26, 27] and nerve grafts [28, 29] have been implanted successfully using the inosculation process. Pre-vascularization techniques, described in Chapter 1, depend on the inosculation between the pre-vascularized tissues and the

host vasculature. Anastomoses between vessels formed *in vitro* (pre-vascularized tissue) and the animal vasculature were first shown in 2005 by Tremblay et al [30].

There are two types of inosculation processes that can occur once the scaffold is implanted: internal and external inosculation [26, 31]. Internal inosculation occurs when host and pre-formed vessels residing in the implant connect within the implant. This type of inosculation occurs when vascular regression/shrinkage takes place within the implant causing the host vessels to first infiltrate into the implant prior to inosculating with the implant vessels [32]. On the other hand, external inosculation occurs when pre-formed vessels that originated from the graft come out of the graft and inosculate with the host vasculature outside of the graft, then this is referred as external inosculation [33]. In addition to connecting to the host vasculature outside the graft, the pre-formed vessels are able form new vessels within the pre-vascularized implant region [33].

As vascular grafts are implanted, an inflammatory and angiogenic response can occur within the implant region [34]. Damaged tissue can initiate the wound healing cascade causing the release of pro-angiogenic growth factors [35]. Unlike angiogenesis which takes weeks to occur, anastomoses can happen as early as four to five days [26, 36].

In addition to surgical anastomoses, natural anastomoses also occur during the angiogenesis process, described in section 2.2. Phng et al. [37] suggest that both Notch and Wnt signaling control the stabilization of vessel anastomoses and vessel pruning during the angiogenesis process. Studies suggest that exploring the link between the two signaling pathways can lead to controlling the number of vessels (vessel density) within constructs prior to implantation. [31, 37]

2.5 Vascularization Techniques in Tissue Engineering

Regenerative medicine – also known as tissue engineering – was proposed as a solution in the middle of the 1980s, due to the limited number of organs available for donation [38]. This multidisciplinary field encompasses many disciplines including biology, materials science, medicine, and engineering and focuses on developing different tissues that can be used in research, tissue/organ repair, or replacement [39, 40].

Cellular and acellular tissue engineering are two of the main strategies being explored in this field. Cellular strategies rely on implanting different cells in engineered scaffolds prior to *in vivo* implantation [39]. In the case of re-vascularization, the scaffolds are designed to permit sprout infiltration into the scaffolds and to allow anastomoses between the host and endothelial sprouts residing in the implant. These scaffolds are then expected to degrade with time without causing negative effects in the host. Acellular tissue engineering focuses on developing materials and embedding signaling molecules such as growth factors that can recruit and/or stimulate the host cells within the implant area [39]. Cell removal from tissues is also a method being explored in order to use the structure of the tissue without worrying about immunological response from foreign cells within the host [39].

To test hypotheses related to vascular tissue engineering, researchers employ various cells (ECs, pericytes, etc.), materials, and growth factors in an array of *in vivo* and *in vitro* models. This section will describe the main cells and materials used for vascularization, and the main *in vitro* and *in vivo* models currently used in this field.

2.5.1 Cells

Stem cells are often used in tissue engineering since they have the ability of differentiating into different lineages. Their differentiation capability is dependent on their classification. Embryonic stem cells (ES) can differentiate into all the three germ layers – endoderm, mesoderm, and ectoderm – that are formed during embryonic development [41]. The endoderm forms the epithelial layer of multiple organs including the pancreas, pharynx, and liver; the mesoderm makes the skeleton, muscle, and other systems including the circulatory system; and the ectoderm makes the nervous system [42]. Adult stem cells are more specialized and constrained in their ability to differentiate based on their origin [43].

Endothelial Cells

Endothelial cells are the first cells to form and the dominant cell in the vascular system [44]. EC fibers are affected by blood flow properties including velocity, pressure, turbulence, and viscosity [45, 46]. There are many different endothelial cells employed to engineer vascular tissues. Endothelial progenitor cells, human umbilical vein endothelial cells, and microvascular endothelial cells, all described below, are the EC types used in this dissertation. Although all of the aforementioned cells are endothelial cells, they each come from different locations in the body, and their shape, function, and other properties are also different [47, 48].

Endothelial progenitor cells (EPCs) are a type of adult stem cell that can form vessels [49]. EPCs circulate in the blood and adhere to the vessel walls when the endothelium lining is deprived or has limited amount of oxygen [50]. EPCs derived from bone marrow behave differently than the ones circulating in the blood. In general, EPC identification, function, and source(s) are still being investigated [51].

In the body, ECs that make up microvessels such as microvascular endothelial cells (MVECs) are more elongated and flatter than ECs comprising large vessels, like HUVECs, which have a cobblestone shape [48]. ECs from microvessels also proliferate slower than ECs from bigger vessels [48]. HUVECs were more often employed than MVECs in the past because they were easier to harvest and proliferate [47].

Two-dimensional characterization of human umbilical vein endothelial cell (HUVECs) was first done in 1963 [52] followed by additional characterization and long term studies [53]. Long term capillary endothelial 2D culture originated in 1979 [54]. It has been demonstrated that sprouting venous endothelial cells are able to differentiate into arteries and capillaries during development [55]. Therefore, HUVECs are still often employed in vasculogenesis and angiogenesis studies. This field continues to explore all these EC types to determine which one creates a better vascular tissue for tissue/organ regeneration.

Mural Cells

Mural cells help form and stabilize blood vessels by secretion of basal membrane components [13]. In vascularization strategies, mural cells such as mesenchymal stem cells (MSCs), fibroblasts, and vascular smooth muscle cells (vSMCs) are co-cultured with endothelial cells in both *in vivo* and *in vitro* systems [56-59]. Mural cells are divided into pericytes and vascular smooth muscle cells based on their location. Pericytes surround capillaries, while bigger vessels such as arteries and veins are surrounded by one or more layers of basement membrane/tissue, depending on the vessel, and a layer of vascular smooth muscle cells. [60]

Mesenchymal stem cells (MSCs) are formed in the connective tissue developed in the middle layer of the embryo [38]. They are one of the most researched adult stem cells in areas such as liver and cardiovascular diseases [41]. MSC isolation can be done from placenta, umbilical

cords, blood, and fatty tissues [41]. However, the source of MSC isolation will alter the behavior of MSCs. A study found that MSCs derived from bone marrow supports vessel formation in a 3D *in vitro* system; however MSCs isolated from umbilical cord arteries and veins did not function in the same manner [57].

Like MSCs, fibroblasts are also used as pericytes in both *in vitro* and *in vivo* systems. They secrete extracellular matrix components like collagen I, angiogenic growth factors like fibroblast growth factor (FGF), and matrix metalloproteinases which play a role in vascularization [61]. Dermal fibroblasts and normal human lung fibroblasts are two types of fibroblast that promote vessel formation *in vitro* and *in vivo* [62, 63]. Our groups employ normal human lung fibroblasts (NHLFs) and MSCs for vasculogenesis and angiogenesis assays. However, previous work has also utilized vascular smooth muscle cells.

Vascular smooth muscle cells (vSMCs) support the larger vessels, and due to their contractile properties, they can regulate the blood flow through those vessels [60]. vSMCs proliferate and produce extracellular matrix components that are part of the vessel wall [64]. A study showed that the incorporation of smooth muscle cells within an implant scaffold resulted in similar physiological functionality and mechanical properties found in normal vessels [38]. Endothelial cells and different stimuli like vessel injury affect the phenotype and behavior of vSMCs [64].

In addition to endothelial cells and stromal cells, bone marrow-derived mononuclear cells (BMMNCs), embryonic stem cells (ES), and induced pluripotent stem cells (iPS) are other cells being studied for tissue regeneration [38]. Current cell therapies being explored include the injection of BMMNCs and other mononuclear cells into ischemic areas with the goal of re-

vascularizing those regions [9, 14]. These BMMNCs can differentiate into multiple lineages and have many cytokines that aid in vascular development [38].

2.5.2 Biomaterials

Biomaterials are employed in tissue engineering with the ultimate goal of repairing a tissue/organ in the body. Prior to developing a scaffold or material, it is important to first determine the target tissue. Choice of material depends on which properties can provide more benefits for that specific tissue or disease. Polymers are most often used as biomaterials due to their structural similarities to various tissues and their adjustable mechanical properties [40]. However, ceramics, composites, and metals are also used as biomaterials [39].

The US Food and Drug Administration (FDA) categorizes any material that will be implanted in the body as a class II medical device [65]. However, due to their complexity some biomaterials are no longer considered class II medical devices by the FDA and must be tested separately to determine their FDA classification [65]. Biocompatibility and biodegradability are also important when designing biomaterials [66, 67]. Tissue replacements must be designed to prevent any extreme reactions in the body after implantation. The criteria for biocompatibility varies depending on the targeted tissue application [39]. As the implant inside the body degrades with time, it begins leaching extra components that must also be biocompatible or else additional complications can occur [66].

Natural Materials

Biomaterials can be synthetic, natural, or a combination of both and can be made into scaffolds for tissue and/or organ replacement [39, 65]. Two main natural materials that are often

used in vasculogenesis and angiogenesis assays are fibrin and collagen [68]. Although there are other natural materials including alginate [69] employed to promote vascularization, fibrin and collagen are highlighted in this section since they are the ones mainly used in this dissertation.

Fibrin plays an important role in the blood clotting cascade which occurs during the wound healing process [70-73]. The polymerization of fibrin is dependent on multiple steps and factors that affect the physical and structural properties [58, 59, 71, 74] of the resulting fibrin hydrogel/scaffold [70]. For this reason, this viscoelastic material [75] is often utilized in tissue engineering to study vasculogenesis, angigonesis, and inosculation processes both *in vitro* and *in vivo*. However, proper understanding of *in vivo* fibrin polymerization is necessary to engineer these fibrin scaffolds.

The polymerization of fibrin occurs in several steps including the formation of fibrin monomers, fibrin oligomers, protofibrils, fibrin fibers, and the final fibrin network [70]. The fibrin precursor, fibrinogen, has six chains made up of two identical polypeptide sets $(A\alpha\ B\beta\ \gamma)_2$ that are connected by 24 disulfide bonds (R-S-S-R) and result in a 45 nm length [70]. This protein (340 kDa) circulates in the blood at 3 mg/mL concentration [71, 76] and is converted into fibrin $(\alpha\ \beta\ \gamma)_2$ via thrombin [77]. In brief, the formation of fibrin monomers $(\alpha\ \beta\ \gamma)_2$ occurs when the fibrinopeptides A and B (FpA, and FpB) located in the N-termini of the Aα and Bβ chains of fibrinogen are cleaved by thrombin [70]. The fibrinogen conformation alters the access of thrombin to FpA and FpB, affecting their thrombin cleavage rate [70]. Oligomer and protofibril production occurs with the polymerization of the fibrin monomers [70, 78]. As protofibrils grow to a specific length, they begin the packing process and side-by-side association to form fibrin fibers [79]. Finally, fiber branching creates a fibrin network, allowing fibrin to form either as a clot (*in vivo*) or a hydrogel (*in vitro*) [70, 78, 79].

Factor XIII (FXIII, A_2B_2) is an oligomer that has four subunits – half are A-subunits and the other half are B-subunits [80]. Thrombin also plays an additional role in the fibrin polymerization process by activating Factor XIII. Once activated, Factor XIIIa is in charge of covalently crosslinking fibrin to stabilize and strengthen it [70, 77]. It can also reduce fiber thickness and increase fiber density during fibrin formation to strengthen them and make them more resistant to fibrinolysis [80].

This complex fibrin mechanism can be affected by genetic variations of the fibrinogen/fibrin structure, the components and their concentrations used in the polymerization process, and the exposure to different cell type(s) and blood flow rates [70]. For example, if only one fibrinopeptide is cleaved instead of both during the polymerization process, then thinner fibers are formed in the fibrin clot [70]. Myocardial infarction and ischemic stroke are some of the many diseases that can cause or be caused by improper fibrin polymerization [70].

Collagen is the main constituent of connective tissues' ECM [81]. There are more than 20 types of collagen that are present in the body. Collagen IV is present in the basement membrane around the vessels. [81] The most abundant protein in the body, collagen I, is most often used in vascularization strategies due to its strength and other structural properties [82, 83]. Type I collagen has a triple helix structure with an approximately 1 to 5 nm width and 300 nm length, with over 1000 amino acids [82]. Both ECs and pericytes can produce and secrete collagen in 2D assays [84, 85].

Synthetic Materials

Synthetic materials are designed to have specific strength, degradation rates, and many other properties that can be independently modulated without affecting other properties, unlike in the case of natural materials [69]. Polyglycolic acid (PGA) is a synthetic material often used due

to its hydrolysis degradation which can be tuned by combining it with other materials [86]. Polyethylene glycol (PEG) is another synthetic material that is often used in vascular studies because it is biocompatible and it does not interact with the body unless it's first functionalized with peptides or other molecules/materials [69]. PEG has also been shown to reduce immunological reactions, and its mechanical and degradation properties can be chemically altered [69].

2.5.3 *In Vivo* Models

Many *in vivo* models have been created to study angiogenesis and drug development [87]. Some of these models are more popular than others because they are more cost-effective and facilitate screening of multiple drugs at a time. These models can be qualitative and/or quantitative and often introduce a tumor or a scaffold/implant into animal(s). These procedures create wound/inflammatory response that promote new sprout formation within the affected regions. [87]

In 1974, both tumor growth and angiogenesis were investigated by implanting tumors into rabbits' corneas due to their avascular and transparent properties [88, 89]. This *in vivo* assay is still being utilized nowadays to study angiogenesis mechanisms and drug delivery formulations [89]. Transparent chambers have also been implanted *in vivo* to investigate and monitor angiogenesis. The first chamber was introduced in 1924 in the rabbit's ear [90]. Some other implantation areas of these chambers include hamster cheek [91], rodent cranial windows, and dorsal skinfold in mice [92], hamsters, rabbits, and rats [93]. There are many additional *in vivo* angiogenesis models including the chick chorioallantoic membrane (CAM) [93, 94], the sponge implant model [95], muscle angiogenesis assay [96], and the zebrafish model [97, 98].

The CAM assay is one of the most popular angiogenesis assays due to its very low cost [93, 94]. This assay was mainly used to screen different materials to determine if they could inhibit or induce angiogenesis; however, it was later adapted for quantitative measurements [99]. There are various protocols for this assay including the creation of a small window in the shell of the chicken egg, or the entire shell removal during incubation [93]. For the quantitative assay, the eggs are first incubated for multiple days, followed by the removal of the entire shell and placement of the egg into a Petri dish. A scaffold is then created by loading growth factor(s) into hydrogels that are placed between two meshes and later on top of chick embryos [99]. Vessel quantification is done by determining the number of vessels formed within the top mesh of the hydrogel [99].

Another method to measure vessel formation is the sponge implant model. This model requires the implantation of a sponge into animals such as dogs [100], rabbits [101], and rats [102] to allow vessel ingrowth into the sponge. Sponges are made of different materials such as cellulose acetate, polyether, polyester, polyurethane, or polyvinyl [95]. After vessel ingrowth occurs, the sponge is removed, and many parameters including blood vessels, cytokines, chemokines, hemoglobin, collagen deposition found within the sponge are quantified [95].

The muscle angiogenesis model consists of implanting either an electrode or an electrical stimulator subcutaneously [96]. A set voltage and stimulation time is chosen to contract muscles once the electrode is implanted. This stimulation increases angiogenesis (vessel density) and remains constant even after stimulation is suspended. [103]

One of the newest angiogenesis models, uses zebrafish since it develops many transparent embryos at a time, facilitating visualization at different stages of embryonic development. Even though these animals are not mammals, the zebrafish assays provide results that can be used in humans. This fish is not only used for cardiovascular drug studies, but also to model other diseases

including cancer, diabetes, muscular dystrophy, and Huntington's disease. Fluorescent labelling of vessels is often done in this model to facilitate angiogenesis studies. [97, 98]

2.5.4 *In Vitro* Models

Cellular Scaffolds

As previously mentioned, fibrin is a natural polymer used in many tissue engineering applications because its physical properties can be altered by varying multiple factors including fibrin fiber diameter and density, the number and distance of branch points, and the porosity of the material [70]. Multiple cells including endothelial and mural cells discussed above bind to fibrin and form sprouts within the fibrillar fibrin network. Fibrin can also be used as a delivery vehicle transporting cells, growth factors, drugs, and other materials to specific areas in the body [75]. However, this section will focus on its use in vasculogenesis and angiogenesis *in vitro* assays.

Angiogenesis studies were first done in animal models as described in the section above. Folkman and Haudenschild published the first *in vitro* angiogenesis model in 1980 [104]. This two-dimensional (2D) model showed that tube formation occurred after capillary endothelial cells were isolated and cultured on gelatin-coated plates using tumor-conditioned media [104]. Three-dimensional models are more useful than 2D models since cells embedded in 3D hydrogels behave more like *in vivo* conditions than cells seeded on top of 2D surfaces [105].

Nehls and Drenckhahn [106] developed an *in vitro* angiogenesis system that could facilitate sprout quantification. This system uses microcarrier beads coated with gelatin to allow endothelial attachment. Once attached, the cellular microcarrier beads are embedded in fibrin hydrogels where they migrate and form sprouts within the hydrogel. This angiogenesis model is still being employed to study endothelial sprouting, inosculation, and other vascular mechanisms which are

affected when adjusting parameters including but not limited to cell type(s), their proximity to each other, and matrix properties [58, 107-110]. Other angiogenesis assays include the human arterial ring angiogenesis assay which entails embedding human umbilical artery rings in basement membrane extracts [111], and the human aortic ring assays which are aortic rings embedded in fibrin or collagen hydrogels [112].

Many researchers continue to investigate how to develop vascular tissues and vasculogenesis/angiogenesis *in vitro* assays by combining different cells and materials [36, 108, 113]. Some of the cells employed in these assays include adipose tissue fragments (ATF) [114], bovine aortic endothelial cells (BAEC) [115-117], bovine capillary endothelial cells (BCEC) [118, 119], embryonic stem cells (ES) [120, 121], endothelial progenitor cells (EPCs) [122], microvascular endothelial cells (MVECs) [123], and human umbilical vein endothelial cells [124]. In addition to fibrin, other biomaterials like collagen, Matrigel, and plasma clots are also used to encapsulate cells and study their functionality [125].

Vasculogenesis studies in the Putnam and Stegemann labs have shown the potential of human umbilical vein endothelial cells (HUVECs) and stromal cells (e.g. mesenchymal stem cells - MSCs, NHLFs, etc.) to form networks when embedded in 3D fibrin macro gels [58, 108, 126-128]. Higher fibrinogen concentrations have been shown to increase the number of fibers and branch points formed within the matrix resulting in higher hydrogel stiffness. [79] Other biomaterials such as collagen are also used with fibrin to increase the overall matrix stiffness.

A previous study from the Stegemann lab [126] demonstrated that HUVECs-MSCs co-cultures form vascular networks of different network lengths depending on the collagen-fibrin concentrations, as well as the HUVECs-MSCs co-culture ratio utilized to make these gels. The study demonstrated that HUVECs-MSCs co-cultures embedded in 40-60 collagen-fibrin macro

gels achieved a network formation comparable to when this same co-culture was embedded in fibrin alone. However, the strengths of these two matrices were different. Fig. 2-1 displays the results of HUVECs-NHLFs experiments, which qualitatively demonstrate that HUVECs-NHLFs co-cultures can also form networks similarly in pure fibrin and 40-60 collagen-fibrin systems even though their mechanical properties are different.

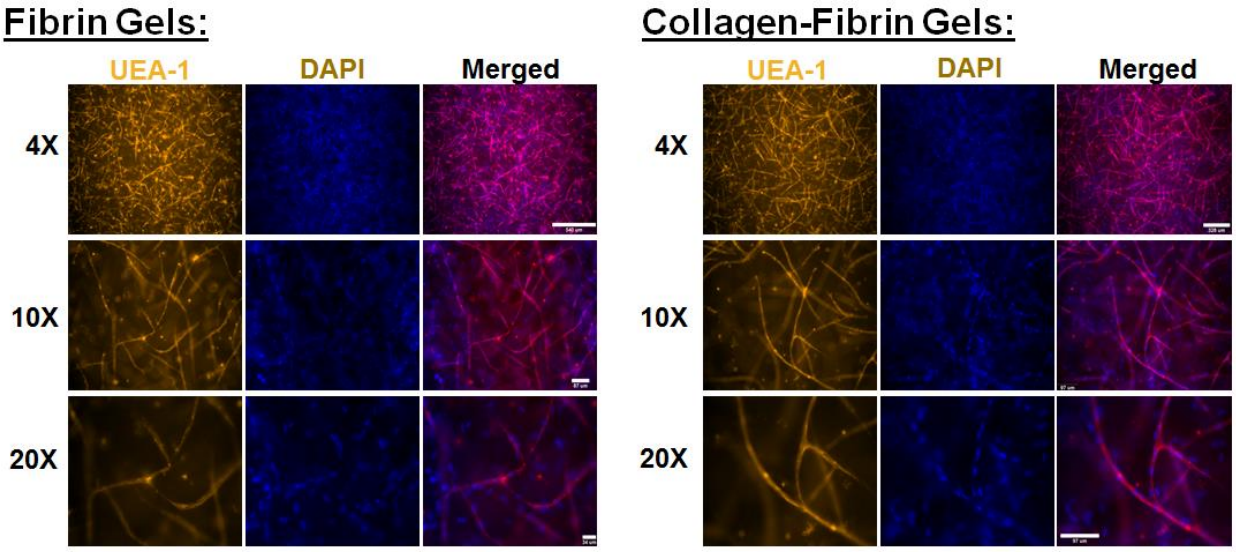

Figure 2-1 HUVECs-NHLFs (1:1) co-culture in 3D fibrin (left) and collagen-fibrin (right) gels at 4x, 10x, and 20x magnifications.

Modular Tissue Engineering Technique

Cells residing in most tissues in the body receive oxygen and nutrients via blood from capillaries that are spaced approximately 100 to 200 μm apart [129, 130]. Although oxygen can diffuse further, cell apoptosis occurs in constructs larger than 200 μm due to oxygen and nutrient consumption limitations. Creating small microtissues diminishes mass transfer limitations while permitting cells residing within the microtissues to attach, spread, and function depending on the

tissue type. The modular tissue engineering technique assembles these microtissues by aggregation or by printing them in specific regions to develops larger tissues [131].

These microtissues can also be injected into disease areas to regenerate tissue [132]. In the case of vascularization, the idea is to encapsulate endothelial and mural cells within the microbeads to allow sprout formation to occur prior to implantation in ischemic areas. Preliminary studies done in our labs showed that HUVECs-NHLFs collagen-fibrin microbeads embedded in fibrin hydrogels containing fibroblasts (*in vivo* like condition) or lacking fibroblasts can form sprouts (Fig. 2-2). To distinguish the microbeads from the surrounding hydrogel, microbeads were made with FITC fibrinogen. Samples were stained with UEA-I (endothelial cell marker, red) and DAPI (nuclei, blue) to distinguish the two cell types.

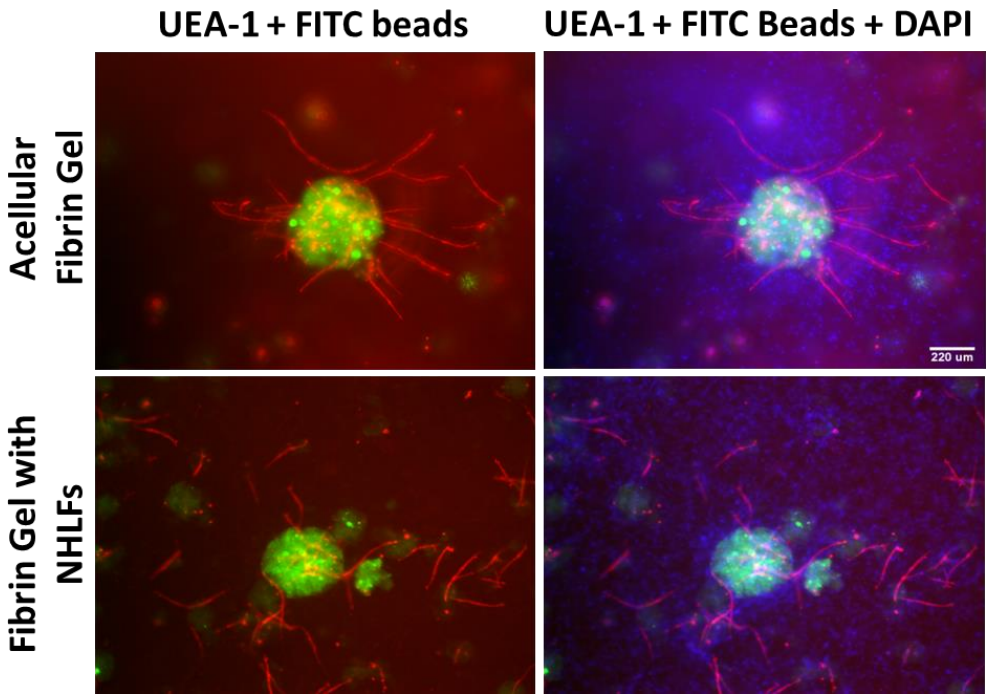

Figure 2-2: Demonstration of sprouting of HUVECs-NHLFs collagen-fibrin microbeads. HUVEC marker (red): UEA-I, cell nuclei (blue): DAPI, microbeads (green): FITC, scale bar = 200 μm.

Cell Patterning Techniques

Cell patterning techniques for tissue development are also employed in tissue engineering [133]. The idea of using microfabrication is that tissues can be built with the necessary blood supply for cells to survive, and ultimately develop an entire organ such as the heart [133]. Photolithography, microcontact printing and microfluidic devices (MFD) are some of the microfabrication techniques employed. In particular, MFDs are often used since cells can be localized within different channels to study their functionality based on biomaterials being used and local effects of flow within the system [133].

2.6 Conclusion

There are multiple processes that occur in vascular tissues including vasculogenesis, angiogenesis, and arteriogenesis. This chapter describes these important processes and the main cells that are part of these processes. Some of the natural materials, e.g. fibrin and collagen, used in tissue engineering are described along with some synthetic materials. There are also multiple *in vitro*/*in vivo* models developed in the tissue engineering field, including the ones developed in this work, to study the cells, materials, and vascular processes. The goal is that someday one or a combination of these strategies will lead to vascular tissue regeneration in ischemic regions.

2.7 References

1. Carlson, B.M., *Chapter 17 - Cardiovascular System*, in *Human Embryology and Developmental Biology (Fifth Edition)*. 2014, W.B. Saunders: Philadelphia. p. 408-452.
2. Risau, W., *Differentiation of endothelium.* FASEB J, 1995. **9**(10): p. 926-33.

3. Risau, W. and I. Flamme, *Vasculogenesis.* Annual review of cell and developmental biology, 1995. **11**(1): p. 73-91.

4. Udan, R.S., J.C. Culver, and M.E. Dickinson, *Understanding vascular development.* Wiley Interdisciplinary Reviews-Developmental Biology, 2013. **2**(3): p. 327-346.

5. Azar, Y. and H. Eyal-Giladi, *Marginal zone cells--the primitive streak-inducing component of the primary hypoblast in the chick.* J Embryol Exp Morphol, 1979. **52**: p. 79-88.

6. Risau, W., *Mechanisms of angiogenesis.* Nature, 1997. **386**(6626): p. 671.

7. Noden, D.M., *Origins and Assembly of Avian Embryonic Blood Vesselsa.* Annals of the New York Academy of Sciences, 1990. **588**(1): p. 236-249.

8. Engerman, R.L., D. Pfaffenbach, and M. Davis, *Cell turnover of capillaries.* Laboratory investigation; a journal of technical methods and pathology, 1967. **17**(6): p. 738-743.

9. Al Mheid, I. and A.A. Quyyumi, *Cell therapy in peripheral arterial disease.* Angiology, 2008. **59**(6): p. 705-16.

10. Buschmann, I. and W. Schaper, *Arteriogenesis versus angiogenesis: two mechanisms of vessel growth.* Physiology, 1999. **14**(3): p. 121-125.

11. Felmeden, D., A. Blann, and G. Lip, *Angiogenesis: basic pathophysiology and implications for disease.* European Heart Journal, 2003. **24**(7): p. 586-603.

12. Pepper, M.S., *Manipulating Angiogenesis.* From Basic Science to the Bedside, 1997. **17**(4): p. 605-619.

13. D'Amore, P.A. and R.W. Thompson, *Mechanisms of angiogenesis.* Annu Rev Physiol, 1987. **49**: p. 453-64.

14. Hazarika, S. and B.H. Annex, *Gene and Cell Therapy for Critical Limb Ischemia*, in *Critical Limb Ischemia*. 2017, Springer. p. 491-501.

15. Shutter, J.R., et al., *Dll4, a novel Notch ligand expressed in arterial endothelium.* Genes & development, 2000. **14**(11): p. 1313-1318.

16. Gerhardt, H., et al., *VEGF guides angiogenic sprouting utilizing endothelial tip cell filopodia.* The Journal of cell biology, 2003. **161**(6): p. 1163-1177.

17. Hellström, M., et al., *Dll4 signalling through Notch1 regulates formation of tip cells during angiogenesis.* Nature, 2007. **445**(7129): p. 776-780.

18. Siekmann, A.F. and N.D. Lawson, *Notch signalling and the regulation of angiogenesis.* Cell adhesion & migration, 2007. **1**(2): p. 104-105.

19. Ausprunk, D.H. and J. Folkman, *Migration and proliferation of endothelial cells in preformed and newly formed blood vessels during tumor angiogenesis.* Microvascular research, 1977. **14**(1): p. 53-65.

20. Sholley, M., et al., *Mechanisms of neovascularization. Vascular sprouting can occur without proliferation of endothelial cells.* Laboratory investigation; a journal of technical methods and pathology, 1984. **51**(6): p. 624-634.

21. Nomi, M., et al., *Principals of neovascularization for tissue engineering.* Molecular aspects of medicine, 2002. **23**(6): p. 463-483.

22. Burri, P.H. and V. Djonov, *Intussusceptive angiogenesis—the alternative to capillary sprouting.* Molecular aspects of medicine, 2002. **23**(6): p. 1-27.

23. Burri, P.H., R. Hlushchuk, and V. Djonov, *Intussusceptive angiogenesis: its emergence, its characteristics, and its significance.* Developmental Dynamics, 2004. **231**(3): p. 474-488.

24. Schaper, W. and D. Scholz, *Factors regulating arteriogenesis.* Arteriosclerosis, thrombosis, and vascular biology, 2003. **23**(7): p. 1143-1151.

25. Carmeliet, P., *Mechanisms of angiogenesis and arteriogenesis.* Nature medicine, 2000. **6**(4): p. 389.

26. Laschke, M.W., B. Vollmar, and M.D. Menger, *Inosculation: connecting the life-sustaining pipelines.* Tissue Engineering Part B: Reviews, 2009. **15**(4): p. 455-465.

27. Clemmesen, T. and D.A. R $ osnhovde, *Restoration of the blood-supply to human skin autografts.* Scandinavian journal of plastic and reconstructive surgery, 1968. **2**(1): p. 44-46.

28. Best, T.J., et al., *Revascularization of peripheral nerve autografts and allografts.* Plastic and reconstructive surgery, 1999. **104**(1): p. 152-160.

29. Chalfoun, C., et al., *Primary nerve grafting: A study of revascularization.* Microsurgery, 2003. **23**(1): p. 60-65.

30. Tremblay, P.L., et al., *Inosculation of tissue-engineered capillaries with the host's vasculature in a reconstructed skin transplanted on mice.* American journal of transplantation, 2005. **5**(5): p. 1002-1010.

31. Laschke, M. and M. Menger, *Vascularization in tissue engineering: angiogenesis versus inosculation.* European Surgical Research, 2012. **48**(2): p. 85-92.

32. Capla, J.M., et al., *Skin graft vascularization involves precisely regulated regression and replacement of endothelial cells through both angiogenesis and vasculogenesis.* Plastic and reconstructive surgery, 2006. **117**(3): p. 836-844.

33. Laschke, M.W., et al., *Improvement of vascularization of PLGA scaffolds by inosculation of in situ-preformed functional blood vessels with the host microvasculature.* Annals of surgery, 2008. **248**(6): p. 939-948.

34. Rücker, M., et al., *Angiogenic and inflammatory response to biodegradable scaffolds in dorsal skinfold chambers of mice.* Biomaterials, 2006. **27**(29): p. 5027-5038.

35. Eming, S.A., et al., *Regulation of angiogenesis: wound healing as a model.* Progress in histochemistry and cytochemistry, 2007. **42**(3): p. 115-170.

36. Chen, X., et al., *Rapid anastomosis of endothelial progenitor cell-derived vessels with host vasculature is promoted by a high density of cotransplanted fibroblasts.* Tissue Eng Part A, 2010. **16**(2): p. 585-94.

37. Phng, L.-K., et al., *Nrarp coordinates endothelial Notch and Wnt signaling to control vessel density in angiogenesis.* Developmental cell, 2009. **16**(1): p. 70-82.

38. Sugiura, T., A.Y. Lee, and T. Shinoka, *Tissue Engineering in Vascular Medicine.* Frontiers, 2017. **4**: p. 3-35.

39. Chen, Q., S. Liang, and G.A. Thouas, *Elastomeric biomaterials for tissue engineering.* Progress in polymer science, 2013. **38**(3): p. 584-671.

40. Hubbell, J.A., *Biomaterials in tissue engineering.* Nature Biotechnology, 1995. **13**(6): p. 565-576.

41. Wang, S., X. Qu, and R.C. Zhao, *Clinical applications of mesenchymal stem cells.* Journal of hematology & oncology, 2012. **5**(1): p. 19.

42. Pansky, B., *Review of medical embryology*. 1982: Macmillan.

43. Hodgkinson, T., X.-F. Yuan, and A. Bayat, *Adult stem cells in tissue engineering.* Expert Review of Medical Devices, 2009. **6**(6): p. 621-640.

44. Eichmann, A., et al., *Vascular development: from precursor cells to branched arterial and venous networks.* International Journal of Developmental Biology, 2003. **49**(2-3): p. 259-267.

45. Herman, I.M., T.D. Pollard, and A.J. Wong, *Contractile proteins in endothelial cells.* Annals of the New York Academy of Sciences, 1982. **401**(1): p. 50-60.

46. White, G.E., M.A. Gimbrone, and K. Fujiwara, *Factors influencing the expression of stress fibers in vascular endothelial cells in situ.* The Journal of Cell Biology, 1983. **97**(2): p. 416-424.

47. Craig, L.E., et al., *Endothelial cells from diverse tissues exhibit differences in growth and morphology.* Microvascular research, 1998. **55**(1): p. 65-76.

48. Kumar, S., D.C. West, and A. Ager, *Heterogeneity in endothelial cells from large vessels and microvessels.* Differentiation, 1987. **36**(1): p. 57-70.

49. Tepper, O.M., et al., *Endothelial progenitor cells: the promise of vascular stem cells for plastic surgery.* Plastic and reconstructive surgery, 2003. **111**(2): p. 846-854.

50. Yoder, M.C., *Human Endothelial Progenitor Cells.* Cold Spring Harbor Perspectives in Medicine, 2012. **2**(7): p. a006692.

51. Urbich, C. and S. Dimmeler, *Endothelial progenitor cells.* Circulation research, 2004. **95**(4): p. 343-353.

52. Maruyama, Y., *The human endothelial cell in tissue culture.* Zeitschrift für Zellforschung und Mikroskopische Anatomie, 1963. **60**(1): p. 69-79.

53. Jaffe, E.A., et al., *Culture of Human Endothelial Cells Derived from Umbilical Veins. IDENTIFICATION BY MORPHOLOGIC AND IMMUNOLOGIC CRITERIA.* Journal of Clinical Investigation, 1973. **52**(11): p. 2745-2756.

54. Folkman, J., C.C. Haudenschild, and B.R. Zetter, *Long-term culture of capillary endothelial cells.* Proceedings of the National Academy of Sciences, 1979. **76**(10): p. 5217-5221.

55. Red-Horse, K., et al., *Coronary arteries form by developmental reprogramming of venous cells.* Nature, 2010. **464**(7288): p. 549-53.

56. Weinberg, C.B. and E. Bell, *A blood vessel model constructed from collagen and cultured vascular cells.* Science, 1986. **231**: p. 397-401.

57. Trkov, S., et al., *Micropatterned 3-Dimensional Hydrogel System to Study Human Endothelial-Mesenchymal Stem Cell Interactions.* Journal of tissue engineering and regenerative medicine, 2010. **4**(3): p. 205.

58. Ghajar, C.M., et al., *Mesenchymal stem cells enhance angiogenesis in mechanically viable prevascularized tissues via early matrix metalloproteinase upregulation.* Tissue Eng, 2006. **12**(10): p. 2875-88.

59. Chen, X., et al., *Prevascularization of a fibrin-based tissue construct accelerates the formation of functional anastomosis with host vasculature.* Tissue Eng Part A, 2009. **15**(6): p. 1363-71.

60. Gerhardt, H. and C. Betsholtz, *Endothelial-pericyte interactions in angiogenesis.* Cell and tissue research, 2003. **314**(1): p. 15-23.

61. Costa-Almeida, R., et al., *Cellular strategies to promote vascularisation in tissue engineering applications.* Eur Cell Mater, 2014. **28**: p. 51-66.

62. Guerreiro, S.G., et al., *Implanted neonatal human dermal fibroblasts influence the recruitment of endothelial cells in mice.* Biomatter, 2012. **2**(1): p. 43-52.

63. Newman, A.C., et al., *The requirement for fibroblasts in angiogenesis: fibroblast-derived matrix proteins are essential for endothelial cell lumen formation.* Molecular biology of the cell, 2011. **22**(20): p. 3791-3800.

64. Owens, G.K., *Regulation of differentiation of vascular smooth muscle cells.* Physiological reviews, 1995. **75**(3): p. 487-517.

65. Amato, S.F. and R.M. Ezzell Jr, *Regulatory affairs for biomaterials and medical devices*. 2014: Elsevier.

66. Langer, R. and J.P. Vacanti, *Tissue Engineering.* Science, 1993. **260**(5110): p. 920-926.

67. Santerre, J., et al., *Understanding the biodegradation of polyurethanes: from classical implants to tissue engineering materials.* Biomaterials, 2005. **26**(35): p. 7457-7470.

68. Feng, X., et al., *Fibrin and collagen differentially but synergistically regulate sprout angiogenesis of human dermal microvascular endothelial cells in 3-dimensional matrix.* International journal of cell biology, 2013. **2013**.

69. Ducheyne, P., et al., *Comprehensive biomaterials*. Vol. 1. 2015: Newnes.

70. Weisel, J.W. and R.I. Litvinov, *Mechanisms of fibrin polymerization and clinical implications.* Blood, 2013. **121**(10): p. 1712-1719.

71. Ceccarelli, J. and A.J. Putnam, *Sculpting the blank slate: how fibrin's support of vascularization can inspire biomaterial design.* Acta biomaterialia, 2014. **10**(4): p. 1515-1523.

72. Laurens, N., P. Koolwijk, and M.P. de Maat, *Fibrin structure and wound healing.* J Thromb Haemost, 2006. **4**(5): p. 932-9.

73. Martino, M.M., et al., *Extracellular matrix and growth factor engineering for controlled angiogenesis in regenerative medicine.* Frontiers in bioengineering and biotechnology, 2015. **3**.

74. Kniazeva, E., S. Kachgal, and A.J. Putnam, *Effects of extracellular matrix density and mesenchymal stem cells on neovascularization in vivo.* Tissue Eng Part A, 2011. **17**(7-8): p. 905-14.

75. Litvinov, R.I. and J.W. Weisel, *Fibrin mechanical properties and their structural origins.* Matrix Biology, 2016.

76. Clark, R., *The molecular and cellular biology of wound repair*. 2013: Springer Science & Business Media.

77. Medved, L. and J. Weisel, *Recommendations for nomenclature on fibrinogen and fibrin.* Journal of Thrombosis and Haemostasis, 2009. **7**(2): p. 355-359.

78. Chernysh, I.N., C. Nagaswami, and J.W. Weisel, *Visualization and identification of the structures formed during early stages of fibrin polymerization.* Blood, 2011. **117**(17): p. 4609-4614.

79. Weisel, J., *Structure of fibrin: impact on clot stability.* Journal of Thrombosis and Haemostasis, 2007. **5**(s1): p. 116-124.

80. Hethershaw, E., et al., *The effect of blood coagulation factor XIII on fibrin clot structure and fibrinolysis.* Journal of Thrombosis and Haemostasis, 2014. **12**(2): p. 197-205.

81. Mienaltowski, M.J. and D.E. Birk, *Structure, Physiology, and Biochemistry of Collagens*. 2014, SPRINGER-VERLAG BERLIN: BERLIN. p. 5.

82. Henriksen, K. and M.A. Karsdal, *Chapter 1 - Type I Collagen*, in *Biochemistry of Collagens, Laminins and Elastin*. 2016, Academic Press. p. 1-11.

83. Walters, B.D. and J.P. Stegemann, *Strategies for directing the structure and function of three-dimensional collagen biomaterials across length scales.* Acta biomaterialia, 2014. **10**(4): p. 1488-1501.

84. Jaffe, E.A., et al., *Synthesis of basement membrane collagen by cultured human endothelial cells.* J exp med, 1976. **144**(1): p. 209-225.

85. Cohen, M., R. Frank, and A. Khalifa, *Collagen production by cultured retinal capillary pericytes.* Investigative ophthalmology & visual science, 1980. **19**(1): p. 90-94.

86. Peck, M., et al., *The evolution of vascular tissue engineering and current state of the art.* Cells Tissues Organs, 2011. **195**(1-2): p. 144-158.

87. Staton, C.A., M.W. Reed, and N.J. Brown, *A critical analysis of current in vitro and in vivo angiogenesis assays.* International journal of experimental pathology, 2009. **90**(3): p. 195-221.

88. Gimbrone, M.A., et al., *Tumor growth and neovascularization: an experimental model using the rabbit cornea.* Journal of the National Cancer Institute, 1974. **52**(2): p. 413-427.

89. Morbidelli, L. and M. Ziche, *The Rabbit Corneal Pocket Assay.* Angiogenesis Protocols, 2016: p. 299-310.

90. Sandison, J.C., *A new method for the microscopic study of living growing tissues by the introduction of a transparent chamber in the rabbit's ear.* The Anatomical Record, 1924. **28**(4): p. 281-287.

91. Goodall, C., A. Sanders, and P. Shubik, *Studies of vascular patterns in living tumors with a transparent chamber inserted in hamster cheek pouch.* Journal of the National Cancer Institute, 1965. **35**(3): p. 497-521.

92. Sckell, A. and M. Leunig, *Dorsal Skinfold Chamber Preparation in Mice: Studying Angiogenesis by Intravital Microscopy.* Angiogenesis Protocols, 2016: p. 251-263.

93. Jain, R.K., et al., *Quantitative angiogenesis assays: progress and problems.* Nature medicine, 1997. **3**(11): p. 1203-1208.

94. Auerbach, R., et al., *A simple procedure for the long-term cultivation of chicken embryos.* Developmental Biology, 1974. **41**(2): p. 391-394.

95. Andrade, S.P. and M.A.N. Diniz Ferreira, *The sponge implant model of angiogenesis.* Angiogenesis Protocols: Second Edition, 2009: p. 295-304.

96. Egginton, S., *In Vivo Models of Muscle Angiogenesis.* Angiogenesis Protocols, 2016: p. 355-373.

97. Ristori, E., S. Donnini, and M. Ziche, *Studying Vascular Angiogenesis and Senescence in Zebrafish Embryos.* Angiogenesis Protocols, 2016: p. 387-400.

98. Rubinstein, A.L., *Zebrafish: from disease modeling to drug discovery.* Current Opinion in Drug Discovery and Development, 2003. **6**(2): p. 218-223.

99. Nguyen, M., Y. Shing, and J. Folkman, *Quantitation of Angiogenesis and Antiangiogenesis in the Chick Embryo Chorioallantoic Membrane.* Microvascular Research, 1994. **47**(1): p. 31-40.

100. Grindlay, J.H. and J.M. Waugh, *Plastic sponge which acts as a framework for living tissue: experimental studies and preliminary report of use to reinforce abdominal aneurysms.* AMA archives of surgery, 1951. **63**(3): p. 288-297.

101. Edwards, R., S. Sarmenta, and G. Hass, *Stimulation of granulation tissue growth by tissue extracts. Study in intramuscular wounds in rabbits.* Archives of pathology, 1960. **69**: p. 286.

102. Woessner, J.F. and R.J. Boucek, *Enzyme activities of rat connective tissue obtained from subcutaneously implanted polyvinyl sponge.* J Biol Chem, 1959. **234**: p. 3296-3300.

103. Linderman, J.R., M.R. Kloehn, and A.S. Greene, *Development of an implantable muscle stimulator: measurement of stimulated angiogenesis and poststimulus vessel regression.* Microcirculation, 2000. **7**(2): p. 119-128.

104. Folkman, J. and C. Haudenschild, *Angiogenesis in vitro.* 1980.

105. Edmondson, R., et al., *Three-Dimensional Cell Culture Systems and Their Applications in Drug Discovery and Cell-Based Biosensors.* Assay and Drug Development Technologies, 2014. **12**(4): p. 207-218.

106. Nehls, V. and D. Drenckhahn, *A novel, microcarrier-based in vitro assay for rapid and reliable quantification of three-dimensional cell migration and angiogenesis.* Microvascular research, 1995. **50**(3): p. 311-322.

107. Griffith, C.K., et al., *Diffusion limits of an in vitro thick prevascularized tissue.* Tissue engineering, 2005. **11**(1-2): p. 257-266.

108. Ghajar, C.M., et al., *The effect of matrix density on the regulation of 3-D capillary morphogenesis.* Biophys J, 2008. **94**(5): p. 1930-41.

109. Nakatsu, M.N. and C.C. Hughes, *An optimized three-dimensional in vitro model for the analysis of angiogenesis.* Methods in enzymology, 2008. **443**: p. 65-82.

110. Tattersall, I.W., et al., *In vitro modeling of endothelial interaction with macrophages and pericytes demonstrates Notch signaling function in the vascular microenvironment.* Angiogenesis, 2016. **19**(2): p. 201-215.

111. Seano, G. and L. Primo, *Human Arterial Ring Angiogenesis Assay.* Angiogenesis Protocols, 2016: p. 191-203.

112. Zippel, N., Y. Ding, and I. Fleming, *A Modified Aortic Ring Assay to Assess Angiogenic Potential In Vitro.* Angiogenesis Protocols, 2016: p. 205-219.

113. Rowe, S.L. and J.P. Stegemann, *Microstructure and Mechanics of Collagen-Fibrin Matrices Polymerized Using Ancrod Snake Venom Enzyme.* Journal of biomechanical engineering, 2009. **131**(6): p. 061012-061012.

114. Montesano, R. and L. Orci, *Tumor-promoting phorbol esters induce angiogenesis in vitro.* Cell, 1985. **42**(2): p. 469-477.

115. Schor, A.M., S.L. Schor, and T.D. Allen, *Effects of culture conditions on the proliferation, morphology and migration of bovine aortic endothelial cells.* Journal of cell science, 1983. **62**(1): p. 267-285.

116. Vernon, R.B. and E.H. Sage, *A novel, quantitative model for study of endothelial cell migration and sprout formation within three-dimensional collagen matrices.* Microvascular research, 1999. **57**(2): p. 118-133.

117. Korff, T. and H.G. Augustin, *Tensional forces in fibrillar extracellular matrices control directional capillary sprouting.* J Cell Sci, 1999. **112**(19): p. 3249-3258.

118. Montesano, R., L. Orci, and P. Vassalli, *In vitro rapid organization of endothelial cells into capillary-like networks is promoted by collagen matrices.* The Journal of cell biology, 1983. **97**(5): p. 1648-1652.

119. Montesano, R., et al., *Phorbol ester induces cultured endothelial cells to invade a fibrin matrix in the presence of fibrinolytic inhibitors.* Journal of cellular physiology, 1987. **132**(3): p. 509-516.

120. Doetschman, T.C., et al., *The in vitro development of blastocyst-derived embryonic stem cell lines: formation of visceral yolk sac, blood islands and myocardium.* Development, 1985. **87**(1): p. 27-45.

121. Vittet, D., et al., *Embryonic stem cells differentiate in vitro to endothelial cells through successive maturation steps.* Blood, 1996. **88**(9): p. 3424-3431.

122. Ziebart, T., et al., *Bisphosphonates: restrictions for vasculogenesis and angiogenesis: inhibition of cell function of endothelial progenitor cells and mature endothelial cells in vitro.* Clinical oral investigations, 2011. **15**(1): p. 105-111.

123. Tiruvannamalai Annamalai, R., et al., *Vascular Network Formation by Human Microvascular Endothelial Cells in Modular Fibrin Microtissues.* ACS Biomaterials Science & Engineering, 2016. **2**(11): p. 1914-1925.

124. Chen, Z., et al., *In vitro angiogenesis by human umbilical vein endothelial cells (HUVEC) induced by three-dimensional co-culture with glioblastoma cells.* Journal of neuro-oncology, 2009. **92**(2): p. 121-128.

125. Vailhé, B., D. Vittet, and J.-J. Feige, *In vitro models of vasculogenesis and angiogenesis.* Laboratory investigation, 2001. **81**(4): p. 439.

126. Rao, R.R., et al., *Matrix composition regulates three-dimensional network formation by endothelial cells and mesenchymal stem cells in collagen/fibrin materials.* Angiogenesis, 2012. **15**(2): p. 253-64.

127. Grainger, S.J., et al., *Stromal cell identity influences the in vivo functionality of engineered capillary networks formed by co-delivery of endothelial cells and stromal cells.* Tissue Eng Part A, 2013. **19**(9-10): p. 1209-22.

128. Carrion, B., et al., *Recreating the perivascular niche ex vivo using a microfluidic approach.* Biotechnol Bioeng, 2010. **107**(6): p. 1020-8.

129. Novosel, E.C., C. Kleinhans, and P.J. Kluger, *Vascularization is the key challenge in tissue engineering.* Adv Drug Deliv Rev, 2011. **63**(4-5): p. 300-11.

130. Jain, R.K., et al., *Engineering vascularized tissue.* Nat Biotechnol, 2005. **23**(7): p. 821-3.

131. Nichol, J.W. and A. Khademhosseini, *Modular tissue engineering: engineering biological tissues from the bottom up.* Soft matter, 2009. **5**(7): p. 1312-1319.

132. Leung, B.M. and M.V. Sefton, *A modular approach to cardiac tissue engineering.* Tissue Engineering Part A, 2010. **16**(10): p. 3207-3218.

133. Andersson, H. and A. Van Den Berg, *Microfabrication and microfluidics for tissue engineering: state of the art and future opportunities.* Lab on a Chip, 2004. **4**(2): p. 98-103.

CHAPTER 3

Engineering Modular Microtissues

3.1 Introduction

It is estimated that two million Americans suffer from critical limb ischemia (CLI) caused by peripheral arterial disease, chronic kidney disease, and severe diabetes [1-3]. CLI occurs when there is a poor supply of oxygenated blood to the lower extremities of the body due to artery blockage. CLI is a chronic condition and current treatments are aimed mainly at preventing progression of the disease or salvaging existing vasculature to provide partial flow to the affected limb. However, there is a need for more permanent and effective solutions that can create new vasculature to provide sufficient oxygen and nutrients to cells in the affected tissue, and thereby prevent tissue necrosis and amputation.

A variety of strategies have been investigated to improve tissue vascularization [4]. Delivery of vascular endothelial growth factor (VEGF) is a direct approach based on the known ability of this signaling molecule to stimulate endothelial cell recruitment and subsequent neovessel formation [5-7]. Other growth factors that facilitate and increase capillary formation include basic fibroblast growth factor (bFGF), hepatocyte growth factor (HGF), and transforming growth factor beta (TGF-β) [8-11] Gene delivery has also been used to upregulate production of pro-angiogenic factors [12, 13]. A challenge in applying gene and/or growth factor delivery is

determining the dosage needed to improve blood perfusion while preventing overproduction of leaky and disorganized vessels, which can occur at high dosages [5, 14, 15].

Attempts have also been made to re-vascularize ischemic tissue using transplanted cells in animal studies as well as in patients with progressed ischemic conditions [16, 17]. Although cell-based therapies have the potential to treat CLI, protocols for selection and delivery of these progenitor cells via injection into ischemic regions create challenges in terms of cell survival and engraftment. Patients are also less likely to respond to this treatment after a single dose, emphasizing the importance of optimizing the dose as well as the cell functionality being delivered to the patient [18].

Pre-vascularization of engineered tissues is a strategy that has been explored to allow more rapid engraftment after transplantation. *In vitro* pre-vascularization is typically achieved by designing and fabricating tissue constructs using appropriate extracellular matrix materials, cell types, and culture conditions to allow self-assembly of a microvascular network [19-21], or via cell seeding of a pre-defined architecture [22]. *In vivo* pre-vascularization relies on implanting an engineered scaffold in a region close to an artery to allow vessel ingrowth and network formation within the implant. A major advantage of pre-vascularized tissue constructs is that the host vasculature can rapidly inosculate with the pre-formed vascular network of the construct [23-25], thereby accelerating the wound healing and remodeling needed to restore tissue functionality [21, 26, 27]. However, a major limitation with current pre-vascularization strategies is the requirement for invasive surgery to implant the engineered tissue at the target site.

Fibrin is the primary structural component of blood clots and plays an important role in the provisional matrix that is remodeled during wound healing [28]. Type I collagen is a well characterized structural protein and an important component of the extracellular matrix of many

tissues [29]. Each of these materials has been used separately as 3D matrices for vascularization because of their demonstrated ability to support the formation of endothelial networks [30-34]. These natural matrices provide cell-adhesion sites and can be enzymatically remodeled by cells. However, combinations have also been used to support vascularization, in part to harness their composite mechanical and biochemical functionalities [31, 35, 36].

Elongation and vascular network formation by endothelial cells embedded in fibrin, collagen, and COL-FIB composite materials has been shown to be influenced by the properties of the matrix [31, 36, 37], and by the presence of stromal cells. Mesenchymal stem cells (MSCs), smooth muscle cells, and fibroblasts are stromal cells that interact with endothelial cells and contribute to the formation, remodeling, and stabilization of blood vessels in part by providing paracrine cues [38-43].

In the present study, we developed and characterized modular protein microbeads designed as a minimally invasive, cell-based therapy for re-vascularization of ischemic tissue. Human endothelial cells and fibroblasts were embedded in pure fibrin and collagen-fibrin microbeads using a simple water-in-oil emulsification process. We examined how cell concentration and matrix composition influenced cell incorporation into microbeads, and characterized cell viability and proliferation in the matrix. Selected microbeads were subsequently embedded into surrounding fibrin hydrogels to study vascular network formation. The morphology and extent of endothelial sprout formation inside and outside microbeads was quantitatively assessed over time in culture. In addition, anastomosis of vessel segments from neighboring microbeads was characterized. The overall goal of this work was to combine cell-based approaches to vasculogenesis with pre-vascularization strategies to produce a potential therapy for the rapid and efficient restoration of blood flow to regions of tissue ischemia.

3.2 Materials and Methods

3.2.1 Cell Culture

Umbilical cords were obtained from the University of Michigan Mott Children's Hospital via an IRB-exempt protocol and human umbilical vein endothelial cells (HUVECs) were isolated via methods similar to those previously described [30]. In brief, the umbilical cord was washed in phosphate buffer saline (PBS) and digested in collagenase type I solution (195 U/mL, Worthington Biochemical, Lakewood, NJ) at 37 °C for 20 min. The digested tissue was washed in PBS and subsequently centrifuged (200xg for 5 min). HUVECs were plated in tissue culture flasks and supplied with endothelial growth media (EGM-2, Lonza). After 24 hours, HUVECs were rinsed with PBS thrice to remove non-adherent cells and supplied with fresh media that was changed every 48 hours. Cells from passages 3 and 4 were utilized for experiments. Normal human lung fibroblasts (NHLFs, Lonza Inc., Walkersville, MD) were cultured in Media 199 (M199, Life Technologies, Grand Island, NY) with 10% fetal bovine serum (FBS), and 1% penicillin/streptomycin (Life Tech). Culture media was replaced every 48 hours and cells from passages 7-12 were used in experiments.

3.2.2 Microbead Fabrication

The process used to create protein microbeads is shown schematically in Figure 3-1. Two matrix formulations were used: 100% fibrin (FIB) and 40/60 wt% collagen/fibrin (COL-FIB). Collagen stock solution (4.0 mg/mL) was made under sterile conditions by dissolving lyophilized type I bovine collagen (MP Biomedicals, Solon, OH) in 0.02 N acetic acid. Fibrinogen stock solution (4.0 mg/mL clottable protein) was made by dissolving bovine fibrinogen (Sigma Aldrich,

St. Louis MO) in serum-free endothelial growth medium (SFEGM-2) at 37 °C. The solution was then filter sterilized after completely dissolving the protein. Equal numbers of HUVECs and NHLFs were suspended in FIB or COL-FIB composite hydrogel solutions at specific cell concentrations (Low: $5x10^5$ cells/mL, High: $2x10^6$ cells/mL). To make 1.0 mL of cellular FIB hydrogel solution, the following components were added to the cell pellet and mixed thoroughly: 255 µL SFEGM-2, 100 µL of FBS (10% final), 20 µL of 50 U/mL thrombin (1 U/mL final), and 625 µL fibrinogen stock solution (2.5 mg/mL final). To make 1.0 mL of cellular COL-FIB composite hydrogel solution, the following components were added to the cell pellet and mixed thoroughly: 93 µL SFEGM-2, 100 µL FBS (10% final), 100 µL of 5X Dulbecco's Modified Eagle Medium (DMEM (10% Final), 12 µL of 87.5 mM glyoxal (1 mM Final, Sigma) for crosslinking collagen, 50 µL of 0.1 N NaOH to neutralize acidic collagen, 20 µL of 50 U/mL thrombin (1 U/mL final), 250 µL collagen stock solution (1.25 mg/mL final), and 375 µL fibrinogen stock solution (1.5 mg/mL final).

To create protein microbeads, 3.0 mL of matrix/cell suspension was quickly added to a stirred bath (600 rpm) containing 75 mL of 100 cSt polydimethylsiloxane (PDMS, Dow Corning) cooled in an ice bath. Emulsification proceeded for 5 min, and the temperature of the PDMS bath was then increased to 37 °C to induce gelling for an additional 25 min. The mixture of PDMS and formed microbeads was then transferred to 50 mL centrifuge tubes and 5 mL of PBS containing 0.1% L101 surfactant (PBS-L101; BASF, Florham Park, NJ) was added to each tube and mixed gently by inverting for 5 min. The mixture was then centrifuged at 200xg for 5 min. The PDMS layer was carefully removed and then pelleted microbeads were washed again using PBS-L101. Once the microbeads were thoroughly washed, they were supplied with an appropriate amount of culture medium (EGM-2) and used for further experiments.

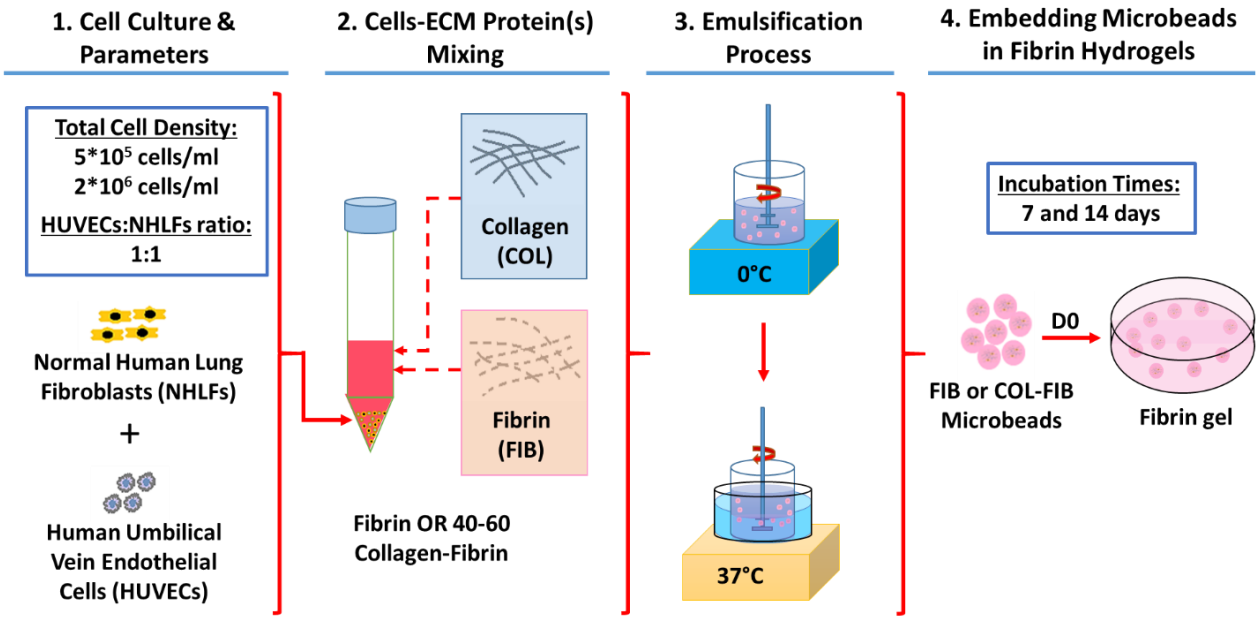

Figure 3-1: Microbead fabrication process. HUVECs and NHLFs were incorporated in a 1:1 ratio at an initial cell density of $5*10^5$ cells/mL or $2*10^6$ cells/mL in either pure fibrin or collagen-fibrin (40-60) microbeads via an oil-and-water emulsification process. Resultant microbeads were subsequently embedded in fibrin hydrogels, cultured for 7 or 14 days, and then analyzed.

3.2.3 Characterization of Cell Incorporation and Microbead Morphology

The number of cells incorporated within microbeads was determined by staining with 4′,6-diamidino-2-phenylindole (DAPI, Life Technologies). The FIB and COL-FIB samples were collected and fixed with zinc-buffered formalin solution (Z-fix, Anatech, Battle Creek, MI) for 5 min. Fixed samples were washed in PBS and stained with 10 nM DAPI solution for 10 min. Bright field and fluorescent images were taken using an optical microscope (Olympus IX81, Olympus, Center Valley, PA). The number of cells per microbead and microbead diameters were determined from these images using ImageJ (National Institutes of Health, Bethesda, MD).

At least 100 randomly selected microbeads per condition and per experiment were used for image analysis to determine microbead diameter, cell distribution, and number of cells incorporated into the microbeads.

3.2.4 Cell Viability and Proliferation Assays

The viability of cells encapsulated in microbeads and in bulk gels was determined using the Live/Dead® staining kit (Life Technologies). Bulk gel samples with the same protein and cell concentration as the microbeads were also prepared by allowing the hydrogel/cell mixture to gel in 24-well plates (500 µL per well) at room temperature for 5 minutes, followed by an additional 20 to 25 min at 37 °C in an incubator. Samples were collected, washed in 10 mM PBS and re-suspended in PBS containing 1 µM calcein-AM and 2 µM ethidium homodimer for 45 min at 37 °C. Samples were then imaged using a fluorescence microscope.

Both cell seeded COL-FIB and FIB microbeads were embedded in fibrin gels after their fabrication process. To embed microbeads in gels, one tenth of a 3 mL microbead preparation was collected and pelleted to make three fibrin hydrogels with microbeads per time point (~500 µL per hydrogel). These hydrogels were made by adding the following components to the microbead pellet and mixing thoroughly: 382.5 µL SFEGM-2, 150 µL of FBS (10% final), 30 µL of 50 U/mL thrombin (1 U/mL final), and 937.5 µL fibrinogen stock solution (2.5 mg/mL final). Hydrogels were molded into standard 24-well culture plates, and were left at room temperature for 5 min before being placed in an incubator for 25 minutes at 37 °C. One milliliter of EGM-2 was added to each hydrogel containing the cellular microbeads. Culture medium was replaced the next day and then on every second day for the duration of the culture period.

Cell proliferation was determined by quantifying total DNA in samples collected at specific time intervals. To isolate the total DNA from the samples, fibrin gels containing microbeads were digested in 10 mM Tris-HCL/0.4 M Guanidine hydrochloride solution for 3 hours. The digested samples were then centrifuged at 10,000 × g for 10 min and the supernatant containing the DNA was aspirated, and then diluted with water to reduce Guanidine-HCL interference with the DNA

assay. DNA content was determined using the PicoGreen® DNA assay kit (Invitrogen). Calf thymus DNA standards were used to generate standard curves.

3.2.5 Imaging and Analysis of Endothelial Sprouts

To distinguish the microbeads from the 3D fibrin environment in which they were embedded, FIB and COL-FIB microbeads fabricated as described above were subsequently coated with a FITC-fibrinogen layer by incubating them in FITC-fibrinogen (9 μg/mL, Life Technologies) in EGM-2 at 37 °C for 25 min prior to embedding within the larger hydrogel. The same embedding process utilized for the proliferation assay (Section 3.2.4) was employed to incorporate the cellular microbeads within acellular fibrin hydrogels. To visualize vascular sprouts, the endothelial cell-specific marker Ulex Europaeus Agglutinin I (UEA-I, Vector Laboratories, Burlingame, CA) was used. In brief, samples were collected at specified time intervals, washed twice in PBS, and fixed in zinc-buffered formalin (Z-fix, Anatech) at room temperature. Fixed samples were then washed and incubated in staining solution containing 1% BSA, 20 μg/mL rhodamine-labeled UEA-I, and 10 nM DAPI in PBS for 45 min at room temperature. Before imaging, samples were rinsed twice with PBS for 5 min to remove unbound residual stains.

Endothelial sprouts were characterized by measuring average sprout lengths, numbers of segments (branching), branch points, and lengths of each segment both inside and outside the microbeads through image analysis using a protocol similar to previous studies [30, 37, 44]. Inosculation of adjacent sprouts protruding from adjacent microbeads was assessed qualitatively. Fluorescence images were acquired using an optical microscope and randomly selected microbeads were used for quantification using ImageJ. All image analysis was performed using a

blinded image evaluation method in which random images were provided to the evaluator with no information about the experimental conditions.

3.2.6 Statistical Analysis

Statistical analyses were performed using STATISTICA (StatSoft. Inc, Tulsa, OK) software. At least 3 independent experiments were performed for each assay and data are reported as mean ± standard error of the mean (SEM). One-way ANOVA followed by unequal N post-test was used to compare multiple conditions. Values of $p \leq 0.05$ were considered statistically significant.

3.3 Results

3.3.1 Cell Encapsulation and Retention in Microbeads

HUVECs and NHLFs were encapsulated at a 1:1 ratio in FIB and COL-FIB microbeads, at either low cell concentration (LC: $5.0x10^5$ cells/mL) or high concentration (HC: $2.0x10^6$ cells/mL). At the same starting concentration, larger microbeads contained greater total numbers of cells, as expected (Fig. 3-2A). The average microbead diameter was approximately 140 µm for both FIB formulations and the low cell concentration COL-FIB formulation; however, the high cell concentration COL-FIB microbeads were significantly larger (approximately 200 µm in diameter, Fig. 3-2B, $p<0.05$). The distribution in the number of cells per microbead of the treatment populations was broader for the high cell concentration conditions, in contrast to microbeads containing the low cell concentration, which exhibited a sharper peak and a more homogeneous distribution (Fig. 3-2C). Overall cell incorporation increased as higher cell

concentrations were used with the same material formulation (Fig. 3-2D, $p<0.05$). Microbeads with high cell concentration contained an average of 30-35 cells per microbead, while those with low cell concentration contained 5-10 cells per microbead. There was no statistical difference in the total number of cells incorporated between COL-FIB and pure FIB microbeads, when comparing at either the low concentration or high cell concentration conditions.

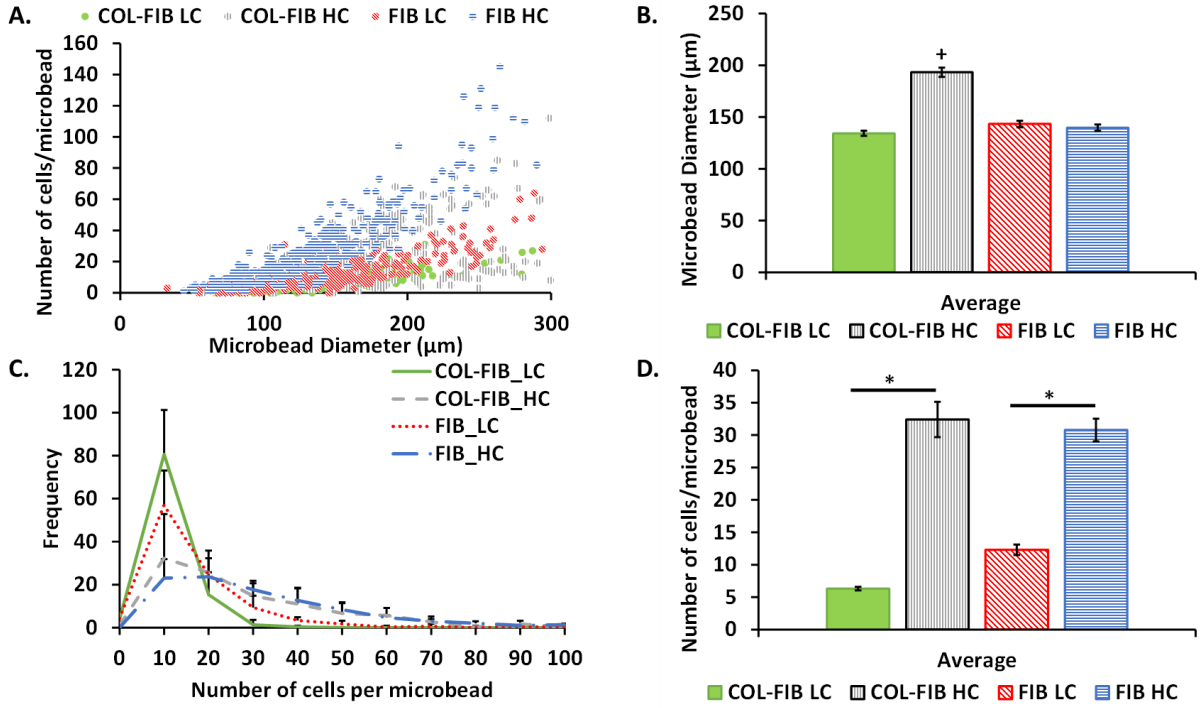

Figure 3-2: Microbead characterization. (A) The number of cells per microbead was quantified as a function of microbead diameter. Average microbead diameters (B), cell number distributions (C), and average number of cells (D) within COL-FIB and FIB microbeads at low (LC) and high (HC) cell densities were quantified. Statistical differences ($p<0.05$) between conditions are denoted by *, while differences between one group and the remaining groups are denoted by ***. (n=3, at least 100 microbeads per n).

3.3.2 Viability and Proliferation of Cells Encapsulated in Microbeads

The viability of cells encapsulated in FIB and COL-FIB microbeads in the high cell concentration ($2.0x10^6$ cells/mL) was quantified and compared to values from bulk macroscopic hydrogels (Fig. 3-3). Representative live (green)/dead (red) images of COL-FIB microbeads (Fig.

3-3A), FIB microbeads (Fig. 3-3B), COL-FIB bulk hydrogels (Fig. 3-3C), and FIB bulk hydrogels (Fig. 3-3D) show uniform cell distributions in both the microbeads and the hydrogels, with no spatial variations in viability evident.

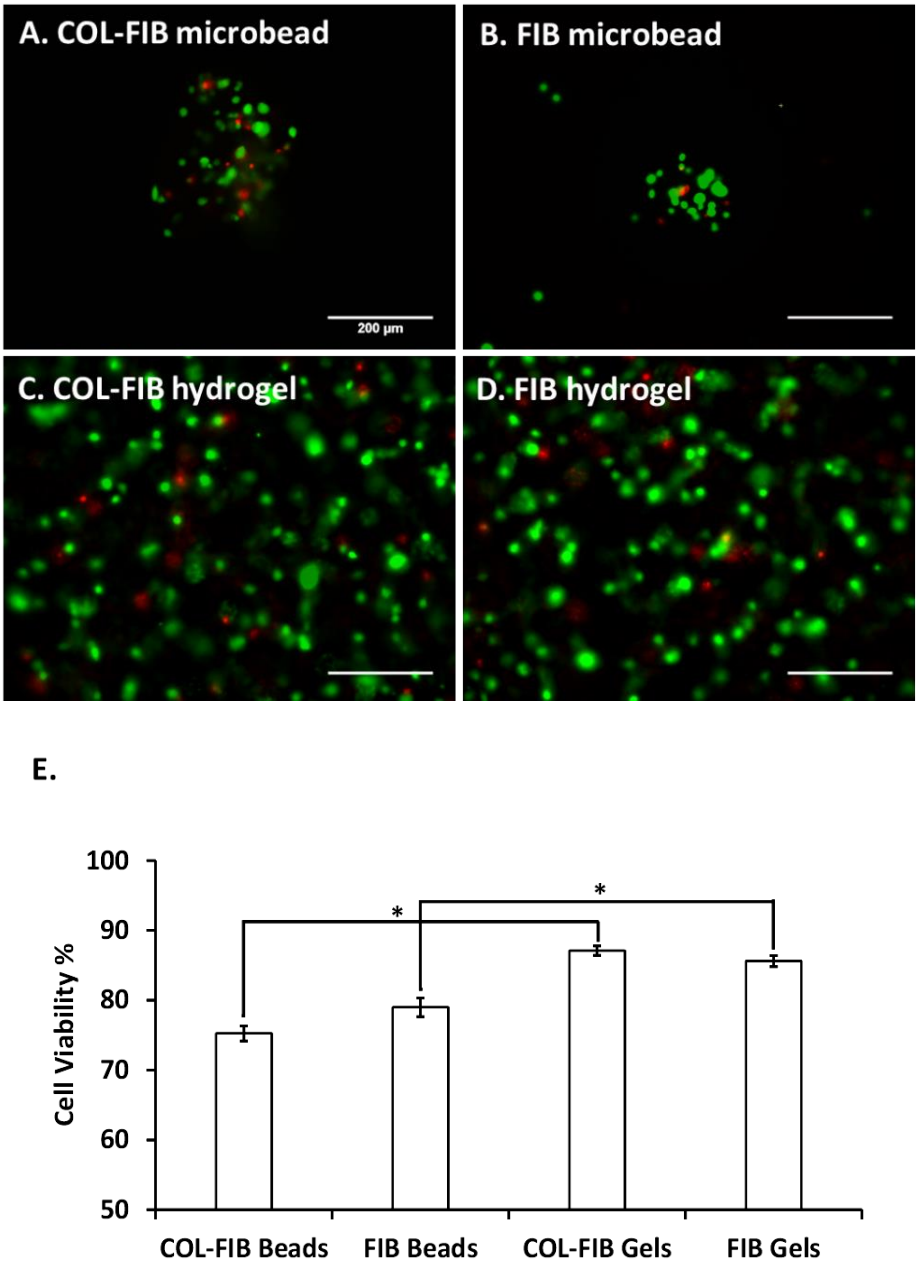

Figure 3-3: Cell viability in microbeads. Representative live (green)/dead (red) images of cells (HUVECs:NHLFs co-cultures) incorporated in (A) COL:FIB microbeads, (B) FIB microbeads, (C) COL-FIB, and (D) FIB hydrogels after their respective fabrication process. (E) Images were quantified to compare the viabilities of cells in microbeads and hydrogels. Statistical differences between conditions are denoted by * ($p<0.05$). (n=3). Scale bar = 200 µm.

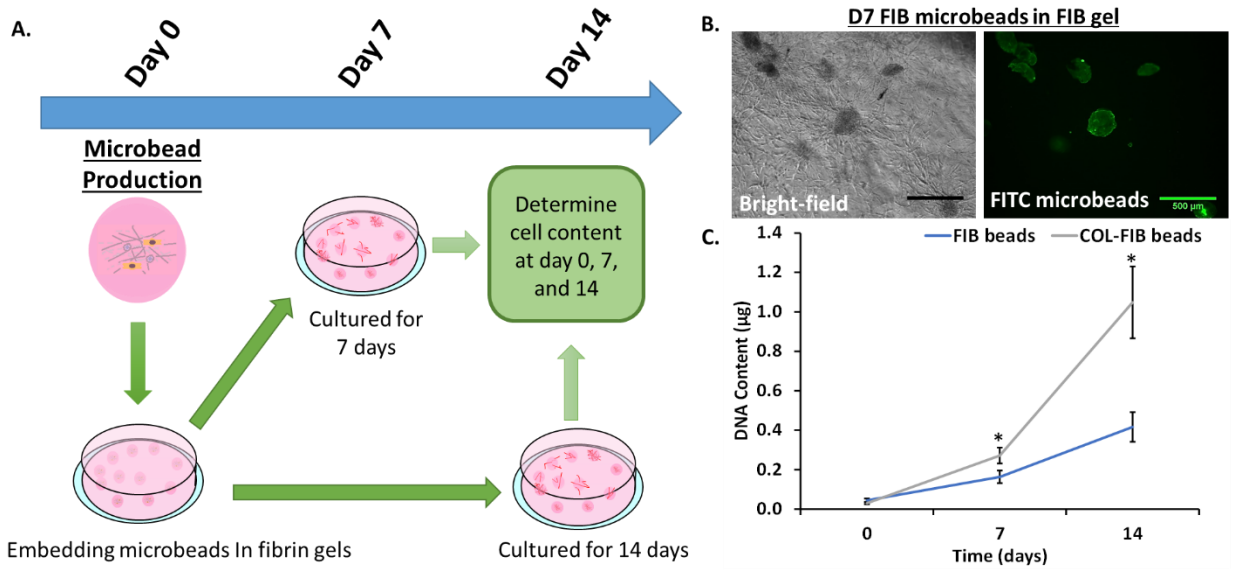

Figure 3-4: Cell proliferation in microbeads. (A) Schematic depicting experimental procedure for cell proliferation studies in which either COL-FIB or FIB microbeads were embedded in FIB hydrogels and cultured for 7 and 14 days. (B) Representative bright-field and fluorescence images of FIB microbeads (green in the fluorescent image) embedded at day 0 and cultured for 7 days. (Microbeads were fabricated with FITC-fibrinogen to illustrate the location of the microbeads within the fibrin matrix in this image. However, non-fluorescent fibrinogen was employed in the actual proliferation studies.) (C) DNA content of cells embedded within COL-FIB or FIB microbeads was quantified after 1 and 2 weeks in culture. Statistical differences between microbead types at both day 7 and day 14 are denoted by * ($p<0.05$, $n\geq3$). Scale bar = 500 µm.

Cell viabilities in both COL-FIB and FIB microbeads were high (75% and 79% viable cells, respectively), with no statistically significant differences between the formulations. However, cell viability was significantly lower in the microbeads compared to their bulk hydrogel counterparts, which exhibited 87% and 85% viable cells, respectively (Fig. 3-3E).

COL-FIB and FIB microbeads made at the high cell concentration ($2.0x10^6$ cells/mL) were embedded in surrounding 2.5 mg/mL fibrin hydrogels to examine cell proliferation and endothelial sprout formation. Figure 3-4A shows a schematic of the protocol used for cell proliferation studies. Microbeads were visualized inside the larger fibrin matrix using bright-field and fluorescent microscopy (Fig. 3-4B). In these images, FIB microbeads were embedded in a FIB hydrogel immediately after fabrication and were cultured for 7 days before imaging. In the fluorescence

image, microbeads were tagged with FITC to distinguish the microbead matrix from the surrounding fibrin. At day 0, both microbead formulations showed equal DNA content, which then increased over time in culture as cells proliferated. At day 7, there was a significant difference ($p<0.05$) in the DNA content between FIB and COL-FIB microbeads. By day 14, the DNA content was 2.5-fold higher ($p<0.05$) in COL-FIB microbeads than in corresponding FIB microbeads, indicating a significantly higher number of cells within these beads (Fig. 3-4C).

3.3.3 Endothelial Sprouting from Microbeads Embedded in Fibrin Matrix

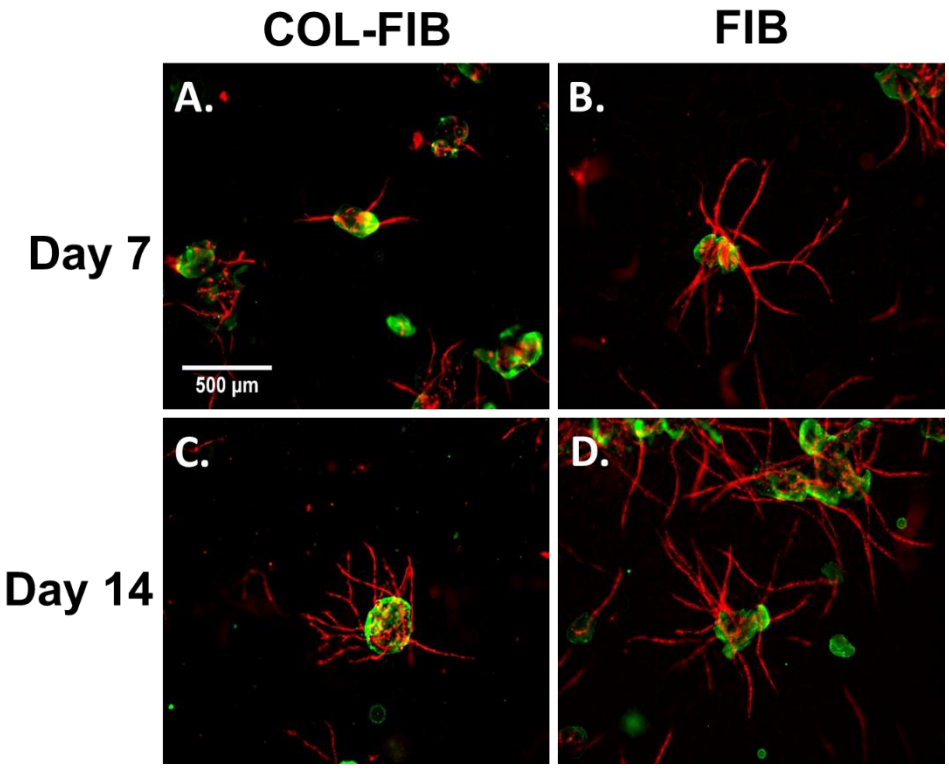

Figure 3-5: Endothelial sprouting within and from microbeads. Representative images of HUVECs (red) and microbeads (green) in either COL-FIB (A, C) or FIB microbeads (B, D) embedded immediately after processing, and cultured for an additional 7 and 14 days within FIB constructs. Sprouts originate from within the beads and invade the surrounding matrix. Scale bar = 500 µm.

COL-FIB microbeads made with the lower cell concentration did not support endothelial sprouting when embedded in fibrin hydrogels (data not shown), while those made with the higher cell concentration retained the capacity for sprout formation when embedded in fibrin hydrogels. Therefore, the vasculogenic capacity of COL-FIB and FIB microbeads were compared only at the higher initial cell concentration. COL-FIB and FIB microbeads containing HUVECs and NHLFs were embedded in fibrin hydrogels and cultured for 7 and 14 days (representative images shown in Fig. 3-5). The microbead matrix was tagged with FITC (green) and the endothelial cells were identified by UEA-1 staining (red). In both microbead formulations, endothelial sprouts initially formed inside the microbead matrix and then invaded into the surrounding fibrin hydrogel.

The extent of sprouting both within the microbeads and in the surrounding matrix were characterized in terms of the number of segments (Fig. 3-6A), the average segment length (Fig. 3-6B), the number of branch points (Fig. 3-6C), and the total sprout length (Fig. 3-6D) (see also Tables 3-1 and 3-2). Microbeads contained an average of 4 to 5 vessel segments by the end of 7 days in culture, with no further change in the number of segments within the microbeads by day 14 (Fig. 3-6A, "inside microbead"). The number of segments that extended from the FIB microbeads was significantly higher compared to COL-FIB microbeads at both time points. A higher number of segments protruding the COL-FIB microbeads was found with an additional week of culture (Fig. 3-6A, "outside microbead"). By day 14, the total number of vessel segments per microbead was 10-14, and this measure was significantly higher in FIB microbeads than in COL-FIB microbeads at both day 7 and day 14 of culture (Fig. 3-6A, "total per microbead").

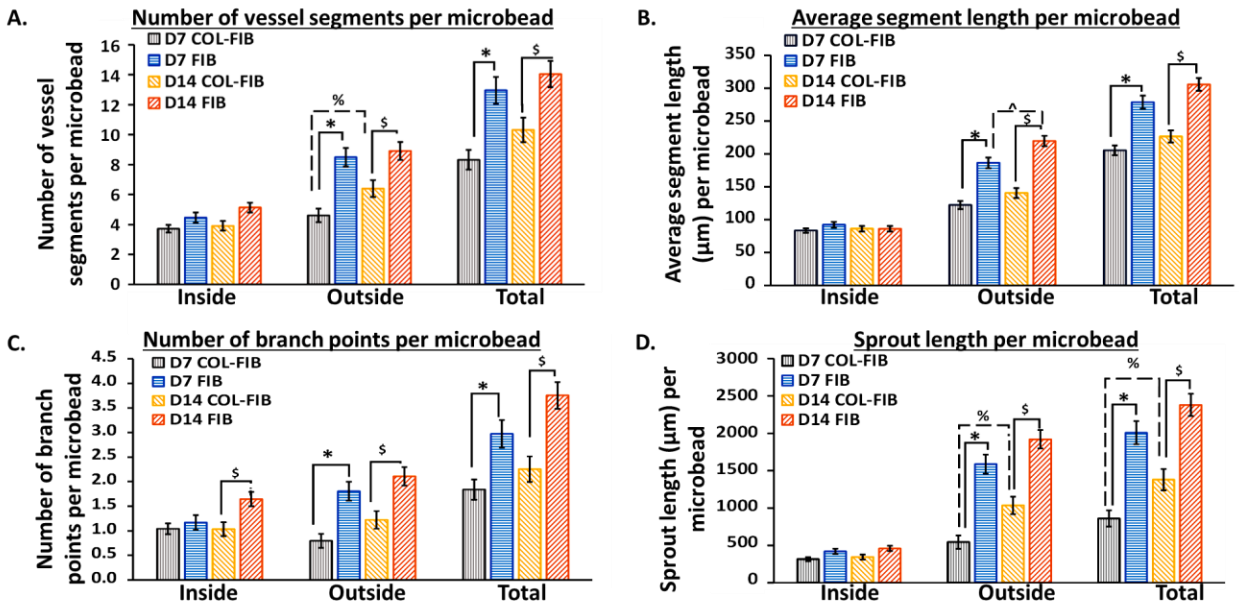

Figure 3-6: Quantification of endothelial sprout lengths and branching. (A) The numbers of vessel segments, (B) average segment lengths, (C) numbers of branch points, and (D) sprout lengths for the nascent microvessel-like networks originating from COL-FIB and FIB microbeads embedded in fibrin gels at day 0, and cultured for an additional 7 and 14 days. Statistical differences ($p<0.05$) are denoted by the following symbols: * for the differences between microbeads at D7, $ for the differences between microbeads at D14, ^ for differences across culture time (D7 vs. D14) for microbeads of the same composition, and # for differences in culture time and microbead composition ($n\geq3$).

Table 3-1: Endothelial sprouting measurements inside microbeads

	Inside the microbeads					
	COL-FIB		**FIB**		**Statistical Significance between FIB and COL-FIB**	
	Day 7	**Day 14**	**Day 7**	**Day 14**	**Day 7**	**Day 14**
No. of segments	3.7 ± 0.3 SEM	3.9 ± 0.3 SEM	4.5 ± 0.3 SEM	5.1 ± 0.3 SEM	p>0.05 NS	p>0.05 NS
No. of branch points	1.0 ± 0.1 SEM	1.0 ± 0.1 SEM	1.2 ± 0.2 SEM	1.6 ± 0.1 SEM	p>0.05 NS	**p<0.05**
Avg. Segment Length (µm)	87 ± 3 SEM	87 ± 4 SEM	93 ± 4 SEM	87 ± 4 SEM	p>0.05 NS	p>0.05 NS
Sprout Length (µm)	315 ± 25 SEM	344 ± 33 SEM	420 ± 36 SEM	459 ± 35 SEM	p>0.05 NS	p>0.05 NS

The average vessel segment length inside microbeads was approximately 90 µm, with no significant differences across matrix formulations or time points (Fig. 3-6B, "inside microbead"). Outside the microbeads, longer segments were produced by FIB microbeads than COL-FIB microbeads ($p<0.05$), and segment length increased significantly outside FIB microbeads between 7 and 14 days (Fig. 3-6B, $p<0.05$). Both COL-FIB and FIB microbeads on average contained at least one branch point, and the number of branch points was significantly higher in FIB microbeads at day 14 (Fig. 3-6C, $p<0.05$), compared to the other formulation and time point. The number of branch points outside the microbeads and the total number of branch points were also significantly higher in FIB microbeads compared to COL-FIB at both time points (Fig. 3-6C, $p<0.05$).

Table 3-2: Endothelial sprouting measurements protruding from the microbeads into the surrounding fibrin matrix

	Outside the microbeads					
	COL-FIB		**FIB**		**Statistical Significance between FIB and COL-FIB**	
	Day 7	**Day 14**	**Day 7**	**Day 14**	**Day 7**	**Day 14**
No. of segments	4.6 ± 0.5 SEM	6.4 ± 0.6 SEM	8.5 ± 0.6 SEM	8.9 ± 0.6 SEM	**p<0.05**	**p<0.05**
No. of branch points	0.8 ± 0.1 SEM	1.2 ± 0.2 SEM	1.8 ± 0.2 SEM	2.1 ± 0.2 SEM	**p<0.05**	**p<0.05**
Avg. Segment Length (µm)	131 ± 6 SEM	142 ± 8 SEM	189 ± 8 SEM	222 ± 8 SEM	**p<0.05**	**p<0.05**
Sprout Length (µm)	544 ± 90 SEM	1035 ± 117 SEM	1588 ± 127 SEM	1920 ± 123 SEM	**p<0.05**	**p<0.05**

The combination of vessel network characteristics described also resulted in differences in the total sprout network length (Fig. 3-6D). The average total sprout length inside microbeads was 315-460 µm, and there were no statistically significant differences between matrix formulations

or time points. However, the vessel networks that penetrated into the surrounding fibrin hydrogel were significantly longer when emerging from FIB microbeads compared to COL-FIB microbeads at both day 7 and 14 (Fig. 3-6D, "outside microbeads", $p<0.05$). Total sprout length increased significantly in COL-FIB microbeads over time, but was lower than in FIB microbeads at all time points (Fig. 3-6D, "total per microbead", $p<0.05$). By day 14, the microvascular network produced by HUVECs and NHLFs encapsulated within FIB microbeads approached 2500 µm in total length. See Table 3-1, and 3-2 for numerical values graphed in Figure 3.6.

3.3.4 Inosculation Between Endothelial Sprouts from Adjacent Microbeads

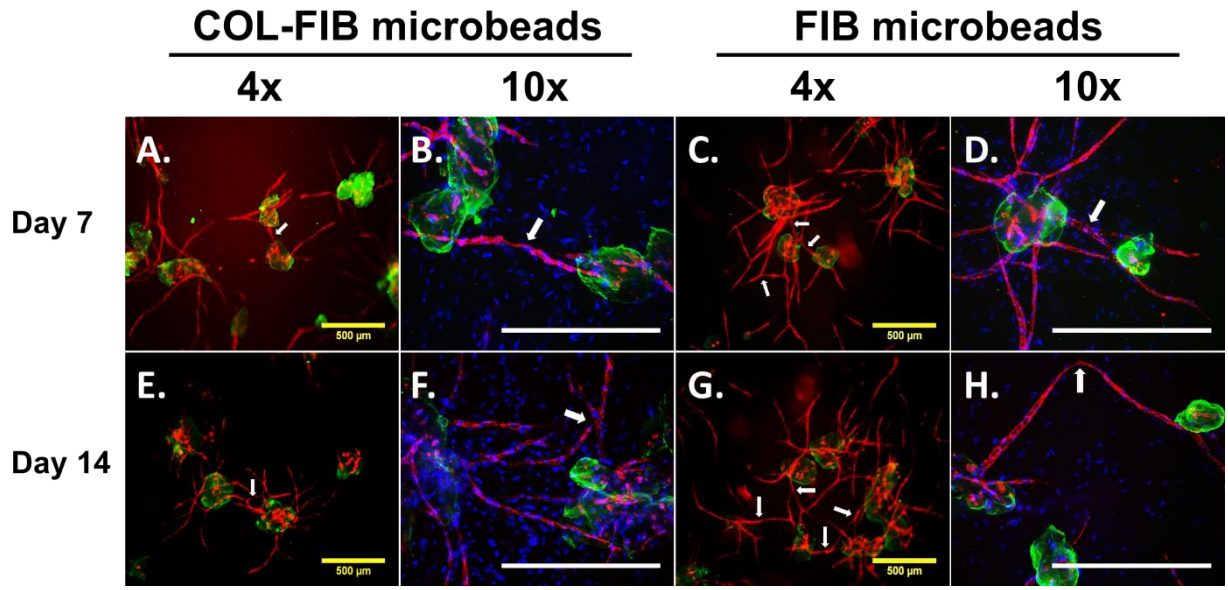

Figure 3-7: Formation of anastomoses between sprouts to form larger microvascular networks. Connections (white arrows) formed via inosculation of endothelial sprouts from adjacent COL-FIB (A, B, E, F) or FIB (C, D, G, H) microbeads embedded in FIB hydrogels immediately post fabrication, and cultured for 7 days (A-D) and 14 days (E-H). Images are 4x and 10x magnification. HUVECs are displayed in red, microbeads in green, and cell (both HUVECs and NHLFs) nuclei in blue. Scale bar = 500 µm.

COL-FIB and FIB microbeads embedded in fibrin hydrogels were cultured for 1 or 2 weeks. The microbead matrix was tagged green prior to the embedding process to distinguish them

from the surrounding fibrin matrix, while the HUVECs were stained in red (Fig. 3-7). Microbeads were generally separated from each other in the surrounding gel, though some clumping was observed. As described quantitatively in Figure 3-6, endothelial cell networks extended from the embedded microbeads by day 7 (Fig. 3-7 A-D), and were more prominent in the pure FIB samples. The arrows in Figure 3-7 show anastomoses between endothelial sprouts from adjacent microbeads. This phenomenon is evident in both microbead formulations at both day 7 and day 14 and at 4x and 10x magnification. The nuclei of both ECs and NHLFs were stained in blue (Fig. 3-7B, D, F, and H). It can be seen that NHLFs migrated out of the microbeads and into the surrounding matrix, and that endothelial sprouts extended and anastomosed between microbeads. By day 14, relatively long distances (1000-2000 μm) were traversed by joined endothelial sprouts (Fig. 3-7 E-H).

3.4 Discussion

Cells in most tissues in the body receive oxygen and nutrients via blood from capillaries that are spaced approximately 100-200 μm apart [24, 45, 46]. In larger engineered tissue constructs, oxygen and nutrients are consumed by cells that reside within this diffusion limit, while those cells that reside beyond the limit typically undergo apoptosis. Therefore, modular approaches are being explored to reduce diffusion limitations that occur in large engineered tissues [47-52]. One strategy has been to create very small "microtissues" with diffusion path lengths on the scale of 10-100 μm. These building blocks are designed to avoid mass transfer limitations, and in some cases can be delivered minimally invasively and assembled into larger tissue structures [53-60].

In the present study, a simple water-in-oil emulsification technique was used to fabricate protein microbeads with diameters in the range of 100-200 μm. Endothelial cells and fibroblasts

were fully embedded within the microbeads. These cell types have been used widely to initiate vasculogenesis and angiogenesis [37, 61], through a process in which fibroblast-derived factors provide signals to promote and stabilize network formation by the endothelial cells [42, 43]. Collagen and fibrin were used in microbeads as extracellular matrix proteins because of their demonstrated ability to support vascular network formation [35, 36, 62]. It has been shown that the composition of the matrix affects the process of neovessel formation [31, 36], and that fibrin is a particularly permissive environment for angiogenesis [20, 30, 32]. However, most studies have been performed in bulk hydrogel materials, and the properties and dynamics of the extracellular matrix in microtissues may be different from larger-scale models. Therefore, this study focused on determining a suitable cell and matrix composition to achieve sprout formation by endothelial cells within collagen-fibrin and pure fibrin microbeads.

The microbeads produced by the emulsification and collection process were generally spheroidal with a diameter of 100-200 μm, and therefore the maximum diffusion path length to a cell in the interior was approximately 100 μm. Cells were incorporated into the microbead matrix in general proportion to the starting cell concentration; however, cell loss did occur during processing. Microbeads fabricated with an initial concentration of $5.0x10^5$ cells/mL contained an average of only 5-10 cells, which was not supportive of the creation of vascular networks within the microbead volume. The low cell number meant that there were insufficient endothelial cells to connect and form networks, as well as reduced paracrine signaling from the relatively few supporting fibroblasts. Therefore, subsequent experiments on vessel network formation were performed using only microbeads fabricated at higher cell concentration. With a starting concentration of $2.0x10^6$ cells/mL of protein matrix, microbeads contained an average of 30-35

cells. Approximately half of these cells could be expected to be endothelial cells, which provided a number sufficient to initiate the formation of small vascular structures within the microbeads.

Cell viability in microbeads was lower than in bulk hydrogels of corresponding composition, but was still in the range of 75-80%. The decrease in cell viability was most likely due to the processing required to fabricate and collect the microbeads, which included multiple wash and centrifugation steps to separate the microbeads from the silicone oil. However, cells survived within microbeads over time in culture, as evidenced by their maintained ability to proliferate and change morphology in the matrix. Cells in both microbead types proliferated in culture, but over the 14-day period studied there was a significantly greater degree of cell proliferation in COL-FIB microbeads, as compared to pure FIB microbeads. Tracking of total DNA content did not allow discrimination of which cell types were proliferating. However endothelial network length was greater in FIB microbeads than in COL-FIB microbeads, suggesting that the increased DNA content in the latter formulation was predominantly the result of fibroblast proliferation.

Endothelial sprout formation and anastomosis between sprouts was examined by embedding microbeads in an acellular surrounding hydrogel consisting of pure fibrin. The surrounding matrix isolated the microbeads from each other and allowed the examination of endothelial network extension outside of the microbeads. Using this system, both COL-FIB and FIB materials supported endothelial network formation inside the microbead matrix, as well as their extension into the surrounding fibrin hydrogel. Over time, anastomosis of endothelial sprouts from adjacent microbeads was also observed in both microbead formulations. The extent of the internal networks was generally the same regardless of microbead composition, but the extension of sprouts into the surrounding matrix was significantly enhanced using pure FIB microbeads. The

networks in FIB microbeads also were more branched with longer inter-branch segments than their COL-FIB counterparts. The longer and more extensive networks produced by FIB microbeads may have a greater chance of creating inter-network connectivity.

Endothelial cell sprouting and migration have been shown to be dependent on matrix composition, stromal cell type, and serum concentration [43, 63, 64]. Since our studies used the same stromal cell type and serum concentration in both microbead formulations, the differences in sprouting in our study are mainly attributable to matrix composition. Previous studies have shown that collagen, fibrin, and their composites support endothelial network formation to different extents [62], and these effects have been correlated to matrix mechanical properties [31]. In addition, fibrin(ogen) (through its heparin-binding domain) binds to many growth factors that stimulate angiogenesis [65] and enhance wound healing [66, 67]. In contrast, the growth factor binding affinity of type I collagen is very low since no growth factor binding sites have been identified in this structural matrix protein [68]. Therefore, both compositional differences and the degree of local growth factor sequestration may explain the increased propensity of vessel networks to extend from pure fibrin microbeads.

3.5 Conclusion

These studies (Fig. 3-8) demonstrate that protein-based microbeads containing endothelial cells and fibroblasts can support the formation of vascular networks by sprouting from individual microbeads, and that adjacent networks can inosculate by anastomoses to produce larger structures. Pure fibrin microbeads triggered the formation of more branched and longer networks, compared to collagen-fibrin composite microbeads. The use of pure protein microbeads has the advantage that the matrix composition is simpler and more readily developed as a cell therapy.

Such microbeads may find utility as a method to deliver vascularizing modules to treat ischemic conditions, and may also be useful to study the processes of vasculogenesis and angiogenesis.

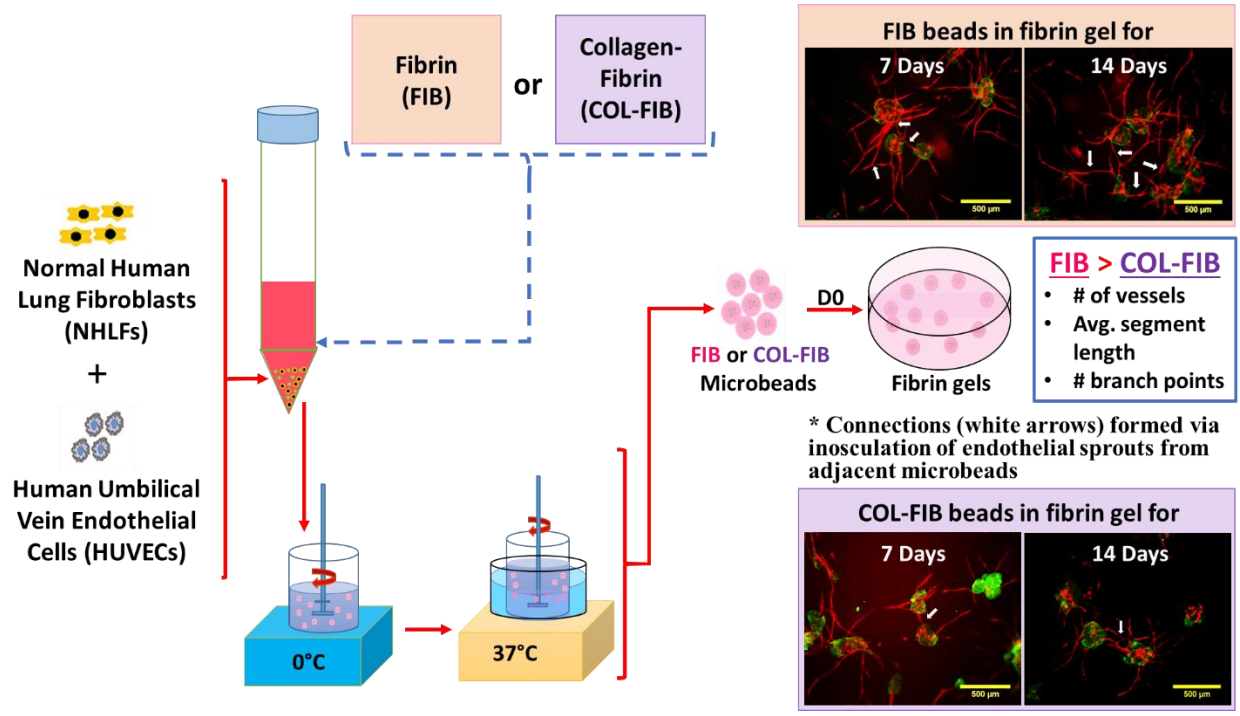

Figure 3-8: Chapter 3 graphical summary. Summary of study in graphical form; from fibrin and collagen-fibrin microbead fabrication to embedding of microbeads into fibrin gel for vessel length quantification.

3.6 References

1. Falluji N, Mukherjee D. Critical and acute limb ischemia: an overview. Angiology 2014;65:137-46.

2. Norgren L, Hiatt WR, Dormandy JA, Nehler MR, Harris KA, Fowkes FG, et al. Inter-Society Consensus for the Management of Peripheral Arterial Disease (TASC II). Journal of vascular surgery 2007;45 Suppl S:S5-67.

3. Golden MA, Ullery, B.W. Essentials of Vascular Surgery for the General Surgeon. New York: Springer New York; 2015.

4. Lovett M, Lee K, Edwards A, Kaplan DL. Vascularization strategies for tissue engineering. Tissue engineering Part B, Reviews 2009;15:353-70.

5. Yancopoulos GD, Davis S, Gale NW, Rudge JS, Wiegand SJ, Holash J. Vascular-specific growth factors and blood vessel formation. Nature 2000;407:242-8.
6. Sun QH, Silva EA, Wang AX, Fritton JC, Mooney DJ, Schaffler MB, et al. Sustained Release of Multiple Growth Factors from Injectable Polymeric System as a Novel Therapeutic Approach Towards Angiogenesis. Pharm Res-Dord 2010;27:264-71.

7. Kannan RY, Salacinski HJ, Sales K, Butler P, Seifalian AM. The roles of tissue engineering and vascularisation in the development of micro-vascular networks: a review. Biomaterials 2005;26:1857-75.

8. Nehls V, Drenckhahn D. A Novel, Microcarrier-Based in Vitro Assay for Rapid and Reliable Quantification of Three-Dimensional Cell Migration and Angiogenesis. Microvascular Research 1995;50:311-22.

9. Klagsbrun M, D'Amore PA. Regulators of angiogenesis. Annual review of physiology 1991;53:217-39.

10. Montesano R, Matsumoto K, Nakamura T, Orci L. Identification of a fibroblast-derived epithelial morphogen as hepatocyte growth factor. Cell 1991;67:901-8.

11. Morishita R, Aoki M, Hashiya N, Makino H, Yamasaki K, Azuma J, et al. Safety evaluation of clinical gene therapy using hepatocyte growth factor to treat peripheral arterial disease. Hypertension 2004;44:203-9.

12. Masaki I, Yonemitsu Y, Yamashita A, Sata S, Tanii M, Komori K, et al. Angiogenic gene therapy for experimental critical limb ischemia: acceleration of limb loss by overexpression of vascular endothelial growth factor 165 but not of fibroblast growth factor-2. Circulation research 2002;90:966-73.

13. Makino H, Aoki M, Hashiya N, Yamasaki K, Azuma J, Sawa Y, et al. Long-term follow-up evaluation of results from clinical trial using hepatocyte growth factor gene to treat severe peripheral arterial disease. Arteriosclerosis, thrombosis, and vascular biology 2012;32:2503-9.

14. Henry TD, Rocha-Singh K, Isner JM, Kereiakes DJ, Giordano FJ, Simons M, et al. Results of intracoronary recombinant human vascular endothelial growth factor (rhVEGF) administration trial. J Am Coll Cardiol 1998;31:65a-a.

15. Mikos AG, Herring SW, Ochareon P, Elisseeff J, Lu HH, Kandel R, et al. Engineering complex tissues. Tissue engineering 2006;12:3307-39.

16. Kalka C, Masuda H, Takahashi T, Kalka-Moll WM, Silver M, Kearney M, et al. Transplantation of ex vivo expanded endothelial progenitor cells for therapeutic neovascularization. Proceedings of the National Academy of Sciences 2000;97:3422-7.

17. Tateishi-Yuyama E, Matsubara H, Murohara T, Ikeda U, Shintani S, Masaki H, et al. Therapeutic angiogenesis for patients with limb ischaemia by autologous transplantation of bone-marrow cells: a pilot study and a randomised controlled trial. The Lancet 2002;360:427-35.

18. Gupta R, Losordo DW. Cell therapy for critical limb ischemia: moving forward one step at a time. Circulation Cardiovascular interventions 2011;4:2-5.

19. Tian L, George SC. Biomaterials to prevascularize engineered tissues. Journal of cardiovascular translational research 2011;4:685-98.

20. Chen X, Aledia AS, Ghajar CM, Griffith CK, Putnam AJ, Hughes CC, et al. Prevascularization of a fibrin-based tissue construct accelerates the formation of functional anastomosis with host vasculature. Tissue engineering Part A 2009;15:1363-71.

21. Levenberg S, Rouwkema J, Macdonald M, Garfein ES, Kohane DS, Darland DC, et al. Engineering vascularized skeletal muscle tissue. Nature biotechnology 2005;23:879-84.

22. Baranski JD, Chaturvedi RR, Stevens KR, Eyckmans J, Carvalho B, Solorzano RD, et al. Geometric control of vascular networks to enhance engineered tissue integration and function. Proceedings of the National Academy of Sciences 2013;110:7586-91.

23. Rouwkema J, Rivron NC, van Blitterswijk CA. Vascularization in tissue engineering. Trends in biotechnology 2008;26:434-41.

24. Novosel EC, Kleinhans C, Kluger PJ. Vascularization is the key challenge in tissue engineering. Adv Drug Deliver Rev 2011;63:300-11.

25. Rivron NC, Liu JJ, Rouwkema J, de Boer J, van Blitterswijk CA. Engineering vascularised tissues in vitro. European cells & materials 2008;15:27-40.

26. Tremblay PL, Hudon V, Berthod F, Germain L, Auger FA. Inosculation of tissue-engineered capillaries with the host's vasculature in a reconstructed skin transplanted on mice. American journal of transplantation: official journal of the American Society of Transplantation and the American Society of Transplant Surgeons 2005;5:1002-10.

27. Shepherd BR, Enis DR, Wang FY, Suarez Y, Pober JS, Schechner JS. Vascularization and engraftment of a human skin substitute using circulating progenitor cell-derived endothelial cells. Faseb J 2006;20:1739-+.

28. Ceccarelli J, Putnam AJ. Sculpting the blank slate: how fibrin's support of vascularization can inspire biomaterial design. Acta biomaterialia 2014;10:1515-23.

29. Walters BD, Stegemann JP. Strategies for directing the structure and function of three-dimensional collagen biomaterials across length scales. Acta biomaterialia 2014;10:1488-501.

30. Ghajar CM, Blevins KS, Hughes CC, George SC, Putnam AJ. Mesenchymal stem cells enhance angiogenesis in mechanically viable prevascularized tissues via early matrix metalloproteinase upregulation. Tissue engineering 2006;12:2875-88.

31. Rao RR, Peterson AW, Ceccarelli J, Putnam AJ, Stegemann JP. Matrix composition regulates three-dimensional network formation by endothelial cells and mesenchymal stem cells in collagen/fibrin materials. Angiogenesis 2012;15:253-64.

32. Kniazeva E, Kachgal S, Putnam AJ. Effects of extracellular matrix density and mesenchymal stem cells on neovascularization in vivo. Tissue engineering Part A 2011;17:905-14.

33. Grainger SJ, Carrion B, Ceccarelli J, Putnam AJ. Stromal cell identity influences the in vivo functionality of engineered capillary networks formed by co-delivery of endothelial cells and stromal cells. Tissue engineering Part A 2013;19:1209-22.

34. Carrion B, Huang CP, Ghajar CM, Kachgal S, Kniazeva E, Jeon NL, et al. Recreating the Perivascular Niche Ex Vivo Using a Microfluidic Approach. Biotechnol Bioeng 2010;107:1020-8.

35. Peterson AW, Caldwell DJ, Rioja AY, Rao RR, Putnam AJ, Stegemann JP. Vasculogenesis and angiogenesis in modular collagen-fibrin microtissues. Biomater Sci-Uk 2014;2:1497-508.

36. Rowe SL, Stegemann JP. Microstructure and Mechanics of Collagen-Fibrin Matrices Polymerized Using Ancrod Snake Venom Enzyme. J Biomech Eng-T Asme 2009;131.

37. Ghajar CM, Chen X, Harris JW, Suresh V, Hughes CC, Jeon NL, et al. The effect of matrix density on the regulation of 3-D capillary morphogenesis. Biophysical journal 2008;94:1930-41.

38. Kirkpatrick CJ, Fuchs S, Unger RE. Co-culture systems for vascularization--learning from nature. Adv Drug Deliv Rev 2011;63:291-9.

39. Au P, Daheron LM, Duda DG, Cohen KS, Tyrrell JA, Lanning RM, et al. Differential in vivo potential of endothelial progenitor cells from human umbilical cord blood and adult peripheral blood to form functional long-lasting vessels. Blood 2008;111:1302-5.

40. Merfeld-Clauss S, Gollahalli N, March KL, Traktuev DO. Adipose tissue progenitor cells directly interact with endothelial cells to induce vascular network formation. Tissue engineering Part A 2010;16:2953-66.

41. Shepherd BR, Jay SM, Saltzman WM, Tellides G, Pober JS. Human aortic smooth muscle cells promote arteriole formation by coengrafted endothelial cells. Tissue engineering Part A 2009;15:165-73.

42. Nakatsu MN, Sainson RCA, Aoto JN, Taylor KL, Aitkenhead M, Pérez-del-Pulgar S, et al. Angiogenic sprouting and capillary lumen formation modeled by human umbilical vein endothelial cells (HUVEC) in fibrin gels: the role of fibroblasts and Angiopoietin-1☆. Microvascular Research 2003;66:102-12.

43. Montesano R, Pepper MS, Orci L. Paracrine induction of angiogenesis in vitro by Swiss 3T3 fibroblasts. Journal of cell science 1993;105 (Pt 4):1013-24.

44. Griffith CK, Miller C, Sainson RC, Calvert JW, Jeon NL, Hughes CC, et al. Diffusion limits of an in vitro thick prevascularized tissue. Tissue engineering 2005;11:257-66.

45. Jain RK, Au P, Tam J, Duda DG, Fukumura D. Engineering vascularized tissue. Nature biotechnology 2005;23:821-3.

46. Carmeliet P, Jain RK. Angiogenesis in cancer and other diseases. Nature 2000;407:249-57.

47. Kelm JM, Djonov V, Ittner LM, Fluri D, Born W, Hoerstrup SP, et al. Design of custom-shaped vascularized tissues using microtissue spheroids as minimal building units. Tissue engineering 2006;12:2151-60.

48. McGuigan AP, Sefton MV. Vascularized organoid engineered by modular assembly enables blood perfusion. Proceedings of the National Academy of Sciences of the United States of America 2006;103:11461-6.

49. Youssef J, Nurse AK, Freund LB, Morgan JR. Quantification of the forces driving self-assembly of three-dimensional microtissues. Proceedings of the National Academy of Sciences of the United States of America 2011;108:6993-8.

50. Dean DM, Morgan JR. Cytoskeletal-mediated tension modulates the directed self-assembly of microtissues. Tissue engineering Part A 2008;14:1989-97.

51. Dean DM, Napolitano AP, Youssef J, Morgan JR. Rods, tori, and honeycombs: the directed self-assembly of microtissues with prescribed microscale geometries. Faseb J 2007;21:4005-12.

52. Dean DM, Rago AP, Morgan JR. Fibroblast elongation and dendritic extensions in constrained versus unconstrained microtissues. Cell motility and the cytoskeleton 2009;66:129-41.

53. Gupta R, Sefton MV. Application of an endothelialized modular construct for islet transplantation in syngeneic and allogeneic immunosuppressed rat models. Tissue engineering Part A 2011;17:2005-15.

54. Cheng HW, Luk KD, Cheung KM, Chan BP. In vitro generation of an osteochondral interface from mesenchymal stem cell-collagen microspheres. Biomaterials 2011;32:1526-35.

55. Wang L, Rao RR, Stegemann JP. Delivery of mesenchymal stem cells in chitosan/collagen microbeads for orthopedic tissue repair. Cells, tissues, organs 2013;197:333-43.

56. Wise JK, Alford AI, Goldstein SA, Stegemann JP. Comparison of uncultured marrow mononuclear cells and culture-expanded mesenchymal stem cells in 3D collagen-chitosan microbeads for orthopedic tissue engineering. Tissue engineering Part A 2014;20:210-24.

57. Leung BM, Miyagi Y, Li RK, Sefton MV. Fate of modular cardiac tissue constructs in a syngeneic rat model. Journal of tissue engineering and regenerative medicine 2013.

58. Tiruvannamalai-Annamalai R, Armant DR, Matthew HW. A glycosaminoglycan based, modular tissue scaffold system for rapid assembly of perfusable, high cell density, engineered tissues. PloS one 2014;9:e84287.

59. Futrega K PJ, Kinney M, Lott WB, Ungrin MD, Zandstra PW, Doran, MR. The microwell-mesh: a novel device and protocol for the high throughput manufacturing of cartilage microtissues. Biomaterials 2015.

60. Yen C-M, Chan C-C, Lin S-J. High-throughput reconstitution of epithelial–mesenchymal interaction in folliculoid microtissues by biomaterial-facilitated self-assembly of dissociated heterotypic adult cells. Biomaterials 2010;31:4341-52.

61. Thompson HG, Truong DT, Griffith CK, George SC. A three-dimensional in vitro model of angiogenesis in the airway mucosa. Pulmonary Pharmacology & Therapeutics 2007;20:141-8.

62. Chung E, Rytlewski JA, Merchant AG, Dhada KS, Lewis EW, Suggs LJ. Fibrin-based 3D matrices induce angiogenic behavior of adipose-derived stem cells. Acta biomaterialia 2015;17:78-88.

63. Dietrich F, Lelkes PI. Fine-tuning of a three-dimensional microcarrier-based angiogenesis assay for the analysis of endothelial-mesenchymal cell co-cultures in fibrin and collagen gels. Angiogenesis 2006;9:111-25.

64. Go RS, Ritman EL, Owen WG. Angiogenesis in rat aortic rings stimulated by very low concentrations of serum and plasma. Angiogenesis 2003;6:25-9.

65. Becker JC, Domschke W, Pohle T. Biological in vitro effects of fibrin glue: fibroblast proliferation, expression and binding of growth factors. Scandinavian journal of gastroenterology 2004;39:927-32.

66. Martino MM, Brkic S, Bovo E, Burger M, Schaefer DJ, Wolff T, et al. Extracellular matrix and growth factor engineering for controlled angiogenesis in regenerative medicine. Frontiers in bioengineering and biotechnology 2015;3.

67. Martino MM, Briquez PS, Ranga A, Lutolf MP, Hubbell JA. Heparin-binding domain of fibrin(ogen) binds growth factors and promotes tissue repair when incorporated within a synthetic matrix. Proceedings of the National Academy of Sciences of the United States of America 2013;110:4563-8.

68. Martino MM, Briquez PS, Güç E, Tortelli F, Kilarski WW, Metzger S, et al. Growth factors engineered for super-affinity to the extracellular matrix enhance tissue healing. Science 2014;343:885-8.

CHAPTER 4

In vitro and *In vivo* Vessel Formation from Vascular Modular Microtissues

4.1 Introduction

Peripheral arterial disease (PAD) is most commonly caused by atherosclerosis, plaque formation in the arterial wall that prevents or limits normal blood flow in the body [1]. Risk factors for PAD include smoking and diabetes [2]. Diabetic patients who suffer from PAD have a higher rate of ischemic events than non-diabetic PAD patients [3]. In the United States, 82% of lower limb amputations are related to diabetes [4]. This increase in limb amputations in diabetics is usually due to patients having infected foot ulcers [5]. Ulcers and gangrene are more common in diabetic PAD patients than in non-diabetic PAD patients [6]. Bypass surgeries can directly re-vascularize the affected region(s) in PAD patients' bodies and prevent long term damage [7]. Unfortunately, diabetic PAD patients are often unable to receive invasive surgeries due to other comorbidities. For this reason, it is important to develop therapeutic techniques that can re-vascularize ischemic regions without the need for open surgery.

Pre-vascularization is a technique that can restore microvasculature by accelerating inosculation with host vessels in non-healthy tissue. The survival of the implant can be enhanced by introducing pre-formed vascular networks and its ability to re-vascularize ischemic regions [8]. In addition to accelerating re-vascularization, pre-vascularization has been shown to improve cell viability after transplantation procedures [9]. Both *in vivo* and *in vitro* pre-vascularization

techniques are being explored to improve blood perfusion and provide sufficient oxygen and nutrients for host cells to survive and prevent and/or limit tissue necrosis. These techniques typically involve vascularizing a scaffold prior to implantation in the ischemic region. In the *in vivo* technique, scaffolds are implanted close to an artery and/or vein allowing sprout infiltration and formation to occur within the implant, which occurs several weeks' post implantation [10, 11]. The vascularized scaffolds are then transferred to the ischemic region where the implant and the host vessels are connected surgically via sutures, returning regular blood flow within the affected area. The number of surgeries (three) and the lengthy time for the implanted scaffold to vascularize reduces the likelihood of using this technique in human clinical studies, especially since major surgical complications including damage to the vasculature and nerves can occur as surgeons search for the best location to implant the construct [10,11].

In vitro pre-vascularization, on the other hand, limits the number of surgical interventions by developing vascularized tissues outside of the body. Multiple proteins with different endothelial and stromal cell co-cultures have been combined to develop vascularized macro tissues *in vitro*. Fibrin has been commonly used as a three-dimensional (3D) matrix in this approach since it supports endothelial vessel formation. Multiple 3D vascular macro tissues have been developed by combining this protein with other biomaterials and/or cell types [12-16]. Stromal cells and/or fibroblasts are often included in these tissues as they provide paracrine signals that are important for endothelial vessel formation and stabilization [17-24]. Endothelial sprout length has been found to depend not only on the stromal cell type employed, but also on the properties of the extracellular matrix properties to which the endothelial cells are exposed [25, 26]. In *in vitro* pre-vascularization, the host vasculature is only required to grow and inosculate with the outer regions of the construct, where many sprouts are found. Once this occurs, the entire construct is supplied

with oxygen and nutrients via the vessel network assembled within the implant [10-12]. Studies have shown that these pre-vascularized networks created *in vitro* connect to the host vasculature post-implantation [13-15]. Although this technique proposes a solution to limit re-vascularization time, one surgery is still required to improve blood vessel perfusion.

Modular approaches to tissue re-vascularization represent a new approach to restoring vasculature in ischemic tissues. The small sizes of tissue modules provide an advantage over macroscopic tissue constructs in terms of size-related oxygen and nutrient diffusion limitations, as cells within modules 100-300 μm in diameter are better sustained with diffusion alone [27-32]. Furthermore, modular approaches may change the way that diabetic PAD patients can be treated since microtissues can be delivered in a minimally invasive manner and subsequently self-assemble into macroscale vascularized networks in situ. Like macroscale tissue constructs, microtissue modules can be fabricated with different materials and cells to engineer tissues, depending on the tissue type and disease being treated [33-40]. Microtissues' matrices may also allow the encapsulated cells to better survive tissue implantation and regeneration [41, 42].

We have shown that EC encapsulated with fibroblasts in modular microbeads fabricated from natural proteins can initiate sprouting both inside and outside the microtissues when embedded in 3D fibrin hydrogels. These EC sprouts also inosculate with sprouts from neighboring microtissues in this 3D model [25]. Although cells encapsulated within these engineered modular constructs may survive because of their small diameters [32], their viability is likely to decrease when implanted in large ischemic regions. For this reason, it is necessary to develop vascular microtissues that (1) can be delivered in a minimally invasive manner via injection, (2) can be pre-cultured for multiple days while fostering endothelial sprout formation to occur, and (3) can inosculate with sprouts from neighboring microbeads as well as with the host vasculature. These

pre-vascularized microbeads will already have existing networks, which we expect will facilitate oxygen diffusion throughout the construct immediately upon inosculation with the host vasculature. The oxygen diffusion will prevent cell apoptosis within the constructs and ultimately decrease the time it takes to regenerate vasculature in the ischemic region.

4.2 Materials and Methods

4.2.1 Cell Culture

Human umbilical vein endothelial cells (HUVECs) and normal human lung fibroblasts (NHLFs) from Lonza Inc, Walkersville, MD were purchased and passaged. Endothelial cells were grown in endothelial growth media (EGM-2, Lonza), while fibroblasts were cultured in Media 199 (M199, Life Technologies, Grand Island, NY) with 10% fetal bovine serum (FBS). Passages 4-7 of HUVECs and passages 9-14 of NHLFs were employed in *in vitro* and *in vivo* experiments.

4.2.2 Fibrin Microbead Production

HUVECs and NHLFs were cultured and trypsinized using 0.05% Trypsin-EDTA (Gibco). Both cell types were re-suspended in their appropriate media. An automated cell counter (Multisizer 3, Beckman Coulter, Brea, CA) was utilized to count the number of cells. For preliminary *in vitro* studies, $2x10^6$ of each cell type was used to make 3 mL of the initial fibrin microbead stock ($2x10^6$ total cells/mL). The cell density was increased from $2x10^6$ total cells/mL to $5x10^6$ total cells/mL for *in vivo* studies and *in vitro* implant characterization.

Fibrin microbeads were made in a water-in-oil emulsification process, as previously described [25]. Prior to starting the emulsification process, 75 mL of 100 cSt polydimethylsiloxane

(PDMS) oil (Clearco Products Co. Inc. Bensalem, PA) was placed into a 100 mL beaker and left on ice. Cells were pipetted in a conical tube at the initial cell density of $2x10^6$ total cells/mL (*in vitro* studies) or $5x10^6$ total cells/mL (*in vivo* studies). Each batch of microbeads was made by mixing 765 µL serum-free endothelial growth media (SFEGM-2), 300 µL fetal bovine serum (FBS, 10% final), 60 µL of 50 U/mL thrombin (1 U/mL final), and 1875 µL of clottable fibrinogen protein stock (2.5 mg/mL final) with the HUVECs-NHLFs pellet. The cell and protein mixture was then added to the PDMS bath, which was kept on ice at 0 °C. Fibrinogen (FGN) stock was made by mixing protein with SFEGM-2 at 37 °C.

The cell-fibrin solution was mixed at 600 RPM for 5 min at 0 °C, and then stirred at the same speed for 25 min at 37 °C. The microbeads and PDMS solution were collected and separated with the addition of PBS with 100 ppm of L101 surfactant (PBS-L101; BASF, Florham Park, NJ), inversion mixing, followed by 4-5 centrifugation steps (200 g for 5 min/each). After each centrifugation step, PDMS was removed from the FIB microbeads. The microbeads were then re-suspended with EGM-2 and placed in vented 15 mL conical tubes with filters (CELLTREAT Scientific Products, Shirley, MA) prior to starting any experimental procedures. Media were changed the day after microbead fabrication and every other day.

4.2.3 Embedding of Microbeads in FIB Hydrogels (3D *in vitro* model)

FIB microbeads were embedded in fibrin hydrogels immediately, 1, 3, 5, or 7 days after their fabrication process. 300 µL of the 3 mL microbead stock was utilized to make 3 fibrin hydrogels, ~100 µL of microbeads per hydrogel. FIB hydrogels were made by mixing the cell pellet thoroughly with 382.5 µL of SFEGM-2, 150 µL of FBS (10% final), 30 µL of 50 U/mL thrombin (1 U/mL final), and 937.5 µL of fibrinogen stock solution (2.5 mg/mL final). 500 µL of

the cell-protein mixture was added per well of a standard 24-well culture plate, and left at room temperature for 5 min before being placed in the incubator for 25 min at 37 °C. EGM-2 was added to each hydrogel after the complete gelation process (1 mL per well). Media were replaced the next day and every other day for the duration of the culture.

4.2.4 Endothelial Cell Staining, Imaging, and Quantification

Prior to staining, microbeads alone or embedded in FIB hydrogel were fixed with the zinc-buffered formalin solution (Z-fix, Anatech, battle Creek, MI). After 10 min, the fixative was removed and the samples were washed two times with phosphate buffer saline (PBS). The endothelial cell specific marker Ulex Europaeus Aglutinin I (UEA-I, Vector Laboratories, Burlingame, CA) was utilized to stain the endothelial cells. The staining solution was made of 1% BSA, 20 µg/mL rhodamine-labeled UEA-I, and 10 nM DAPI in PBS. The staining solution was then added to microbead samples and left for 45 min at room temperature. Samples were then washed with PBS for 2-4 times prior to imaging.

FIB hydrogels were taken out of the wells of the 24-well plate and placed in a microscope slide (Superfrost Plus precleaned, Fisher Scientific, Pittsburgh, PA), a microscope cover glass (Vista Vision cover glass, VWR International, LLC, Radnor, PA) was then added on top, in order to keep the hydrogel in the center. Fluorescent images of endothelial networks formed in fibrin microbeads that had been embedded in FIB hydrogels were then captured using an Olympus IX81 microscope (Olympus, Center Valley, PA) using the “scan slide” tool in the Metamorph software to image the entire construct. NIH ImageJ software (National Institutes of Health, Bethesda, MD) was utilized to merge fluorescent and bright-field images. Prior to quantification, all endothelial images were cropped and processed using the Kirsch filter to detect edges of endothelial sprouts.

The processing and imaging settings were kept constant for all conditions. The Angiogenesis Tube Formation module within the Metamorph software was then used to quantify the total area covered by endothelial tubes within each fibrin hydrogel containing microbeads.

4.2.5 Preparation of Samples for Subcutaneous Studies

To ensure equal numbers of cells were injected into mice for each of the different 3 cellular experimental groups, a method was developed to quantify the number of cells within the microbead preparations after fabrication. After microbeads were fabricated, the microbead pellet from each batch was re-suspended in 1 mL of EGM-2 and transferred into vented 15 mL conical tube with filters (CELLTREAT Scientific Products, Shirley, MA). The total volume of the microbead and media was noted, and 100 µL of it was taken out and placed in a well of a 96-well plate. 100 µL of nattokinase solution was then added on top and mixed. The plate was then transferred into the incubator for 30 minutes to allow the microbeads to dissociate and facilitate cell count. The nattokinase solution was prepared as published [43].

Briefly, nattokinase (NSK-SD, Japan Bio Science Laboratory Co., Ltd) and EDTA were dissolved in Dulbecco's phosphate-buffered saline (DPBS, no Calcium, no Magnesium) at a concentration of 50 FU (fibrin degradation units) per mL and 1 mM respectively. Using a hemacytometer, a cell count was found and adjusted based on the original volume. Each implant contained approximately $2.4x10^6$ total cells, half HUVECs and half NHLFs. This number was adjusted for each batch prior to injection, except for the pre-cultured implants.

Nattokinase didn’t degrade the entire microbead matrix after 3 days of pre-culture. For this reason, the number of cells in the pre-cultured microbeads were quantified a day after they were made (day 1). Prior to cell quantification, pre-cultured microbeads were centrifuged at 200 g for 1

min, supernatant was removed, and 1 mL of media/microbead pellet was left in each tube. 10 mL of EGM-2 was replaced after cell counts of each batch were adjusted to $2.4x10^6$ total cells/batch, and cultured for an additional two days (total 3 days).

Acellular microbeads, cells only, or microbeads containing cells were centrifuged at 200 g for 1-5 min, supernatant was then removed. Samples were re-suspended in FIB hydrogel pre-cursors. Each FIB hydrogel precursor was composed of 270 µL of SFEGM-2, 60 µL of FBS (10% final), 12 µL of thrombin (1 U/mL final), and 258 µL of fibrinogen stock solution (2.5 mg/mL final).

The solution with the samples was well mixed and placed into a 5-mL syringe with a 20-gauge x 1 inch BD PrecisionGlideTM Needle. Roughly 500 µL of the 600 µL solution was then injected into the animal, delivering approximately $2.0x10^6$ total cells per cellular implant.

4.2.6 Subcutaneous Injections

CB17/SCID mice, 6 to 8 weeks old, (Taconic Labs, Hudson, NY) were acclimated for 72 hours prior to beginning any surgical procedures. The animal protocol employed in this study was approved by the University of Michigan Committee on Use and Care of Animals. An analgesic/anesthetic drug mixture of ketamine (80-120 mg/kg), xylazine (5-10 mg/kg), and buprenorphine (0.05-0.01 mg/kg) was administered to each animal via intraperitoneal injection. Animals were returned to cages placed on top of a warm blanket until the anesthesia took effect. Ophthalmic ointment (Puralube® vet ointment, Dechra, Overland Park, KS) was applied to the eyes of each mouse. The dorsal lumbar flanks were shaved, and depilatory agent (Nair, Fisher Scientific, Pittsburg, PA) was applied to remove any remaining hair. The injection sites were sterilized by wiping the flanks with ethanol and betadine (Thermo Fisher Scientific, Fremont, CA).

A sterile surgical field was created prior to each injection, and the researchers followed sterile protocol (gloves, gowns, masks, etc.).

Four experimental conditions were injected into the mice: Acellular microbeads, cellular hydrogel, control (freshly made, D0) microbeads, and pre-cultured (3 days post-fabrication) microbeads. The samples were prepared, mixed, and injected subcutaneously into the dorsal flank of the mouse. The needle was left in the injection site for ~30 seconds to allow the solution to gel. Two implants were injected per animal, one on each flank. A second dose of buprenorphine (0.05-0.01 mg/kg) was administered to each animal 12 hours after subcutaneous injections. Animals were monitored every day post-surgery.

4.2.7 Laser Doppler Perfusion Imaging (LDPI)

Laser Doppler Perfusion Imaging (LDPI, Perimed AB, Sweden) was employed at discrete time points to non-invasively characterize blood perfusion to the implant regions. A minimum of three scans per animal were performed and then averaged to determine average blood perfusion through each implant. Scans were performed before implants were injected, immediately after implant injection, and at 3 and 7 days after injection. Animals were anesthetized (described in the previous section) prior to imaging.

4.2.8 Implant Retrieval and Post-Processing

After 3 or 7 days, animals were euthanized. Implants were removed with scissors and forceps and placed immediately in 20 mL glass bottles with Z-fix. Implants were fixed for 24 hours at 4 °C. Z-fix was removed, and implants were washed with PBS 3 to 4 times (5 min/wash). 70%

ethanol was then added to implants and left at 4 °C until further processing. Samples were then placed in pink cassettes (UNISETTE cassette with lid, Simport, Canada), embedded in paraffin using the tissue embedding processor (KD-BM II, KEDEE, China), and sectioned with a Thermo Scientific™ HM 325 rotary microtome (6 µm sections) for further analysis.

4.2.9 Hematoxylin and Eosin (H&E) staining

Sections were stained with Mayer's Hematoxylin (Electron Microscopy Sciences 26252) and Eosin Y (Sigma HT110132). Slides were dewaxed with xylene twice (5 minutes/wash), and then transferred to 100%, 95%, 70% ethanol, and deionized baths (3 minutes/wash, two baths per ethanol concentration). Slides were submerged in hematoxylin bath for 15 minutes, and then rinsed with tap water for an additional 15 minutes. Slides were then placed in 95% ethanol for 30 seconds, followed by their immersion in Eosin for 1 minute. Slides were subsequently transferred into 95% ethanol bath for 1 minute, and 2 separate 100% ethanol baths (1 minute/bath). Samples were cleared by submerging them into 2 xylene baths (3 minutes/wash). Toluene mounting solution was added to each slide prior to placing the cover-slips. Slides were left to dry prior to imaging.

4.2.10 CD31 and Alpha-Smooth Muscle Actin (α-SMA) Staining

The location of each implant within the explanted tissue section was first identified with H&E staining. The subsequent serial section of each implant was then deparrafinized with xylene and then rehydrated through a series of graded ethanol washes and ending with water. Slides were placed in antigen retrieval solution (Dako, Carpinteria, CA) and placed in steamer (95- 99 °C) for 35 minutes. The antigen retrieval solution with the samples was then removed and left until room

temperature was reached. Slides were rinsed 3x with tris-buffered saline (TBS-T), 2 min/wash. The area around the tissue was marked with an ImmEdge™ pen (Vector Laboratories, Inc., Burlingame, CA). The Dako EnVision System-HRP (DAB) kit (Dako) was utilized for CD31 staining. Slides were rinsed with TBS-T (3 times, 2 minutes/wash) before any solution from the Dako kit was added to the samples. First, peroxidase blocking solution was added to each tissue for 5 minutes. Dako mouse anti-human CD31 primary antibody (1:50 dilution in TBS-T) was then added to each tissue and kept at 4 °C for 16 hours.

The HRP-conjugated anti-mouse secondary antibody was added to each sample and left for 30 minutes. Samples were then kept with DAB+ substrate-chromogen buffer solution for 5 minutes. A negative control reagent was used in some samples to confirm the specificity of the staining. Most samples were counter-stained with hematoxylin and/or eosin. Slides were then washed with 95% ethanol, 100% ethanol, and xylene. Toluene mounting medium was added prior to covering the samples with cover-slips.

The Dako EnVision System-HRP (DAB) kit (Dako, Carpinteria, CA), antigen retrieval, dewaxing, and dehydration/hydration steps described above were also used in the alpha-smooth muscle actin (α-SMA) staining process. The only differences between the CD31 staining and the α-SMA staining were that smooth muscle actin monoclonal antibody (1A4 (asm-1)) (Invitrogen: Thermo Fisher Scientific) was used as the primary antibody, and its two-hour incubation time was at room temperature.

4.2.11 Vessel Quantification

Bright-field images (4x and 20x) of each complete implant were taken with an inverted Nikon microscope (Nikon Instruments Inc., Melville, NJ). A minimum of four 20x CD31 images

from each implant were quantified to determine average vessels per implant. A vessel was considered any area defined by the presence of a lumen with red blood cells inside and marked with a complete brown rim of positive human CD31 staining. A one-sided blinded study was performed by re-labeling all samples to prevent any bias by those assigned to manually count vessels. Auto stitch software, developed by Brown and Lowe [44], was utilized to create complete images of each implant from the 4x images taken. The total area of each implant was quantified using ImageJ. The number of vessels per selected implant area was found by multiplying the average vessel number times the number of times a 20x image fitted into each complete implant region.

4.2.12 Implant Shear Modulus Measurement

Implant preparation was done similarly to the protocol employed for subcutaneous injections (see section 4.2.5). Once the samples were re-suspended in fibrin hydrogel precursors, rather than injecting them into the animal, they were pipetted into wells of 24-well plates and left in the incubator for 25 to 30 minutes for gelation to occur. EGM-2 media was added on top of hydrogels, and samples were left in the incubator overnight. The shear modulus of the hydrogels was characterized using a TA instruments AR-G2 rheometer with an 8-mm parallel-plate geometry. The top plate was lowered towards a sample hydrogel in a stepwise manner (50 to 100 microns) from a height that is greater than the theoretical height of a 500 μL hydrogel in a 24-well plate. At each step height, the shear modulus of the hydrogel was evaluated and recorded. As the gap decreased, the shear modulus versus height curve switched from a gradual linear regime to a steeper linear regime. The nominal hydrogel shear modulus and height were evaluated by finding the intersection of these two linear regime tangent lines. Samples were kept at 37 °C while

measurements were being taken to prevent changes in the samples' properties while measurements were recorded. Shear moduli of D0 implants were measured by pipetting the implant and fibrin solution directly on top of the rheometer stage prior to gelation. The sample was left on the stage for 45 minutes to allow for complete gelation and to acquire the shear modulus curve.

4.2.13 Measurement of Implant Volumes

Cellular implants were prepared the same way as described in section 4.2.5. Instead of injecting them into the animals, the same implant volume (500 µL) was pipetted into transparent caps of 5 mL Eppendorf Tubes® that had been placed in wells of 6-well plates. Samples were then placed in the incubator for 25 to 30 minutes at 37 °C to allow complete gelation. To prevent samples from drying, 6 mL of EGM-2 was added to each construct, and constructs were then flipped upside-down and left in the incubator overnight. Spectral ultrasound imaging (SUSI) was employed using the Vevo 770 (VisualSonics Inc., Toronto, Canada) with the same parameters described previously [45] to image cellular implants and quantify their volumes. The implant volumes were normalized to the volume of the pre-cultured condition, which was found to be close to 500 µL, the expected initial implant volume. Implant volume for each test condition was averaged over three implants.

4.2.14 Regional Mechanical Testing using Dual-Mode Ultrasound Elastography (DUE)

After the samples were imaged with the Vevo 700 system (section 4.2.13), the viscoelastic properties of the fibrin hydrogels with microbeads and cells were measured using the dual-mode

ultrasound elastography (DUE) technique. This technique can measure viscoelastic properties at the microscale, non-invasively. Samples were compressed using acoustic radiation force (ARF) produced by a 2 MHz focused ultrasound (FUS) transducer with a circular aperture (H148; Sonic Concepts, Woodinville, WA). Simultaneously, an ultrasound imaging system ran in M-mode with a 10 MHz transducer (Olympus, Waltham, MA; 55 mm focal distance, - 6 dB beam width of 1 mm) measured the samples' deformation caused by the compression. This methodology along with additional information on experimental set-up and calibration has been previously published [46].

Prior to starting FUS compressions, a pulser-receiver (5900 PR; Olympus) was used to drive the imaging transducer at a 1 Hz pulse repetition frequency (PRF) for 20 seconds to first determine the base-line signals for the sample at undeformed state. FUS pulses (pulse duration: 0.99 seconds or 99% duty cycle) at 1 Hz PRF were then applied for 3 minutes while ultrasound imaging pulses (pulse duration of 0.4 μs or duty cycle of 0.00004%) were applied simultaneously, to assess the deformation done by the FUS pulses. A pulse/delay generator (Model 565; BNC, San Rafael, CA) and two waveform generators (33220A; Agilent, Santa Clara, CA) synchronized the FUS and imaging pulses.

The 99% duty cycle for the FUS pulses put the sample under a nearly constant compression load while permitting detection of sample deformation with ultrasound imaging. The transducer received the backscattered radio frequency (RF) signals during, before, and after FUS compression to determine deformation (strain) of the material. Three individual samples for each condition were analyzed; four different locations from each implant were averaged to obtain the average viscoelastic properties of each sample.

4.2.15 Viscoelastic Properties' Analysis and Burger's Viscoelastic Model Fitting

The viscoelastic properties of each implant were determined by fitting the creep data to the Burger's viscoelastic model, as previously shown [46, 47]. This model combines both the spring and dashpot in series (Maxwell model) and the spring and dashpot in parallel (Voigt Model) (Fig. 4-1).

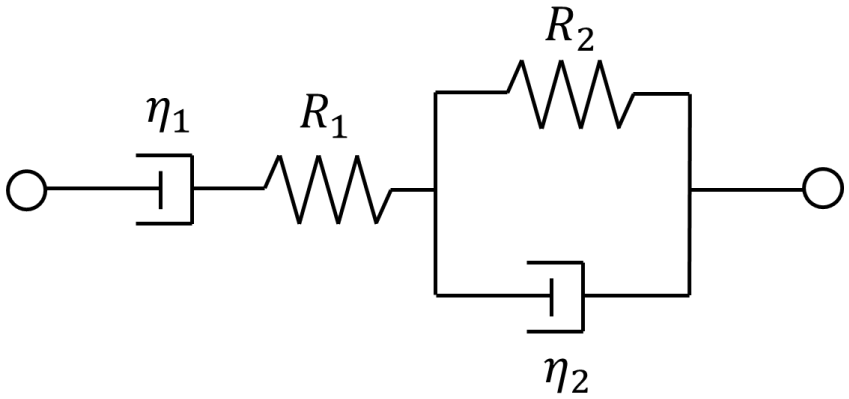

Figure 4-1: Burger's viscoelastic model

These viscous (η_1 and η_2) and elastic (R_1 and R_2) parameters as well as the viscoelastic creep constant, η_2/R_2 [46, 48] – elements in the Burger model – are acquired by fitting the creep data to the following strain response equation [49]

$$\boldsymbol{\varepsilon_{creep}(t) = \frac{\sigma_0}{R_1} + \frac{\sigma_0 t}{\eta_1} + \frac{\sigma_0}{R_2}\left[1 - \exp\left(-\frac{t}{\frac{\eta_2}{R_2}}\right)\right]}$$

where $\boldsymbol{\sigma_0}$ is the applied stress.

4.2.16 Statistical Analysis

Statistical analyses were performed using one-way ANOVA with Unequal N post hoc test using STATISTICA software (StatSoft. Inc, Tulsa, OK). For *in vitro* studies, 12 individual hydrogels were quantified to determine if there were differences between conditions, while 4 to 5 random images of each implant (3 to 4 implants/condition) were quantified for *in vivo* studies. Data are reported as mean ± standard error. Values of $p \leq 0.05$ were considered statistically significant.

4.3 Results

4.3.1 Overview of Microbead Study

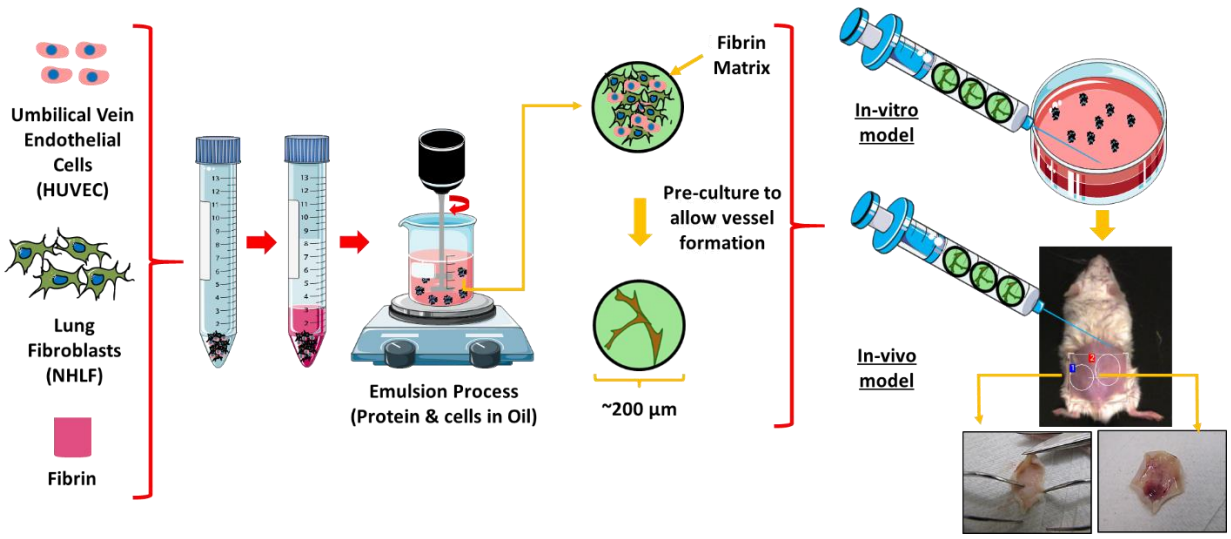

Figure 4-2: Experimental design of *in vitro* and *in vivo* vascular study. Fibrin microbeads containing human umbilical vein endothelial (HUVECs) and normal human lung fibroblasts (NHLFs) were made via emulsification process. Initial cell density was increased from 2M cells/mL for *in vitro* studies to 5M cells/mL for *in vivo* studies. Microbeads were embedded in fibrin hydrogels to determine the optimal microbead pre-culture condition for *in vivo* subcutaneous studies. Left and right implants show the acellular microbeads and cellular D0 microbeads after 7 days of injection, respectively. Some images were adapted from Servier Medical Arts clipart (*www.servier.com*).

Fibrin microbeads containing HUVECs-NHLFs co-cultures were made via an emulsification process, and were immediately embedded in acellular fibrin hydrogels immediately or after being pre-cultured (Fig. 4-2). For *in vitro* studies, microbeads were pre-cultured for 1, 3, 5, and 7 days and embedded and kept in culture for an additional 7 days. In subcutaneous studies, cellular microbeads were injected right away or after 3 days in culture. Acellular microbeads (negative control) and cells (positive control) were also injected. All implants were first re-suspended in a fibrin hydrogel precursor prior to injection. Implants were left in mice for 3 and 7 days. The left and right panels under the *in vivo* model in Fig. 4-2 show acellular microbeads (left) and D0 cellular microbeads (right) extracted 7 days after being injected subcutaneously.

4.3.2 Microbead Pre-culture and *In Vitro* Characterization

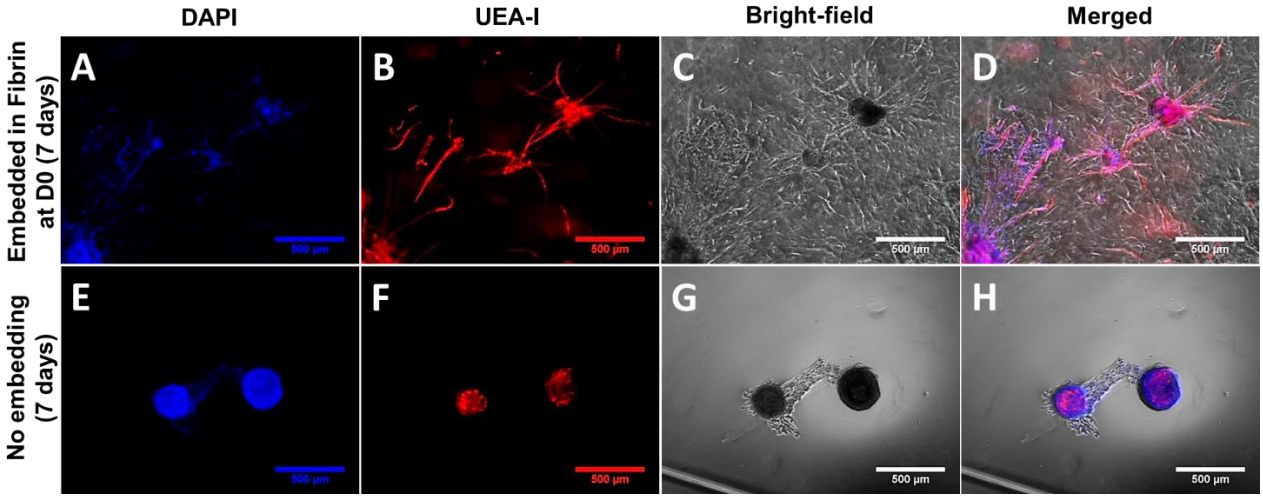

Figure 4-3: Endothelial sprout formation occurred inside HUVECs-NHLFs fibrin microbeads without the need of an additional fibrin microenvironment. Bright-field images show that cells from microbeads migrated into the surrounding fibrin hydrogels (A-D), while cells from microbeads with no additional surrounding matrix had limited mobility (E-H). Merged images of microbeads (D) embedded in fibrin hydrogels for 1 week, or (H) kept in tube culture for 7 days without embedding show endothelial sprouting formation within the microbeads. Nuclei of endothelial cells and fibroblasts were stained with DAPI - blue (A, E), and endothelial cells were stained in red with UEA-I (B, F). Scale bar – 500 µm.

As previously shown [25], endothelial cells encapsulated with fibroblasts in fibrin microbeads form sprouts within the microbead and outside the microbeads when embedded in fibrin hydrogels right after being made. The nuclei of endothelial cells and fibroblasts within and around the microbeads (Fig. 4-3E) and within and around the microbeads and fibrin hydrogel can be seen (Fig. 4-3A). UEA-I images show that endothelial cells will remain in the microbeads (Fig. 4-3F) unless microbeads are embedded in an additional fibrin matrix (Fig. 4-3B). Bright-field images were taken to demonstrate that some microbeads were (Fig. 4-3C) embedded in a fibrin hydrogel, while others were cultured statically in a tube for 7 days without an additional matrix, and then transferred to a tissue culture dish for imaging (Fig. 4-3 E-H). The DAPI/UEA-I/bright-field merged images are shown in Fig. 4-3D, H. It can be observed in Fig. 4-3H that although microbeads are not embedded in an additional extracellular matrix, cells within the microbeads still migrate towards each other during the pre-culture period.

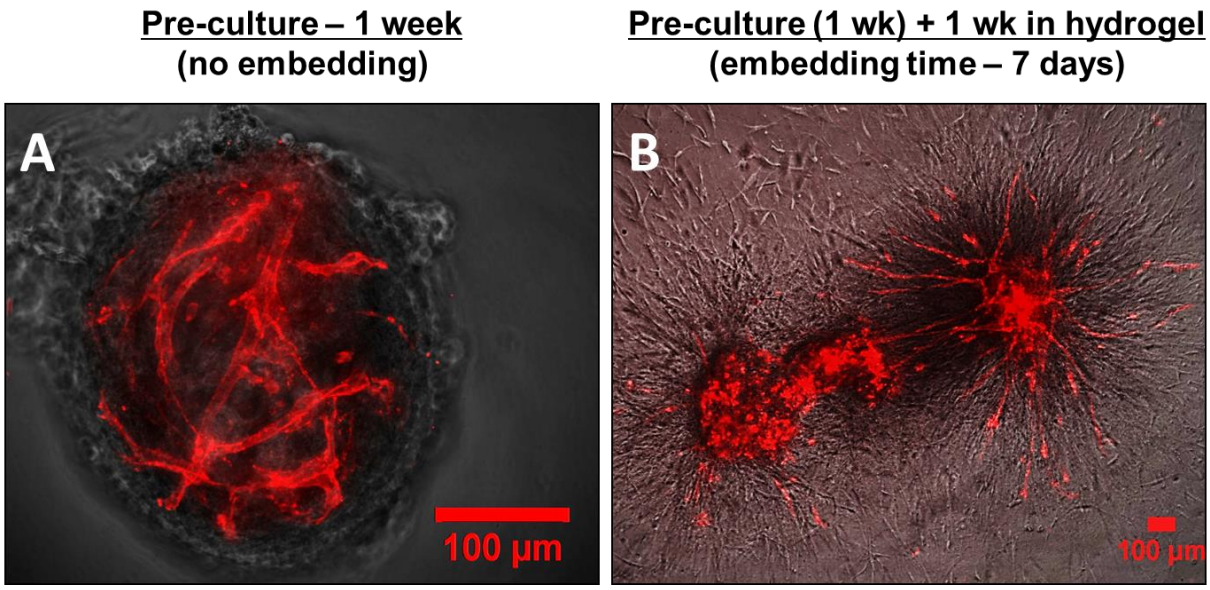

Figure 4-4: Proof of concept - Pre-cultured microbeads form endothelial sprouts and can inosculate with other sprouts from neighboring microbeads after being embedded in 3D fibrin hydrogels. (A) Microbeads were pre-cultured for 7 days and (B) embedded in a fibrin hydrogel for an additional week to allow inosculation to occur. Scale bar – 100 µm.

After FIB microbeads were kept in static culture for 7 days, endothelial sprouts formed within the FIB matrix (Fig. 4-4A). The D7 fibrin microbeads were then embedded in fibrin hydrogels and kept in culture for an additional week (Fig. 4-4B). Similar to the endothelial cells encapsulated in microbeads and embedded in fibrin hydrogels immediately after fabrication (Fig. 4-4 A-D), the endothelial cells in the D7 microbeads also formed sprouts after being embedded for 7 days (Fig. 4-4B).

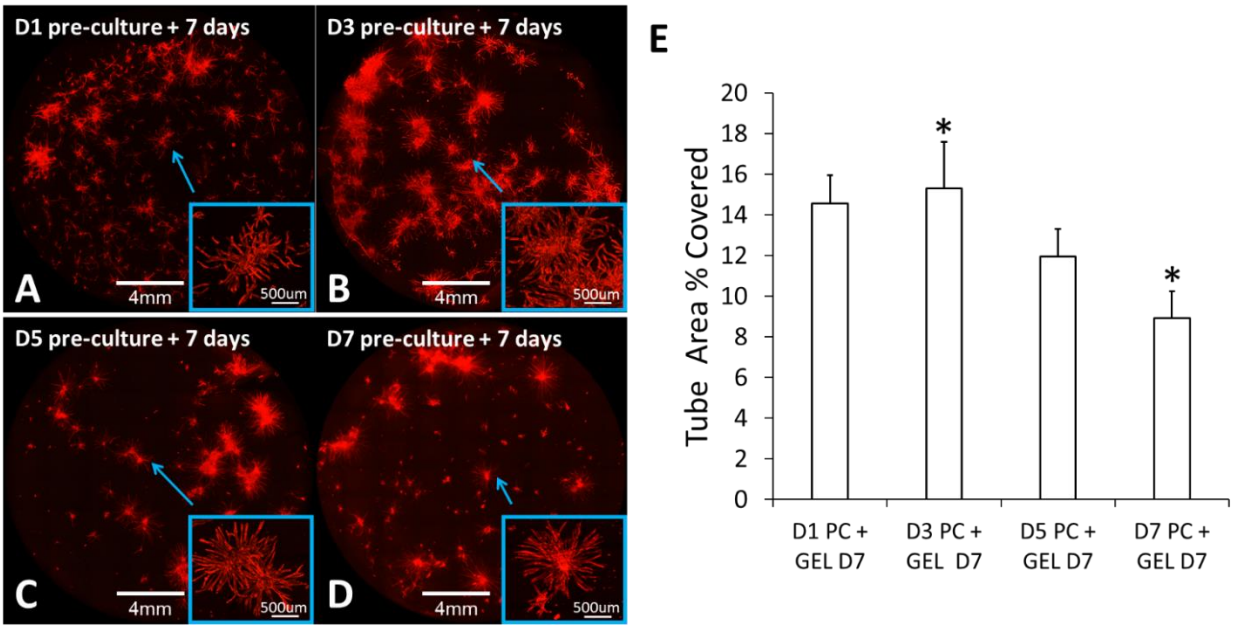

Figure 4-5: Pre-culture time affects endothelial tube coverage. Microbeads were pre-cultured for (A) 1 day, (B) 3 days, (C) 5 days, and (D) 7 days, and then embedded in fibrin hydrogels for an additional 7 days. (E) The pre-culture time with the most endothelial network coverage was found to be 3 days. Inset shows regions of the hydrogel that were magnified and adjusted with a Kirsch filter to facilitate edge detection and software quantification. Scale bar of hydrogels is 4 mm, and 500 µm for insets.

Fibrin microbeads were then pre-cultured for 1 (Fig. 4-5A), 3 (Fig. 4-5B), 5 (Fig. 4-5C), and 7 days (Fig. 4-5D) and embedded in fibrin hydrogels for an additional week to determine the pre-culture time that would provide higher endothelial coverage within the fibrin hydrogels. Insets show close-up regions in the hydrogels where endothelial sprouting occurred. A reduction in

endothelial cell coverage within the fibrin hydrogel was found with longer pre-culture times (Fig. 4-5E). D3 pre-culture time was employed in subcutaneous studies as it produced a higher tube area coverage.

4.3.3 Laser Doppler Perfusion Imaging

Laser Doppler perfusion images were taken immediately after implant injection (Fig. 4-6A, B), creating a pocket in the implant site and preventing blood perfusion from occurring within the injection areas. The left implant contained acellular microbeads in a fibrin hydrogel, while the right implant was the cellular hydrogels. It appears, qualitatively that after 3 days (Fig. 4-6C), blood perfusion did not seem to differ between the acellular and cellular implants. In addition, it did not differ much from the blood perfusion image of the mouse with no implants (Fig. 4-6D).

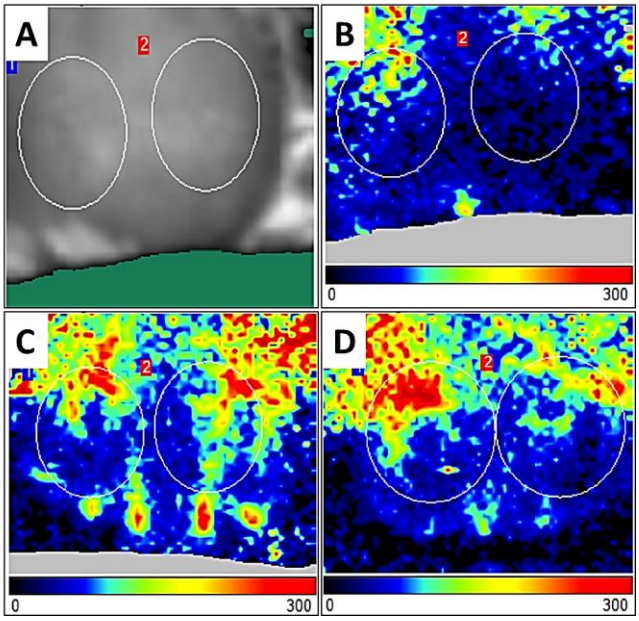

Figure 4-6: Laser Doppler Perfusion Imaging. Image of mice implant selection immediately after implantation (A), LDPI image of the implants: acellular microbeads on the left and cellular hydrogel on the right (B) immediately after injection, (C) 3 days after injection, and (D) with no implant injection – normal blood perfusion.

Quantification of the images are shown in Fig. 4-7. As seen from the images, the percent relative perfusion decreased by about 50% after the injections of the implants. After 3 and 7 days, the percent relative perfusion returned to normal. No statistical differences were found between the percent relative perfusion between D3 and D7 implants.

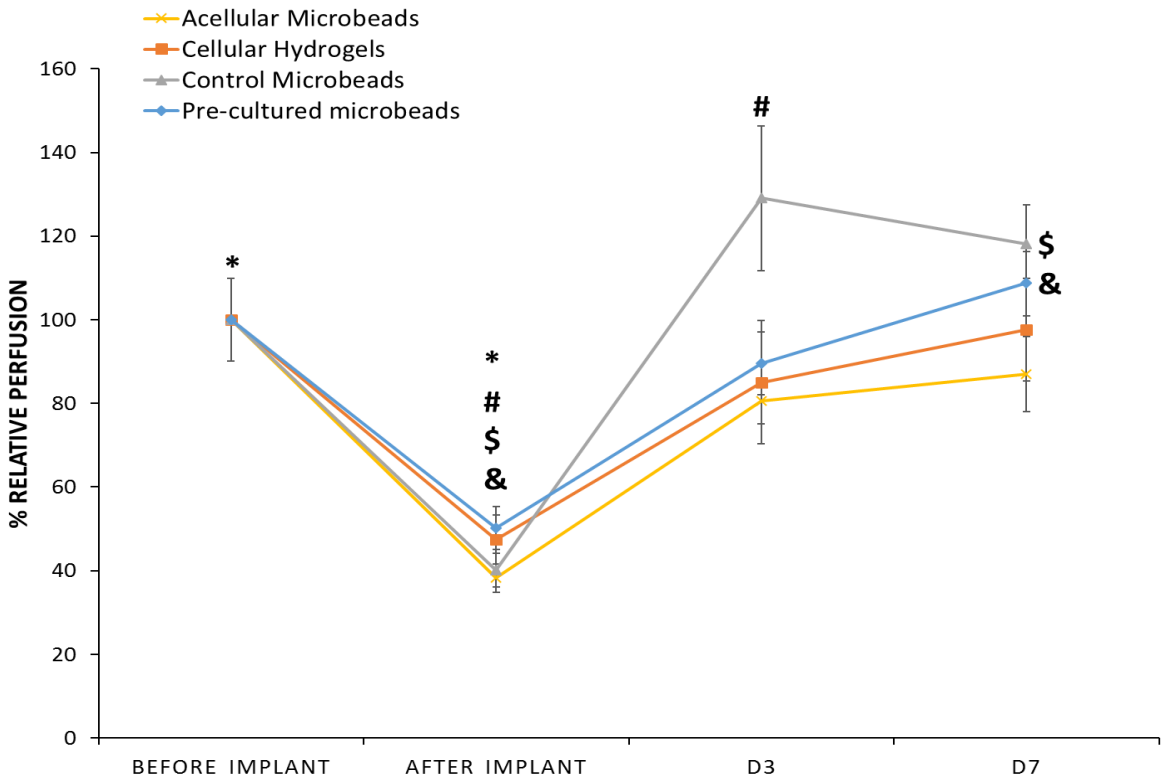

Figure 4-7: Percent relative perfusion decreased after implants were injected, and returned to normal after 3 days in the animal.

4.3.4 Vessel Formation and Cell Infiltration in Subcutaneous Implants

Acellular microbeads (Fig. 4-8 A, E), cellular hydrogels (Fig. 4-8B, F), control microbeads (Fig. 4-8C, D), and pre-cultured microbeads were extracted from the mouse after 3 (Fig. 4-8 A-D), and 7 days (Fig. 4-8 E-H) post injection. Tissues were processed, stained with H&E, and imaged at 20x. Eosin stained the fibrin microbeads and the surrounding hydrogel injected, while

the Hematoxylin stained the human endothelial cells and fibroblasts in the implants as well as the host cells. Host cells infiltrate between acellular microbeads both after 3 and 7 days (Fig. 4-8A, E). Endothelial vessels were found in cellular hydrogels, control microbeads, and pre-cultured microbeads after 7 days in situ (Fig. 4-8 F-H). Some endothelial vessels were also distinguishable after 3 days in situ in the pre-cultured microbead condition. Black circles with a "B" next to them highlight microbeads in the implants. Black asterisks show mouse red blood cells, while black arrows point at blood vessels formed within the implants.

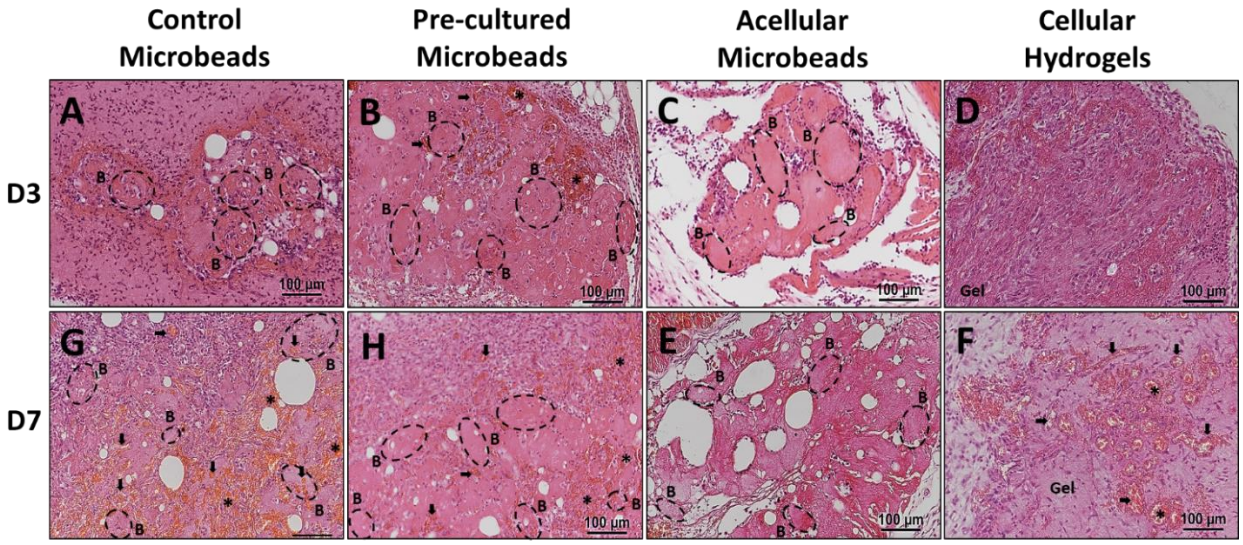

Figure 4-8: Hematoxylin and Eosin staining show vessel formation and cell infiltration in implants. Control microbeads (A, G), pre-cultured microbeads (B, H), acellular microbeads (C, E), and cellular hydrogels (D, F) were injected in the back of the mice for 3 days (A-D) and 7 days (E-H). Black dashed circles with a letter "B" highlight microbeads within the implants, black asterisks identify red blood cells within the implant regions, while black arrows show vessels. Scale bar – 100 µm.

4.3.5 Pre-cultured Microbeads Inosculate with the Host Vasculature

Pre-cultured microbeads were injected into the animal and extracted after 3 (Fig. 4-9 A-C) and 7 days (Fig. 4-9 D-G). The implant region was found by staining the samples with CD31 to locate the microbeads containing human endothelial cells (brown). Tissues were counter-stained

with hematoxylin and eosin to facilitate the visualization of the implant and the host cells and vasculature. Fig. 4-9A shows the implant region with the endothelial cells along with the mouse tissue and vasculature. The mouse vessels (white arrows) are not stained with anti-human CD31. This demonstrates that anti-human CD31 is only specific to human endothelial cells. A magnified image of the pre-cultured microbead implant (Fig. 4-9B) shows a vessel (white asterisk) characterized by a brown anti-human CD31 rim surrounding red blood cells (white asterisks).

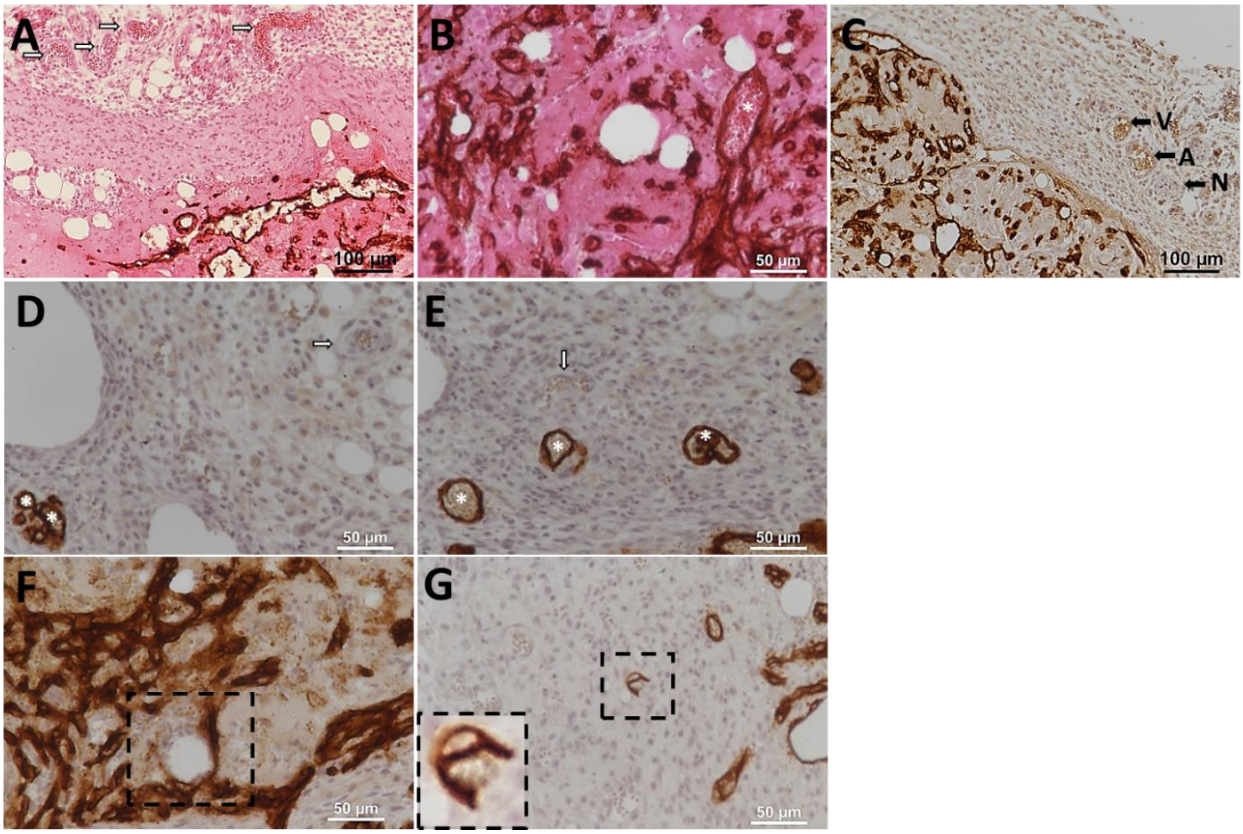

Figure 4-9: Pre-cultured microbeads injected in the animal for 3 and 7 days inosculate with the host vasculature and form endothelial vessels. Hematoxylin, eosin, and CD31 staining of D3 pre-cultured microbead implants and surrounding tissue 3 days (A-C) and 7 days (D-G) post-implantation. White arrows show mouse vasculature, white asterisks highlight regions of red blood cells, and black arrows display the mouse nerve, "N", artery, "A", and vein, "V", close to the microbead implant. Black rectangles show connections formed with mouse and human cells (F, G). The inset in G shows a magnified version of the chimeric vessel to demonstrate that there are red blood cells within the vessel containing both mouse and human endothelial cells.

Eosin staining is not necessary to locate the implant and the host tissue/ vasculature (Fig. 4-9C). In addition to the implant, the mouse vein "V", artery "A", and nerve "N" complex was found close to the implant (black arrows). Mouse and human endothelial vessels were found near each other after pre-cultured microbeads were in the host for 7 days (Fig. 4-9 D-E). Black rectangles (Fig. 4-9 F-G) show a connection between human endothelial cells (in brown) and mouse endothelial cells (not stained). A vessel formed from human and mouse endothelial cells with red blood cells was found in Fig. 4-9G (chimeric vessel). A magnified version of the rectangle is shown in the bottom left corner of the image as an inset to highlight the red blood cells (Fig. 4-9G).

4.3.6 Quantification of Vessel Density, Area, and Total Vessel Count

Average vessel quantification was done by staining samples with CD31 and hematoxylin (Fig. 4-10). Acellular microbeads (Fig. 4-10 A-D), cellular fibrin hydrogels (Fig. 4-10 E-H), control microbeads (Fig. 4-10 I-L), and pre-cultured microbeads (Fig. 4-10 M-P) were extracted 3 days (Fig. 4-10 A, B, E, F, I, J, M, N) and 7 days (Fig. 4-10C, D, G, H, K, L, O, P) after being injected in mice. The second (Fig. 4-10B, F, J, N) and fourth columns (Fig. 4-10 D, H, L, P) show magnified areas (40x) of the first and third column, respectively. No significant differences in the average vessel count per mm^2 (vessel density) were found between any cellular implant type at day 3 (Fig. 4-10Q) or day 7 (Fig. 4-10R).

Representative images of CD31 positive (+) areas were measured in control microbeads (Fig. 4-11A, D), pre-cultured microbeads (Fig. 4-11B, E), and cellular hydrogels (Fig. 4-11C, F). The differences in the average CD31+ area, mm^2, and the total number of vessels per implant area after 3 and 7 days are displayed in Fig. 4-11G and H. Control microbeads and fibrin hydrogels had

a similar CD31+ areas (Fig. 4-11G) and total number of vessels within these areas (Fig. 4-11I) after 3 days' post implantation. Whereas, pre-cultured microbeads had a wider CD31+ area and higher total number of vessels per selected implant area at the same time point. Statistical differences were found between pre-cultured microbeads and the other cellular conditions as well as the acellular microbeads ($p \leq 0.05$). After 7 days in the host, control microbeads (Fig. 4-11D) and pre-cultured microbeads (Fig. 4-11E) had similar CD31+ areas that were higher than both the acellular microbeads and cellular hydrogels (Fig. 4-11F). However, statistical differences in CD31+ area after 7 days were only found between the two cellular microbead conditions and the acellular one (Fig. 4-11H). In addition, statistical differences in number of vessels per implant area, at day 7, were only found between the control microbeads and the acellular microbeads (Fig. 4-11J).

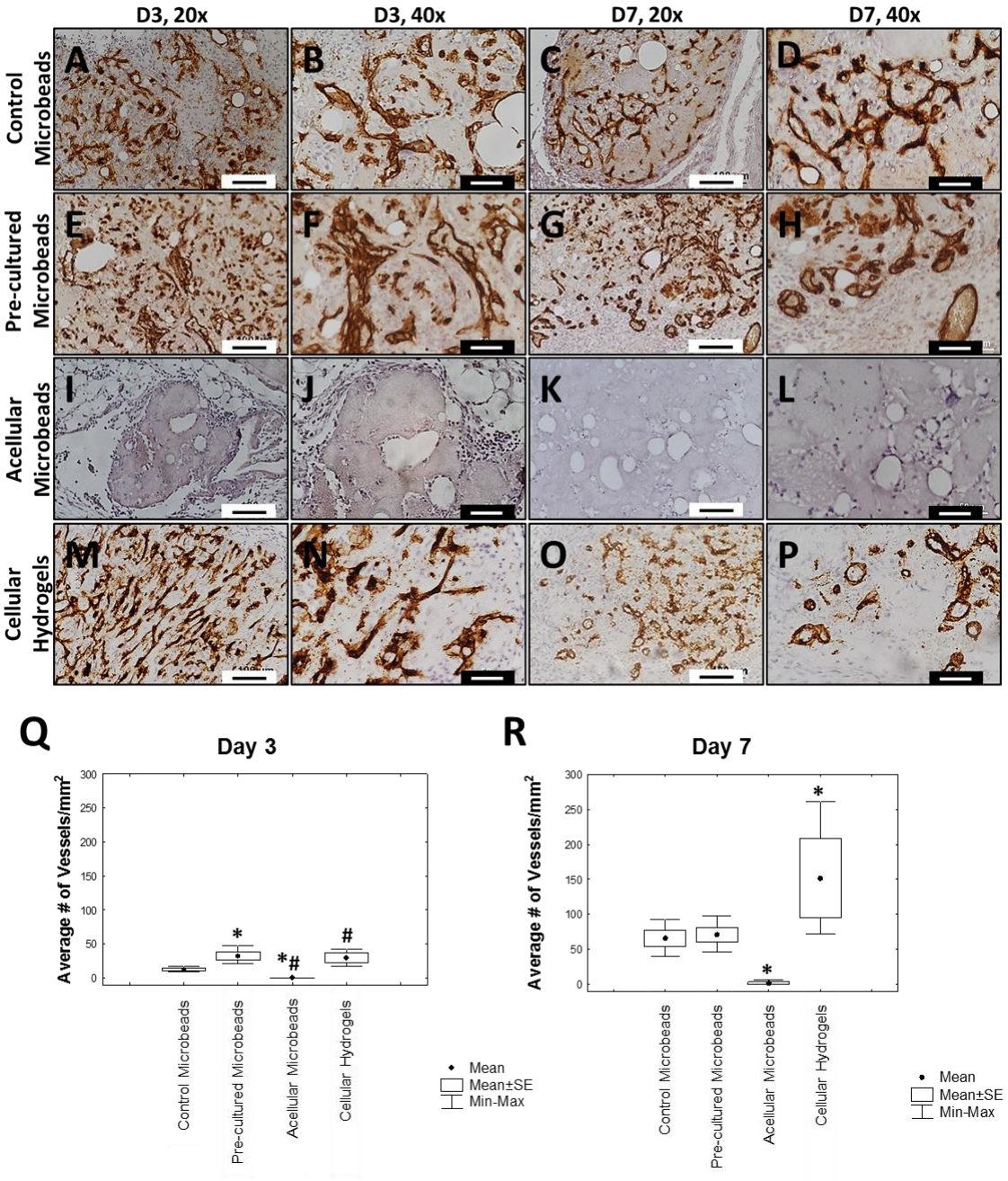

Figure 4-10: No significant differences were found in the average number of vessels per area between any of the implants that contained human endothelial cells after 3 and 7 days after injection. Control microbeads (A-D), pre-cultured microbeads (E-H), acellular microbeads (I-L), and cellular hydrogels (M-P) were injected in the back of mice for 3 days (A, B, E, F, I, J, M, N) and 7 days (C, D, G, H, K, L, O, P) and stained with CD31. Human endothelial cells were found (brown) within all implants except for acellular microbeads. Quantification of endothelial vessels for each condition after 3 days (Q) and 7 days (R) is displayed in rectangular plots. The average is shown in black dots, the standard error is highlighted by the bottom and top of the rectangles, and the min and max points are displayed with the whiskers. No differences between cellular conditions were found at day 3 or day 7. Scale bar – 100 µm (20x images) and 50 µm (40x images).

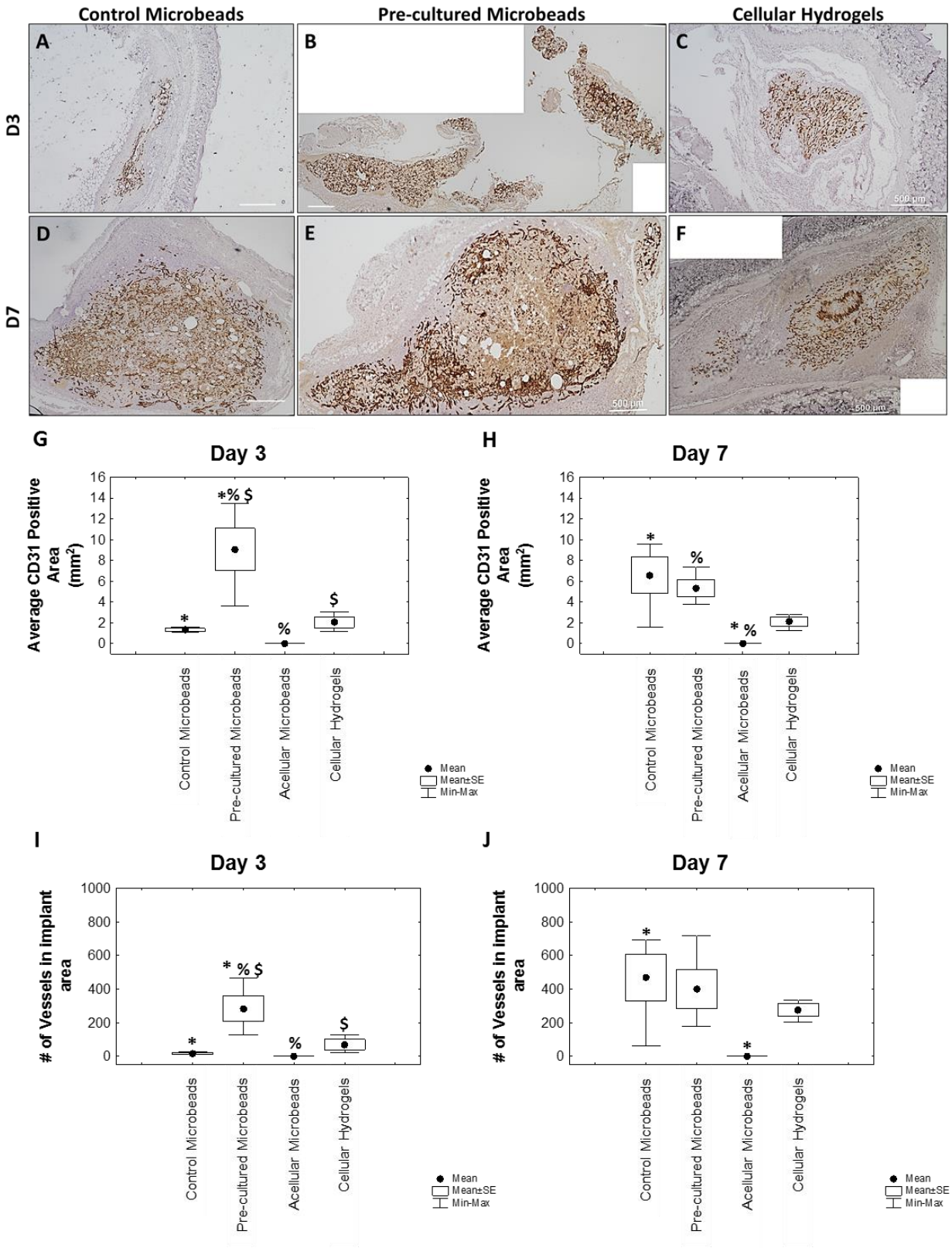

Figure 4-11: Pre-cultured microbeads, on average, had a bigger implant area and higher number of vessels in implant than other cellular conditions. Representative images of entire implant areas were taken (A-F). Control microbeads

(A, D), pre-cultured microbeads (B, E), and cellular hydrogels (C, F) were left in the animal for 3 (A-C), and 7 days (D-F). All implants were labeled differently during experiment to avoid tissue processing bias. All tissues were excised and average implant areas were found after 3 days (G) and 7 days (H). Total numbers of vessels in selected implant areas were then calculated and displayed (I, J). After 3 days in subcutaneous model, D3 microbead implant size was found to be bigger than the other conditions. The total number of vessels per implant was also higher in D3 microbead implants compared to control microbeads ($p = .04 < 0.05$) and cellular hydrogels ($p = 0.08 < 0.10$). No significant differences were found between implant areas or total number of vessels of D7 implants. The average is shown in black dots, the standard error is highlighted by the bottom and top of the rectangles, and the min and max points are displayed with the whiskers.

4.3.7 Vessel Maturity via Alpha-Smooth Muscle Actin Staining

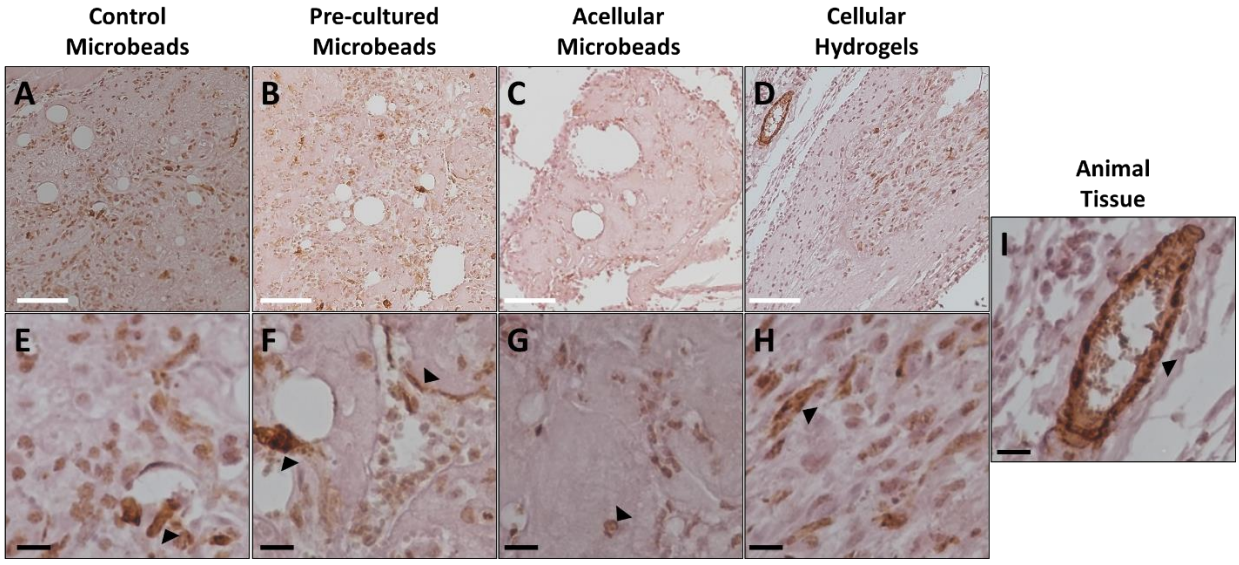

Figure 4-12: Alpha-smooth muscle actin staining (black arrows) in Day 3 (A,E) control microbeads, (B,F) pre-cultured microbeads, (C,G) acellular microbeads, (D,H) cellular hydrogels at (A-D) 10x and (E-I) 40x magnification. (I) Animal tissue with vessel surrounded by smooth muscle cells at 40x magnification. Black scale bar – 100 µm, and white scale bar – 50 µm.

Day 3 and 7 implants were stained with alpha-smooth muscle actin (α-SMA) antibody to assess the presence of smooth muscles within these implants. There was little to no presence of smooth muscle cells (α-SMA, brown stain with black arrows) within day 3 (Fig. 4-12A, E) control microbeads, (Fig. 4-12B, F) pre-cultured microbeads, (Fig. 4-12C, G) acellular microbeads, and (Fig. 4-12D, H) cellular hydrogels (Fig. 4-12). Images were magnified from (Fig. 4-12 A-D) 10x to (Fig. 4-12 E-I) 40x to highlight the stain. Positive α-SMA staining was observed in the outer

region of a vessel found outside of the cellular implant area, displayed at the top left corner of Fig. 4-12D, and magnified in Fig. 4-12I.

After an additional 4 days, 7-day (Fig. 4-13A, E) control microbeads, (Fig. 4-13B, F) pre-cultured microbeads, (Fig. 4-13 C, G) acellular microbeads, and (Fig. 4-13D, H) cellular hydrogels implants displayed a stronger α-SMA staining compared to day 3 (Fig. 4-12). Once again, 10x images (Fig. 4-13 A-D) were magnified (Fig. 4-13 E-H) to highlight the staining while black arrows indicated α-SMA positive regions within the implant. Pre-cultured microbeads (Fig. 4-13B, F) had the highest amount of stromal cell presence within their implant, followed by cellular hydrogels (Fig. 4-13D, H), and control microbeads (Fig. 4-13A, E). A weak α-SMA staining was found in some of the outer areas of the acellular microbeads (Fig. 4-13C, G).

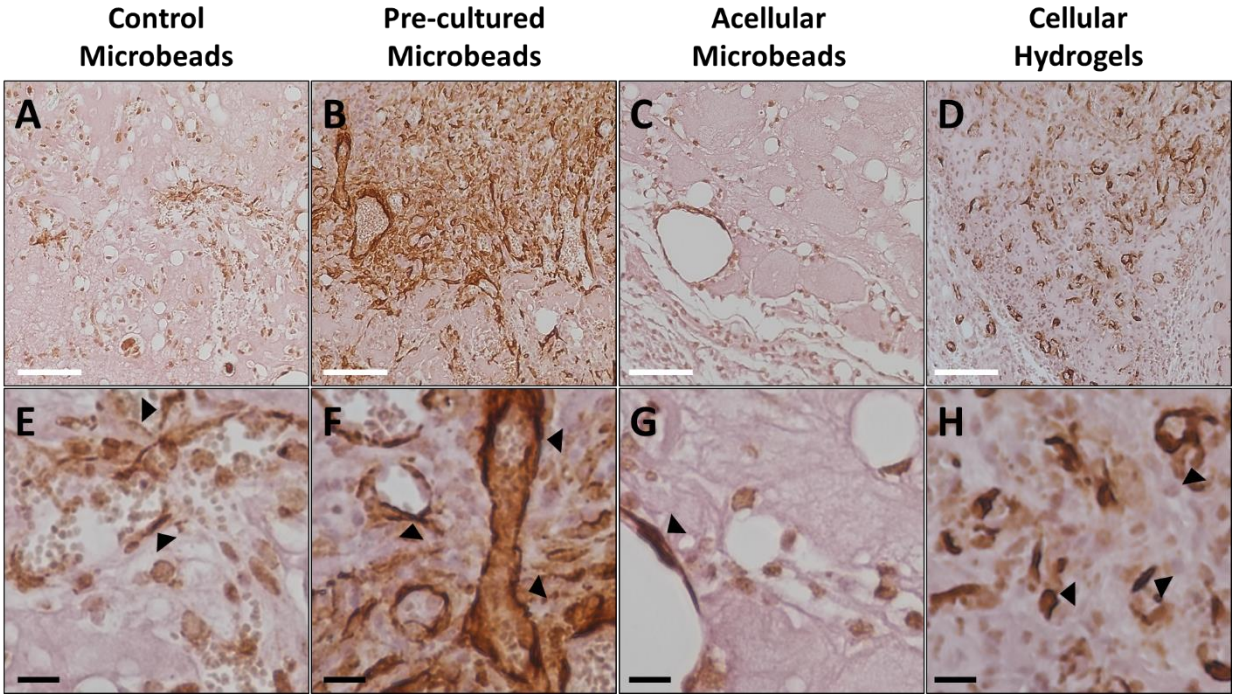

Figure 4-13: Day 7 (A, E) control microbeads, (B,F) pre-cultured microbeads, (C, G) acellular microbeads, (D,H) and cellular hydrogels containing smooth muscle cells (black arrows) around or inside the implant at (A-D) 10x and (E-H) 40x magnification. Black scale bar – 100 µm, and white scale bar – 50 µm.

4.3.8 *In Vitro* Mechanical Characterization of Implants

Volume Measurements (Implant Compaction)

In vitro implant volume was measured the day after implant production. There were no changes in volume of the fibrin gels containing the pre-cultured microbeads (Fig. 4-14A). The implant volumes of the control microbeads and cellular hydrogels were normalized to the pre-cultured volume and found to be lower. There was an approximately 0.17 relative decrease in the volume of control (not pre-cultured) microbeads (Fig. 4-14B) and 0.47 decrease in volume of cellular hydrogel implants (Fig. 4-14C), compared to the pre-cultured microbeads. All volumes were found to be statistically different from one another (Fig. 4-14D).

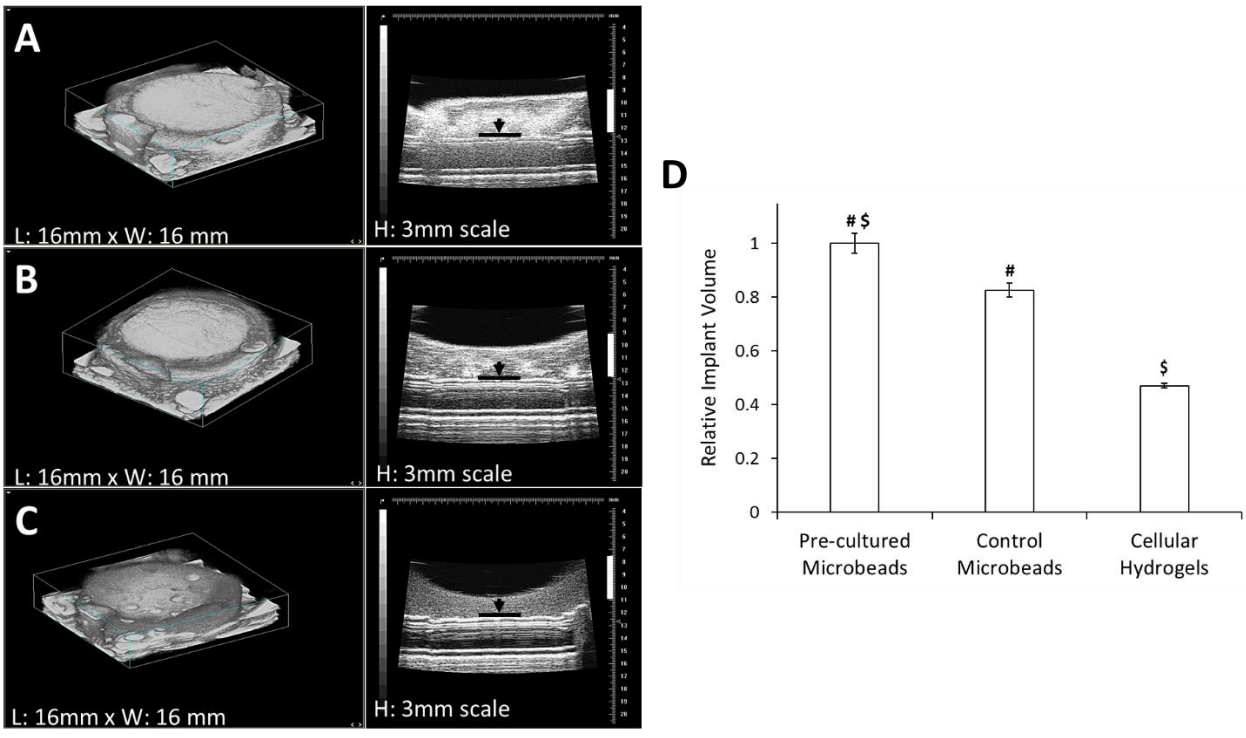

Figure 4-14: Pre-cultured microbeads implants don't compact after 1 day of *in vitro* culture. Ultrasound 3D images of pre-cultured microbeads (A), control microbeads (B), cellular hydrogels (C). Black lines and arrows show the bottom of the implant and 3 mm scale bars are displayed as white vertical lines. (D) Relative implant volume was calculated based on pre-cultured microbead implants which volumes were not altered after 24 hours of *in vitro* culture.

Implant Macro/Bulk Rheology Measurements

As cellular samples gelled, their shear moduli were measured. Acellular hydrogels were also measured and compared to previously collected data for measurement validation (data not shown). Fig. 4-15 shows the shear modulus versus time for implants during the gelation process. Cellular hydrogels had the highest shear modulus (G'), followed by the control microbeads, pre-cultured microbeads, and acellular hydrogels, which had the lowest shear modulus (Fig. 4-16). All implants were statistically different from each other, with the exception of the pre-cultured microbeads and acellular fibrin hydrogels (Fig. 4-16A).

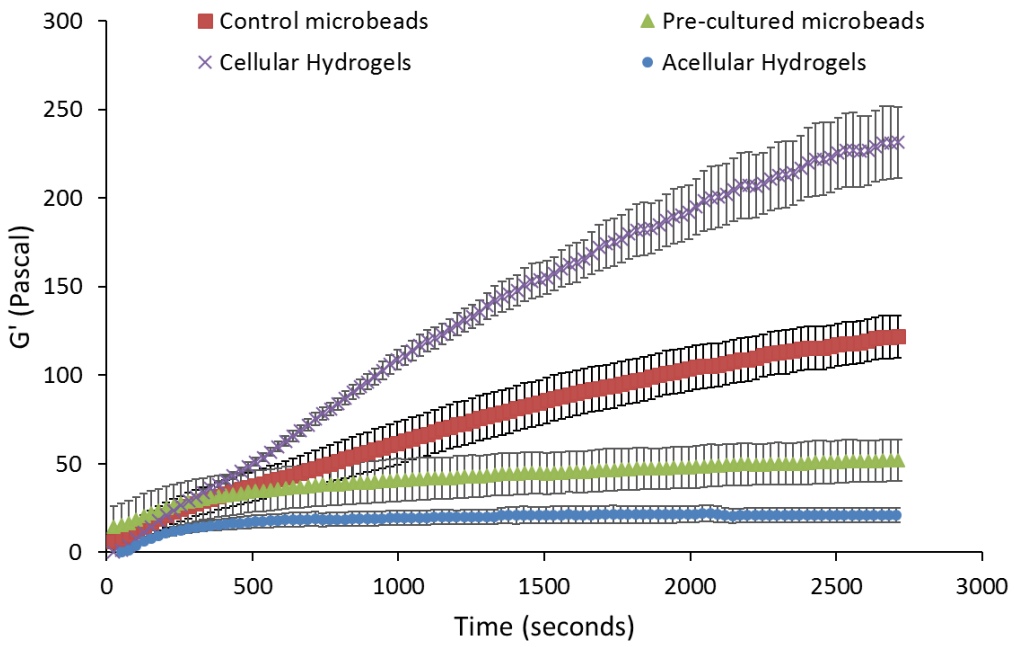

Figure 4-15: Addition of cells and cellular microbeads into fibrin hydrogels increases the implants' shear modulus (*in vitro* study). Cellular hydrogels and control microbeads have a higher shear modulus (G', Pascal) than acellular fibrin hydrogels (control microbeads>cellular hydrogels>acellular hydrogels). Pre-culturing the microbeads decreases the shear modulus, lower than both control microbeads and cellular hydrogels. Graph shows average and standard error of the mean.

The shear modulus of the implants left overnight increase, except for the cellular hydrogels (Fig. 4-16). However, the only statistical difference found after one day was the shear modulus of

control microbeads (Fig. 4-16). The shear modulus of the pre-cultured microbeads was also higher when the implants were left overnight, but not statistically different.

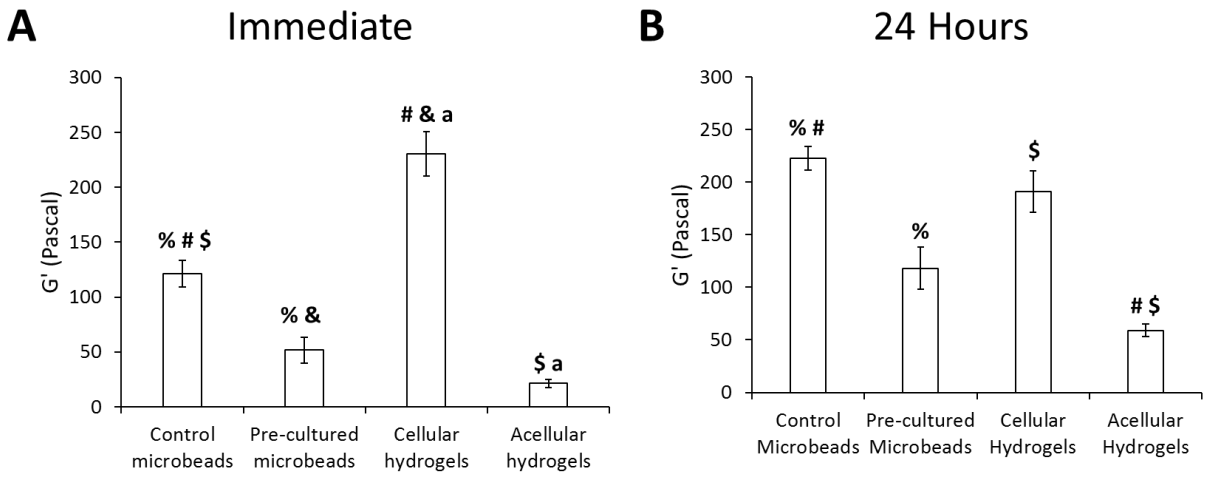

Figure 4-16: Shear modulus of all implants, except of cellular hydrogels, increased when left in-culture overnight. Shear modulus of all the cellular implants and acellular hydrogels were found immediately during their gelation (A) or after being in-culture overnight (B).

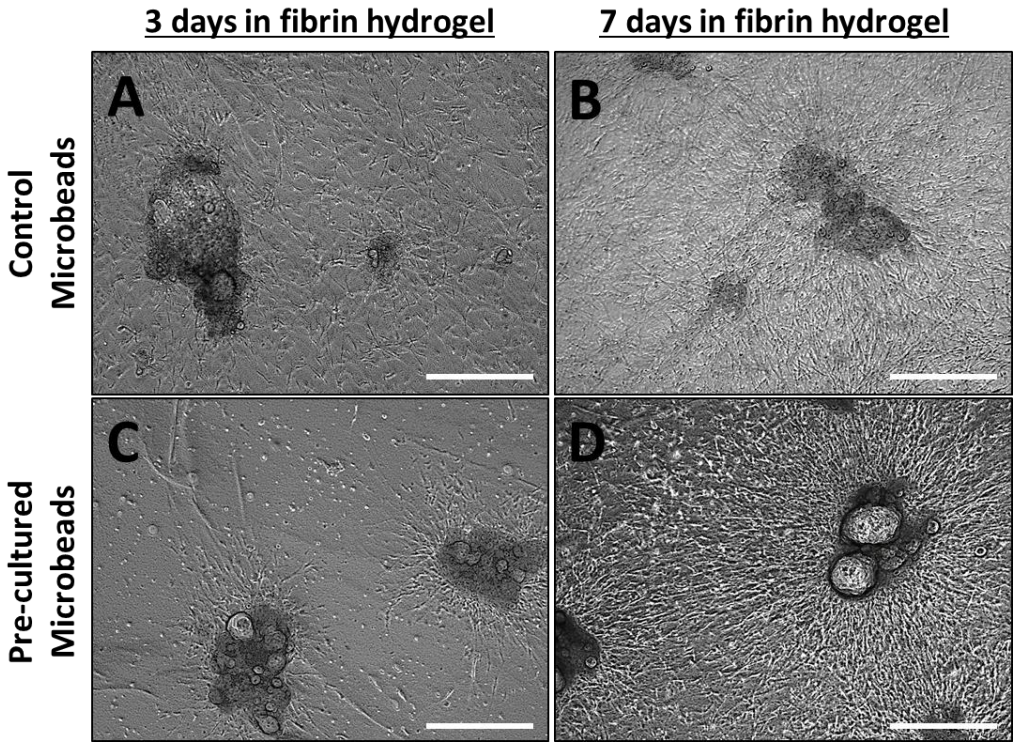

Figure 4-17: Cells migrate from microbeads into fibrin hydrogels. Bright-field images of control (A,B) and pre-cultured (C,D) microbeads ($3x10^6$ total cells/mL - initial cell density) embedded in fibrin hydrogels for 3 (A,C) and 7 days (B,D). Scale bar – 500 µm.

Control and pre-cultured microbeads were embedded in fibrin hydrogel for 3 and 7 days. Cells encapsulated in the acellular hydrogel begin to move out of the microbeads into the hydrogels. The bright-field images show that fewer cells are coming out of the pre-cultured microbeads than the control microbeads (Fig. 4-17). This observation is more clear when microbeads are left in the fibrin hydrogels for 3 days (Fig. 4-17A, C) rather than 7 days (Fig. 4-17B, D) since there is less time for cells to remodel the matrix.

For these observations, a lower initial cell density ($2x10^6$ cells/mL of microbead volume) was used to enhance visible differences in the number of migrated cells. At the higher density used for the implants ($5x10^6$ cells/mL of microbead volume), the fibrin hydrogel was crowded in all cases, and migration differences were obscured (data not shown).

Microscale Implant Characterization

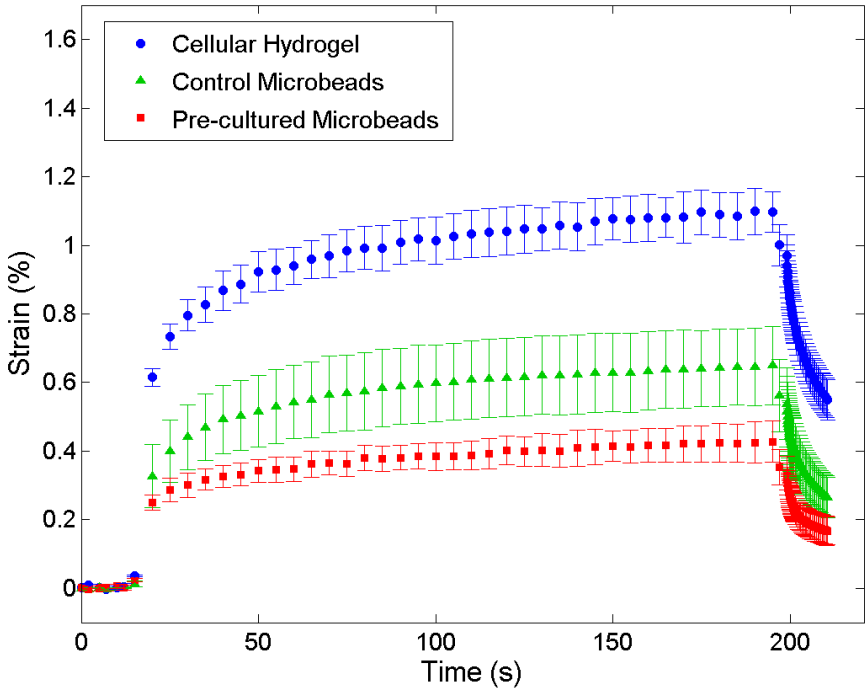

Figure 4-18: Pre-cultured microbeads had lower strain % compared to both control microbeads and cellular hydrogels.

To determine what the cells can sense within a region of the implant, regional mechanical measurements were taken using the dual-mode ultrasound elastography (DUE). This technique allows for surface deformation measurements within the microbead and hydrogel interface, rather than the entire deformation measured with the rheometer. Strain % versus time of the cellular implants are shown in Fig. 4-18. The strain was highest in the implants containing cells only (cellular hydrogels), followed by the control microbeads, and the lowest being the pre-cultured microbeads.

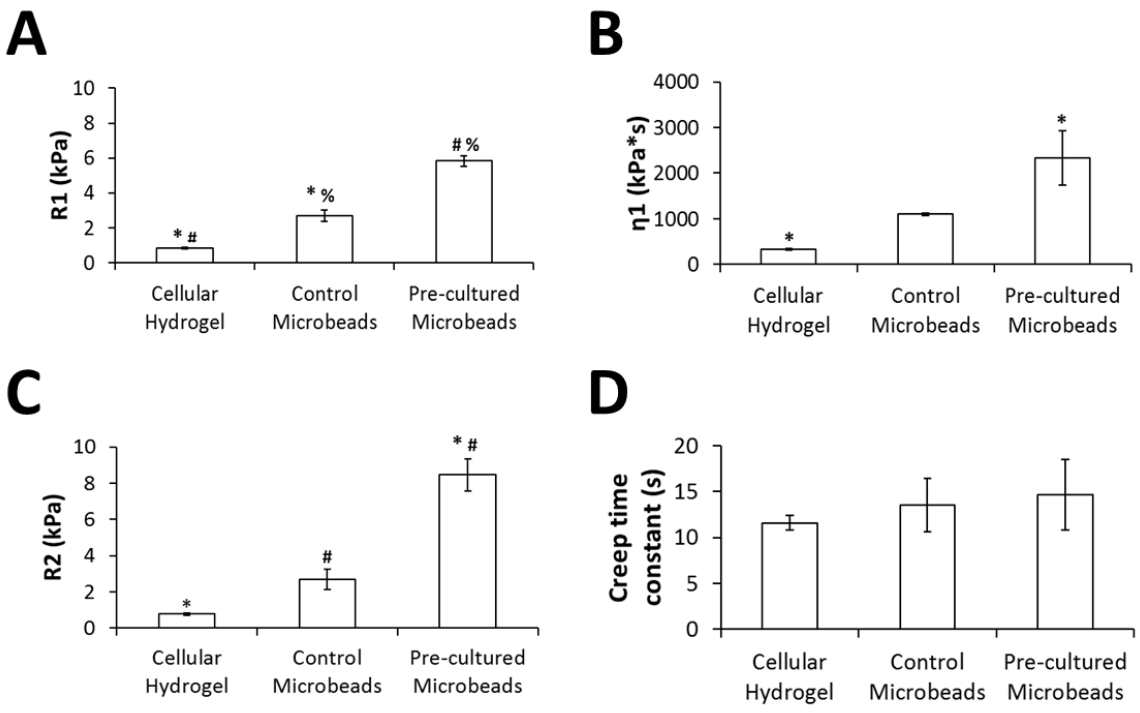

Figure 4-19: Parameters of implants calculated using the Burger's Viscoelastic model. (A) R_1, (B) η_1, (C) R_2, and (D) the creep time constant (η_2/R_2).

The immediate elastic response of the material to stress is controlled by the elastic modulus R_1. Therefore, a stiffer material has a bigger R_1, and a smaller strain results. Pre-cultured

microbeads have the highest R_1, followed by control microbeads and cellular hydrogels with the lowest R_1 value (Fig. 4-19A).

The viscous damping parameter in the Burger's model, η_1, was higher in the pre-cultured microbeads than the other two cellular implants (Fig. 4-19B). This parameter is theoretically the zero-shear viscosity (viscosity for a very weak stress), and it controls the rate of plastic (non-recoverable) deformation in creep. The larger the value of η_1, the more viscous the material is. Pre-cultured microbeads seem to be more viscous than the control microbeads and the cellular hydrogels (statistically higher). R_2 is the retarded modulus and controls the long-term viscoelastic creep response. At long time, R_2 behaves like the stiffness R_1, but achieving the strain requires maintaining the stress long enough to overcome a viscous resistance. Once again, the pre-cultured microbeads had a statistically higher R_2 value than the control microbeads, and cellular hydrogels (Fig. 4-19C). The creep time constant, η_2/R_2, controls the rate of viscoelastic response. The smaller the time constant, the faster the material responds after the immediate strain [46]. No statistical differences were found between the creep time constants of the three cellular implants (Fig. 4-19D).

4.4 Discussion

Although current tissue engineering approaches including *in vivo* and *in vitro* pre-vascularization techniques have potential to re-vascularize ischemic regions, open surgery is still required to implant the pre-vascularized tissue in the injured site. Unfortunately, CLI patients who suffer from other chronic diseases such as diabetes may be ineligible for open surgery due to additional complications. Therefore, it is important to develop an alternative solution to re-vascularize ischemic regions without the need of major surgery.

Modular vascular tissue engineering approaches may provide an alternative path to open surgery, since these microtissues can be injected via syringe. The microtissue approach meets the requirements and flexibility of macro tissues such as being developed with different cell types, densities, and biomaterials; and they permit sprout formation and/or blood perfusion. In addition, these modular microtissues are scalable and moldable into different vascularized constructs. [31-33, 50]

Even though modular microtissues with an exterior coating of endothelial cells have shown vascular potential *in vitro* and *in vivo* [51], we sought to pre-vascularize microtissues by encapsulating cells within a matrix. We encapsulated HUVECs and NHLFs in a 1:1 ratio in fibrin microbeads to form vessels within the microtissues via pre-culture, to allow for minimally invasive delivery via injection, and to inosculate with the host vasculature. Fibrin was employed because it improves cell survival during injection [42], and it promotes wound healing and endothelial sprout formation in particular [25, 52]. Additionally, fibrin structure, permeability, clotting rate, and polymerization rate can be modified [53, 54], making it an ideal material for microtissue development.

Endothelial sprouting occurred after control microbeads (freshly made, D0) were embedded in a fibrin matrix and cultured for one to two weeks *in vitro*. Cells encapsulated in fibrin microbeads formed vessels in static pre-culture for up to 7 days without the need of embedding them in an additional fibrin matrix. And once embedded, like control microbeads, endothelial sprouts from adjacent pre-cultured microbeads also formed connections with each other within the fibrin matrix *in vitro*.

Pre-culture time was investigated by quantifying the percent area covered by endothelial tubules in a model tissue. Microbeads were pre-cultured for 1, 3, 5, and 7 days prior to being

embedded in acellular fibrin hydrogels. The percent tube coverage area was greatest with 3 days of microbead pre-culture time; longer pre-culture times led to lower tube area coverage, which could be due to aggregation of microbeads, causing a more localized and less homogenous microbead distribution within the fibrin hydrogel (see Chapter 5).

Microbeads and/or cells (control microbeads, pre-cultured microbeads, acellular microbeads, and cells) were delivered with a mixture of fibrin precursor, FBS, and thrombin into the animal. Blood perfusion within the resulting implants was measured using LDPI immediately after implantation and prior to implant removal (days 3 and 7). The results from this technique were not accurate when compared to the histological data. This could be because the implants are surrounded by vascularized host tissue, and they compact differently, making it difficult to track their locations with time and obtain accurate blood perfusion readings.

The implant regions were excised, embedded in paraffin, and sectioned 3 and 7 days after implant injections. Samples were then stained with hematoxylin and eosin to locate the implants within the host tissue embedded in the paraffin blocks. Host cell infiltration was observed in all cellular and acellular implants. Anti-human CD31 staining was then used to identify the implanted human endothelial cells and distinguish them from mouse ECs. Both human and mouse vessels were found within the implant region, corroborating the specificity of the antibody due to the lack of cross-reactivity with mouse endothelial cells. Red blood cells found in the lumens formed by human endothelial cells demonstrate that inosculation occurred between the host vessels and the human vessels within the implant area.

There were no statistical differences in number of vessels/mm^2 of the cellular implants at day 3 or day 7. The cellular hydrogels had a higher average number of vessels/mm^2 than the two microbead types at day 7, but a wider variability between each sample, unlike the control and pre-

cultured microbeads. The average CD31+ area of each implant gave a measure of total vessel coverage within an implant section. Three days after implant injections, the pre-cultured microbeads had a statistically larger vessel coverage compared to the other cellular implants and the acellular microbeads. The vessel coverage area of the control microbeads increased when the implants were kept in the animal for an additional 4 days (7 days total). This area was similar to the area of the pre-cultured microbead implant at the same time point. Cellular hydrogel CD31+ area was also smaller than the pre-cultured microbeads on day 3 and did not increase by day 7, suggesting that cellular hydrogels compacted.

The cellular hydrogel implant had both small CD31+ area and the highest number of vessels/mm^2, suggesting that compaction increased vessel density. An increase in number of lumens/mm^2 due to compaction has been previously observed in an *in vitro* model developed by Morin et al. [14]. In addition, the CD31+ area data suggests that implants containing microbeads did not compact as much as the cellular hydrogels, especially if pre-cultured prior to being embedded. Despite having the highest number of vessels/mm^2, the cellular hydrogel did not have the highest total number of vessels.

The CD31+ area (mm^2) was multiplied by the number of vessels/mm^2 to approximate the total number of vessels found within the implant at days 3 and 7. The total number of vessels in the cellular hydrogels was lower than the number of vessels found in the pre-cultured microbead implant. However, the control microbeads had the lowest total vessel number as it had a low average number of vessels/mm^2 and the smallest CD31+ area. When the implants were kept for an additional 4 days (day 7), the total number of vessels within the control microbead implant was similar to that of the pre-cultured microbead implant at day 3. This suggests that it takes 4

additional days for the endothelial cells in the control microbead implant to form as many vessels as the pre-cultured microbeads.

Many factors characterize vessel maturity and functionality including the expression of physiological markers and the presence of perivascular mural cells [55]. The presence of smooth muscle cells in the outer regions of the vessel is particularly linked to vessel maturity [56-58]. Therefore, day 3 and day 7 implants were stained with α-SMA to determine the maturity of the vessels within the implant. At day 3, mature vessels were found in the mouse tissue while the cellular implants contained some weak α-SMA expression. On the other hand, the cellular implants after 7 days in the host displayed a higher expression of α-SMA. However, it appeared that smooth muscle cells presence was higher in the outer regions of the implants and lower in the center (data not shown). Overall, pre-cultured microbeads had a higher α-SMA expression than all the other implants, suggesting that more mature vessels form in the pre-cultured microbeads condition.

To characterize the compaction observed in implants *in vivo*, an ultrasound analysis was employed on implants cultured *in vitro*. Rather than injecting the implants into the animals, the same implant volume was pipetted into a cylindrical container, gelled at 37 °C, and left in culture overnight with media. A similar trend to *in vivo* implant compaction was found *in vitro*. Pre-cultured microbead implants did not compact compared to an approximate 20% compaction in the control microbeads and ~50% compaction of cellular hydrogel implant relative to the pre-cultured microbead implants. Implants containing pre-cultured microbeads appeared to be denser than other materials based on the higher attenuation displayed in the ultrasound image of pre-cultured microbeads relative to the other constructs.

The stiffness of each implant, during gelation and 24 hours after gelation, was measured using the rheometer. During the gelation process, the implants' shear moduli were found to be

positively correlated with the implant compaction. The cellular hydrogels which had compacted the most over 24 hours had a higher shear modulus, while pre-cultured microbeads had less compaction and lower shear modulus. Control microbeads were between the two conditions in both compaction and shear modulus. However, when the implants' shear moduli were measured after 24 hours, the positive correlation with implant compaction no longer existed; control microbead implants became as stiff as cellular hydrogels and stiffer than pre-cultured microbead implants. The cellular hydrogel implant's shear modulus did not vary during the 24 hours. In addition, the shear moduli of both the acellular hydrogel and pre-cultured microbeads were not statistically different.

Our lab has observed that the addition of cells to the fibrin hydrogel increases the shear modulus of the hydrogel (data not shown). This suggests that cells encapsulated in the pre-cultured microbeads may take longer to infiltrate the remaining fibrin hydrogel than the ones residing in the control microbeads. This idea agrees with observations of slower cell migration from pre-cultured microbeads after 3-day and 7-day embedding in the fibrin hydrogels.

Since the microbeads embedded in the fibrin hydrogel make up about 25% of the entire implant volume, the stiffnesses of the microbeads/fibrin regions were measured to determine if they were different from the overall implant stiffness. Regional mechanical measurements were taken with dual-mode ultrasound elastography to determine the stiffness in the microbead/hydrogel area. The areas with pre-cultured microbeads in fibrin were found to be stiffer and more viscous than both areas with control microbeads and also homogeneous cellular hydrogel.

We found that nattokinase, which degrades fibrin, could not degrade the fibrin microbeads after 3 days of pre-culture. Therefore, cells may be remodeling the microbeads and secreting additional matrix during pre-culture. This cellular remodeling of the pre-cultured microbeads may

compact, densify (based on ultrasound images), and stiffen the microbeads. Previous studies have shown that cell migration and matrix remodeling are dependent on material properties including ECM density and stiffness [59-62]. Likewise, the encapsulation of cells within stiffer/denser pre-cultured microbeads may slow down further cell remodeling and migration into the remaining fibrin hydrogel compared to control microbeads and homogeneous cellular hydrogels.

4.5 Conclusion

This study demonstrated that pre-cultured microbeads embedded in fibrin hydrogels provide a wider implant area with a higher number of vessels, prevent further implant compaction upon implantation, and improve vessel quality compared to other cellular implants. By encapsulating HUVECs and NHLFs in fibrin microbeads, vessel formation within the microtissues can occur if pre-cultured statically, prior to injection. This is particularly important for future studies that will investigate the re-vascularization potential of the pre-cultured microbeads in ischemic regions, since cell survival time may be limited by the lack of oxygen and nutrients in the injection site of ischemic tissues [41]. Whereas immature cells might not survive long enough to form vessels from scratch, these pre-cultured microbeads could jump-start inosculation with pre-formed vessels to rapidly supply oxygen and nutrients for cellular implant survival.

4.6 References

1. Kullo, I.J. and T.W. Rooke, *Peripheral artery disease.* New England Journal of Medicine, 2016. **374**(9): p. 861-871.

2. Fowkes, F.G., et al., *Comparison of global estimates of prevalence and risk factors for peripheral artery disease in 2000 and 2010: a systematic review and analysis.* Lancet, 2013. **382**(9901): p. 1329-40.

3. Marso, S.P. and W.R. Hiatt, *Peripheral arterial disease in patients with diabetes.* J Am Coll Cardiol, 2006. **47**(5): p. 921-9.

4. Dillingham, T.R., L.E. Pezzin, and E.J. MacKenzie, *Limb amputation and limb deficiency: epidemiology and recent trends in the United States.* South Med J, 2002. **95**(8): p. 875-83.

5. Moxey, P.W., et al., *Lower extremity amputations--a review of global variability in incidence.* Diabet Med, 2011. **28**(10): p. 1144-53.

6. Jude, E.B., et al., *Peripheral arterial disease in diabetic and nondiabetic patients: a comparison of severity and outcome.* Diabetes Care, 2001. **24**(8): p. 1433-7.

7. Vartanian, S.M. and M.S. Conte, *Surgical intervention for peripheral arterial disease.* Circ Res, 2015. **116**(9): p. 1614-28.

8. Shepherd, B.R., J.B. Hoying, and S.K. Williams, *Microvascular transplantation after acute myocardial infarction.* Tissue Eng, 2007. **13**(12): p. 2871-9.

9. Sakakibara, Y., et al., *Prevascularization with gelatin microspheres containing basic fibroblast growth factor enhances the benefits of cardiomyocyte transplantation.* J Thorac Cardiovasc Surg, 2002. **124**(1): p. 50-6.

10. Lind, B., et al., *Arteriovenous loop grafts for free tissue transfer.* Vascular and endovascular surgery, 2012. **46**(1): p. 30-33.

11. Rouwkema, J., N.C. Rivron, and C.A. van Blitterswijk, *Vascularization in tissue engineering.* Trends in biotechnology, 2008. **26**(8): p. 434-441.

12. Chen, X., et al., *Rapid anastomosis of endothelial progenitor cell-derived vessels with host vasculature is promoted by a high density of cotransplanted fibroblasts.* Tissue Eng Part A, 2010. **16**(2): p. 585-94.

13. Chen, X., et al., *Prevascularization of a fibrin-based tissue construct accelerates the formation of functional anastomosis with host vasculature.* Tissue Engineering Part A, 2008. **15**(6): p. 1363-1371.

14. Morin, K.T., J.L. Dries-Devlin, and R.T. Tranquillo, *Engineered microvessels with strong alignment and high lumen density via cell-induced fibrin gel compaction and interstitial flow.* Tissue Engineering Part A, 2013. **20**(3-4): p. 553-565.

15. Riemenschneider, S.B., et al., *Inosculation and perfusion of pre-vascularized tissue patches containing aligned human microvessels after myocardial infarction.* Biomaterials, 2016. **97**: p. 51-61.

16. Tian, L. and S.C. George, *Biomaterials to prevascularize engineered tissues.* Journal of cardiovascular translational research, 2011. **4**(5): p. 685.

17. Kirkpatrick, C.J., S. Fuchs, and R.E. Unger, *Co-culture systems for vascularization--learning from nature.* Adv Drug Deliv Rev, 2011. **63**(4-5): p. 291-9.

18. Au, P., et al., *Differential in vivo potential of endothelial progenitor cells from human umbilical cord blood and adult peripheral blood to form functional long-lasting vessels.* Blood, 2008. **111**(3): p. 1302-1305.

19. Merfeld-Clauss, S., et al., *Adipose tissue progenitor cells directly interact with endothelial cells to induce vascular network formation.* Tissue Eng Part A, 2010. **16**(9): p. 2953-66.

20. Shepherd, B.R., et al., *Human aortic smooth muscle cells promote arteriole formation by coengrafted endothelial cells.* Tissue Eng Part A, 2009. **15**(1): p. 165-73.

21. Nakatsu, M.N., et al., *Angiogenic sprouting and capillary lumen formation modeled by human umbilical vein endothelial cells (HUVEC) in fibrin gels: the role of fibroblasts and Angiopoietin-1 ☆.* Microvascular Research, 2003. **66**(2): p. 102-112.

22. Montesano, R., M.S. Pepper, and L. Orci, *Paracrine induction of angiogenesis in vitro by Swiss 3T3 fibroblasts.* J Cell Sci, 1993. **105 (Pt 4)**: p. 1013-24.

23. Thompson, H.G., et al., *A three-dimensional in vitro model of angiogenesis in the airway mucosa.* Pulmonary Pharmacology & Therapeutics, 2007. **20**(2): p. 141-148.

24. Ghajar, C.M., et al., *The effect of matrix density on the regulation of 3-D capillary morphogenesis.* Biophys J, 2008. **94**(5): p. 1930-41.

25. Rioja, A.Y., et al., *Endothelial sprouting and network formation in collagen- and fibrin-based modular microbeads.* Acta Biomater, 2016. **29**: p. 33-41.

26. Rao, R.R., et al., *Matrix composition regulates three-dimensional network formation by endothelial cells and mesenchymal stem cells in collagen/fibrin materials.* Angiogenesis, 2012. **15**(2): p. 253-64.

27. Dean, D.M., et al., *Rods, tori, and honeycombs: the directed self-assembly of microtissues with prescribed microscale geometries.* FASEB J, 2007. **21**(14): p. 4005-12.

28. Dean, D.M. and J.R. Morgan, *Cytoskeletal-mediated tension modulates the directed self-assembly of microtissues.* Tissue Eng Part A, 2008. **14**(12): p. 1989-97.

29. Dean, D.M., A.P. Rago, and J.R. Morgan, *Fibroblast elongation and dendritic extensions in constrained versus unconstrained microtissues.* Cell Motil Cytoskeleton, 2009. **66**(3): p. 129-41.

30. Youssef, J., et al., *Quantification of the forces driving self-assembly of three-dimensional microtissues.* Proc Natl Acad Sci U S A, 2011. **108**(17): p. 6993-8.

31. McGuigan, A.P. and M.V. Sefton, *Vascularized organoid engineered by modular assembly enables blood perfusion.* Proceedings of the National Academy of Sciences, 2006. **103**(31): p. 11461-11466.

32. Kelm, J.M., et al., *Design of custom-shaped vascularized tissues using microtissue spheroids as minimal building units.* Tissue engineering, 2006. **12**(8): p. 2151-2160.

33. Gupta, R. and M.V. Sefton, *Application of an endothelialized modular construct for islet transplantation in syngeneic and allogeneic immunosuppressed rat models.* Tissue Eng Part A, 2011. **17**(15-16): p. 2005-15.

34. Cheng, H.W., et al., *In vitro generation of an osteochondral interface from mesenchymal stem cell-collagen microspheres.* Biomaterials, 2011. **32**(6): p. 1526-35.

35. Wang, L., R.R. Rao, and J.P. Stegemann, *Delivery of mesenchymal stem cells in chitosan/collagen microbeads for orthopedic tissue repair.* Cells Tissues Organs, 2013. **197**(5): p. 333-43.

36. Wise, J.K., et al., *Comparison of uncultured marrow mononuclear cells and culture-expanded mesenchymal stem cells in 3D collagen-chitosan microbeads for orthopedic tissue engineering.* Tissue Eng Part A, 2014. **20**(1-2): p. 210-24.

37. Leung, B.M., et al., *Fate of modular cardiac tissue constructs in a syngeneic rat model.* J Tissue Eng Regen Med, 2013.

38. Futrega K, P.J., Kinney M, Lott WB, Ungrin MD, Zandstra PW, Doran and MR, *The microwell-mesh: a novel device and protocol for the high throughput manufacturing of cartilage microtissues.* Biomaterials 2015.

39. Yen, C.-M., C.-C. Chan, and S.-J. Lin, *High-throughput reconstitution of epithelial–mesenchymal interaction in folliculoid microtissues by biomaterial-facilitated self-assembly of dissociated heterotypic adult cells.* Biomaterials, 2010. **31**(15): p. 4341-4352.

40. Daley, E.L., R.M. Coleman, and J.P. Stegemann, *Biomimetic microbeads containing a chondroitin sulfate/chitosan polyelectrolyte complex for cell-based cartilage therapy.* J Mater Chem B Mater Biol Med, 2015. **3**(40): p. 7920-7929.

41. Aguado, B.A., et al., *Improving viability of stem cells during syringe needle flow through the design of hydrogel cell carriers.* Tissue Eng Part A, 2012. **18**(7-8): p. 806-15.

42. Christman, K.L., et al., *Injectable fibrin scaffold improves cell transplant survival, reduces infarct expansion, and induces neovasculature formation in ischemic myocardium.* Journal of the American College of Cardiology, 2004. **44**(3): p. 654-660.

43. Carrion, B., et al., *A safe and efficient method to retrieve mesenchymal stem cells from three-dimensional fibrin gels.* Tissue Eng Part C Methods, 2014. **20**(3): p. 252-63.

44. Brown, M. and D.G. Lowe, *Automatic panoramic image stitching using invariant features.* International Journal of Computer Vision, 2007. **74**(1): p. 59-73.

45. Gudur, M.S.R., et al., *Noninvasive quantification of in vitro osteoblastic differentiation in 3D engineered tissue constructs using spectral ultrasound imaging.* PloS one, 2014. **9**(1): p. e85749.

46. Hong, X., J.P. Stegemann, and C.X. Deng, *Microscale characterization of the viscoelastic properties of hydrogel biomaterials using dual-mode ultrasound elastography.* Biomaterials, 2016. **88**: p. 12-24.

47. Berglund, J.D., R.M. Nerem, and A. Sambanis, *Viscoelastic testing methodologies for tissue engineered blood vessels.* Journal of biomechanical engineering, 2005. **127**(7): p. 1176-1184.

48. Dey, A. and P.K. Basudhar, *Parameter estimation of four-parameter viscoelastic Burger model by inverse analysis: case studies of four oil-refineries.* Interaction and Multiscale Mechanics, 2012. **5**(3): p. 211-228.

49. Rowe, S.L. and J.P. Stegemann, *Microstructure and Mechanics of Collagen-Fibrin Matrices Polymerized Using Ancrod Snake Venom Enzyme.* Journal of biomechanical engineering, 2009. **131**(6): p. 061012-061012.

50. Rioja, A.Y., et al., *Distributed Vasculogenesis from Modular Agarose-Hydroxyapatite-Fibrinogen Microbeads.* Acta Biomaterialia, 2017.

51. Chamberlain, M.D., R. Gupta, and M.V. Sefton, *Chimeric vessel tissue engineering driven by endothelialized modules in immunosuppressed Sprague-Dawley rats.* Tissue Engineering Part A, 2010. **17**(1-2): p. 151-160.

52. Ghajar, C.M., et al., *Mesenchymal stem cells enhance angiogenesis in mechanically viable prevascularized tissues via early matrix metalloproteinase upregulation.* Tissue engineering, 2006. **12**(10): p. 2875-2888.

53. Laurens, N., P. Koolwijk, and M.P. de Maat, *Fibrin structure and wound healing.* J Thromb Haemost, 2006. **4**(5): p. 932-9.

54. Ceccarelli, J. and A.J. Putnam, *Sculpting the blank slate: how fibrin's support of vascularization can inspire biomaterial design.* Acta biomaterialia, 2014. **10**(4): p. 1515-1523.

55. Nor, J.E., et al., *Engineering and characterization of functional human microvessels in immunodeficient mice.* Lab Invest, 2001. **81**(4): p. 453-63.

56. Nillesen, S.T.M., et al., *Increased angiogenesis and blood vessel maturation in acellular collagen–heparin scaffolds containing both FGF2 and VEGF*. Biomaterials, 2007. **28**(6): p. 1123-1131.

57. Taylor, A.P., et al., *Altered tumor vessel maturation and proliferation in placenta growth factor-producing tumors: potential relationship to post-therapy tumor angiogenesis and recurrence.* Int J Cancer, 2003. **105**(2): p. 158-64.

58. Risau, W., *Differentiation of endothelium.* FASEB J, 1995. **9**(10): p. 926-33.

59. Lu, P., et al., *Extracellular Matrix Degradation and Remodeling in Development and Disease.* Cold Spring Harbor perspectives in biology, 2011. **3**(12): p. 10.1101/cshperspect.a005058 a005058.

60. Rozario, T. and D.W. DeSimone, *The Extracellular Matrix In Development and Morphogenesis: A Dynamic View.* Developmental biology, 2010. **341**(1): p. 126-140.

61. Palecek, S.P., et al., *Integrin-ligand binding properties govern cell migration speed through cell-substratum adhesiveness.* Nature, 1997. **385**(6616): p. 537-40.

62. Swartz, D.D., J.A. Russell, and S.T. Andreadis, *Engineering of fibrin-based functional and implantable small-diameter blood vessels.* American Journal of Physiology - Heart and Circulatory Physiology, 2005. **288**(3): p. H1451-H1460.

CHAPTER 5

Alternative Microbead Development for Distributed Vasculogenesis

5.1 Introduction

Peripheral arterial disease (PAD) is caused by the obstruction/reduction of blood flow in the arteries due to atherosclerotic plaque formation. As PAD progresses, patients begin to experience pain in the limbs even at rest. This chronic and final stage of PAD, critical limb ischemia (CLI), can result in the loss of the affected limb due to ulceration or gangrene [1, 2]. Though CLI patients represent only 1% of all PAD sufferers, this condition is associated with significant rates of mortality (nearly 50% after 5 years) as well as a substantial economic burden [2].

CLI treatment involves restoration of blood flow to the extremities to prevent tissue necropathy and eventual amputation. While pharmaceutical options such as statin therapy are available to treat CLI [3], surgical interventions are sometimes employed if the patient is healthy enough for surgery. However, patients with medical co-morbidities may be poor candidates for highly invasive surgical procedures [2]. For these patients, it is advantageous to treat the ischemic tissue directly by repairing the microvasculature in a minimally invasive manner. Treating CLI in a more localized fashion may reduce ulceration and improve outcomes in diabetic patients.

Currently there is no specific treatment for the repair of damaged microvasculature that causes ulceration in CLI. However, by combining cells, growth factors and biomaterial scaffolds, a tissue engineering strategy offers a compelling and potentially minimally invasive means of promoting the repair of microvasculature in ischemic tissues. A variety of materials, cells, and growth factors have been employed to treat ulcers [4-6]. Modular tissue engineering offers a refinement of the tissue engineering strategy in which small scaffold "building blocks" can be generated and assembled into larger engineered constructs [7]. The use of engineered microtissues has been shown to reduce the oxygen and nutrient diffusion limitations that hamper larger constructs [8-13]. Moreover, microtissues can be designed to be delivered in a minimally invasive manner or assembled into macrostructures.

A key consideration when developing engineered vascular microtissues is enabling the establishment of vascularization *in vitro* prior to implantation. After implantation in an ischemic site, pre-vascularized microtissues could accelerate the restoration of the microvasculature by jump-starting anastomosis with blood vessels in the surrounding healthy tissue. In addition, pre-vascularization may also improve the survival of the cells within the construct. A variety of materials and cell populations can be employed to engineer microtissues, depending on the application [14-21]. For re-vascularization strategies, pure fibrin and composites made from fibrin, agarose, collagen, and gelatin have been used to develop engineered tissues capable of supporting endothelial vessel formation [22-25].

Past work by our group has shown that cell-encapsulating fibrin and collagen-fibrin microtissues can foster endothelial sprout formation and inosculation in a three-dimensional (3D) *in vitro* model [25, 26]. In particular, we have used co-cultures of endothelial cells and stromal cells to promote vessel formation in engineered tissues. Paracrine signals provided by fibroblasts

or other stromal cells are important in the formation and stabilization of endothelial cell networks [23, 27-33]. *In vitro* studies have shown that endothelial sprout length is dependent on a variety of conditions, including extracellular matrix properties and stromal cell type [23, 25, 34].

In the present study, we build upon our previous work by developing microtissues designed to promote widespread vascular network formation, using a defined combination of naturally-derived, biomimetic biomaterials. Agarose is a relatively inert polysaccharide used in a variety of tissue engineering applications for structural support [21, 35]. It does not permit cell attachment, and therefore is often used in combination with other materials that facilitate cell adhesion and proliferation [36-38]. Hydroxyapatite (HA) is a main component of mineralized biological tissues that has been shown to adsorb and retain proteins [39-41], and may also promote vasculogenesis [42-44]. Fibrinogen (FGN) is a circulating precursor of the blood clotting protein fibrin, which is known to bind growth factors and proteins through its heparin-binding domain [45]. Incorporation of HA and FGN into agarose microtissues therefore provides a mechanically robust environment with the ability to sequester proteins and provide sites for cell attachment. Our goal was to combine these materials to create novel "microbeads" that exhibit: 1) higher production yield through a reduction in adhesion and aggregation, 2) improved injectability through reduced size and increased sphericity, and 3) more widespread vascular network formation via inosculation between sprouts from neighboring microbeads.

5.2 Materials and Methods

5.2.1 Cell Culture

Human umbilical vein endothelial cells (HUVECs) from two different sources were used in these studies. For microbead characterization experiments, HUVECs were isolated from

umbilical cords obtained via an IRB-exempt process from the University of Michigan Mott Children's Hospital using previously described methodology [34]. Umbilical cords were rinsed with phosphate buffer saline (PBS) prior to digestion. Collagenase type I solution (195 U/mL, Worthington Biochemical, Lakewood, NJ) was utilized to digest cords for 20 minutes at 37 °C. Digested tissues were rinsed with PBS and centrifuged at 200 g for 5 minutes. HUVECs were plated in T25 flasks with endothelial growth media (EGM-2, Lonza). Flasks were rinsed with PBS three times, the next day, prior to media change. Additional media changes were done every 2 days. HUVECs from a commercial source (Lonza Inc, Walkersville, MD), were utilized for network length studies. We employed two different HUVECs sources to ensure the robustness of the observed phenomena independent of endothelial cell source. All experiments employed HUVECs from passages 4-7.

Normal human lung fibroblasts (NHLFs, Lonza Inc., Walkersville, MD) from passages 9-14 were cultured in Media 199 (M199, Life Technologies, Grand Island, NY) with 10% fetal bovine serum (FBS). Culture media of HUVECs and NHLFs were replaced every other day prior to experimental processing. EGM-2 is composed of 500 mL of endothelial basal medium, 10 mL of FBS (2% concentration), 0.5 mL of vascular endothelial growth factor (VEGF), 0.5 mL of gentamicin, amphotericin-B (GA-1000), 0.2 mL of human fibroblastic growth factor (hFGF-B), 0.5 mL of R3-IGF-1, 0.5 mL of ascorbic acid, 0.5 mL hydrocortisone, 0.5 mL of human epidermal growth factor (hEGF), and 2.0 mL of heparin. Component' concentrations are not provided by Lonza, Inc.

5.2.2 Production of Agarose-based Microbeads

Cell-encapsulating, agarose-based microbeads were produced using a water-in-oil emulsification process (Fig 5-1) [46]. Emulsification was carried out in autoclaved 100 cSt polydimethylsiloxane (PDMS) oil (Clearco Products Co. Inc. Bensalem, PA).

In preparation for microbead production, HUVECs and NHLFs were detached using 0.05% Trypsin-EDTA (Gibco), re-suspended in endothelial growth media (EGM-2), and counted using an automated cell counter (Multisizer 3, Beckman Coulter, Brea, CA). Fibrinogen (Sigma Aldrich, St. Louis MO) was dissolved in serum-free endothelial growth media (SFEGM-2) at 37 °C (4.0 mg/mL active clottable protein concentration), sterile filtered and kept on ice until ready for use. Agarose was warmed to 65 °C.

Microbeads components included HUVECs and NHLFs ($1x10^6$ of cell type per mL of aqueous components), agarose (8.0 mg/mL final concentration), fetal bovine serum (FBS), hydroxyapatite (HA), and fibrinogen (FGN). The components were loaded into a 10 mL syringe and injected into the PDMS through a 25-gauge needle. A two-paddle impeller stirred the mixture at 700 rpm for 6 min at 37 °C and then for 30 min on ice to gel the resulting microbeads. Previous work has shown that use of FBS acts as a surfactant that facilitates the separation of the beads from the oil phase during production, and also aids in maintaining high cell viability [17, 21].

After mixing, the microbeads were separated from the PDMS using three centrifugation and PBS wash steps. The microbeads were then re-suspended in EGM-2 and cultured in 15 mL vented conical tubes (CELLTREAT Scientific Products, Shirley, MA). Media of constructs was changed the day after preparation and every other day after.

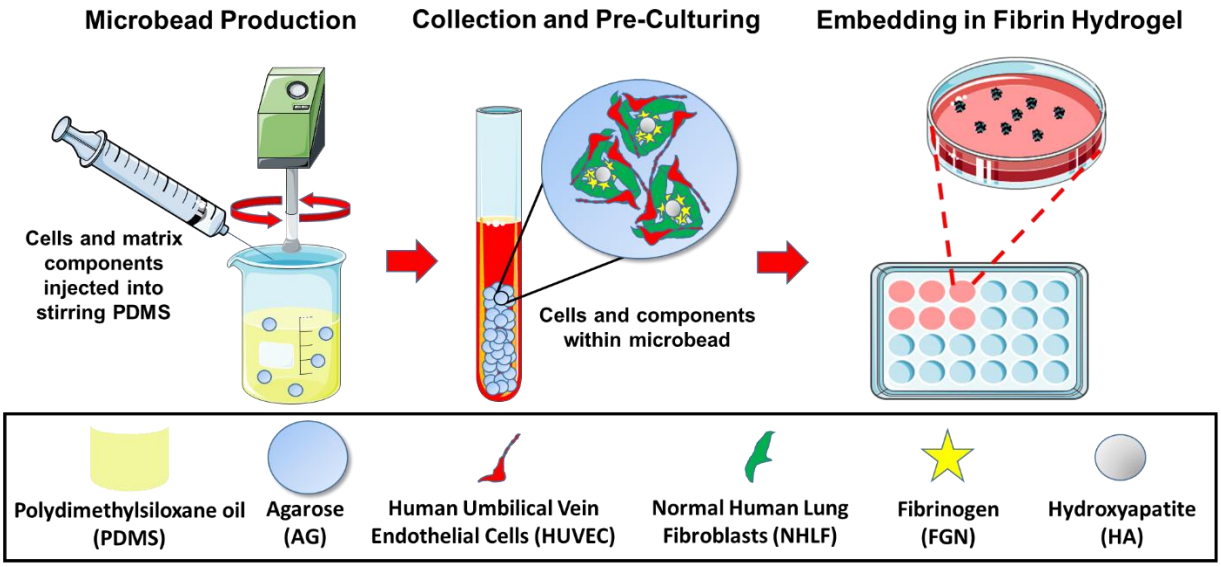

Figure 5-1: Microbead production and culture. Agarose-based, cell-encapsulating microbeads were produced using a water-in-oil emulsion process. HUVECs and NHLFs were incorporated in a 1:1 ratio at $2x10^6$ total cells per mL of aqueous microbead components. Microbeads were pre-cultured for Days 1 and/or 7 and then embedded in fibrin hydrogels. Some images were adapted from Servier Medical Arts clipart (*www.servier.com*).

5.2.3 Embedding of Microbeads in Fibrin (FIB) Hydrogels

Microbeads were embedded in fibrin hydrogels similarly to what was previously done [25]. The 15 mL vented conical tubes containing the media-microbead solution were centrifuged prior to the separation of the supernatant from the microbeads. All tubes were aliquoted the same way to keep comparison between batches consistent. 255 µL of microbeads were transferred from the culture tubes and placed into new tubes. 100 µL of FBS (10% final), 20 µL of 50 U/mL thrombin (1 U/mL final), and 625 µL of fibrinogen stock (2.5 mg/mL final clottable protein concentration) were added atop of the microbeads and mixed thoroughly to make 2 fibrin hydrogels with microbeads. 500 µL of the total solution was added to each well of a 24-well plate and left in the incubator for approximately 30 minutes to allow complete gelation of the fibrin hydrogels. 1 mL of media was added to each hydrogel after the gelation process. Media was replaced the next day and every other day until the experimental end points.

5.2.4 Microbead Characterization

Prior to microbead size quantification, images of microbeads were taken using Nikon DS-Ri2 camera. The rectangular selection tool in ImageJ (National Institutes of Health, Bethesda, MD) was utilized to measure microbead size. The average horizontal and vertical diameter of the first 25 microbeads per image (100 microbeads total) were quantified to determine the average microbead diameter of each batch.

To calculate microbead yield, microbeads were counted using a hemocytometer in the same manner cell counting is done. Ten independent counts were done per microbead batch. A single-blind study was used for both microbead size and yield quantification.

5.2.5 Viability of Encapsulated Cells

Cell viability was quantified using a fluorescent live/dead assay (Thermo Fisher) as per the manufacturer's protocols. Images were captured using a fluorescent source 465-495/515-555 nm excitation/emission (calcein-AM, live cells) and 540/605 nm (ethidium bromide, dead cells) filter sets (Nikon Instruments Inc., Melville, NJ). Cells were counted using ImageJ analysis software and a custom macro (US National Institutes of Health, Bethesda, MD). Cells staining positive for calcein-AM and negative for ethidium bromide were considered live at the beginning of the assay.

5.2.6 Staining and Visualization of Microbead Protein Content

A non-specific protein-binding dye (EZBlue, Sigma-Aldrich) was used to visualize protein content. Microbeads were washed in PBS, and fixed overnight in buffered zinc formalin (Z-Fix, Anatech Ltd, Battle Creek, MI). Microbeads were then stained for 10 min at room temperature.

5.2.7 HUVEC Sprout Staining and Quantification

Z-fix was employed to fix constructs 7 days after microbeads were embedded in fibrin hydrogels. Samples were rinsed two times before and after fixation. Ulex Europaeus Agglutinin I (UEA-I, Vector Laboratories, Burlingame, CA), an endothelial cell-specific marker, was utilized to stain the endothelial cells. Samples were stained with a 1% BSA buffer in PBS containing 10 nM DAPI and 20 µg/mL rhodamine-labeled UEA-I. After the 45 min room temperature incubation, samples were washed 2-4 times with PBS.

Prior to imaging, samples were taken out from the 24-well tissue culture plates and placed on slides. Coverslips were added on top prior to imaging. An optical microscope (Olympus IX81, Olympus, Center Valley, PA) and the scan slide tool in the Metamorph software were employed to take fluorescent images of endothelial networks formed in HUVECs-NHLFs microbeads that had been embedded in FIB hydrogels. The angiogenesis analyzer tool [71] and the ImageJ software were employed to measure total network length in each fibrin hydrogel. The background, brightness, contrast, and threshold of each hydrogel scan was adjusted preceding analysis. The correct scale and possible outlier parameters were also defined before running the angiogenesis analyzer. The aforementioned processing settings were kept constant for each hydrogel scan.

5.2.8 Statistical Analysis

Statistical analyses were performed running a one-way ANOVA with Dunnett's T3 post hoc test using SPSS software (IBM, Armonk, NY). Experiments were repeated at least twice and each contain at least three replicates for each group. Data are reported as mean ± standard deviation. Values of $p \leq 0.05$ were considered statistically significant.

5.3 Results and Discussion

5.3.1 Microbead Formulation and Production

The goal of this study was to develop modular tissue engineering constructs that could be easily handled and promote vascular network formation over a broad area. Our strategy centered on agarose (AG)-based microbeads encapsulating a co-culture of endothelial cells and fibroblasts, because these cell types have been shown to form robust vascular networks in other applications. Agarose was chosen to form the bulk of the microbead volume because of its ability to produce stable, spherical microbeads while limiting the adherence of the microbeads to each other and to the surface of the cultureware used in processing and handling. Hydroxyapatite (HA) and fibrinogen (FGN) were added to the microbead formulations at defined levels to encourage cell adherence and spreading, and to promote cell-specific functions that can enhance vasculogenesis.

Water-in-oil emulsification and an alternating heating/cooling cycle consistently resulted in spherical AG-based microbeads with mean diameters ranging from 80 to 110 μm, as shown in Figure 5-2. Pure 8.0 mg/mL AG microbeads (Fig. 5-2A) were clear, colorless, and highly spherical. Addition of HA and FGN to these AG-based microbeads resulted in incorporation of the active matrix components to differing degrees. HA alone dispersed evenly throughout the microbead (Fig. 5-2B), whereas FGN alone was not well incorporated (Fig. 5-2C) and remained in the supernatant when microbeads were collected. However, addition of both HA and FGN resulted in the formation of dense and homogenously distributed HA/FGN complexes (Fig. 5-2 D-E). These data suggest that HA serves to bind and incorporate FGN into the microbeads. The HA surface lattice contains Ca^{2+} and PO_3^- ions that promote the adsorption of a wide range of proteins

with positively or negatively charged moieties [72]. In the context of vasculogenic microbeads, the use of HA was intended to improve the incorporation of FGN into the microbeads during production and to provide a substrate for serum proteins that could further enhance cell attachment and sprout formation. Fabrication of microbeads using only 4.0 mg/mL agarose resulted in fragile microbeads and poor encapsulation of HA and FGN (Fig. 5-2F).

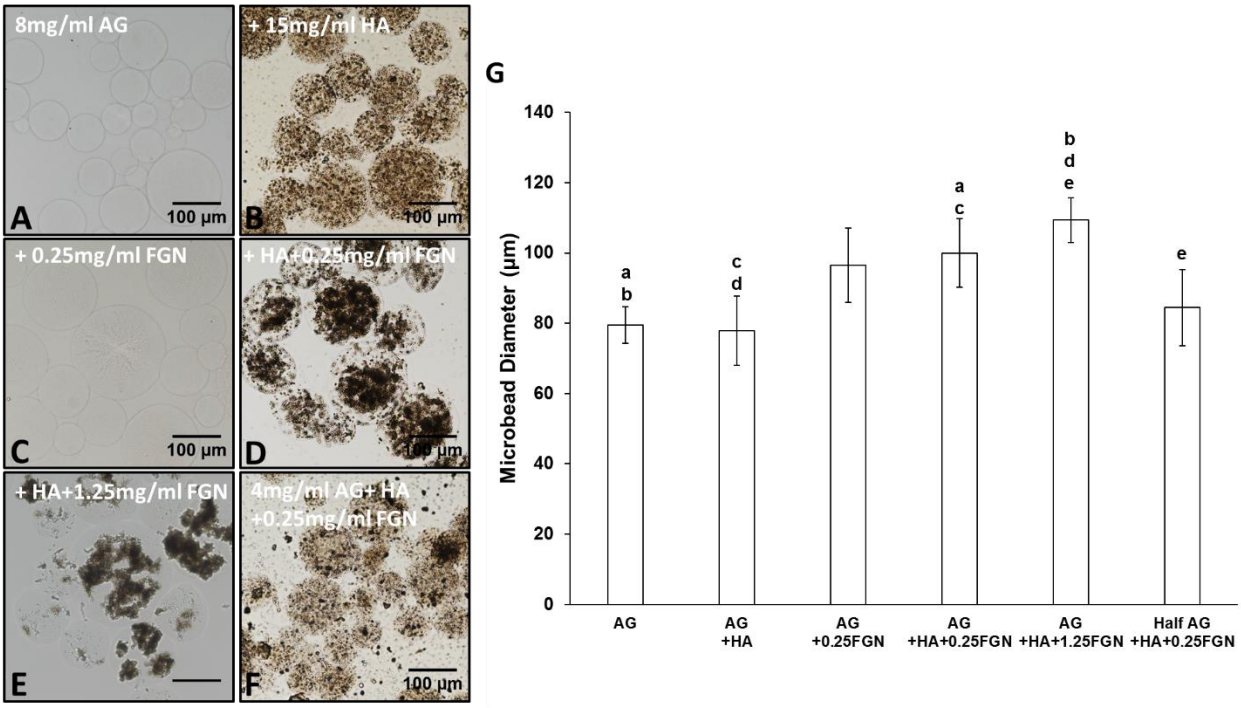

Figure 5-2: Microbead formulation characterization. Bright-field images showing incorporation of varying concentrations of FGN and HA into AG-based microbeads: (A) AG only microbeads and those made from 8 mg/mL AG + (B)HA, (C)FGN, (D)HA+ FGN, (E) 15 mg/mL HA+1.25 mg/mL FGN and (F) 4 mg/mL AG+15 mg/mL HA+0.25 mg/mL FGN. (G) Microbead size quantification. Lowercase letters indicate comparisons for which $p \leq 0.05$ (one-way ANOVA).

Addition of HA and FGN resulted in significantly larger microbeads compared to pure AG or AG+HA microbeads (Fig. 5-2G). However, there was no significant difference in diameters between microbeads containing AG+HA+0.25FGN and those containing AG+HA+1.25FGN. While average microbead diameters depended on the proportion of constituent materials, the

resulting microbeads were consistent with a relatively narrow size distribution, as indicated by the error bars in Fig. 5-2G. In all cases, the microbeads were <120 µm in diameter, such that any encapsulated cell would be less than 60 µm from the perimeter. This small diffusion distance is an advantage of the microbead format because it ensures availability of nutrients and oxygen to embedded cells.

5.3.2 Microbead Characterization

Protein staining was used to visualize the distribution of the active matrix components and cells encapsulated within AG-based microbeads, as shown in Figure 5-3. Pure AG microbeads (Fig. 5-3A) entrapped cells efficiently, but there was no evidence of cell spreading by Day 1 in HUVECs-NHLFs co-culture. Microbeads made with added FGN alone showed little incorporation of protein or cell spreading, though in the higher concentration some protein strands were evident (Fig. 5-3B, C). Addition of HA alone (Fig. 5-3D) to the microbeads indicated some entrapment of protein, presumably from the surrounding culture medium. However, addition of HA+FGN (Fig. 5-3E, F) resulted in very clear and widespread incorporation of protein into the microbeads, with concomitant evidence of cell adhesion and spreading. FGN is a soluble plasma protein that contains RGD domains that permit direct binding of cells [73], and its relatively high solubility enables its incorporation in the microbead fabrication process. Our results further support the idea that the incorporation of HA serves to sequester FGN, which in turn promotes cell attachment and function.

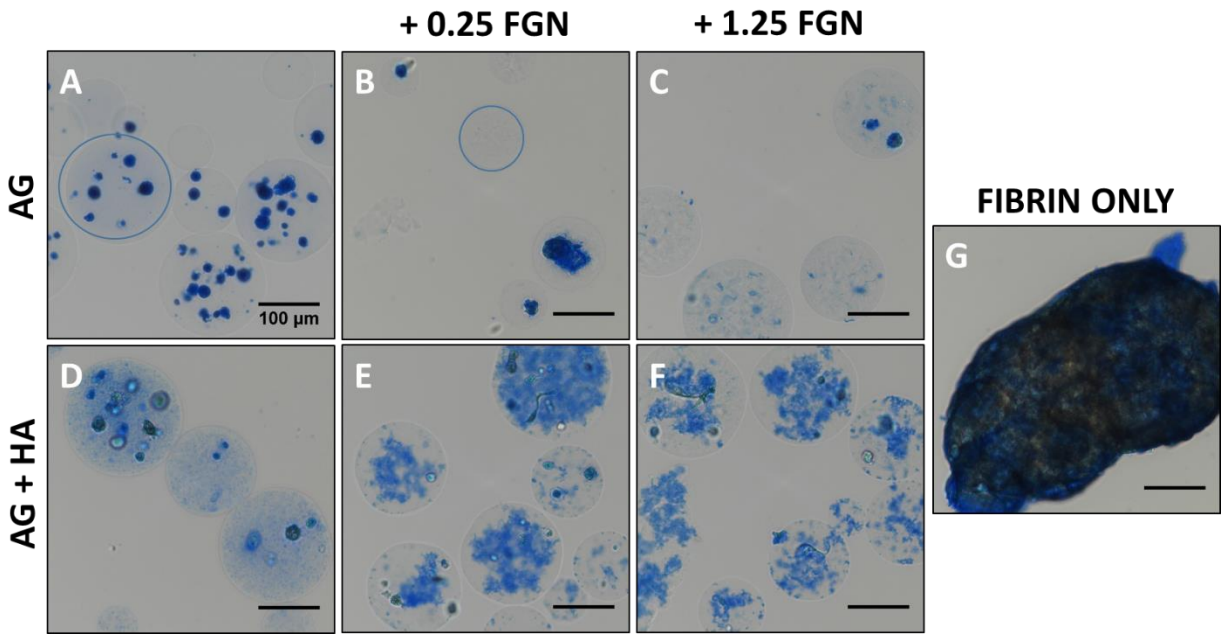

Figure 5-3: Greater concentrations of FGN permit the formation of homogenous, non-adherent HUVECs-NHLFs microbeads. (A) AG, (B) AG+0.25FGN, (C) AG+1.25FGN, (D) AG+HA, (E) AG+HA+0.25FGN, (F) AG+HA+1.25FGN, and (G) fibrin microbeads stained using EZ blue to visualize microbead protein content after processing. Microbead boundary indicated with blue circle. Scalebar = 100 µm.

Pure fibrin (FIB) microbeads were also produced and cultured in the same manner as AG-based microbeads. However, under these conditions FIB microbeads tended to agglomerate into masses several hundred microns in diameter in culture (Fig. 5-3G). In contrast, AG-based microbeads remained as discrete spherical units, and did not change appreciably in size or shape. Reduced aggregation allows microbeads to be cultured *in vitro* over time before being injected as a slurry. Such *in vitro* culture periods allow the phenotype of the embedded cells to be more carefully controlled, and therefore may lead to more effective function when implanted.

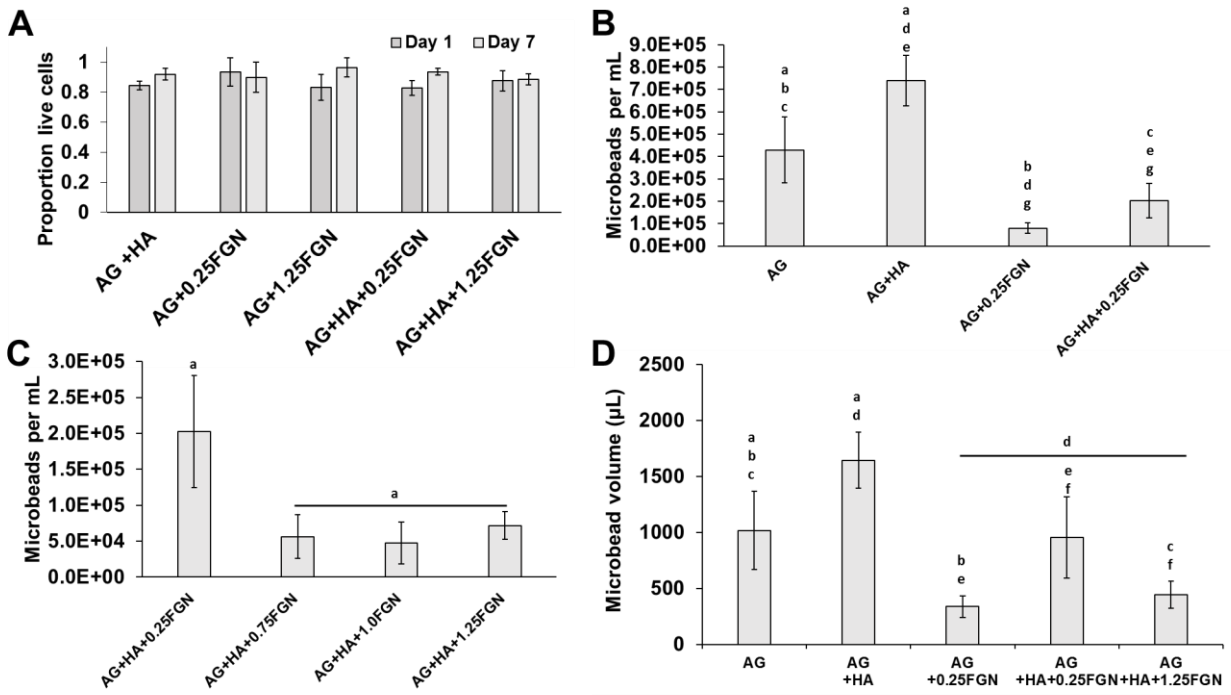

Figure 5-4: Effects of the different components on microbead yield and HUVECs-NHLFs viability. (A) HA or FGN content had no significant effect on the viability of encapsulated cells one day after microbead production and after pre-culture. (B,C) Microbead yield increase with the addition of HA and decreased with the addition of FGN, until it reached steady-state at 0.75FGN. (D) Microbead volume based on microbead yield and microbead diameter. (Lowercase letters indicate comparisons for which $p \leq 0.05$ (one-way ANOVA).

Cell viability in all microbead formulations was high (Fig. 5-4A). Viability of HUVECs and NHLFs was generally >80% in all microbead types, with no statistical differences between formulations or time in culture over a one week period. These results show that the encapsulation process itself is not harmful to cells, and that cells can maintain their viability when being cultured in microbeads. The clear survival of cells over a week in culture suggests that mass transfer limitations are not a barrier, and it is expected that cells could therefore also survive for longer periods.

Microbead composition affected the number and volume of microbeads yielded by the production process (Fig. 5-4B). The numerical yield of AG-only microbeads was approximately

$4x10^5$/mL, while the addition of HA alone increased the yield to over $7x10^5$/mL. It is likely that the relatively high specific gravity of HA (3.08) reduced the buoyancy of HA-containing microbeads and thereby contributed to improved separation during centrifugation [74]. Incorporation of FGN alone decreased the microbead yield, while including HA+FGN caused a recovery in numerical yield, though not to the level of the pure AG microbeads. To further assess the effects of the active matrix components on microbead yield, AG-based microbeads were made with HA and from 0.25 to 1.25 mg/mL FGN (Fig. 5-4C).

Numerical yield dropped significantly when the FGN content was increased from 0.25 to 0.75 mg/mL. However, further increases in FGN concentration did not significantly affect yield. It should be noted that while large differences were observed in the numerical yields between microbead formulations, the difference in the volume of microbeads collected was not as great. This discrepancy is due to the differences in microbead size (Fig. 5-2G), and estimation of the microbead volume showed no significant differences between the yields of AG-only and AG+HA+0.25 mg/mL FGN microbeads (Fig. 5-4D).

5.3.3 HUVEC Sprouting and Network Formation

Figure 5-5 shows images of AG+HA+0.25FGN with encapsulated HUVECs and NHLFs in culture. These experiments were performed to verify whether endothelial cells can form sprouts within and from these microbeads, as a precursor to examining more global network formation. When microbeads were embedded in a bulk 3D fibrin gel (Fig. 5-5A), it was evident that HUVECs could sprout from microbeads into the surrounding matrix over a week in culture, and nascent vessel networks were observed. Culture of microbeads within bulk fibrin gels is used to recreate a 3D matrix to mimic the *in vivo* tissue environment, and similar systems have been employed to

study angiogenesis and vasculogenesis [25, 26]. When microbeads were cultured as discrete units without being embedded in a surrounding gel (Fig. 5-5B), small vessel fragments formed within the microbeads. When such microbeads were pre-cultured for 8 days as discrete modules before being embedded in a surrounding fibrin bulk gel (Fig. 5-5C), the vessel fragments formed within the microbeads could sprout into the surrounding matrix. Taken together, these experiments therefore established that HUVECs can form nascent vessels within AG+HA+FGN microbeads, and can sprout from the microbeads when embedded in a surrounding matrix.

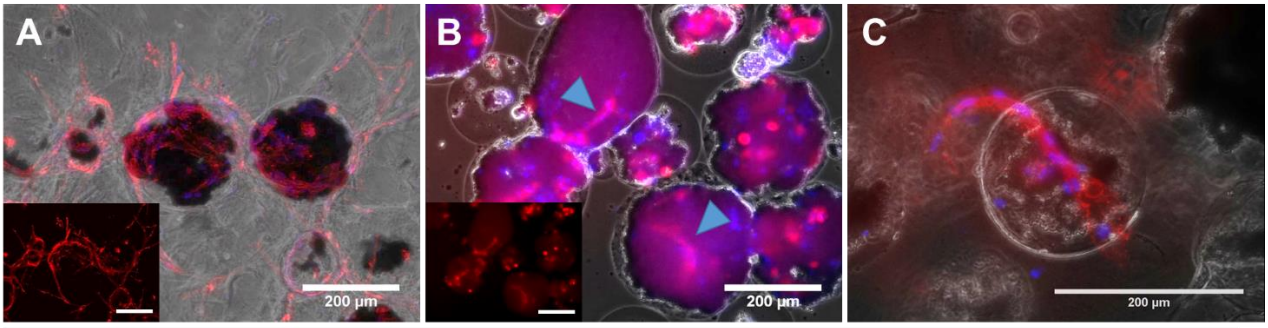

Figure 5-5: Proof of concept EC sprouting from Ag+15 mg/mL HA+0.25 mg/mL FGN microbeads under different culture conditions. (A) After 7 days of embedding in 2.5mg/mL FIB hydrogel (no pre-culture). (B) After 7 days sedimentation in conical tube (no FIB embedding). Arrowheads indicate sprouts forming within microbeads. (C) After 5 days in FIB following 8 days pre-culture in conical tube. Sprouts originated in the HA-FGN complex (black) located within the microbead boundaries (not visible). The inset in image A and B show endothelial cells stained in red. Red = UEA staining, Blue =DAPI. Scale bar = 200 µm.

The composition of the microbeads affected their ability to create distributed (i.e. spanning a large area) vessel networks, as shown in Figure 5-6. In these studies, microbeads were embedded in surrounding fibrin gels one day after microbead production, and were then cultured for seven days. In microbeads without HA (Fig. 5-6 A-C), sprouting was minimal and relatively local in the direct vicinity of the microbeads. Microbeads with HA but no FGN (Fig. 5-6D) also showed minimal and local sprouting. For microbeads that contained both HA and FGN (Fig. 5-6 E, F), the

extent of sprouting was much greater and spanned the entire volume of the surrounding fibrin matrix. In contrast, pure FIB microbeads that were cultured under similar conditions (Fig. 5-6G), exhibited robust but highly focal sprouting (Fig. 5-6G) due to aggregation of the microbeads. The limited aggregation of the AG-based microbeads led to greater homogeneity in the distribution of endothelial networks within the surrounding matrix. This effect is a potentially important feature of AG+HA+FGN microbeads, since upon implantation a more distributed vessel network could increase the probability and rate of inosculation with the host and subsequent re-vascularization of tissue.

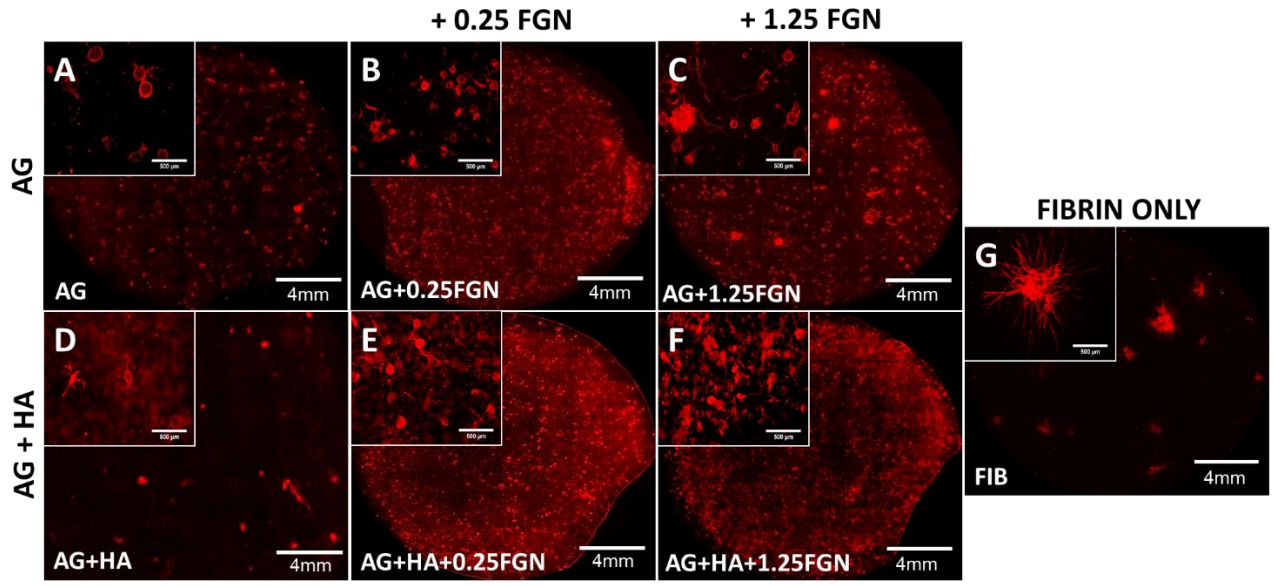

Figure 5-6: The distribution of HUVEC sprouting depends on microbead matrix components. (A) AG, (B) AG+0.25FGN, (C) AG+1.25FGN, (D) AG+HA, (E) AG+HA+0.25FGN, (F) AG+HA+1.25FGN and (G) fibrin microbeads were embedded in 2.5mg/mL FIB hydrogels and cultured for 7 days.

The distribution of fibroblasts and endothelial cells in all four microbead conditions was assess by staining of cells 7 days after being embedded in fibrin hydrogels, as shown in Fig. 5-7. All four microbead conditions formed endothelial sprouts (as previously shown); however, there

were more fibroblasts and a higher number of microbeads with endothelial sprouts in the AG+1.25FGN and the AG+7.5HA+1.25FGN conditions. Fibroblasts migrated from the microbeads into the fibrin hydrogels in all conditions. A more homogeneous distribution of fibroblasts and endothelial cells was observed in the AG+7.5HA+1.25FGN condition.

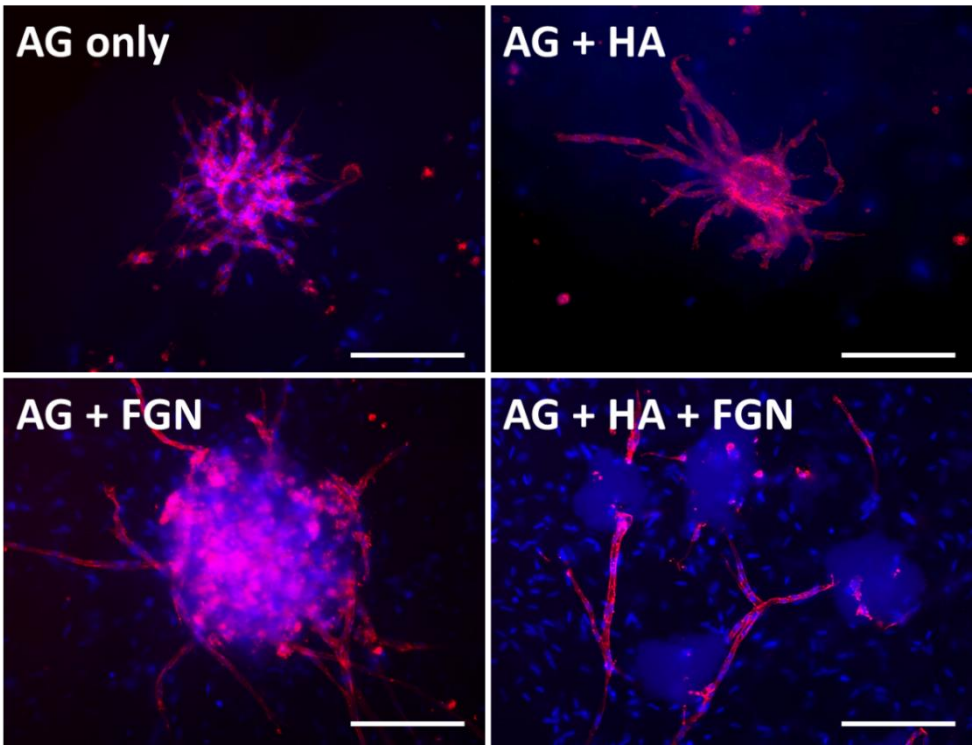

Figure 5-7: Fibroblasts surround endothelial sprouts protruding from microbeads embedded in fibrin hydrogels. One day after fabrication, microbeads of differing formulations were embedded in fibrin hydrogels for 7 days. Endothelial cells were stained with UEA-I (red) while nuclei of both endothelial cells and fibroblasts were stained with DAPI (blue). Scale bar = 200 μm.

The effect of pre-culture on endothelial network formation was also assessed using selected microbead formulations, as shown in Figure 5-8. In these experiments, a lower (7.5 mg/mL) concentration of HA was used to reduce background fluorescence and allow quantification of vessel network length. Microbeads that were embedded in 3D fibrin gels one day after production (Fig. 5-8 A-D) showed again that only local and very modest sprouting occurs into surrounding

matrix, unless both HA and FGN are incorporated. In the latter case, endothelial sprouting is robust and distributed throughout the matrix. When microbeads were pre-cultured for seven days prior to being embedded in fibrin (Fig. 5-8 E-H), the degree of sprouting was decreased in both pure AG and AG+HA samples, but was retained in the FGN and HA+FGN microbeads.

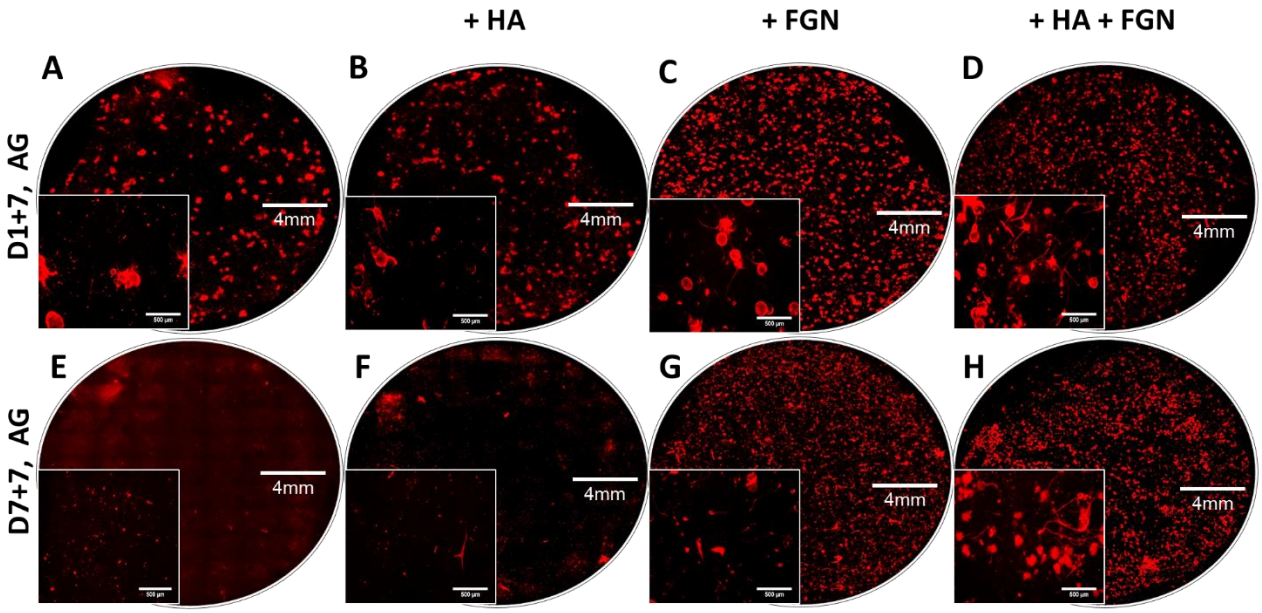

Figure 5-8: Fluorescence imaging reveals that HUVEC sprouting is affected by microbead composition and pre-culture conditions. Images of endothelial sprouting (red) from AG (A,E), AG+7.5HA (B,F), AG+1.25FGN (C,G), and AG+7.5HA+1.25FGN microbeads (D,H) embedded in fibrin hydrogels for 1 week; with (E,F,G,H), and without pre-culture (A,B,C,D).

Quantification of total sprout network length (Fig. 5-9) confirmed these observations. These data show that addition of HA+FGN caused a marked increase in total network length, relative to the other formulations. In addition, pre-culture of the AG+HA+FGN microbeads prior to embedding had a modest positive effect on network length, compared to AG+HA+FGN microbeads that had not been pre-cultured.

The fate of microbeads and the embedded cells after implantation *in vivo* will depend on the matrix formulation. The materials examined in this study assisted with achieving distributed

vascularization, and they can be further optimized to provide desired rates of cell delivery and concomitant matrix degradation. Agarose is resistant to proteolytic degradation, but can be broken down hydrolytically over time, and is susceptible to some lysosomal enzymes. It is therefore likely to be broken down slowly *in vivo*, and can impart stability to the microbeads while promoting cell function. Future work will examine the remodeling and degradation of microbeads after implantation, and will also investigate other materials that can mimic the distributive effects of agarose while offering more control over degradation rate. The tailoring of matrix material properties can be used to control the distribution of vessel networks, and potentially to thereby promote more rapid and efficient inosculation with host tissue after implantation.

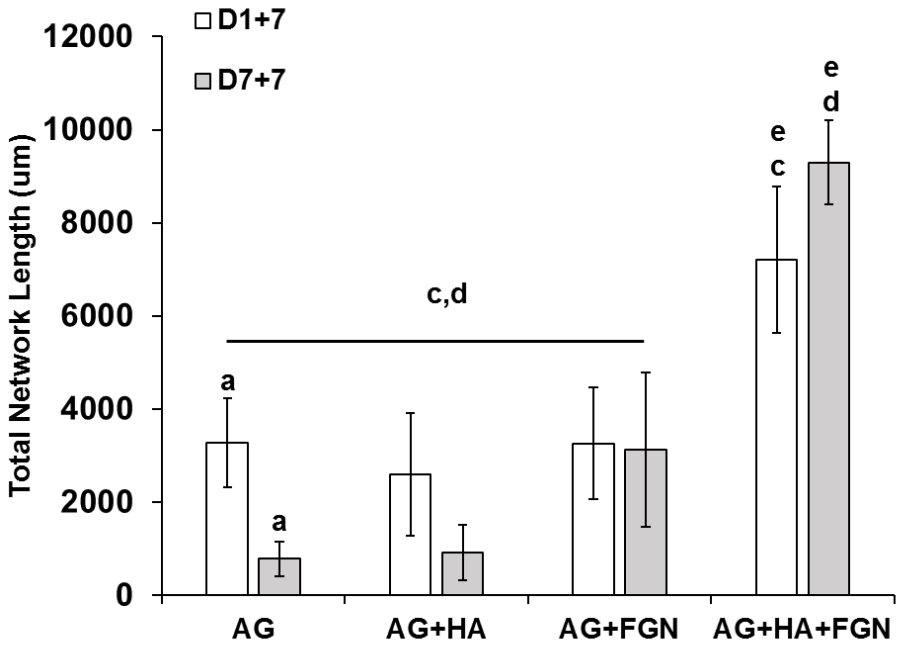

Figure 5-9: Quantification of total network length confirms that HUVEC sprouting is affected by microbead composition and pre-culture conditions. Quantification of microbeads, with/without pre-culture, embedded in fibrin hydrogels for 1 week. Endothelial network length increased significantly when cells were encapsulated with HA and FGN in AG microbeads. Pre-culture had a positive effect on total network length in AG+HA+FGN microbeads only. (Lowercase letters indicate comparisons for which $p \leq 0.05$ (one-way ANOVA).

5.3.4 Supplementary Information

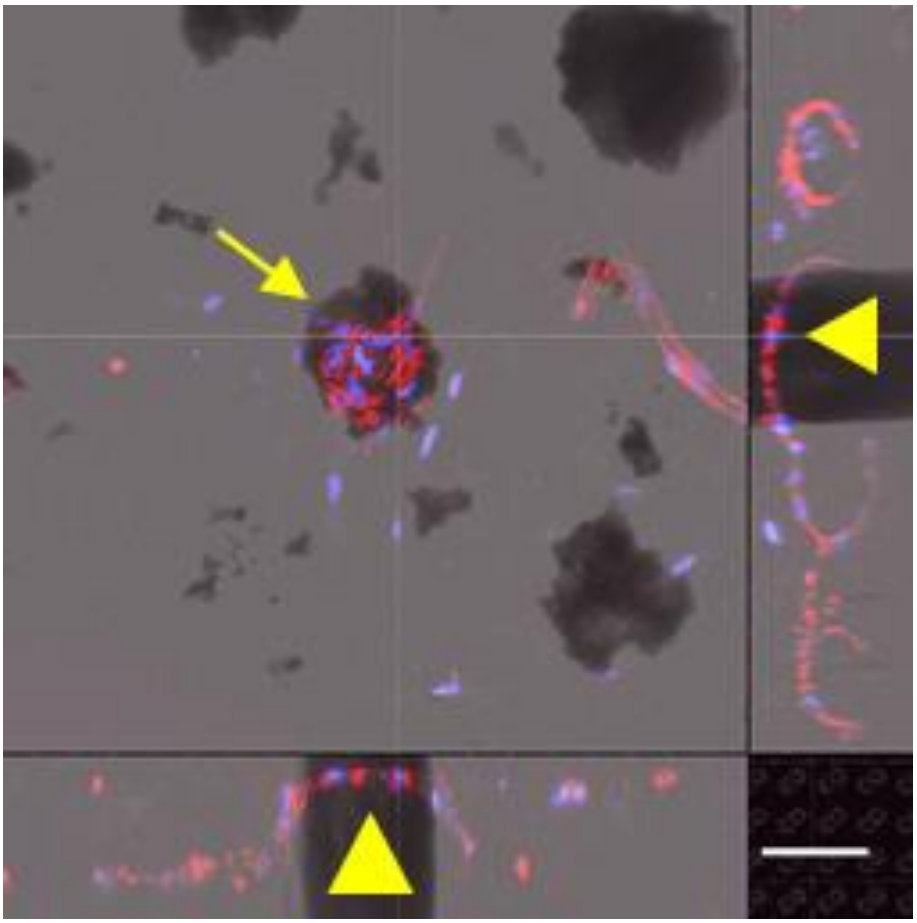

Figure 5-10: Microbeads pre-cultured on AG then embedded in FIB. Cross sections (bottom, side panels) show sprouting (arrowheads) within HA+FGN comples (arrow). Endothelial cells are stained with red: UEA-I, and nuclei stained with blue: DAPI. Scale bar: 100 µm.

AG+HA+FGN microbeads were embedded in a fibrin hydrogel for 7 days following 8 days of pre-culture on a non-adherent agarose hydrogel. The confocal reflectance image shows the cross sections on the bottom and side panels of the microbead (Fig. 5-10). The HA-FGN complex (black) located within the microbead boundaries (not visible) allows endothelial sprouting (yellow arrow heads) to occur. This EC sprouting observed both within and between the microbead, indicates that EC retain their function after being cultured in AG+HA+FGN microbeads alone and that an

adherent pre-conditioning environment surrounding the microbeads is not required for subsequent sprouting.

Endothelial cells (UEA-I, red) and NHLFs encapsulated in AG, AG+HA, AG+FGN, and AG+HA+FGN microbeads, were pre-cultured for 1, 3, and 7 days, and embedded in fibrin hydrogels for 1, 3, and 7 days (Fig. 5-11). The longer the embedding time, the longer the EC sprouts grew within the fibrin hydrogels. More sprouting also occurred in the AG+HA+FGN conditions that the other microbead conditions; while EC morphology may differ depending on the microbead the cells were originally encapsulated in.

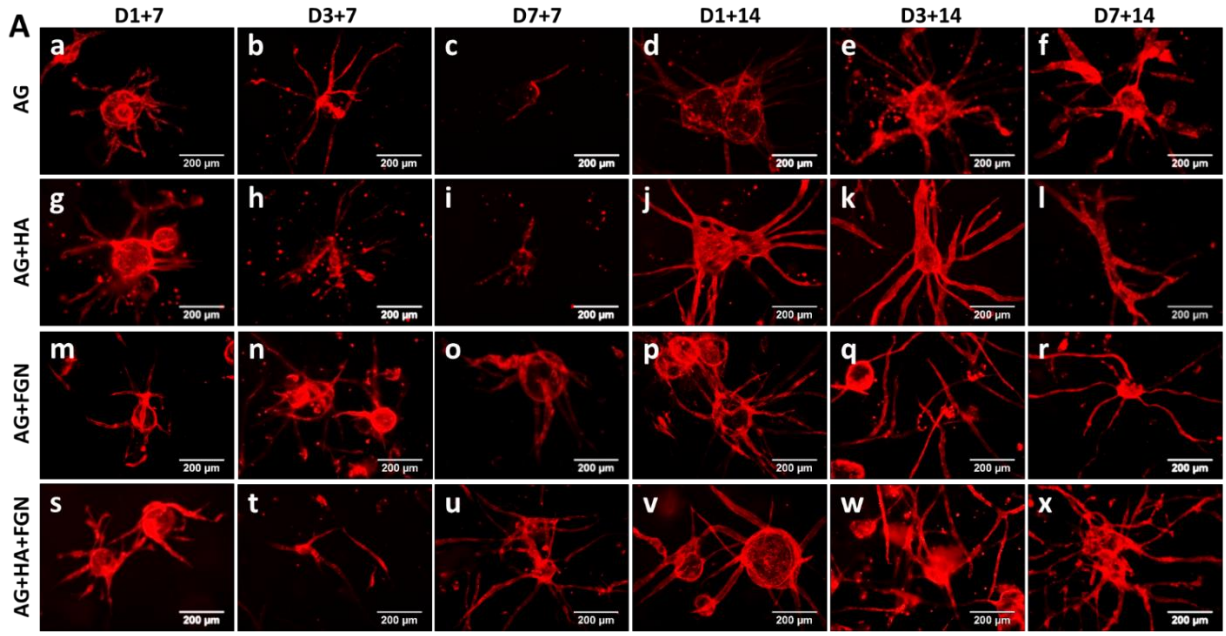

Figure 5-11: Effects of pre-culture on HUVEC sprouting from microbeads embedded in fibrin hydrogel. Images of endothelial sprouting (red) from Agarose (a-f), AG+HA (g-l), AG+FGN (m-r), and (AG+HA+FGN) microbeads embedded in fibrin hydrogel after 1 day (a,g,m,s,d,j,p,v), 3 days (b,h,n,t,e,k,q,w), and 7 days (c,i,o,u,f,l,r,x) and cultured for 1-2 weeks. Scale bar: 200 µm.

These same four types of microbeads were pre-cultured for 1 and 7 days at different microbead concentrations (0.5 mL: 1:2 bead:media volume, and 1 mL: 1:1 bead:media volume) and stained with EZ blue to determine protein content – qualitatively (Fig. 5-12). After 1 day of

pre-culture, microbeads did not show a lot of protein content, except for the AG+HA+FGN condition). Pre-culturing the AG and AG+HA microbeads for 1 day versus 7 days did not affect their microbead content (qualitative). On the other hand, the AG+FN and AG+HA+FGN microbeads pre-cultured for 7 days at a 0.5 mL or 1 mL had more protein, not only within the microbead, but also surrounding multiple microbeads suggesting a possible interaction between the cells of neighboring microbeads.

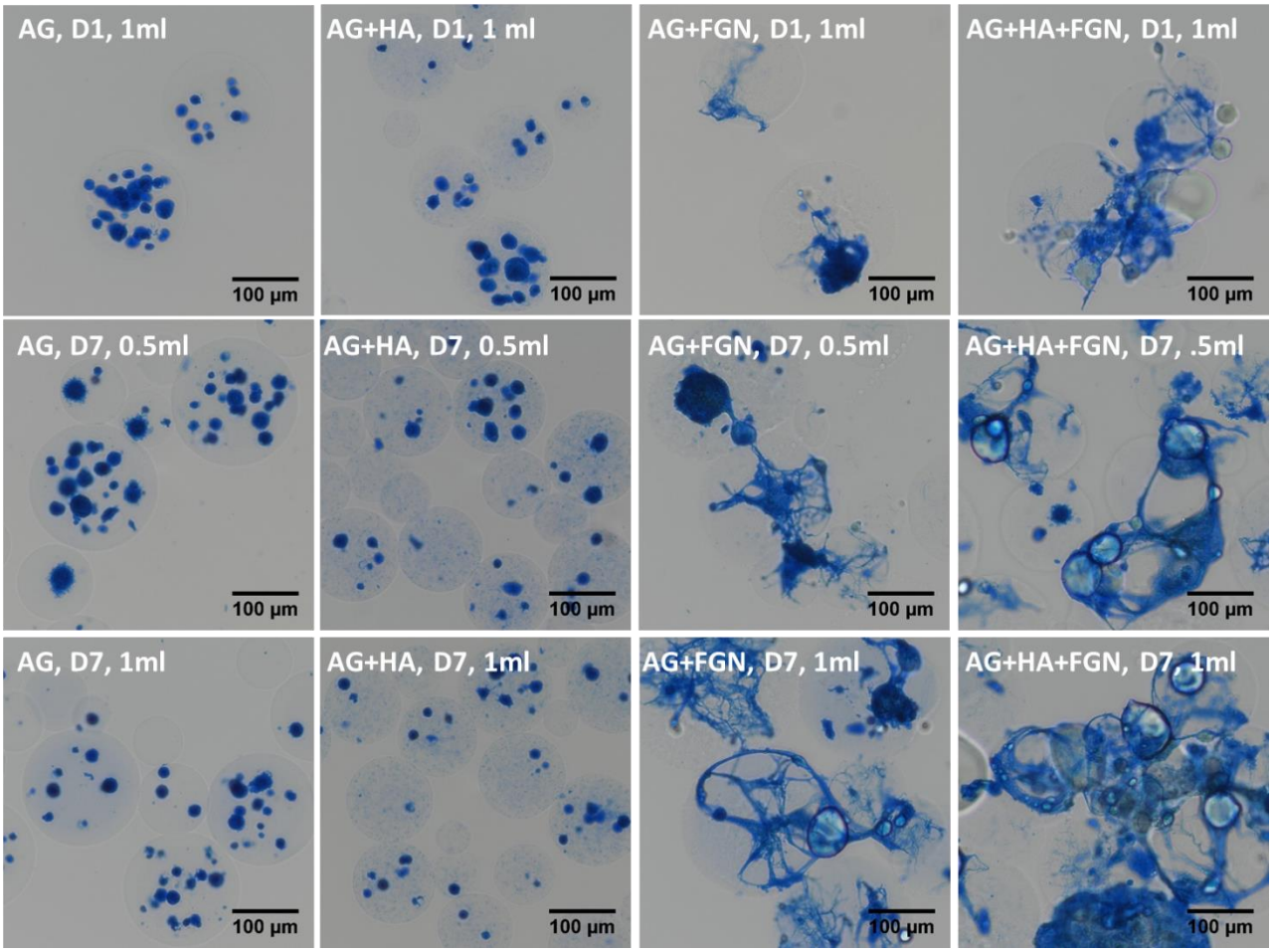

Figure 5-12: Protein content of AG, AG+HA, AG+FGN, and AG+HA+FGN microbeads that had been pre-cultured for 1 and 7 days (0.5ml and 1ml). Scale bar: 100 µm.

Endothelial sprout length and pre-culture medium volume was investigated by pre-culturing the four microbead types (AG, AG+HA, AG+FGN, and AG+HA+FGN) for 7 days in different medium volumes (1x: 1:1 bead:media volume, 2x: 1:2 bead:media volume, and 4x: 1:4 bead:media volume) followed by their embedding in a fibrin hydrogel for an additional week. Quantification of this data was done by hand (one-side blind study). Figure 5-13 shows that total sprout length increased when AG+HA+FGN were pre-cultured with more media for 7 days prior to embedding.

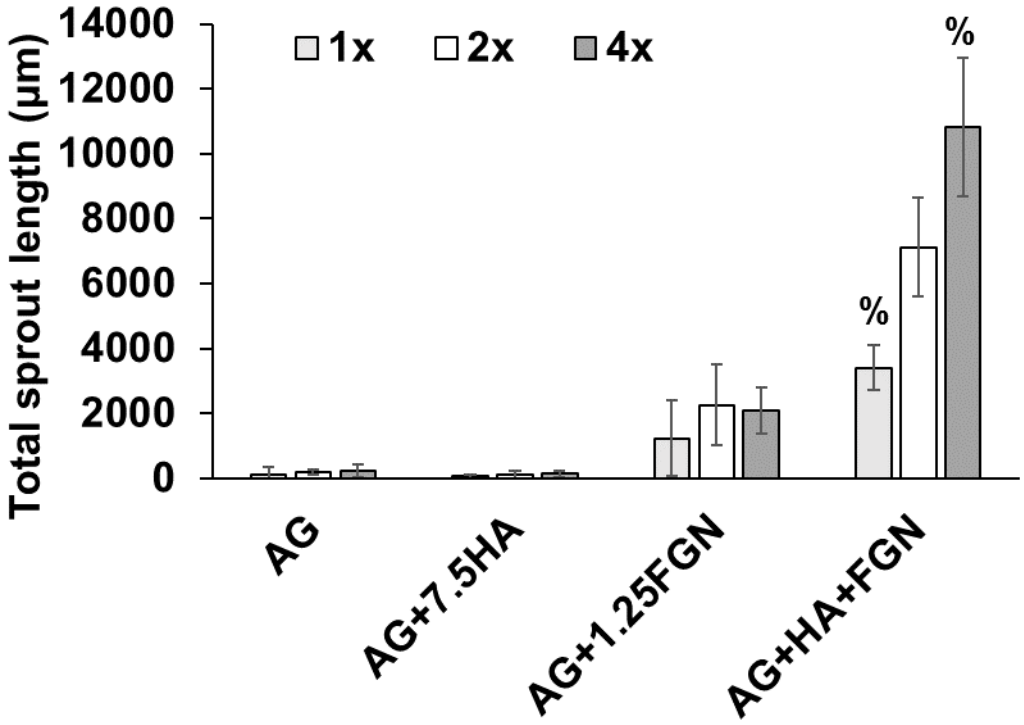

Figure 5-13: Total sprout length increased in AG+HA+FGN microbeads pre-cultured with more EGM-2 media. ANOVA + Dunnett T3 post-hoc % shows differences for $p<0.05$ of AG+HA+FGN only condition

Fig. 5-14 displays the same total sprout length graph shown above, but comparing only the sprout length of microbeads pre-cultured with the same microbead:media volume "*".

AG+HA+FGN microbeads had a higher total sprout length than other microbeads cultured with the same 2x, and 4x bead:media volume. While total EC sprout length of AG+HA+FGN pre-cultured with 1x bead:media volume were only significant higher "**a**" than AG and AG+HA condition, not AG+FGN condition.

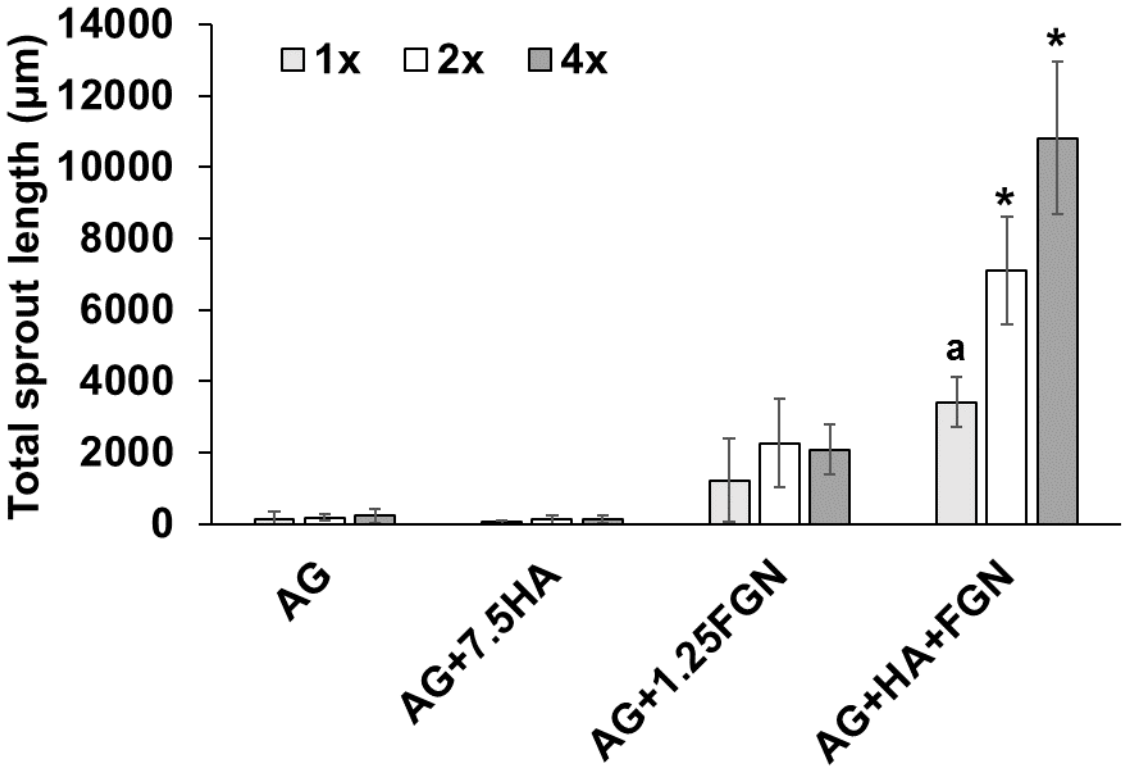

Figure 5-14: Endothelial sprout length based on pre-culture media volume. ANOVA + Dunnett T3 post-hoc "*" compared to others of same volume for $p<0.05$, and "**a**" for $p<0.05$ compared to AG, and AG+HA of same volume.

5.4 Conclusion

AG+HA+FGN microbeads can support endothelial sprouting and provide even distribution of endothelial network formation, via inosculation of endothelial sprouts between adjacent

microbeads embedded in fibrin hydrogels (Fig. 5-15). The use of AG in the matrix prevents aggregation and contributes to the formation of spherical microbeads, which facilitates the culture, collection, and injection processes. The incorporation of HA and FGN within the microbeads permit cell adhesion and spreading within the non-adherent AG. By developing these AG+HA+FGN microbeads, we have increased microbead yield production, improved injectability, and achieved a more homogeneous vascular network. In addition, pre-culture of these microbeads leads to a slight increase in endothelial network length which could be beneficial in ischemic studies.

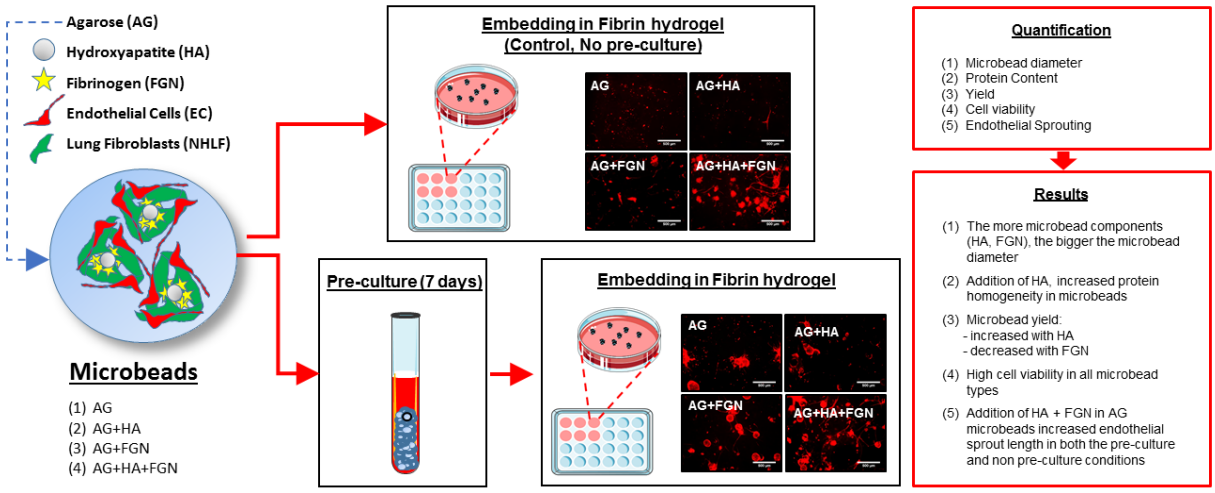

Figure 5-15: Graphical figure summarizing the study.

5.5 References

1. Peripheral Arterial Disease in People With Diabetes. Diabetes Care 2003;26:3333-41.

2. Varu VN, Hogg ME, Kibbe MR. Critical limb ischemia. Journal of vascular surgery 2010;51:230-41.

3. Falluji N, Mukherjee D. Critical and acute limb ischemia: an overview. Angiology 2014;65:137-46.

4. Leaper DJ. Silver dressings: their role in wound management. International wound journal 2006;3:282-94.

5. Kirsner RS, Sabolinski ML, Parsons NB, Skornicki M, Marston WA. Comparative effectiveness of a bioengineered living cellular construct vs. a dehydrated human amniotic membrane allograft for the treatment of diabetic foot ulcers in a real world setting. Wound Repair and Regeneration 2015;23:737-44.

6. Galiano RD, Tepper OM, Pelo CR, Bhatt KA, Callaghan M, Bastidas N, N, Bunting S, Steinmetz HG, Gurtner GC. Topical Vascular Endothelial Growth Factor Accelerates Diabetic Wound Healing through Increased Angiogenesis and by Mobilizing and Recruiting Bone Marrow-Derived Cells. The American Journal of Pathology 2004;164:1935-47.

7. Nichol JW, Khademhosseini A. Modular Tissue Engineering: Engineering Biological Tissues from the Bottom Up. Soft matter 2009;5:1312-9.

8. Dean DM, Napolitano AP, Youssef J, Morgan JR. Rods, tori, and honeycombs: the directed self-assembly of microtissues with prescribed microscale geometries. Faseb J 2007;21:4005-12.

9. Dean DM, Morgan JR. Cytoskeletal-mediated tension modulates the directed self-assembly of microtissues. Tissue engineering Part A 2008;14:1989-97.

10. Dean DM, Rago AP, Morgan JR. Fibroblast elongation and dendritic extensions in constrained versus unconstrained microtissues. Cell motility and the cytoskeleton 2009;66:129-41.

11. Kelm JM, Djonov V, Ittner LM, Fluri D, Born W, Hoerstrup SP, Fussenegger M. Design of custom-shaped vascularized tissues using microtissue spheroids as minimal building units. Tissue engineering 2006;12:2151-60.

12. McGuigan AP, Sefton MV. Vascularized organoid engineered by modular assembly enables blood perfusion. Proceedings of the National Academy of Sciences of the United States of America 2006;103:11461-6.

13. Youssef J, Nurse AK, Freund LB, Morgan JR. Quantification of the forces driving self-assembly of three-dimensional microtissues. Proceedings of the National Academy of Sciences of the United States of America 2011;108:6993-8.

14. Gupta R, Sefton MV. Application of an endothelialized modular construct for islet transplantation in syngeneic and allogeneic immunosuppressed rat models. Tissue engineering Part A 2011;17:2005-15.

15. Cheng HW, Luk KD, Cheung KM, Chan BP. In vitro generation of an osteochondral interface from mesenchymal stem cell-collagen microspheres. Biomaterials 2011;32:1526-35.

16. Wang L, Rao RR, Stegemann JP. Delivery of mesenchymal stem cells in chitosan/collagen microbeads for orthopedic tissue repair. Cells, tissues, organs 2013;197:333-43.

17. Wise JK, Alford AI, Goldstein SA, Stegemann JP. Comparison of uncultured marrow mononuclear cells and culture-expanded mesenchymal stem cells in 3D collagen-chitosan microbeads for orthopedic tissue engineering. Tissue engineering Part A 2014;20:210-24.

18. Leung BM, Miyagi Y, Li RK, Sefton MV. Fate of modular cardiac tissue constructs in a syngeneic rat model. Journal of tissue engineering and regenerative medicine 2013.

19. Futrega K PJ, Kinney M, Lott WB, Ungrin MD, Zandstra PW, Doran, MR. The microwell-mesh: a novel device and protocol for the high throughput manufacturing of cartilage microtissues. Biomaterials 2015.

20. Yen C-M, Chan C-C, Lin S-J. High-throughput reconstitution of epithelial–mesenchymal interaction in folliculoid microtissues by biomaterial-facilitated self-assembly of dissociated heterotypic adult cells. Biomaterials 2010;31:4341-52.

21. Daley EL, Coleman RM, Stegemann JP. Biomimetic microbeads containing a chondroitin sulfate/chitosan polyelectrolyte complex for cell-based cartilage therapy. Journal of materials chemistry B, Materials for biology and medicine 2015;3:7920-9.

22. Rowe SL, Stegemann JP. Microstructure and Mechanics of Collagen-Fibrin Matrices Polymerized Using Ancrod Snake Venom Enzyme. J Biomech Eng-T Asme 2009;131.

23. Ghajar CM, Chen X, Harris JW, Suresh V, Hughes CC, Jeon NL, Putnam AJ, George SC. The effect of matrix density on the regulation of 3-D capillary morphogenesis. Biophysical journal 2008;94:1930-41.

24. Rao RR, Peterson AW, Ceccarelli J, Putnam AJ, Stegemann JP. Matrix composition regulates three-dimensional network formation by endothelial cells and mesenchymal stem cells in collagen/fibrin materials. Angiogenesis 2012;15:253-64.

25. Rioja AY, Tiruvannamalai Annamalai R, Paris S, Putnam AJ, Stegemann JP. Endothelial sprouting and network formation in collagen- and fibrin-based modular microbeads. Acta biomaterialia 2016;29:33-41.

26. Peterson AW, Caldwell DJ, Rioja AY, Rao RR, Putnam AJ, Stegemann JP. Vasculogenesis and angiogenesis in modular collagen-fibrin microtissues. Biomater Sci-Uk 2014;2:1497-508.

27. Kirkpatrick CJ, Fuchs S, Unger RE. Co-culture systems for vascularization--learning from nature. Adv Drug Deliv Rev 2011;63:291-9.

28. Au P, Daheron LM, Duda DG, Cohen KS, Tyrrell JA, Lanning RM, Fukumura D, Scadden DT, Jain RK. Differential in vivo potential of endothelial progenitor cells from human umbilical cord blood and adult peripheral blood to form functional long-lasting vessels. Blood 2008;111:1302-5.

29. Merfeld-Clauss S, Gollahalli N, March KL, Traktuev DO. Adipose tissue progenitor cells directly interact with endothelial cells to induce vascular network formation. Tissue engineering Part A 2010;16:2953-66.

30. Shepherd BR, Jay SM, Saltzman WM, Tellides G, Pober JS. Human aortic smooth muscle cells promote arteriole formation by coengrafted endothelial cells. Tissue engineering Part A 2009;15:165-73.

31. Nakatsu MN, Sainson RCA, Aoto JN, Taylor KL, Aitkenhead M, Pérez-del-Pulgar S, Carpenter PM, Hughes CC. Angiogenic sprouting and capillary lumen formation modeled by human umbilical vein endothelial cells (HUVEC) in fibrin gels: the role of fibroblasts and Angiopoietin-1☆. Microvascular Research 2003;66:102-12.

32. Montesano R, Pepper MS, Orci L. Paracrine induction of angiogenesis in vitro by Swiss 3T3 fibroblasts. Journal of cell science 1993;105 (Pt 4):1013-24.

33. Thompson HG, Truong DT, Griffith CK, George SC. A three-dimensional in vitro model of angiogenesis in the airway mucosa. Pulmonary Pharmacology & Therapeutics 2007;20:141-8.

34. Ghajar CM, Blevins KS, Hughes CC, George SC, Putnam AJ. Mesenchymal stem cells enhance angiogenesis in mechanically viable prevascularized tissues via early matrix metalloproteinase upregulation. Tissue engineering 2006;12:2875-88.

35. Fernandez-Cossio S, Leon-Mateos A, Sampedro FG, Oreja MTC. Biocompatibility of agarose gel as a dermal filler: Histologic evaluation of subcutaneous implants. Plast Reconstr Surg 2007;120:1161-9.

36. Bloch K, Vanichkin A, Damshkaln LG, Lozinsky VI, Vardi P. Vascularization of wide pore agarose-gelatin cryogel scaffolds implanted subcutaneously in diabetic and non-diabetic mice. Acta biomaterialia 2010;6:1200-5.

37. Bhat S, Kumar A. Cell proliferation on three-dimensional chitosan-agarose-gelatin cryogel scaffolds for tissue engineering applications. Journal of bioscience and bioengineering 2012;114:663-70.

38. Bhat S, Tripathi A, Kumar A. Supermacroprous chitosan-agarose-gelatin cryogels: in vitro characterization and in vivo assessment for cartilage tissue engineering. Journal of the Royal Society, Interface / the Royal Society 2011;8:540-54.

39. Yang Q, Zhang YY, Liu ML, Zhang YQ, Yao SZ. Study of fibrinogen adsorption on hydroxyapatite and TiO2 surfaces by electrochemical piezoelectric quartz crystal impedance and FTIR-ATR spectroscopy. Anal Chim Acta 2007;597:58-66.

40. Lü XY, Yan H, Zheng BZ, Wu AP. Comparing adsorptive property of natural and synthesized hydroxyapatite to albumin, fibrinogen and IgG. Key Engineering Materials: Trans Tech Publ; 2007. p. 869-72.

41. Yongli C, Xiufang Z, Yandao G, Nanming Z, Tingying Z, Xinqi S. Conformational Changes of Fibrinogen Adsorption onto Hydroxyapatite and Titanium Oxide Nanoparticles. Journal of colloid and interface science 1999;214:38-45.

42. He J, Genetos DC, Leach JK. Osteogenesis and trophic factor secretion are influenced by the composition of hydroxyapatite/poly(lactide-co-glycolide) composite scaffolds. Tissue engineering Part A 2010;16:127-37.

43. He J, Decaris ML, Leach JK. Bioceramic-mediated trophic factor secretion by mesenchymal stem cells enhances in vitro endothelial cell persistence and in vivo angiogenesis. Tissue engineering Part A 2012;18:1520-8.

44. Mima Y, Fukumoto S, Koyama H, Okada M, Tanaka S, Shoji T, Emoto M, Furuzono T, Nishizawa Y, Inaba M. Enhancement of Cell-Based Therapeutic Angiogenesis Using a Novel Type of Injectable Scaffolds of Hydroxyapatite-Polymer Nanocomposite Microspheres. Plos One 2012;7.

45. Becker JC, Domschke W, Pohle T. Biological in vitro effects of fibrin glue: fibroblast proliferation, expression and binding of growth factors. Scandinavian journal of gastroenterology 2004;39:927-32.

46. Batorsky A, Liao J, Lund AW, Plopper GE, Stegemann JP. Encapsulation of adult human mesenchymal stem cells within collagen-agarose microenvironments. Biotechnology and bioengineering 2005;92:492-500.

47. Carpentier G. ImageJ contribution: Angiogenesis Analyzer. ImageJ News 2012.

48. Hauschka PV, Wians FH, Jr. Osteocalcin-hydroxyapatite interaction in the extracellular organic matrix of bone. The Anatomical record 1989;224:180-8.

49. Gailit J, Clarke C, Newman D, Tonnesen MG, Mosesson MW, Clark RA. Human fibroblasts bind directly to fibrinogen at RGD sites through integrin alpha(v)beta3. Experimental cell research 1997;232:118-26.

50. Grumezescu A. Nanobiomaterials in Galenic Formulations and Cosmetics: Applications of Nanobiomaterials: William Andrew; 2016.

CHAPTER 6

Conclusions and Future Directions

This chapter summarizes the work done in this dissertation including the motivation of the project and the current solutions that exist to resolve the problems caused by the disease within and outside the tissue engineering field. It includes the major findings discovered with the newly developed vascular microbeads and suggestions for future work. Some preliminary data collected for future work is also included to provide insight on the future directions.

6.1 Conclusion

This work aims to develop a potential re-vascularization therapy for patients suffering from critical limb ischemia (CLI). Current solutions for CLI patients include pharmaceutical therapies and surgical interventions. Although less invasive surgeries such as percutaneous transluminal angioplasty are successful at removing plaque from the arterial walls, open bypass surgery still provides better outcomes for CLI patients (improved life quality) than other solutions.

The tissue engineering field began with work to engineer artificial tissues/organs that can replace diseased ones from the body. Although there are many tissue engineering techniques that have re-vascularization potential including *in vivo* and *in vitro* pre-vascularization, patients must still have open surgery for these techniques to work. Unfortunately, there are many patients

who are inoperable due to comorbidities, such as in the case of diabetic patients who develop CLI. These patients often rely on experimental clinical trials to prevent limb amputation and death.

This dissertation describes a method to engineer vascular microbeads capable of forming endothelial sprouts during a pre-culture step and that inosculate with one another when embedded in fibrin hydrogels, both *in vitro* and *in vivo*. In the *in vitro* model, the fibrin hydrogel fixes the microbeads in a physical space and provides a controlled structural environment permitting the investigation of the cells' behavior and response to stimuli, and facilitating sprout quantification. In the *in vivo* model, the fibrin precursor was mixed with the microbeads to facilitate microbead injection [1].

Prior to this work, fibrin microbeads had not been engineered and preliminary studies focused on finding a collagen-fibrin composite for vascular microbeads that could achieve comparable endothelial sprout length to pure fibrin matrices. This study found that endothelial sprouting from embedded endothelial cells and mesenchymal cells was similar in a 40-60wt% COL-FIB matrix and a pure FIB matrix [2].

Our work began by making 40-60 wt% COL-FIB microbeads containing human umbilical vein endothelial cells (HUVECs) and human fibroblast that could sprout when embedded in fibrin hydrogels [3]. We then developed fibrin microbeads and compared them to the existing 40-60wt% COL-FIB microbeads to find differences in endothelial sprouting [4]. Both microbead types were embedded in fibrin hydrogels, cultured for 1 to 2 weeks, and quantified in terms of endothelial tube length. This study found that fibrin microbeads provided a higher endothelial sprouting that the 40-60 wt% COL-FIB microbeads (See Chapter 3). We also demonstrated that microvascular endothelial cells (MVECs) could be used in the fibrin microbead system developed [5].

We established that fibrin microbeads could be pre-cultured to allow endothelial sprout formation to occur within these microbeads without the necessity of embedding them into an additional matrix. We found that fibrin microbeads provided a better endothelial sprout coverage when cultured for 3 days instead of 1, 5, and 7 days prior to embedding them into fibrin hydrogels. A subcutaneous model was then used to determine whether this new modular vascular approach would facilitate vessel formation *in vivo* similarly to what had previously been shown with the delivery of endothelial cells with stromal cells in a fibrin matrix (cellular hydrogels) [6].

In addition to both pre-cultured fibrin microbeads and cellular hydrogels, control (non-pre-cultured) microbeads and acellular microbeads were also investigated with this *in vivo* model. The four groups of implants were injected for 1, 3, 7, and 14 days. However, all data shown in this dissertation comes from day 3 and day 7 implants. Day 1 implants did not provide much endothelial sprouting while some day 14 implants were difficult to find following remodeling (degradation). No vessel density differences were found in cellular experimental groups at either day 3 nor day 7. There was no surprise that human vessels were not found in the acellular microbead implants. Although there were no statistical differences in D7 cellular hydrogels and the fibrin microbeads, the average vessel density was higher in cellular hydrogels compared to the microbeads. However, the high variability between each independent implant meant there were no statistical differences between the cellular implants (See Chapter 4).

One of the most surprising findings was that the pre-cultured microbeads in fibrin hydrogels did not compact as much as the cellular hydrogel implants and the control microbeads after 3 and 7 days in situ. These results were confirmed by measuring implant' volume with ultrasound imaging *in vitro* one day after their production. No correlation was found between the implant mechanical properties, measured with a rheometer, and compaction, as it was found that

cellular hydrogels were stiffer than control microbeads and pre-cultured microbeads. However, pre-cultured microbeads were found to be stiffer than control microbeads, and cellular hydrogels when measuring regional stiffness using a dual-mode ultrasound elastography (DUE) technique.

We hypothesize that cells near the microbeads sense a stiffer matrix and take longer to degrade the matrix and migrate towards the remaining fibrin hydrogel as shown with the bright-field images comparing the pre-cultured and control microbeads embedded in fibrin hydrogels *in vitro*. Consequently, additional experiments must be done to test whether our hypothesis is correct. Nevertheless, we found that pre-cultured microbeads prevent implant compaction and provide a higher absolute number of vessels than the other cellular conditions tested. These results indicate that pre-cultured microbeads may be more useful than the other implants in an ischemic environment as it may be necessary for the implant site injected in the ischemic region to not compact while anastomoses between the host and implanted vessels occur.

Agarose-based microbeads were also developed to improve microbead yield and prevent microbead aggregation during pre-culture [7]. Microbead yield decreased when incorporating proteins in the microbead formula, while the addition of hydroxyapatite recovered some of the decrease in microbead yield. The combination of agarose (AG), hydroxyapatite (HA), and fibrinogen (FGN) in the microbead formula produced a more homogeneous distribution of endothelial sprouts compared to other microbead types embedded in fibrin hydrogels. Pre-culture was found to be slightly beneficial in AG+HA+FGN microbeads and not in the other agarose-based microbeads that did not support endothelial sprouting. Although this method can be employed for further pre-culture studies, its results can't be directly compared to the results from fibrin microbeads shown above as they were developed using a variation in the emulsification process. However, the behavior of different endothelial cells and stromal cells may be studied

using AG+HA+FGN to determine which co-culture can provide more endothelial sprouting (See Chapter 5).

6.2 Future Directions

Further testing is necessary to determine the clinical potential of the modular therapy for ischemia, including injectability studies, suitability with clinically relevant cells, clinically feasible pre-culture technique, evaluation in hind-limb ischemia model, and muscle function measurements. There are multiple *in vitro* and *in vivo* experiments described below to further demonstrate therapeutic potential and help provide additional understanding of this modular vascular system.

Injectability Studies

The model described in this dissertation employed fibrin as a delivery vehicle. The effects of shear stress on the stability of the formed networks can be calculated as previously done by Aguado et al. [8] to determine whether the mechanical properties of the fibrin microbeads need to be enhanced to augment cell viability and sprout integrity within the microbeads during the injection process. If this turns out to be the case, then increasing the fibrin concentration of the delivery vehicle and/or the microbeads themselves may be the solution to this problem.

Using More Clinically Relevant Cells

HUVECs as a therapeutic cell type are hampered by their limited availability. Endothelial progenitor cells (EPC) from cord blood, bone marrow, or peripheral circulation may be more

readily available and autologous [9, 10]. Therefore, future microbead studies should determine if sprout formation varies significantly depending on the endothelial and mural cell types utilized.

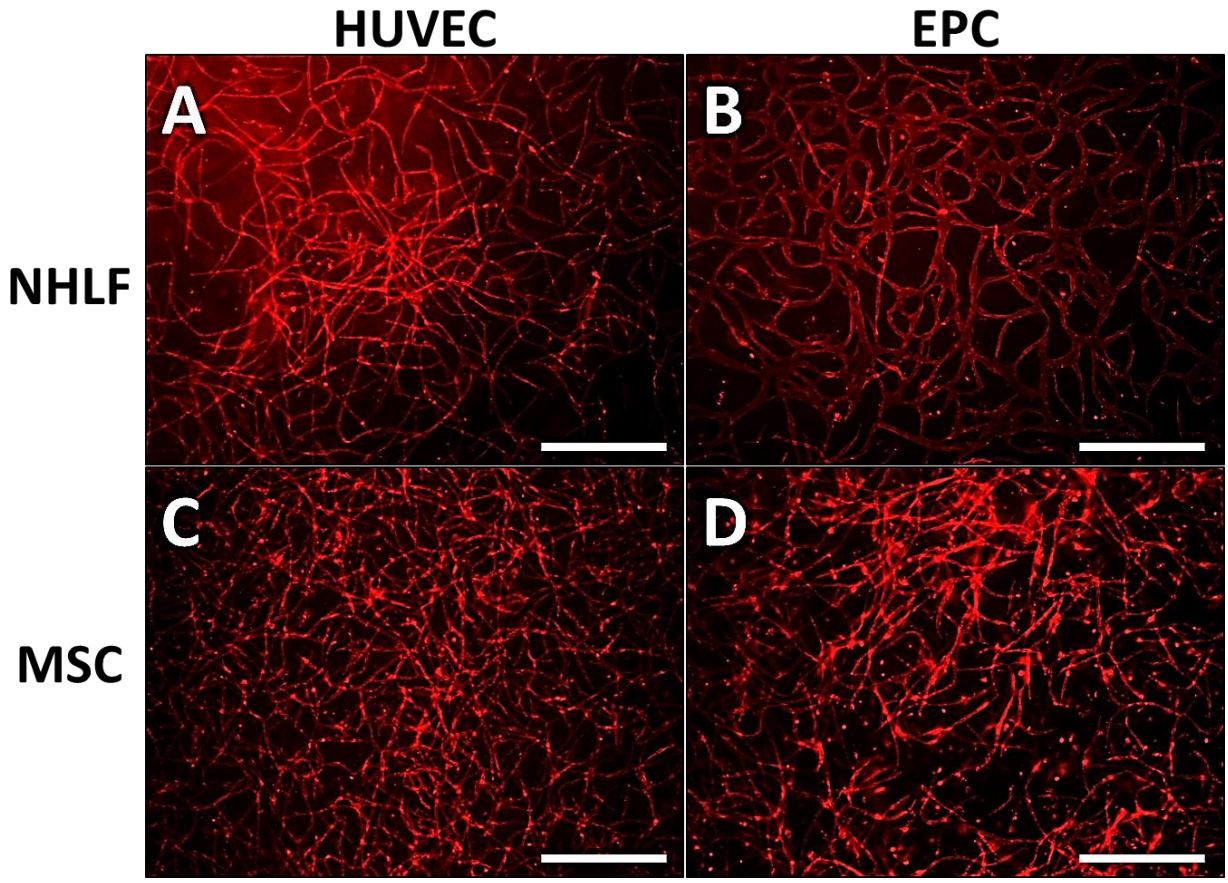

Figure 6-1: Images of endothelial networks in fibrin hydrogels after 7 days of culture. (A) HUVECs-NHLFs, (B) EPCs-NHLFs, (C) HUVECs-MSCs, and (D) EPCs-MSCs embedded in fibrin hydrogels at a 1:1 ratio at a total cell concentration of 500K/mL. Scale bar – 500 µm.

Preliminary studies in 3D fibrin hydrogels (vasculogenesis assay) demonstrated endothelial network formation is dependent on the endothelial cell source and mural cell types. Images of HUVECs-NHLFs (Fig. 6-1A), EPCs-NHLFs (Fig. 6-1B), HUVECs-MSCs (Fig. 6-1C), and EPCs-MSCs (Fig. 6-1D) embedded in a 1:1 ratio at 500K cells/mL show endothelial network differences. At least three individual experiments with 3 or more fibrin hydrogels per

condition/experiment were quantified using the angiogenesis tube module from the Metamorph software. The quantification of the different endothelial tubes/sprouts formed from HUVECs and EPCs co-cultured with NHLFs or MSCs in 3D fibrin hydrogels at three different total cell concentrations (125K, 250K, and 500K cells per mL of fibrin hydrogel solution) are displayed in Fig. 6-2 and Fig. 6-3.

The higher number of cells embedded in the fibrin hydrogel (initial cell concentration) formed a longer total tube length, except for the EPCs-NHLFs condition which total tube length went from ~ 79888 µm ± 15114 µm at 125K/mL to 71351 µm ± 17914 µm at 500K/mL (Fig. 6-2A). The EPCs-NHLFs condition also formed a longer total tube length than the other conditions embedded at 125K cells/mL. EPCs-NHLFs were also higher at 250K/mL; however, only statistically higher than the EPCs-MSCs condition. When co-cultures were embedded at 500K/mL, HUVECs-MSCs had the highest total tube length of all the conditions, but only statistically higher than the EPC-MSCs condition. (Fig. 6-2A).

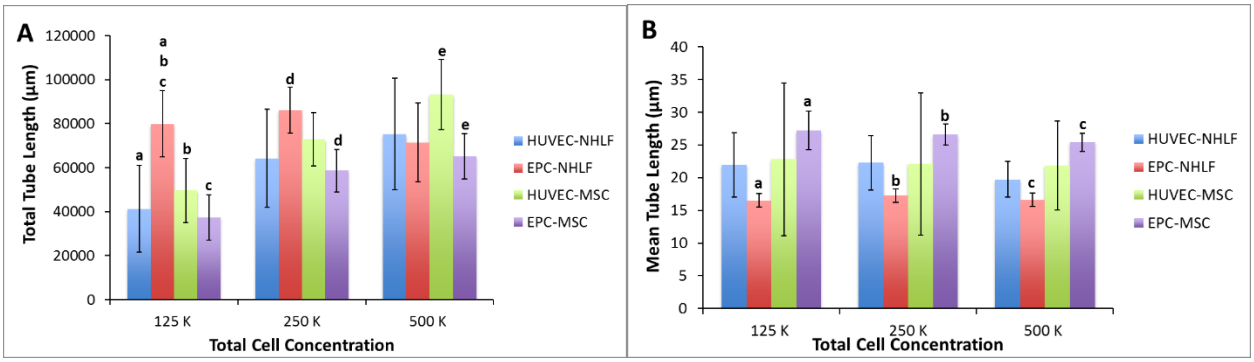

Figure 6-2: Quantification of (A) total endothelial tube length and (B) average tube length of different cell concentrations of endothelial and stromal cells. HUVECs-NHLFs, HUVECs-MSCs, EPCs-NHLFs, and EPCs-MSCs were embedded in fibrin hydrogel at three different cell concentrations (125K, 250K, and 500K/mL) in a 1:1 ratio.

Fig. 6-2B shows that the EPCs-MSCs condition had the highest average tube length compared to the other co-cultures; however, this condition was only statistically different than the

EPCs-NHLFs condition (at 125K/mL) and the EPCs-NHLFs condition (at 250K/mL and 500K/mL cell concentration). The number of segments (Fig. 6-3A), and the number of branch points (Fig. 6-3B) were also quantified from the endothelial networks formed from the different cell co-cultures. EPCs-NHLFs at the 125K/mL cell concentration had the highest number of segments and branch points of all the co-cultures ($p \leq 0.05$). The HUVECs-MSCs condition was the second highest, followed by HUVECs-NHLFs and EPCs-MSCs.

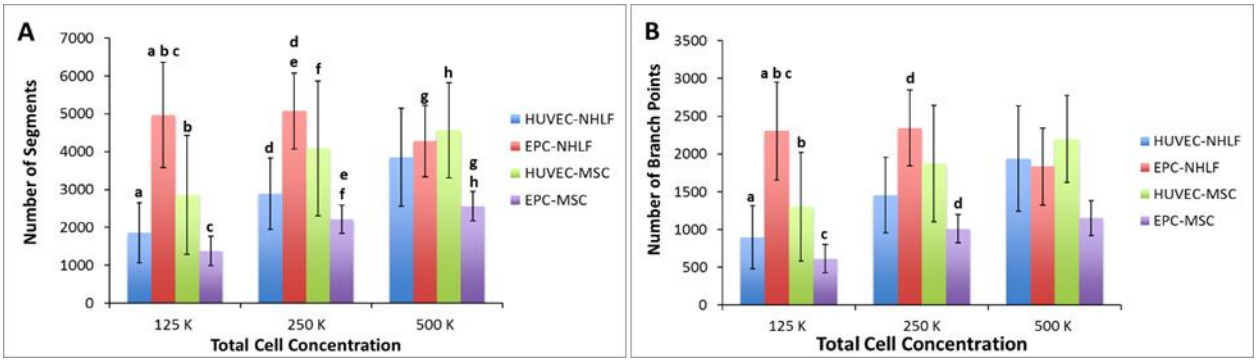

Figure 6-3: Average number of (A) segments and (B) branch points of endothelial cells (HUVECs and EPCs) co-cultured with NHLFs or MSCs at 125K/mL, 250K/mL, and 500K/mL (total cell concentrations) at a 1:1 ratio in 2.5 mg/mL fibrin hydrogels.

At the 250K/mL cell concentration, the EPCs-NHLFs condition had more segments than other conditions, but only statistically more than the HUVECs-NHLFs and the EPCs-MSCs conditions (Fig. 6-3A). On the other hand, EPCs-NHLFs only had a statistically higher number of branch points than the EPCs-MSCs condition at the 250K/mL cell concentration (Fig. 6-3B). Similar to the total tube length, the HUVECs-MSCs condition had higher number of segments than both EPCs-NHLFs and EPCs-MSCs conditions at 500K/mL (Fig. 6-3A). No statistical differences in number of branch points were found at the 500K/mL cell concentration (Fig. 6-3B). All the data graphed in Figs. 6-2 and 6-3 are tabulated for each total cell concentration in tables 6-1, 6-2, and 6-3.

Table 6-1: Endothelial network data of fibrin hydrogels containing endothelial cells co-cultured with NHLFs or MSCs at 125K/mL total cell concentration.

	Total Tube Length	Mean Tube Length	Segments	Branch Points
HUVEC-NHLF	4.1 ± 2.0 cm	22 ± 5 µm	1853 ± 793	897 ± 419
EPC-NHLF	8.0 ± 1.5 cm	17 ± 2 µm	4972 ± 1388	2304 ± 652
HUVEC-MSC	5.0 ± 1.4 cm	23 ± 12 µm	2863 ± 1568	1299 ± 719
EPC-MSC	3.7 ± 1.0 cm	27 ± 3 µm	1376 ± 387	614 ± 185

Table 6-2: Endothelial network data of fibrin hydrogels containing endothelial cells co-cultured with NHLFs or MSCs at 250K/mL total cell concentration.

	Total Tube Length	Mean Tube Length	Segments	Branch Points
HUVEC-NHLF	6.4 ± 2.2 cm	22 ± 4 µm	2894 ± 944	1452 ± 499
EPC-NHLF	8.6 ± 1.0 cm	17 ± 2 µm	5071 ± 1007	2345 ± 502
HUVEC-MSC	7.3 ± 1.2 cm	22 ± 11 µm	4089 ± 1778	1873 ± 769
EPC-MSC	5.9 ± 9.7 cm	27 ± 2 µm	2212 ± 376	1009 ± 188

Table 6-3: Endothelial network data of fibrin hydrogels containing endothelial cells co-cultured with NHLFs or MSCs at 500K/mL total cell concentration.

	Total Tube Length	Mean Tube Length	Segments	Branch Points
HUVEC-NHLF	7.5 ± 2.5 cm	20 ± 3 µm	3852 ± 1291	1940 ± 699
EPC-NHLF	7.1 ± 1.8 cm	17 ± 2 µm	4275 ± 941	1834 ± 511
HUVEC-MSC	9.3 ± 1.6 cm	22 ± 7 µm	4569 ± 1258	2200 ± 576
EPC-MSC	6.5 ± 1.0 cm	25 ± 1 µm	2561 ± 386	1153 ± 232

The EPCs-NHLFs condition shows potential for HUVECs-NHLFs replacement as it provides almost double the total tube length (8.0 cm ± 1.5 cm versus 4.1 cm ± 2.0 cm) at the lowest total cell concentration tested. However, the behavior of endothelial cells and fibroblasts encapsulated in microbeads may be different than in fibrin hydrogels as has been shown in Chapter 4. Therefore, it is important to study whether the above co-cultures will behave similarly in the modular vascular system.

Preliminary work using this modular system showed that EPCs-NHLFs microbeads (Fig. 6-4A, C) can form endothelial sprouts similarly to the HUVECs-NHLFs (Fig. 6-4B, D) conditions, whether with additional fibroblasts during embedding (Fig. 6-4C, D) or without (Fig. 6-4A, B).

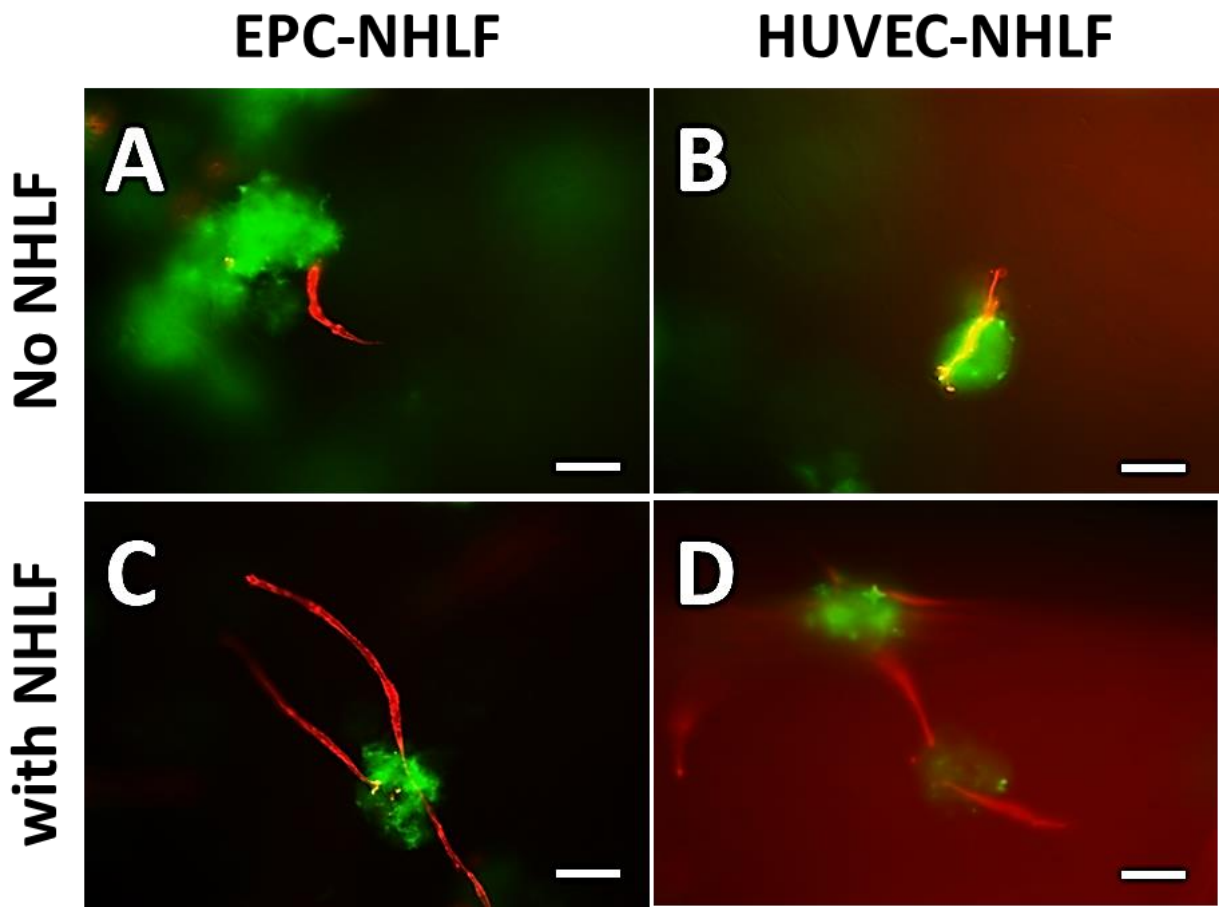

Figure 6-4: COL-FIB Microbeads with NHLFs co-cultured with HUVECs or EPCs. Scale bar – 220 µm.

Both Fig. 6-4 and Fig. 6-5 show microbeads in green (FITC) and endothelial cells in red (UEA-I). The staining procedure is described in Chapter 3. Microvascular endothelial cells (MVECs) are also an endothelial cell source than can be used in clinical studies. To determine if they would sprout, MVECs were also encapsulated with NHLFs in microbeads and embedded in fibrin hydrogels [5]. Fig. 6-5 shows MVEC sprouts come out of the microbeads and into the fibrin

hydrogels like all other endothelial conditions. However, to assess which endothelial cell works best in the microbead system, endothelial network from all the three different endothelial cell types must be studied in a controlled, side-by-side experiment as in the fibrin hydrogel study (Figs. 6-1, 6-2, 6-3). In addition, since MSCs have been shown to provide more stable vessels than NHLFs in animal studies [6], MSCs should also be employed to determine if they can provide a similar degree of network formation as NHLFs in the microbead system.

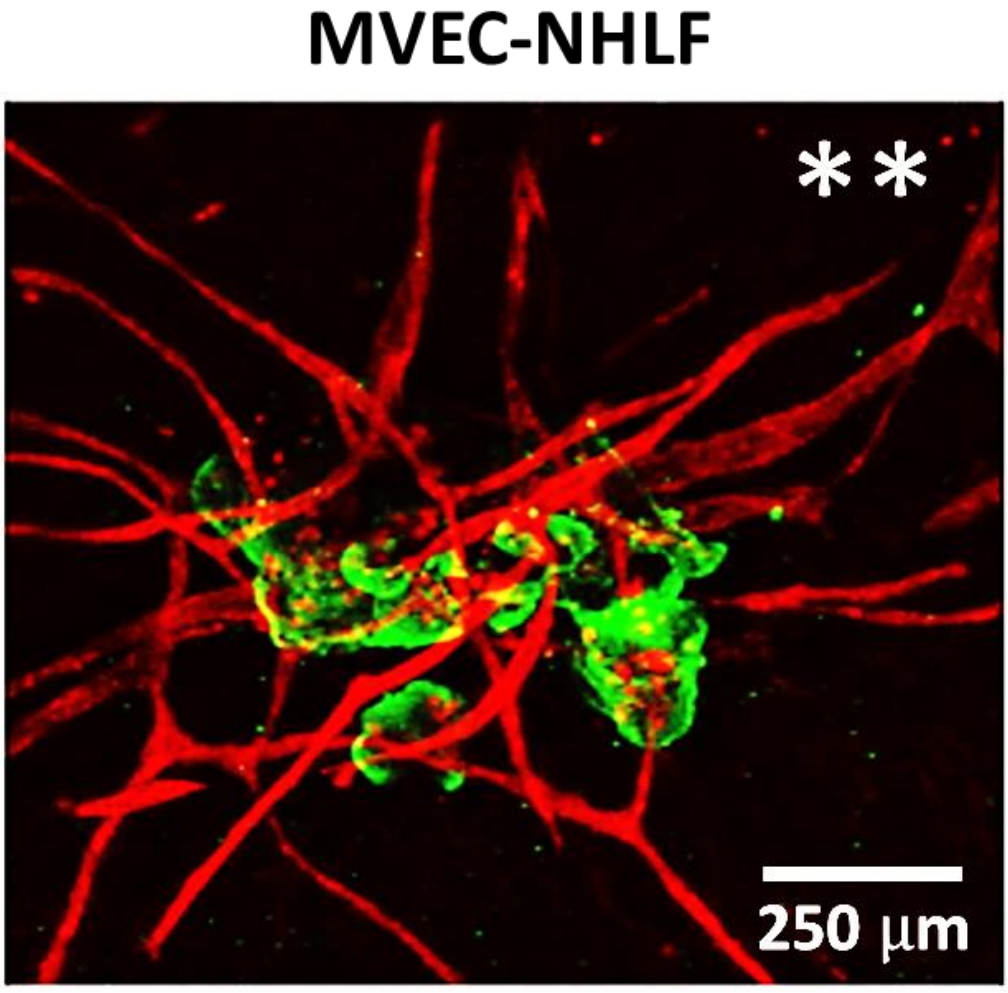

Figure 6-5: MVEC fibrin microbeads form sprout formation after 7 days in fibrin hydrogel immediately after their fabrication process. Scale bar – 250 µm. **Image from Ramkumar TA, Ana Y. Rioja, et al. ACS Biomater. Sci. Eng., 2016 [5].

Pre-culture Techniques

Microbead pre-culture has improved sprout length in both protein-based and agarose-based microbeads. Consequently, it is important to investigate the pre-culture conditions for alternative endothelial cell types and determine if endothelial sprouts can form when encapsulating these other endothelial cells with fibroblast in microbeads and pre-culturing them in the same manner as the HUVECs-NHLFs microbeads. Preliminary work showed that EPCs-NHLFs fibrin microbeads can form sprouts after being cultured statically for 7 days (Fig. 6-6). In addition, other pre-culture conditions can be explored including dynamic culture via the use of spinner flasks.

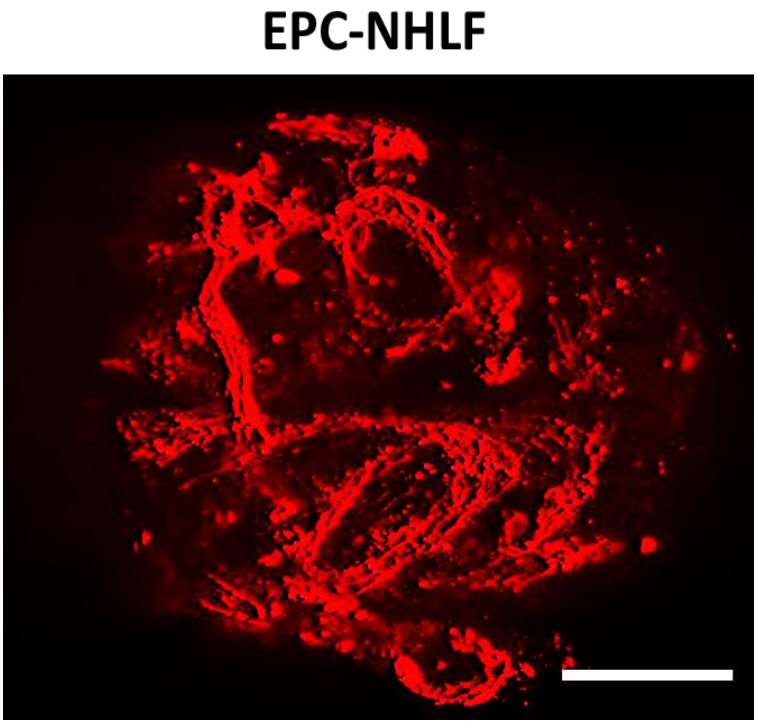

Figure 6-6: EPCs-NHLFs were encapsulated in fibrin microbeads and pre-cultured for 7 days. Scale bar – 100 µm.

Fig. 6-7 shows that HUVECs-NHLFs microbeads aggregated when pre-cultured for 7 days in a spinner flask prior to being embedded in fibrin hydrogels. Fig. 6-7A, B demonstrate that these

cellular microbeads can sprout when embedded immediately, as previously shown; however, once microbeads are pre-cultured for 7 days in the spinner flask at either at (Fig. 6-7C) 30 RPM or (Fig. 6-7D, E) 80 RPM, endothelial sprout formation does not occur after embedding in fibrin hydrogels.

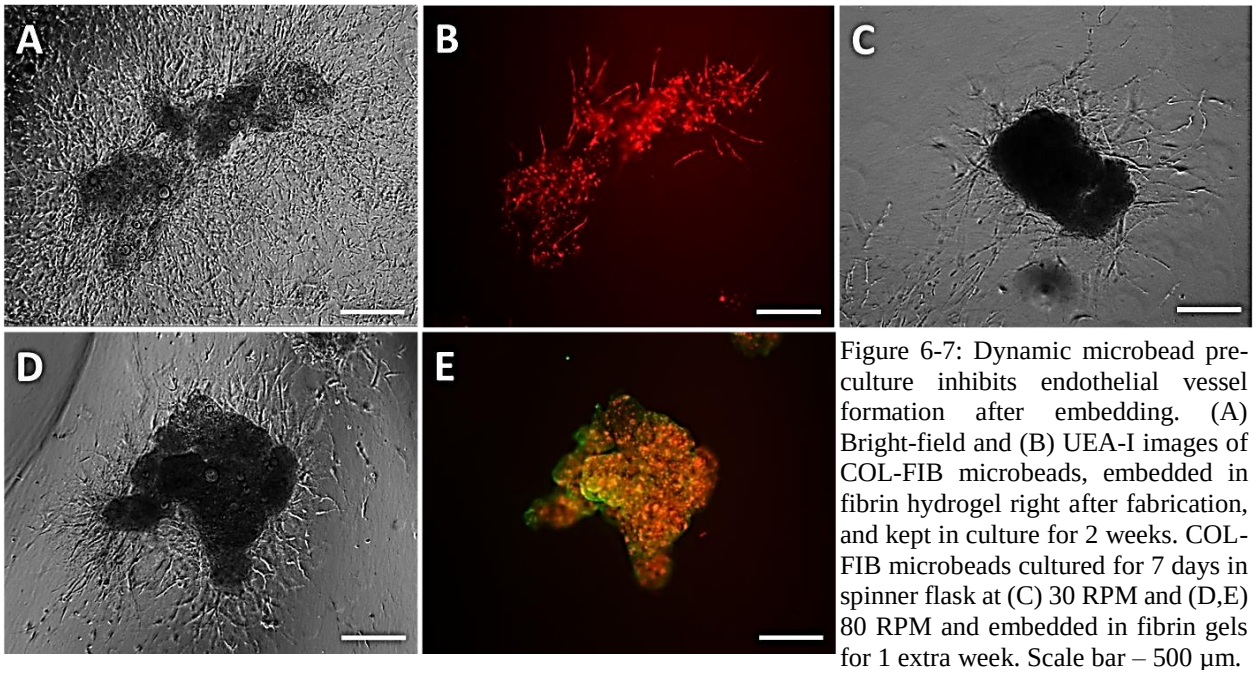

Figure 6-7: Dynamic microbead pre-culture inhibits endothelial vessel formation after embedding. (A) Bright-field and (B) UEA-I images of COL-FIB microbeads, embedded in fibrin hydrogel right after fabrication, and kept in culture for 2 weeks. COL-FIB microbeads cultured for 7 days in spinner flask at (C) 30 RPM and (D,E) 80 RPM and embedded in fibrin gels for 1 extra week. Scale bar – 500 µm.

The protein microtissues may not be useful in dynamic culture as they tend to aggregate during spinner flask culture. On the other hand, the AG+HA+FGN developed in Chapter 5 may be employed for pre-culture studies since they prevent aggregation, which could have a negative impact on endothelial sprouting. Microbead aggregation may decrease cell viability due to oxygen and nutrient diffusion limitations. By using the AG-based microbeads, studies can determine if dynamic culture improves sprout formation over static culture. It's also important to investigate how media volume affects the endothelial sprouting during pre-culture, as previous studies described in Chapter 5 showed that more media volume added to the microbeads led to more

endothelial sprouting after embedding in fibrin hydrogels. However, there may be a limit to this effect.

Use of Hind-limb Ischemia Model

Since the pre-cultured microbeads have been shown to prevent compaction and form a higher number of human endothelial vessels than control (no pre-culture) microbeads and fibrin hydrogels, it is important to study their behavior in ischemic conditions. A hind-limb ischemia model can be employed to evaluate the efficacy of the pre-cultured microbeads to inosculate with the host vasculature in an ischemic region. The model can also show whether HUVECs-NHLFs in fibrin hydrogels or in microbeads can re-vascularize and stabilize the network in an ischemic region in a similar time frame that it takes for the pre-cultured microbeads to do so.

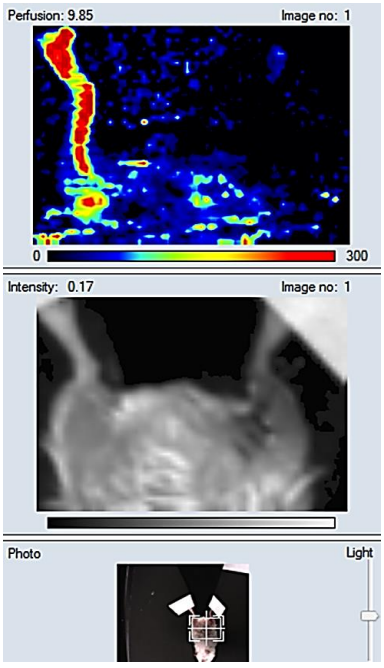

Figure 6-8: Laser Doppler perfusion imaging (LDPI) of ligated limb post-surgery.

An adaptation of the murine model of hind-limb ischemia described by Niiyama et al. 2009 [11] can be employed to assess blood flow restoration in 7- to 9-week-old male SCID mice (CB17/SCID, Taconic Labs, Germantown, NY). In brief, this model consists of surgically ligating of one of the mouse's deep femoral arteries. The procedure must be done carefully to avoid compromising additional vessels and nerves found in the hind limb region. Animals need to be anesthetized properly via intraperitoneal injection or isoflurane inhalation prior to surgery.

Each sample would be injected into the ligated region of the mouse to determine if the inosculation rate of pre-cultured microbeads with the host vasculature is faster than the control (no pre-culture) microbeads, acellular microbeads (negative control), and the cellular hydrogels. Each

implant type should be injected in a separate animal since one of the limbs from each animal must be kept as a basis of comparison. LDPI will be used to measure blood vessel perfusion during study (Fig. 6-8).

Muscle Activity Measurements

Cells residing within an ischemic area begin to die and stop their normal functions. Therefore, in addition to measuring re-vascularization, it is important to assess muscle activity within the region. Mice studies have implemented treadmills or running wheels to determine normal physical activity in mice [12], and they can indirectly measure muscle functionality after ischemia. Electromyography (EMG) analysis can also be used to analyze limb movement during hind-limb ischemia studies [13].

Additional methods such as the one described by Pipinos et al. [14] can also be employed to remove the muscle from the ischemic and control limbs to determine if muscles in the ischemic regions exhibit myopathy or whether the pre-cultured microbeads or other implants can re-vascularize the ischemic region fast enough to prevent muscle myopathy. Western blots and histological analysis can be done to determine muscle myopathy. Superoxide anion production in tissues will be measured using dihydroethidium staining. The main source of superoxide (a reactive oxygen species) production, is mitochondria, best known for energy production [15]. A possible link between improper mitochondria function and superoxide overproduction has been found, as superoxide anion production is higher in ischemic muscles. [15] Triphenyl tetrazolium chloride histochemistry is also used to determine if there are skeletal muscle infarctions in muscles close to the ischemic regions. [15] In addition, manganese superoxide dismutase (MnSOD) is a mitochondrial antioxidant whose expression decreases in ischemic versus normal muscle [14, 15]. MnSOD expression can be measured via western blot analysis as previously described [15].

Mechanistic Studies

Although most future studies will mainly focus on developing the vascular microtissues as a clinical therapy, the microbead model can also be used to study angiogenesis *in vitro*. The microcarrier bead assay [16] developed in 1995 is still being employed for mechanistic angiogenesis studies. However, since our model allows cell encapsulation inside microbeads, future mechanistic insight can be gained from the migration of cells from these microbeads and how microvessels form depending on the protein matrices they are encapsulated in or surrounded by.

One mechanistic study that we started uses a 3D collagen model containing pre-cultured/pre-vascular microbeads with gelatin microspheres. Gelatin microspheres are often used for growth factor delivery. This model was created to determine if the gelatin microspheres alone or loaded with growth factors like VEGF could increase endothelial vessel sprouting. Preliminary data show pre-cultured/pre-vascular HUVECs-NHLFs fibrin microbeads (Fig. 6-9A) embedded in either a 1.0 mg/mL (Fig. 6-9B) or a 2.5 mg/mL (Fig. 6-9D) collagen hydrogel with un-loaded (no growth factor) gelatin microspheres. Some pre-vascular microbeads were also embedded in a 1.0 mg/mL collagen hydrogel without any gelatin microspheres (Fig. 6-9C) to determine if the gelatin microspheres affected endothelial sprouting before growth factors were loaded in the gelatin microspheres. It was interesting to find that the addition of un-loaded gelatin microspheres promoted endothelial sprouting in collagen hydrogels made at 1.0 mg/mL and 2.5 mg/mL final concentrations. Future work is necessary to understand how these gelatin spheres affect the cells and promote sprouting within the collagen hydrogels.

RNA extraction can also be used to measure the levels of angiogenic markers (CD-31, CD-34, and vWF) from all samples via quantitative RT-PCR. These results would supplement the immunohistochemical data shown in the dissertation.

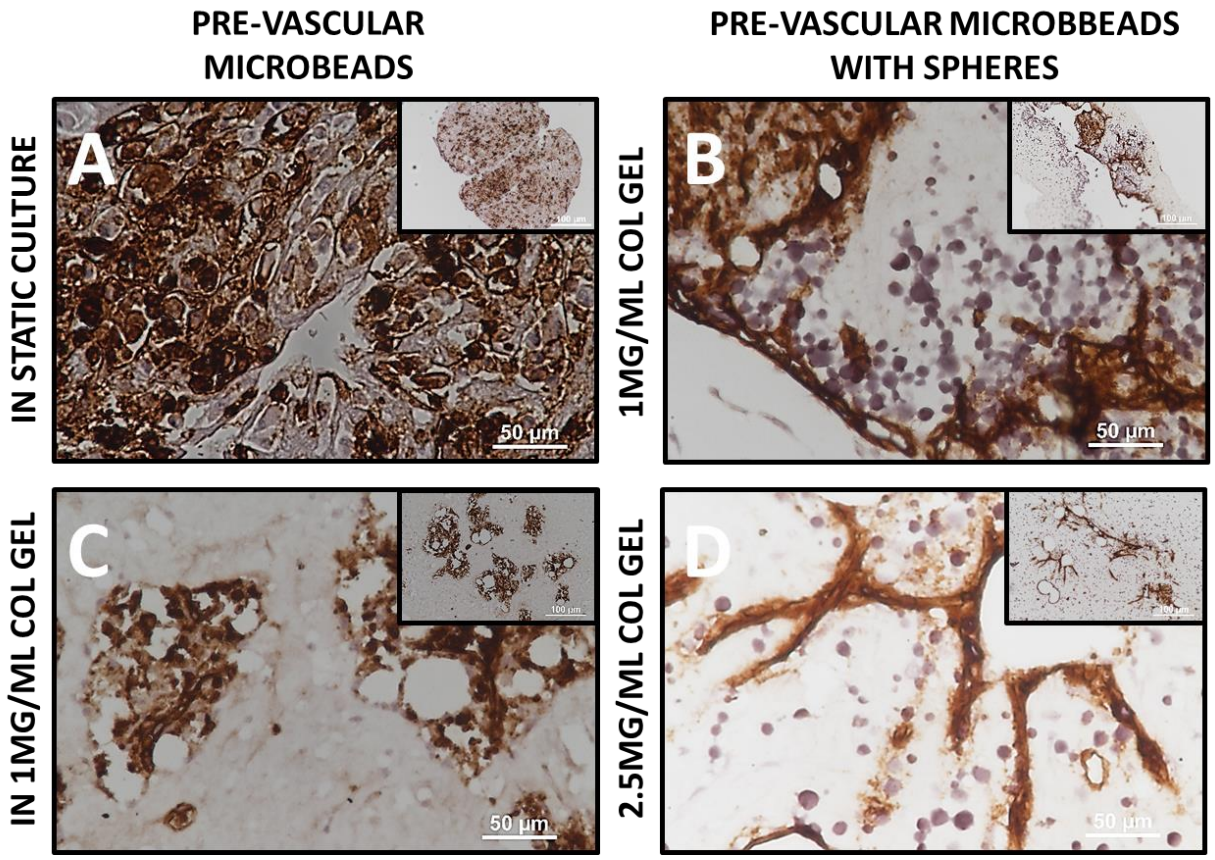

Figure 6-9: CD31 staining of pre-cultured/pre-vascular microbeads (A) after 3 days in static culture, (B) after being embedded and kept in culture in a 1 mg/mL collagen hydrogel (B) with and (C) without gelatin microspheres. These pre-vascular microbeads were also embedded in a (D) 2.5 mg/mL collagen hydrogel with gelatin microspheres. The addition of gelatin microspheres in both collagen hydrogel concentrations promoted endothelial sprouting within the hydrogel unlike in the collagen hydrogel that did not have any gelatin microspheres. Insets show a wider region of the collagen hydrogel containing multiple microbeads. Scale bar of main images – 50 µm and of insets – 100 µm.

In Vitro Inosculation

As previously described, inosculation is the process of vessels connecting to each other. This process is easy to assess *in vivo* as red blood cells can found within the lumens of human

vessels. The only way for red blood cells to be within those lumens is by the connection of the human vessels and the host vasculature. Inosculation *in vitro* is more difficult to demonstrate since the connection between two different endothelial sprouts must be proven. While the data in the previous chapters show that cells appear to be connecting to each other, 3D projections (z-stack) images would perhaps highlight that these connections, and lumen formation, are occurring in our model.

We have shown that lumen formation can occur *in vitro* as MVECs-NHLFs microbeads are embedded and cultured in fibrin hydrogels [5]. However, additional studies can be done to demonstrate that inosculation is occurring *in vitro*. An experimental study using two different endothelial cells with different fluorescent dyes can be utilized to demonstrate that inosculation occurs *in vitro*. In addition, a time-lapse microscope with 3D projection capabilities would show that a connection is occurring from two different endothelial sprouts in the fibrin hydrogels.

Physical and Chemical Characterization

Nuclear magnetic resonance (NMR) spectroscopy is often employed to study protein conformation [17]. For this reason, preliminary studies were conducted using NMR to determine if physical and chemical differences could be detected between different samples employed in the dissertation. First, (from left to right) fibrinogen, fibrin microbeads, and fibrin hydrogels with no cells were dissolved in deuterium oxide (Fig. 6-10). Fibrin hydrogels were more soluble in deuterium oxide (D_2O) than fibrin microbeads (Fig. 6-10). D_2O is water, where its two hydrogen atoms are replaced by their isotope deuterium. To avoid spectra dominated by the solvent signal, most ^1H NMR spectra are recorded in a deuterated solvent. However, deuteration is not 100%, so signals for the residual protons are observed. In water solvent (D_2O), the corresponding DHO peak

as a singlet signal is observed at 4.65 ppm. A detailed protocol of sample processing and NMR analysis can be found in appendix M.

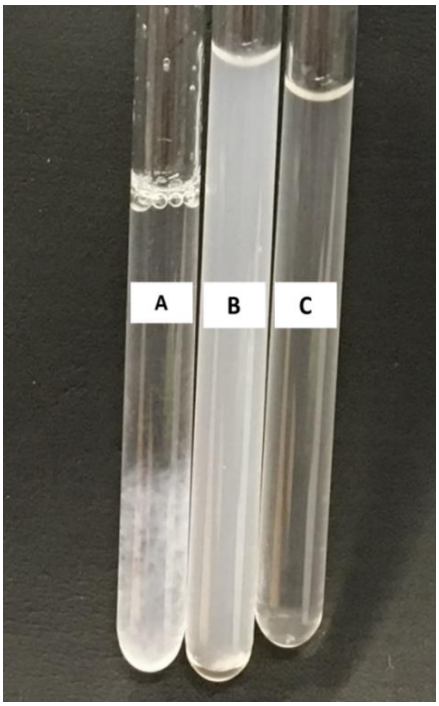

Figure 6-10: Solubility of (A) fibrinogen, (B) fibrin microbeads, and (C) fibrin hydrogels in deuterium oxide water.

Fibrinogen only (Fig. 6-11A), acellular fibrin microbeads (Fig. 6-11B), fibrin hydrogels (Fig. 6-11C), control (no pre-culture) microbeads (Fig. 6-11D), and pre-cultured microbeads (Fig. 6-11E) NMR spectra are shown in Fig. 6-11. Both the (Fig. 6-11D) control and the (Fig. 6-11E) pre-cultured microbeads were embedded in a fibrin hydrogel and left in culture overnight prior to the NMR spectra analysis. The first difference between the NMR spectra of all the samples is that acellular microbeads did not have an N-H peak unlike all other samples (Fig. 6-11B). In addition, the multiple peaks between 0 to 4 ppm found in both fibrinogen (Fig. 6-11A) and fibrin hydrogels (Fig. 6-11B) are missing in the acellular microbeads spectrum (Fig. 6-11B).

The control microbeads embedded in fibrin hydrogels (Fig. 6-11D) have similar, but slightly bigger peaks than the ones found in the fibrin hydrogel NMR spectrum (Fig. 6-11C). On the other hand, the pre-cultured microbeads embedded in a fibrin hydrogel displayed more peaks between the 0 to 4 ppm area (Fig. 6-11E) than both the control microbeads within a fibrin hydrogel (Fig. 6-11D), the acellular microbeads (Fig. 6-11B), and fibrin hydrogels (Fig. 6-11C). This result suggests that there may be additional matrix modifications done by cells encapsulated and left in culture for additional 3 days prior to embedding. Additional NMR descriptions of each sample can be found in Appendix M.

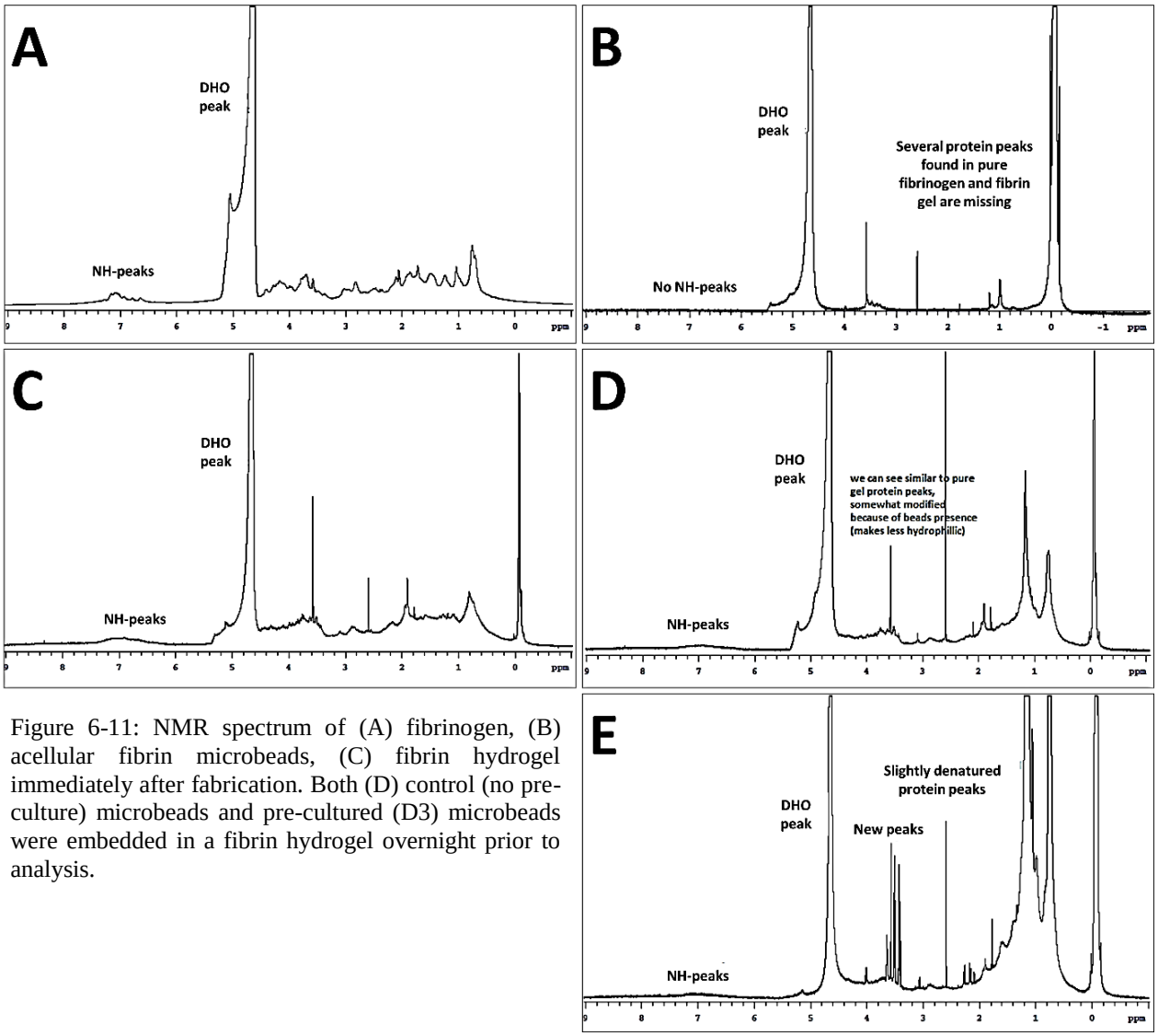

Figure 6-11: NMR spectrum of (A) fibrinogen, (B) acellular fibrin microbeads, (C) fibrin hydrogel immediately after fabrication. Both (D) control (no pre-culture) microbeads and pre-cultured (D3) microbeads were embedded in a fibrin hydrogel overnight prior to analysis.

Future studies will continue to characterize physical and chemical properties of these materials including control and pre-cultured microbeads alone to determine how the conformational changes affect the behavior of the endothelial cells in particular the endothelial sprouting.

6.3 References

1. Christman, K.L., et al., *Injectable fibrin scaffold improves cell transplant survival, reduces infarct expansion, and induces neovasculature formation in ischemic myocardium.* Journal of the American College of Cardiology, 2004. **44**(3): p. 654-660.

2. Rao, R.R., et al., *Matrix composition regulates three-dimensional network formation by endothelial cells and mesenchymal stem cells in collagen/fibrin materials.* Angiogenesis, 2012. **15**(2): p. 253-64.

3. Peterson, A.W., et al., *Vasculogenesis and Angiogenesis in Modular Collagen-Fibrin Microtissues.* Biomater Sci, 2014. **2**(10): p. 1497-1508.

4. Rioja, A.Y., et al., *Endothelial sprouting and network formation in collagen- and fibrin-based modular microbeads.* Acta Biomater, 2016. **29**: p. 33-41.

5. Tiruvannamalai Annamalai, R., et al., *Vascular Network Formation by Human Microvascular Endothelial Cells in Modular Fibrin Microtissues.* ACS Biomaterials Science & Engineering, 2016. **2**(11): p. 1914-1925.

6. Grainger, S.J., et al., *Stromal Cell Identity Influences the In Vivo Functionality of Engineered Capillary Networks Formed by Co-delivery of Endothelial Cells and Stromal Cells.* Tissue Engineering. Part A, 2013. **19**(9-10): p. 1209-1222.

7. Rioja, A.Y., et al., *Distributed Vasculogenesis from Modular Agarose-Hydroxyapatite-Fibrinogen Microbeads.* Acta Biomaterialia, 2017.

8. Aguado, B.A., et al., *Improving viability of stem cells during syringe needle flow through the design of hydrogel cell carriers.* Tissue Eng Part A, 2012. **18**(7-8): p. 806-15.

9. Chen, X., et al., *Rapid anastomosis of endothelial progenitor cell-derived vessels with host vasculature is promoted by a high density of cotransplanted fibroblasts.* Tissue Eng Part A, 2010. **16**(2): p. 585-94.

10. Melero-Martin, J.M. and J. Bischoff, *An in vivo experimental model for postnatal vasculogenesis.* Methods in enzymology, 2008. **445**: p. 303-329.

11. Niiyama, H., et al., *Murine model of hindlimb ischemia.* JoVE (Journal of Visualized Experiments), 2009(23): p. e1035-e1035.

12. Knab, A.M., et al., *Repeatability of exercise behaviors in mice.* Physiology & behavior, 2009. **98**(4): p. 433-440.

13. Akay, T., et al., *Behavioral and Electromyographic Characterization of Mice Lacking EphA4 Receptors.* Journal of Neurophysiology, 2006. **96**(2): p. 642-651.

14. Pipinos, I.I., et al., *Chronically ischemic mouse skeletal muscle exhibits myopathy in association with mitochondrial dysfunction and oxidative damage.* American Journal of Physiology. Regulatory, Integrative and Comparative Physiology, 2008. **295**(1): p. R290-R296.

15. Tran, T.P., et al., *Tourniquet-induced acute ischemia–reperfusion injury in mouse skeletal muscles: Involvement of superoxide.* European journal of pharmacology, 2011. **650**(1): p. 328-334.

16. Nehls, V. and D. Drenckhahn, *A novel, microcarrier-based in vitro assay for rapid and reliable quantification of three-dimensional cell migration and angiogenesis.* Microvascular research, 1995. **50**(3): p. 311-322.

17. Clayden, N. and R. Williams, *Peptide group shifts.* Journal of Magnetic Resonance (1969), 1982. **49**(3): p. 383-396.

Appendix A - HUVEC-NHLF Fibrin Hydrogel (Vasculogenesis Assay)

- Keywords:
  - SFEGM-2: Serum free EGM-2; FIB: Fibrin

- Initial Fibrin Stock (5.4 mg/mL), mix in SFEGM-2.
  - Place fibrinogen powder in 50 mL conical tube
  - Add SFEGM-2 to get a 5.4 mg/mL final concentration (4.0 mg/mL clottable factors)
  - Mix tube well and place it in water bath to help dissolve the fibrinogen
  - Filter the fibrinogen solution and place it on ice

- Fibrin Recipe (2 hydrogels → 1 mL):
  - SFEGM-2: 255 µL
  - FBS: 100 µL
  - Thrombin (1 UT/mL): 20 µL
  - FIB (4.0 mg/mL clottable stock): 625 µL

- Procedure:
  - Trypsinize cells (e.g. HUVECs, NHLFs)
  - Count cells and re-suspend cells with appropriate media [1 Million cells/mL]
    - HUVECs re-suspend in EGM-2 media
    - NHLFs re-suspend in M-199 media
  - Add $1x10^6$ desired cells into new 15 mL conical tube
    - If you use 1:1 HUVECs:NHLFs, then add 500k (500 µL) of each cell type
  - Centrifuge tube at 200g for 5 minutes
  - Take out and label 24 well (non-tissue culture treated) plate
  - Aspirate supernatant and begin adding the components mentioned above in the following order: SFEGM-2, FBS, Thrombin, and Fibrin
  - Mix cells wells after adding FBS and once again after adding fibrin
  - Add 500 µl of cell/fibrin solution to each well of a 24-well plate
  - Leave the 24 well plate in the hood for 5 minutes and then transfer it to the incubator for an additional 20 minutes (minimum)
  - Add 1 mL of EGM-2 to each well and replace media the next day and every other day after that

- Notes:
  - Maximum 3 gels can be made at a time prior to gelation to occur.
  - Make fibrin stock every time you make new gels.
  - Don't place fibrin from the water bath directly to ice. Filter it first and then place it on ice.

Appendix B – Isolation of HUVECs from umbilical cords

Materials [Storage]:

- 2 Haemostats [Tissue Culture room, in drying rack]
- 1 pair of scissors [Tissue Culture room, in drying rack]
- 2 L beaker [Glass cabinet]
- Foil and autoclave tape [Tape drawer, next to office supply drawer]
- 2, 5 mL syringe [Drawer below pH meter]
- 1, 33 mm Millex filter [Shelf on top of centrifuge in culture room]
- 2, 20 mL syringes [Drawer below pH meter]
- Butterfly needle [Shelf - above Marina's desk]
- 1, 18-gauge needle (or 16-gauge needle) [Shelf next to chemical airflow cabinet]
- 40 mL of sterile PBS [Cell culture fridge]
- 5 mL of 0.1% collagenase (sterile-filter) [Cell culture fridge, top-left corner]
- 5 mL of EGM-2 [Cell culture fridge]
- Umbilical Cord [Must be stored in 4 °C fridge A]

Protocol:

Day before doing this protocol:

- Place 2 haemostats, and 1 pair of scissors in a 2 L beaker. *One pair of scissors doesn't work properly; therefore, it's better to add the 2 pairs of scissors to the beaker.*
- Cover the beaker with aluminum foil and then tape one side of the aluminum foil to the beaker using autoclave tape.
- Autoclave beaker using the textiles setting.
    a. Sterilization time: 45 minutes
    b. Drying time: 10 minutes
- Check to make sure water level of pipe in the autoclave is at the specific set level. Then start the process.

---

1. Place the umbilical cord and the sterile PBS in the water bath. *Make sure that the cord is in the biohazard delivery bag to avoid contaminating the water bath.*
2. Make 5 mL of 0.1% of collagenase in PBS. *Make sure to make this solution every time this protocol is repeated, DO NOT store solution after experiment is completed. [Concentration = 5 mg/mL]*

0.1% collagenase in PBS

1	mL of PBS
0.001	0.1%collagenase
0.001	G
1	mg of Collagenase

Concentration: 1mg of collagenase/mL of PBS

Note*- Make 6 mL just to make sure you have enough after sterile filtering.*

3. Sterile filter the 0.1% collagenase solution using a 5 mL syringe with a 33 mm Millex filter.
4. Connect an 18-gauge needle to a 5 mL syringe and suction 5 mL of the sterile-filter collagenase. Place the syringe back in its wrapper for storage.
5. Remove the needle from the syringe carefully and throw it in the sharps needle biohazard container. *Make sure you don't recap the needle.*
6. Suction 20 mL of PBS in each 20 mL syringe. Put the syringes back in their wrappers for storage.
7. Sterilize the hood and all the materials needed in this protocol prior to putting them in the hood.
8. Place paper towels inside the hood *(use sufficient amount to cover your working area properly).*
9. Soak the towels with bleach *(make sure surface is completely wet with bleach).*
10. Put on a second pair of gloves prior to placing the umbilical cord in the container and especially prior to opening the umbilical cord container.
11. Take out the umbilical cord and PBS from the water bath and place them inside the hood after wiping them down with ethanol.
12. Take out the umbilical cord from its container and wipe off the clotted blood in the paper towels.
13. Locate the lines where they clamped the haemostats on both ends of the cord. Cut the cord below the clamp marks. *Use cord container as a waste container for the pieces cut from the cord. The cleaner the cut is the easier it is to locate the veins and arteries.*
14. Gently slide half of the butterfly needle into the vein and clamp the cord with the needle using the haemostat. *You must spiral the needle around because vein spirals around the outside. NOTE – Leave the plastic casing of the butterfly needle covering the needle when inserting it into the vein. The vein looks like a stretch mark. You shouldn't have to put a lot of force when inserting the needle to the vein, there should be no resistance.*
15. Remove the extra part of the butterfly needle so that you only have the tube connected to the butterfly needle. Attach the first 20mL syringe of PBS and inject all of it slowly into the vein making sure there are no clots. *Make sure the cord is on top of the waste container.*
16. Attach the collagenase syringe and begin injecting the solution until the liquid coming down changes its color to gold. (It takes approximately 1 mL of collagenase of color change to occur). *Make sure to put the cord on top of the white towel to make it easier to notice the liquid color change.*
17. Clamp the other end of the cord and very carefully re-inflate the vein with the 4 mL of collagenase remaining in the syringe.

18. Carefully place everything in the autoclaved beaker which initially contained the haemostats and scissors. Cover the top with the aluminum foil taped at one side of the beaker.
19. Remove your outer pair of gloves and take the 2 L beaker to the bottom shelf of the incubator. *If there is no space, then use the top incubator instead. Don't clean up workspace yet.*
20. Leave the cord in the incubator for **20 min**.
21. Put on a second pair of gloves and take out the cord from the incubator. Remove the haemostat that is *not* holding the needle and then attach the last 20 mL syringe of PBS.
22. Place the cord on top of a 50 mL centrifuge tube and begin injecting the PBS in the vein very slowly to wash off the cells but avoid bursting the vein. Collect the entire solution in the 50mL tube and then discard the cord in the waste container after removing the needle and the haemostat holding it in place.
23. Centrifuge the tube in Setting 1 (200g for 5 min).
24. Make sure all waste goes in the biohazard bag. Clean up the hood with bleach and ethanol (rinsing).
25. Take out a 25 mL flask and place it in the clean hood. Label it: "HUVEC P.0, Date, Your initials".
26. Remove the 50 mL tube from the centrifuge and aspirate off the supernatant. *Make sure to do it carefully to avoid aspirating off the HUVECs.*
27. Add 5 mL of EGM-2 into centrifuge tube and mix well. Put the cell-media solution into the 25 mL flask.
28. Place the flask in the incubator overnight.
29. Place flask in the hood and aspirate off the medium. Add 5 mL of PBS and rock the flask.
30. Aspirate off the PBS and add 5 mL of PBS (2X).
31. Remove PBS and add 5 mL of EGM-2.
32. Look at the HUVECs under microscope. Let them grow on the T-25 flask and make sure to check on them every day. Cells should be confluent in less than 1 week. If not, throw the cells away.
33. Once the cells are confluent, trypsinize and passage them into 2 T-75 flasks.
34. Grow to confluency and freeze them down. Label them P.3.

Appendix C – Collagen-Fibrin Microbeads Protocol

- **Composition of 40-60 Col.- Fib. Beads (Total Volume: 3 mL):**
  - Collagen 750µL
  - Fibrinogen 1125µL
  - Thrombin 60µL
  - NaOH 150µL
  - FBS 300µL
  - 5X DMEM 300µL
  - Glyoxal 36µL
  - Media (SFEGM-2) 279µL

- **Storage of Ingredients:**
  - 5.4 mg/mL of Fibrinogen from bovine plasma → ThermoScientific refrigerator (top), outside the tissue culture room. Big container.
  - Thrombin 50 UT/mL → ThermoScientific refrigerator.
  - Oil (PDMS 100 C.S.) → Bench where the hot plate is.
  - Ice Machine is in the autoclave room.
  - Media, 5X DMEM, FBS, glyoxal, and collagen → Refrigerator in the Tissue Culture (TC) room.
  - PBS-L101 → Refrigerator in the TC room.

- **Notes:**
  - If you need 2 mL of fibrin solution, make 3 mL solution instead if 2 mL because you may lose some volume during the experimental process.
  - For vasculogenesis beads use EGM-2 without serum (SFEGM-2) to make the fibrin (this will allow you more time to mix all ingredients before the solution gels completely). For MSC Col-fib beads use serum free DMEM media.

- **Bead Preparation Procedure:**
  - Weight the necessary amount of fibrin (Fibrinogen from bovine plasma) needed for the experiment in a 50 mL tube.
  - Dissolve the fibrin in SFEGM-2 at ***5.4 mg/mL concentration***, sterile filter it, and then place it on ice. (Warm media facilitates the mixing with fibrinogen).

- Spray the bead processing area with 70% ethanol and then place the propeller, beaker, and ice container on their appropriate places. (*The propeller has to be place in the mixer apparatus.*)
- Fill half of the water container with sterile water (autoclaved water or DI water), and place it on top of the hot plate. The temperature of the water should be at 37 ºC prior to beginning the experiment.
- Rinse both endothelial cells (EC) and fibroblasts' flasks with DPBS and then add **3 mL** of trypsin to the EC flask (T-75), and **5 mL** of trypsin to the NHLFs flask (T-150). (*Standard – 3 mL of trypsin in T-75, 5 mL of trypsin in T-150, 10 mL of trypsin in T-225*).
- Place flasks in incubator for **4 to 5 minutes**.
- Check under microscope to make sure that all/most cells have lifted off the plate.
- Neutralize trypsin by adding and mixing the appropriate media to each flask. (*EGM-2 to ECs and M-199 to NHLFs*). [*Standard – 7 mL of media in T-75 flask, 5 mL in T-150 flask, and 10 mL in T-225 flask.*]
- Transfer the media/cell solution from each flask into 15mL conical tubes. After mixing the solution, take out **200 µL** and add it into a plastic coulter container that has been filled with 19.8 mL of Isoton solution (*use one container per cell type)*.
- Centrifuge both ECs and NHLFs 15 mL tubes for **5 min** at **200g**. While cells are in the centrifuge, count the number of cells using the Coulter Counter system.
- Carefully remove the 15mL tubes from the centrifuge and remove the supernatant from each tube. Make sure not to disturb the cell pellet when removing the supernatant.
- Add the necessary media to each tube in order to acquire a final cell concentration of **1 Million cells/mL**. (*Make sure to add the appropriate media to each cell type – EGM-2 for ECs, and M-199 for NHLFs.*)
- Combine both cells types in a new 15mL tube at the desired concentration and place it in the centrifuge for **5 min** at **200g**.
- Place the thrombin in the water bath. (Can do this during the centrifugation process, after the cells have been trypsinized).
- While the cells are in the centrifuge, add 75 mL of oil (PDMS 100C.S.) into a 100 mL beaker that has been placed on top of ice.
    1. Ice is placed in an orange rectangular container that has two rubber bands. Make sure that ice does not fall in the beaker and that the beaker does not move when the propeller is working.
    2. Use the 25 mL pipette to add the PDMS to the beaker; once the last 25 mL of oil has been added to the beaker, remove the automatic pipette and let the oil drip down the pipette.
- Place ice and beaker on the blue platform and raise the platform up until the propeller has been submerged in the PDMS solution.

1. Make sure both parts of the propeller are submerged in the oil without touching the bottom or the sides of the beaker.

- Barnant Mixer Controller → Can adjust time and speed (both variables change the size of the beads). Make sure the speed is set to **600 rpm**.
- When making the bead solution, add the following components:

1- Media. 2- FBS. 3- 5X DMEM. 4- NaOH, 5- Glyoxal. 6- Thrombin. 7- Collagen. 8- Fibrin.

- Mix solution well with a **5 mL** sterile pipette. Keep the pipette in the tube and remove both the tube and the pipette from the hood. *Make sure to c*over the container with your other hand.
- Start the propeller and begin adding the solution to the beaker.
    1. Note- When adding the collagen-fibrin solution, make sure the pipette is close to the shaft to avoid clump formation.
    2. Turn on/off the mixer a couple of times after all the solution has been added to the PDMS.
- After running the solution for **5 min** on ice. Remove the beaker and place it on top of the 37 °C water.
    1. Note- First, hold the beaker with your left hand close to the propeller, and then bring the platform down with the ice container.
    2. Remove the orange container with ice from the blue platform and replace it with the hot plate that has the 37 °C water.
    3. Place the beaker containing the PDMS/COL-FIB cell solution on top of the hot water and raise the beaker making sure that the solution is submerging both shafts of the propeller.
- Secure the beaker with a clamp to make sure that it doesn't move during the mixing process. Let the solution mix for the remaining time (25 min.)
- A few minutes before the mixing process is complete, take out the PBS with the surfactant (L101) [PBS-L101], and place it inside the hood.
- Take out ***two* 50 mL** conical tubes and place it on the rack.
- Once the mixing process is done, remove beaker with solution and place it inside the hood. Make sure to cover the top of the beaker with one hand to avoid any contamination that may occur while transporting the solution into the hood.
- Add **25 mL** of the oil solution to each 50mL conical tube.
    1. Note- Move the pipette clockwise (continuously) while aspirating the solution.
- Remove the remaining solution from the beaker and distribute it evenly between the two tubes.
    1. Note- Move the pipette clockwise while aspirating the solution.
- Add **5 mL** of PBS-L101 to each conical tube.
- Invert the tubes with your hand for **5 minutes**.
- Place the tubes in the centrifuge. **USE SETTING 4** (200g for 5 min).
- Remove oil from the tubes and place it back in the beaker.

- Once most of the oil has been removed from the tubes, wash a NEW pipette with PBS-L101 by aspirating PBS-L101 up and down.
- Using this NEW pipette, aspirate the bead-oil solution from each 50 mL conical tube and place it into a new **15 mL** tube (2 tubes total).
- Add **8 mL** of PBS-L101 to one of the e*mpty* 50 mL tubes, in order to collect any of the remaining beads, and then rinse the second 50 mL tube with the same solution.
- Add **4 mL** of the 8 mL solution to each 15 mL tube (*Note- Final solution per tube is approximately 12 mL when initial col-fib solution is 4.5 mL*).
- Centrifuge tubes once again at **Setting 4**.
- Remove the non-bead solution from both tubes, then with a NEW pipette rinsed with PBS-L101, collect the beads and place them in one new 15 mL conical tube.
- Add **5 mL** of PBS-L101 and mix well. (*Total solution is approximately 6 mL*).
- Place tube for **10 minutes** in the incubator. Make sure the cap in the tube is loose to allow air flow.
- Proceed to centrifuge the beads using **Setting 4**.
- Take out the supernatant and add EGM-2 to the tube. (*Add the same volume of EGM-2 that was originally used in the COL-FIB bead solution*). [If the beads were made with an original 3.0 mL solution, then add 3.0 mL of EGM-2 to the beads].
- Transfer the bead/media solution into a new labeled 15 mL conical tube, and place it in the incubator. Make sure the cap is loose to allow air flow.
- Change the media of the beads the next day and then every other day until the desired time point.
- Dispense the oil in the waste container located on the bench close to the sink.

Appendix D – Fibrin only cellular microbead Protocol

- Total Cell Density:
  - Desired: 2.0M cells/mL
    - 3.0M HUVECs, 3.0M NHLFs = 6.0M total in 3.0 mL FIB solution.

- Total Fibrinogen Needed:
  - 5.4 mg/mL initial fibrinogen concentration (includes the protein and clottable concentration) in SFEGM-2

  - ******* Leave in water bath to assure fibrin is completely dissolved (for a minimum of 30 minutes). Sterile filter solution prior to making the microbeads.

- FIBRIN Recipe: (Total = 3 mL)

  - SFEGM-2 765 µL
  - FBS 300 µL
  - Thrombin 60 µL
  - Fibrin 1875 µL

- Same procedure as COL-FIB microbead procedure (see appendix C)
- Normal three washes were made:

  - Wash #1:
    - Washed the 25-mL plastic pipette with PBS+L101 prior to distributing the beads and PDMS into the 50mL conical tubes.
    - Separated the 75 mL of beads and PDMS solution into two 50 mL conical tubes.
    - Added 5 mL of PBS+L101 solution into each tube and inverted tubes for 5 minutes.
    - Centrifuged for 5 minutes at 200g acceleration and deceleration: 9.

  - Wash #2:
    - Aspirated off the PDMS and rinsed a 10 mL plastic pipette with PBS + L101 solution
    - Took the remaining solution from the 50 mL conical tubes and transfer it into two 15 mL conical tubes. (approximately 8mL per tube)
    - Added 4 mL of PBS+L101 on top of each tube and centrifuged for 5 min (same centrifuge settings as wash #1)

- Wash #3:
    - Removed supernatant and rinsed a 10 mL plastic pipette with PBS+L101 solution
    - Took the remaining bead solution from the 15 mL conical tubes and transfer it into a new 15 mL conical tube.
    - Added 5 mL of PBS+L101 to the bead pellet and mix well.
    - Placed the tube in the incubator for 10 minutes.
    - Centrifuged for additional 5 minutes (same parameters as previous washes).
- Mixed microbead pellet with EGM-2 for sprout length studies.

Notes: The 10-minute incubation time during wash 3 for FIB microbeads was no longer used (in Aim 2) for FIB microbeads pre-culture and in vivo studies since cell viability did not decrease when skipping this step.

Appendix E – Collagen Preparation

Collagen TYPE I

Storage: 4 °C [Fridge next to the CMITE cryogenic tank]

Cat No: 150026 Lot No: 9787K

250mg. MP Biomedicals, LLC. USA Reorder: 800.854.0530

Protocol

- Autoclave a 100 mL bottle with a small stir bar (in one bag), and big tweezers (in a separate bag).

- *Do steps 2 and 3 inside the hood*. Add **250 mg** of collagen to the autoclaved bottle using the autoclaved tweezers. [An entire bottle of collagen contains 250 mg of collagen].

- Add **62.5 mL** of **0.02 N** of **acetic acid** on top of the collagen.

- Close the lid of the bottle and label it appropriately. (i.e. ***4 mg/mL Collagen A.Y.R.***]

- Leave the bottle on top of spinner that is inside the fridge located next to the CMITE cryogenic tank for **1 day** to allow the collagen to dissolve completely.

Appendix F – Preparation of M199 Medium

Note- The following protocol has been taken from the Invitrogen website (see link below); however, some minor changes have been made to it.

1. Measure 5% less distilled water than the desired total volume of medium. *Use a mixing container that is as close to the final volume as possible.*
2. Add powdered medium to room temperature (15 °C to 30 °C) water with gentle stirring. *Do not heat the water.*
3. Rinse out the inside of package to remove all traces of powder. *Use the same water that is in the beaker to rinse out the package. It's easier if you employ a pipette to do this step.*
4. Add **2.2 g** of sodium bicarbonate ($NaHCO_3$) per liter of medium.
5. Dilute the desired volume with water. *Stir until dissolved by putting the beaker and the stirring bar on top of a stirring plate. DO NOT over-mix and do not apply heat.*
6. Adjust the pH to 0.2 and 0.3 units below the desired final working pH by slowly adding, with stirring, 1 N NaOH or 1 N HCl. *The pH may rise 0.1 to 0.3 units upon filtration.*
   Desired pH = 7.4.

7. After pH is adjusted keep container closed until medium is filtered.
8. Adjust the final volume with distilled water.
9. Sterilize immediately by membrane filtration with a 0.2-µm filter using a positive-pressure system.

   Source: http://www.invitrogen.com/site/us/en/home/References/gibco-cell-culture-basics/cell-culture-protocols/media-preparation-from-powder-and-concentrates.html

10. Once the 199 Media has been filtered, take out the desired amount needed for your experiments.
11. Add 10% FBS, 1% penicillin-streptomycin (P/S), and 0.1% Gentamicin reagent solution.

Both Media 199 with and without FBS and antibiotics can be stored in the refrigerator where all the other media is stored.

*Product information can be found in lab notebook 1, Pg. 48. **

Appendix G – Immunofluorescent staining of microbeads and hydrogels

1. Wash samples with **PBS** for 5 minutes by adding **300 µL** of PBS to each well or Eppendrof tube.
2. Fix cells in **10% formalin** for 10 minutes at room temperature by adding **200 µL** of formalin to each well/Eppendorf tube.
3. Wash samples with **PBS** for 5 minutes (4X → 20 minutes total). (**300 µL** of PBS for each sample).
4. Swirl container to make sure samples are rinsed thoroughly.
5. Permeabilize cells with **Tris-buffered saline (TBS) + 0.5% Triton X-100** for 10 minutes (4X → 20 minutes total). Add **200 µL** of TBS + 0.5% Triton X-100 solution to each sample.
6. Swirl container to make sure samples are rinsed thoroughly.
7. Wash samples with **TBS-T (TBS +0.1% Triton)** for 5 minutes by adding **400 µL** of TBS-T to each sample. (4X → 20 minutes total).
8. Swirl container to make sure samples are rinsed thoroughly.
9. Block with **2%BSA in TBS-T (Abdil)** for 20 minutes **at 4°C**. Add 400 µL of Abdil to each sample. [4 grams of albumin in 200 mL of TBS-T).
10. **Primary incubation at 4°C**.
    - **<u>Primary Antibodies (AB):</u>** (**1:100 dilution** → 1 µL of pAB in 100 µL of Abdil) *Use one of the following primary antibodies:*
        1. Mouse laminin [Stored in Fridge A, -20°C, in -20 °C Antibodies box].
        2. Rb to pAB laminin [Stored in Fridge A, -20°C in –Albert's box -20 °C]. (Rabbit to primary antibody laminin).
    - **<u>Phalloidin:</u>** (**1:250 dilution** → 1 µL of phalloidin in 250 µL of Abdil)
        1. Oregon Green 488 Phalloidin [Stored in Fridge XX]
11. Leave overnight.
12. Wash samples for 5 minutes in **TBS-T** (4X → 20 minutes). 400 µL of TBS-T on each sample.
13. Incubate with **secondary antibody** for 1 hour **at 4°C**.
    6 **<u>Secondary Antibodies:</u>** (**1:450 dilution** → 1µL of 2°AB in 450 µL of Abdil) *Use one of the following secondary antibodies:*
        1. Goat Anti-mouse Alexa 488
           [Storage: Fridge B, 4 °C, antibody box, side door]
        2. Goat Anti-rabbit Alexa 488

[Storage: Fridge B, 4 °C, antibody box, side door]

3. Goat Anti-mouse Alexa 594
   [Storage: Fridge B, 4 °C, antibody box, side door]
4. Goat Anti-rabbit Alexa 594
   [Storage: Fridge B, 4 °C, antibody box, side door]

***NOTE*- Make sure that if primary antibody is anti-rabbit, then secondary must be anti-rabbit too. You can't use Rb to pAB laminin for 1° antibody and Goat-anti-mouse for 2°.

14. Wash samples for 5 minutes in **TBS-T** (4X → 20 minutes). 400 µL of TBS-T on each sample.
15. Use **DAPI** to stain the nuclei of the samples (1:10,000 dilution in PBS) for 10 minutes **at 4 °C**. [Stored in Dr. Stegemann's fridge].
    7 0.5 µL in 5 mL PBS
    ***NOTE*- You can use **1:1000 dilution** for better results.

16. Wash samples for 5 minutes in **TBS-T** (4X → 20 minutes). 400 µL of TBS-T on each sample.
17. Store samples with **TBS-T at 4 °C**. Cover the samples with parafilm and foil to make sure that the TBS-T does not evaporate over time and that the samples are not exposed to light. Check over time to make sure TBS-T does not evaporate.

<u>Note:</u> The more times the samples are washed, the less background in the images.

Appendix H – Cell count microbead analysis

- Open Bright-field and DAPI images using ImageJ
- Open cell count analysis excel file

- <u>Measure Bead Diameter:</u>

    - Select bright-field image
    - Draw a horizontal line across the bead, hit **CTRL+M** to measure the diameter of the bead
    - Draw a vertical line across the bead, hit **CTRL+M** to measure the diameter of the bead

- <u>Measure Cell Count:</u>

    - Select DAPI image
    - Click Image → Lookup Tables → Blue
    - If there are more than 2 beads, then overlay bright-field image
        - Image → Overlay → Add Image
            - Select Image to add: **bright-field image**, change the opacity to **50%**
            - Click OK
    - Select Plugins → Analyze → Cell Counter
        - Hit Initialize, and then **type 1 counter**
        - Begin selecting each nucleus
            - The final number will appear on the rectangle to the right of the type 1 counter.
- Add data in excel file

Appendix I – H&E histology staining protocol

Note – This protocol is based on Ethan Daley's optimized protocol

Dewaxing slides

1. Wash slides with Xylene **2x** (5 min/wash) [Dewaxed with Xylene]

Re-hydration of slides

2. Wash slides with 100% ethanol **2x** (3 min/wash)
3. Wash slides with 95% ethanol **2x** (3 min/wash)
4. Wash slides with 70% ethanol **1x** (3 min/wash)
5. Wash slides with DI water **1x** (3 min/wash)

Staining of slides

6. Hematoxylin - 15 minute incubation time
7. Tap water (running water and rinsing) - 15 minutes
8. 95% Ethanol - **1x** (30 seconds)
9. Eosin - **1x** (1 minute)

Dehydration of slides

10. 95% Ethanol - **1x** (1 min/wash)
11. 100% Ethanol - **2x** (1 min/wash)

Clearing of slides

12. Wash slides with Xylene **2x** (3 min/wash)

Mounting coverslips on slides

- **DO NOT** wash coverslips with xylene (dip them in xylene)
- Add 3 to 4 small drops on the coverslip and place it on top of the slides
- Leave slides overnight

Notes

- **Stains:**
    - Mayer's Hematoxylin (Electron Microscopy Sciences 26252)
    - Eosin Y (Sigma HT110132)
- Use absolute ethanol to make reagents
- Always go left to right direction
- Double glove when washing with Xylene

Appendix J – Antigen Retrieval, CD31 Immunohistochemistry Staining

Deparaffinization and Rehydration:

**** Protocol from P. 8 of Dako General Instructions For Immunohistochemical Staining November 2009***

1. Place tap water in the food steamer and turn on while slides are being deparaffinized and rehydrated (steps below)
2. Take out **target retrieval solution** from the fridge and place it in a 100 mL beaker (enough volume to cover the cassette with the slides).
3. Place slides in the cassette.
4. Place slides in a **xylene** bath and incubate for 5 minutes. Transfer to a new xylene bath and leave for 5 minutes.
5. Tap off excess liquid and place slides in **100% ethanol** for 3 minutes. Transfer to a new 100% ethanol bath and leave for 3 minutes.
6. Tap off excess liquid and place slides in **95% ethanol** for 3 minutes. Transfer to a new bath and leave for 3 minutes.
7. Tap off excess liquid and place slides in **distilled water** for 30 seconds.

Antigen Retrieval:

**** Protocol designed with Anu David's helpful tips (Shikanov Lab's Post Doc)***

8. Place cassette in beaker containing the **target retrieval solution.** Use gloves to place the beaker in the food steamer.
9. Leave the beaker in the steamer for **35 minutes** (it takes about 13 minutes for the temperature in the beaker to turn 90 degrees C).
10. While your slides are in the steamer, prepare the slide chamber for the staining protocol.
    a. Cover the bottom of the slide chamber with tissues.
    b. Completely wet tissues with water, make sure some of the water remains in the chamber.
    c. Close the chamber and leave it on the counter until Step 15.
11. Take out beaker and let it cool for **30 minutes.**
12. Wash slides with **TBS-T (2 minutes, 3x)**. Change baths for every TBS-T wash.
13. Remove moisture from slides and tissues carefully.
14. Use **PAP pen** to mark around the tissue. Make sure not to touch the tissue with the pen.

Staining Protocol:

**** Protocol designed with Anu David's helpful tips (Shikanov Lab's Post Doc) and from Dako Envision+ System-HRP (DAB)***

15. Add enough **peroxidase block** to cover specimen completely. Place slides in slide chamber prepared to avoid slides from drying. Incubate for **5 minutes**.
16. Rinse gently with **TBS-T (2 minutes, 3x)**. Change baths for every TBS-T wash.
17. Remove moisture from slides and tissues carefully. Add **primary antibody** to cover entire specimen. 1:50 (i.e **5 µL CD31:245 µL of TBS-T**).
18. Place each slide in slide chamber, prepared to avoid slides from drying. Incubate for **16 hours** at 4 deg C.

---

19. Try to remove antibody carefully (one slide at a time,, 1st dip each slide in TBS-T to remove primary antibody). Then rinse gently with **TBS-T (2 minutes, 3x)**. Change baths for every TBS-T wash.
20. Tap off excess buffer, place slides in slide chamber, and add **peroxidase labelled polymer.** Incubate for **30 minutes.** Start making the Liquid DAB+ Substrate needed in step 23 when there are 10 minutes left of the incubation time.
21. Try to remove peroxidase labelled polymer carefully (one slide at a time). Then rinse gently with **TBS-T (2 minutes, 3x)**. Change baths for every TBS-T wash.
22. Remove moisture from slides and tissues carefully.
23. Place slides in slide chamber and add prepared **Liquid DAB+ substrate-chromogen solution** to slides. Incubate for **5 minutes.**

Preparation of Liquid DAB+ substrate-chromogen solution:

***To make 1 mL of the solution (for up to 10 tissue sections)*

1. Transfer 1 mL aliquot of **buffer substrate** into provided calibrated test tube (~40 µL/drop) [approximately ~33-35 drops]
2. For each 1 mL of buffer, add one drop (20 µL) of **liquid DAB+ Chromogen**
3. Mix immediately and apply to tissue section with pasteur pipette.

Note - *Prepared solution is stable for 5 days when stored at 4 deg C. Make sure solution is well mixed prior to adding to tissues.*

24. Rinse gently in **distilled water**. Collect waste in hazardous waste container.
25. Immerse slides in **hematoxylin and incubate for 15 minutes.**
26. Wash gently with tap water for **10 minutes** (water container, water should be clear)
27. Two washes with **95% ethanol** (1 minute per wash)
28. Two washes with **100% ethanol** (1 minute per wash)
29. Two washes with **xylene** (3 minute per wash)
30. Mount slides with mounting media and cover-slips. Let them dry overnight.

Appendix K – Alpha-smooth muscle actin immunohistochemistry staining

Same protocol as Appendix J, except:

- Primary antibody used: Smooth muscle actin monoclonal antibody (1A4 (asm-1)) [Invitrogen: Thermo Fisher Scientific]
- Concentration of antibody: 1:800 in TBS-T
- Incubation time: 2 hours.

Appendix L – CD31 Vessel Quantification (Single-blind study)

- Open 20x Images from each individual CD31 folder
    - Make sure you select every other 20x image (Images 1, 3, 5, 7, and 9).
    - Some folders may have more images, if this occur then divide the number of images by 5 to get a number "N". Analyze every Nth image (five images total).
        - Example: 40 images then 40/5 = 8, so images that will be analyzed are 8, 16, 24, 32, and 40.
    - Do NOT calibrate images

- **Quantify:** Excel Template

    - Vessel: Brown CD31 rim with erythrocytes
    - The number of vessels with hollow lumens (V_L)
    - The number of vessels with hollow lumens and erythrocytes inside the lumen (V_LE)
    - Measure the diameter of each vessel, make sure you keep track of which diameter belongs to which type of vessel (diameter of V_L vs. diameter of V_LE)
        - Some vessels are positioned longitudinal. In this case, make sure to measure the diameter that represents the entire vessel.
    - Keep track of the number of individual V_L/V_LE vs number of V_L/V_LE connected (i.e. you have a total of 10 V_L, 3 of them are by themselves, 1 group has 2 V_L connected and 1 group has 3 V_L)

- **Protocol:**

    - Open 20x image in ImageJ
    - Analyze → Set Measurements

        - Click area, shape descriptors, Feret's diameter, add to overlay, limit to threshold, and display label.
        - Decimal places: 2
        - Click OK
    - (You can start with diameter measurements first) Measure the diameter of the V_L and V_LE conditions Select the Straight line tool to begin measuring the diameters of V_L and V_LE.
        - Select the inner diameter of the vessel and hit CTRL+M
        - **Important Notes**
            - Keep track of the numbers for the V_L and V_LE diameters and then write it down in excel.
    - Plugins → Analyze → Cell Counter
        - Click on the image, click keep original and then click initialize
        - A new window will pop-up with a copy of your image
        - Click on the **Type 1** counter (blue) in the cell counter window and add every V_L
        - Click on the **Type 7** counter (red) in the cell counter window and start from the beginning counting every V_LE
        - Hit the Results button in the cell counter window and record the numbers from both Type 1 and Type 7 counter in the excel sheet
        - Close the cell counter window
    - Quantify the number of independents vs joint lumens
        - You can use either the first or second image. The cell counter can help facilitate this quantification.
    - Keep a copy of each image after analysis (save as JPEG).
    - Save the diameter results in a different excel file prior to adding these numbers to the CD31 vessel quantification excel sheet.
        - *This will be important in case we need to remove some of the data points based on a diameter size threshold.*
    - There is a Notes column in case you have any questions/comments about certain images.
    - Upload all excel sheets and images in the CD31 Quantification folder: https://drive.google.com/drive/folders/0B0wTvHQYVAykSk5vcHhFd19Ob0k

Appendix M – Nuclear Magnetic Resonance (NMR) analysis

Note – Based on Gopinath Tiruchinapally's protocol and analysis.

- Prepare fibrin constructs and transfer into dialysis bags (8 kDa MWCO).
- Dialyze samples with DI water for 2 days, then proceed to lyophilized to obtain dry samples
- Take 1.2 mg of each sample and dissolve it in 0.5 mL of D_2O.
    - Some samples required an additional 0.1 mL of solvent to dissolve properly.
- ^1H NMR spectra in D_2O were recorded on 700 MHz Varian Mercury systems (Palo Alto, CA) at room temperature.
    - NMR spectra were referenced using Me_4Si (0 ppm), residual D_2O at δ ^1H-NMR 4.65 ppm.

Pure fibrinogen: We observed amide NH-protons at 6.5-7.6 ppm. These are characteristic peaks for Aspartic acid (Asp), Glutamic acid (Glu), Glycine (Gly) and Lysine (Lys) peptide bonds. We observed several multiplets for carbohydrate portions of the protein at 3.00-4.50 ppm. These peaks are for Mannose (Man), Galactose (Gal) and N-acetylgalactosamine (GlcNAc) protons. Other characteristic peaks at 2.00 ppm and 2.60-2.80 ppm were observed for N-acetyl neuraminic acid.

Fibrin hydrogel: All peaks observed were similar to the ones found in pure fibrinogen NMR, but slightly distorted. For example, the amide NH peaks observed at 6.20-7.40 ppm were less intense than what we observed in pure fibrinogen. This could be because several NH peaks may be trapped inside the cross-linking network, and also might be participating in the network formation. We found almost all other peaks for amino acids and carbohydrates to be similar to the fibrinogen NMR. Interestingly two singlet peaks were observed at 2.58 ppm and 3.42 ppm, which is typically found if there is a methylation. We did not use any methylating agent during gel preparation, so this might be due to conformational changes in the sugar which exposes N-acetylneuraminic acid and mannose O-methyl groups.

Fibrin (acellular) microbeads: This NMR data was very different to the previous two NMRs. No NH peaks were found at 6.5-7.4 ppm. This indicates that the protein changed its conformation during the bead preparation. These microbeads were prepared in a hydrophobic mineral oil

(PDMS). During the emulsification process, the oil will most likely interact with the hydrophobic portions of the proteins and the hydrophilic portion (carbohydrate) of the protein may eventually get trapped inside the microbeads. This may be one of the reasons why we don't observe the amide protons. In other words, the inner portion of the protein did not experience the D_2O. Some of the carbohydrates peaks are also missing, which validates the theory that the microbead preparation method has an impact on how the fibrinogen protein individual molecules will arrange (cross-link) during the microbead formation (polymerization). To test our hypothesis, a hydrophilic solvent must be used for the microbead preparation to determine if we can see the NH amide protons.

Cellular control fibrin microbeads (non-pre-cultured) embedded in fibrin hydrogel for 1 day: We detected some low intense NH peaks for amides at 6.50- to 7.40 ppm, which is most likely attributed mainly to the hydrogel amides and not from the microbeads. The control microbeads' NMR was very similar to the fibrin hydrogel NMR with some modifications including some extra peaks at 0.4-1.50 ppm, which may be due to some cell debris (lipids) [1]. Some aliphatic fatty acid (lipids) peaks were found around 0.5-2.00 ppm. The low intensity of these peaks indicates that the more cells are more likely inside the microbeads than within the remaining fibrin hydrogel.

Cellular pre-cultured fibrin microbeads embedded in fibrin gel for 1 day: A more intense NH peak for amides at 6.50- to 7.40 ppm was found compared to the control microbead samples. A reason may be that microbeads may be opening in some areas and the amides from microbeads may be exposed to D_2O solvent, increasing the peak intensity. More aliphatic lipid peaks were observed around 0.5-2.2 ppm than in the control microbeads implant, which may indicate that more microbead openings are taken place during the 3 days. We also see some characteristic carbohydrate peaks around 3.30-3.80 ppm, which indicating that there is more exposure of the carbohydrates portion from the microbeads and the hydrogel. These peaks were not observed in pure fibrin hydrogels, acellular fibrin microbeads and control microbeads. This result suggests that there may be additional matrix modifications done by cells encapsulated and left in culture for additional 3 days prior to embedding.

There are two interesting outcomes from control and pre-cultured microbeads embedded in fibrin hydrogels' NMRs:

1. The time taken to dissociate some portions of the outer layer of the microbead is approximately 3 days.
2. The amount of debris (lipids) from the cells may indicate the amount of the cells come out of the beads into the gel/matrix.

Reference:

1. Duarte, I.F., et al., *Analytical approaches toward successful human cell metabolome studies by NMR spectroscopy*. 2009.

Appendix N – Fibrin Microbead Pre-culture

Protocol:

1. After microbead production, re-suspend the microbead pellet in **10 mL** of EGM-2 media.

2. Place the microbead/media solution in 15 mL Eppendorf tubes with air filters (CELLTREAT Scientific Products, Shirley, MA). Add each batch to a separate Eppendorf tube.

3. Place tubes up-right in the incubator at 37°C overnight.

4. Change media of microbeads, the next day and every other day after that.

5. Media changes are done by first centrifuging the tubes containing the microbeads for 1 min at 200xg to allow microbeads to settle to the bottom.

6. Remove media with plastic pipettes to prevent microbead aspiration.

   Note – Some left over media will be left in the tube ~1 to 1.5 mL of microbeads/media left in tube after media removal.

7. Re-suspend microbeads with 10 mL of fresh EGM-2. Make sure to mix well, at least 3 times up and down with plastic pipette.

8. Place tubes back in the incubator and change media every other day until experimental studies.

Important Notes:

- Fibrin microbeads may aggregate a lot, especially right after their fabrication process. Make sure to mix the microbeads with a plastic 10 mL pipette coated with EGM-2
    - Aspirate EGM-2 with pipette up and down a few times before mixing the media with microbeads to prevent microbeads sticking to the pipette.
    - Make sure NOT to use a P1000 to avoid additional aggregation of microbeads into P1000 tips.
- Media volume added to microbeads is important. Not adding enough media during pre-culture will cause a reduction in cell viability from cells encapsulated in microbeads.

Appendix O – AG+HA+FGN Microbead Processing

Protocol designed by Ana Y. Rioja and Ethan L.H. Daley

- **Cells:**
  - 2M total cells/mL in a 1:1 ratio of HUVECs:NHLFs co-cultures.
  - Each batch was made with 3 mL of solution
  - 2 batches of microbeads were made at a time.

- **Recipes (units in µl)**
  - **8 mg/mL AG**
    - 1200 AG
    - 480 FBS
    - 1320 SFEGM-2/cells
  - **8 mg/mL AG+15 mg/mL HA**
    - 1200 AG
    - 150 HA
    - 330 FBS
    - 1320 SFEGM-2/cells
  - **8 mg/mL AG+0.25 mg/mL FGN**
    - 1200 AG
    - 480 FBS
    - 1132.5 SFEGM-2/cells
    - 187.5 FGN
  - **8 mg/mL AG+1.25 mg/mL FGN**
    - 1200 AG
    - 480 FBS
    - 382.5 SFEGM-2/cells
    - 937.5 FGN
  - **8 mg/mL AG+15 mg/mL HA+0.25 mg/mL FGN**
    - 1200 AG
    - 150 HA
    - 330 FBS
    - 1132.5 SFEGM-2/cells
    - 187.5 FGN

- **8 mg/mL AG+15 mg/mL HA+1.25 mg/mL FGN**
    - 1200 AG
    - 150 HA
    - 330 FBS
    - 382.5 SFEGM-2/cells
    - 937.5 FGN

- **Protocol:**
    - Load the components above into a 10 mL syringe and inject (25-gauge needle) into 100 cSt polydimethylsiloxane (PDMS) oil (Clearco Products Co. Inc. Bensalem, PA).
    - Mix solution in PDMS at 700 rpm for 6 min at 37 °C and then for 30 min on ice to gel the resulting microbeads
    - Wash all microbeads with PBS and re-suspended to a total 9 mL volume (EGM-2 + beads)
    - Place 1 mL aliquots in 15 mL conical tubes with air filters caps (green caps) and leave them in the incubator overnight

- **Abbreviations:**
    - AG=agarose
    - HA= hydroxyapatite nanoparticles
    - FGN=fibrinogen
    - Agarose must be heated to 65 °C prior to use
    - HA needs to be sonicated for 15-20 min prior to use
    - FGN must be prepared the day of use
    - Total aqueous component volume= 3000 μL
    - Concentrations given in recipes are in 3000 μL volume

- **Stock solutions:**
    - AG: 20 mg/mL in dH_20
    - HA: 300 mg/mL in FBS
    - FGN: 4 mg/mL (clotting components) in serum-free EGM-2 (5.4 mg/mL total)

- **Notes -**
    - *Microbeads gelled too fast prior to adding the entire cell/solutions from the recipe above into the PDMS bath.* ***This occurred because AG was added last instead of FGN. Fibrinogen (FGN) must be added last.***

    - *All FGN was made fresh per batch to avoid fast gelation. FGN was left in the water bath for about 20 min max.*

Appendix P – Subcutaneous Injections, Implant Removal and Fixation

Materials:

- BD 1/2 cc Insulin Syringe U-1000 28G 1/2" needle Ref 309306 (Fisher Scientific Company LLC, Pittsburgh, PA)
- Puralube® Vet Ointment – Sterile ocular lubricant (Dechra, Overland Park, KS)
- Small cotton-tipped applicators Cat. No. 23-400-115 (Fisher Scientific)
- Sterile alcohol prep pads (Fisherbrand®)
- Sterling nitrile sterile powder-free exam gloves. KC300 (Kimberly-clark, Roswell, GA)
- Polylined sterile drape field. (18 in. x 26 in.) Ref No. 697 (Bosse, Hauppauge, NY)
- Drugs: Ketamine, xylazine, buprenorphine
- Additional materials: Cap, gown, mask, shoe covers, warming pad/blanket, heating lamp, nair hair removal, hair clipper, betadine antiseptic solution, forceps, and scissors, formalin, 20 mL vials, 70% ethanol.

Subcutaneous Injection Protocol:

1. Mice must be left in their housing facility for 3 days to acclimate prior to surgery
2. Appropriate gown, gloves, face mask, cap, and shoe covers must be worn prior to handling animals

All steps below were done under the hood, except for step #4

3. Administer drugs to each mouse before surgery via intraperitoneal (IP) injection

Drug Dosage (Anesthetic/analgesic):

- Ketamine 80-120 mg/kg IP
- Xylazine 5-10 mg/kg IP
- Buprenorphine: 0.05-0.01 mg/kg IP

4. Transfer each mouse into a cage placed under a warming blanket
5. Apply ointment to eyes of mice, once anesthesia takes effect
6. Shave the back of the mouse and then apply Nair hair removal to make sure injection site does not have any remaining hair
7. Use ethanol alcohol prep pads to remove any remaining Nair hair removal

8. Apply betadine antiseptic solution with small cotton-tipped applicators and alcohol prep pads twice to sterilize the area
9. Make a sterile area by placing a polylined sterile drape in the hood.
10. Drop syringes and needles (two of each) onto the sterile area (step 9)
11. Remove gloves and put on sterling nitrile sterile powder-free exam gloves. In the meantime, second person should prepare samples by adding fibrinogen and thrombin
    Note – Thrombin shouldn't be added until person injecting samples is prepared to do so
12. Mix samples thoroughly and inject each implant subcutaneously on flank of the mouse – one sample per flank. (Lift mouse skin with forceps to create a tent in order to facilitate injection)
13. Let the samples gel for 30 seconds and the rinse the injection site with ethanol alcohol pads.
14. Take Laser Doppler Perfusion Imaging (LDPI) of each mouse
15. After 12 hours, inject mice with a second dose of buprenorphine to prevent surgical pain

Implant Removal and Fixation Protocol:

16. After 1, 3, 7, and 14 days, inject the same drug dosage to mice as done prior to subcutaneous injections (see step 3 from section above)
17. Take Laser Doppler Perfusion Imaging (LDPI) of each mouse
18. Place mice in cage and turn on CO_2
19. Once mice are euthanized, make sure to perform a bilateral pneumothorax to ensure animal does not revive from carbon dioxide overdose
20. Wipe injection are with 70% ethanol
21. Open mouse to remove implant. Make sure to separate as much of the extra tissue from the implant prior to fixation
22. Place each implant into 20 mL vials containing Z-fix formalin
23. Store beakers in fridge for 24 hours
24. Rinse implants with phosphate buffer saline (2 to 4 times)
25. Add 70% ethanol to 20 mL vials containing implant and place it in fridge until tissue processing

- *Tissue processing protocol and additional details have been specified in Chapter 4 Materials and Methods*

Appendix Q – Preliminary Studies on Effects of Gelatin Spheres on Endothelial and Stromal Cells

Work done by Ana Y. Rioja and Paul A. Turner

Overall Project Goal:

Develop gelatin A microspheres crosslinked with genipin to load growth factors such as vascular endothelial growth factors (VEGF) and augment overall sprout length.

Preliminary Study:

Prior to starting VEGF delivery studies, preliminary studies were started to determine whether endothelial cells and other stromal cells could degrade the gelatin microspheres required to release the growth factors, once loaded. First, human umbilical vein endothelial cells (HUVECs), normal human lung fibroblast (NHLFs), adipose stem cells (ASCs), and mesenchymal stem cells (MSCs) were plated on two-dimensional (2D) tissue culture dishes with 200 µg microspheres per well to determine microsphere degradation. The gelatin microspheres were crosslinked with genipin (590 nm /620 nm, Cy5 filter) to measure degradation based on fluorescent readings using a plate reader (Biotek).

Bright-field images of microspheres alone or with HUVECs and NHLFs shows how HUVECs and NHLFs interact with microspheres. The microspheres alone are visualized in the Texas-red fluorescent images (Fig. Q-1). HUVECs degraded the microspheres the most, followed by ASCs, MSCs, and NHLFs (Fig. Q-1G). Microsphere degradation by HUVECs-NHLFs and HUVECs-ASCs were measured and compared to the stromal cells alone. These two stromal cells were used since one provided the least degradation while the other provided the most degradation of all the stromal cells from 2D studies

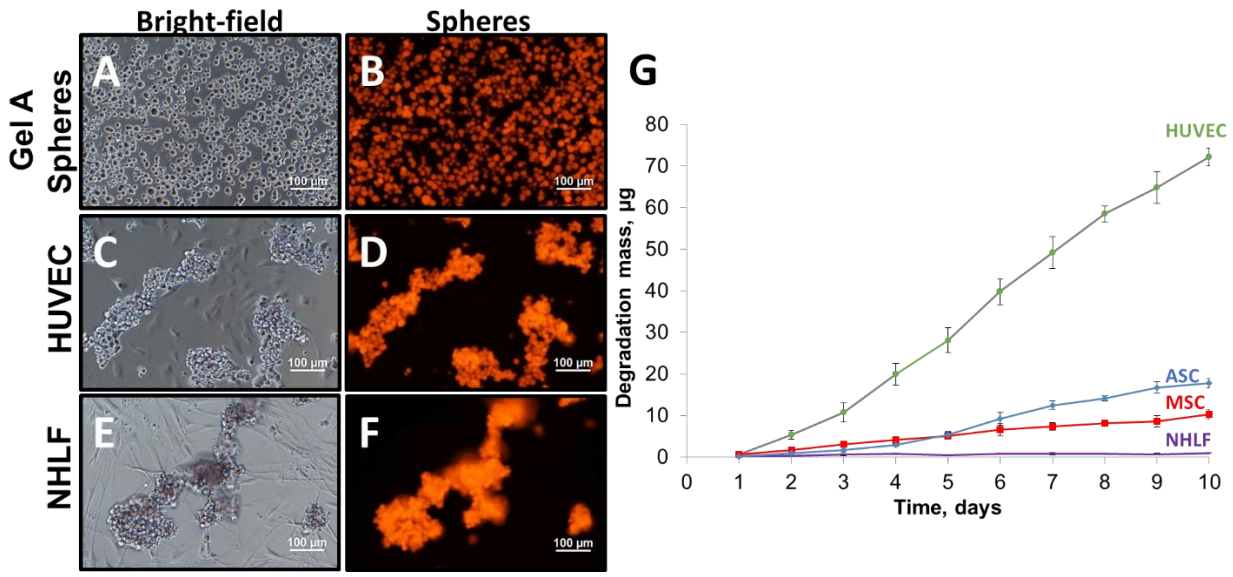

Figure Q-1: Cell type affects microsphere degradation (2D). Representative bright-field images of microspheres with (C, E) and without cells (A), and microsphere Texas-red fluorescent images (B, D, F). Quantification of degradation of microspheres by mono-cultures. Scale bar – 100 µm.

.

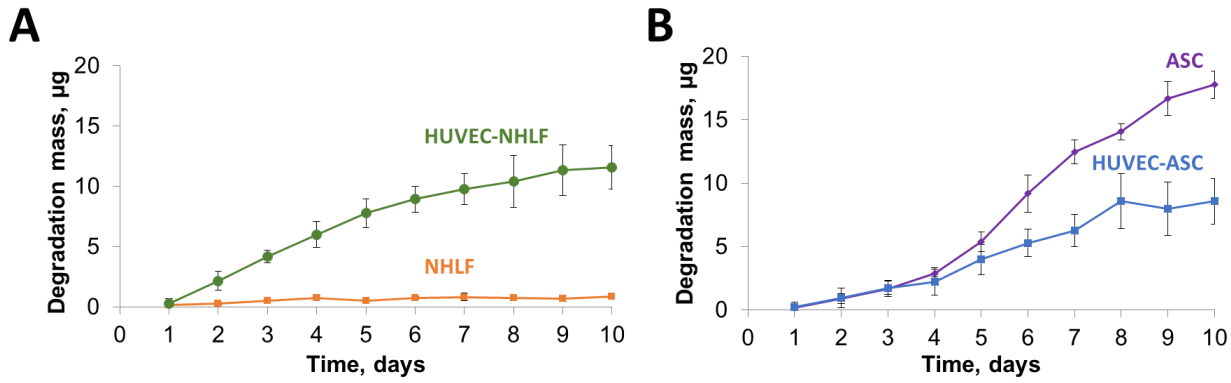

Figure Q-2: Co-cultures affect microsphere degradation (2D). (A) Microsphere degradation was higher when HUVECs-NHLFs were mixed rather than having NHLFs alone. (B) Degradation of microspheres by ASCs was higher than when combined with HUVECs (HUVECs-ASCs).

HUVECs-NHLFs co-cultures degraded the microspheres more than NHLFs alone (Fig. Q-2A), but not as much as HUVECs alone (Fig. Q-1G). On the other hand, ASCs alone degraded more microspheres than HUVECs-ASCs co-cultures (Fig. Q-2B), but once again not as high compared to HUVECs microsphere degradation. Three-dimensional (3D) studies were done to quantify endothelial sprouting and microsphere degradation in both fibrin and collagen hydrogels (Fig. Q-3).

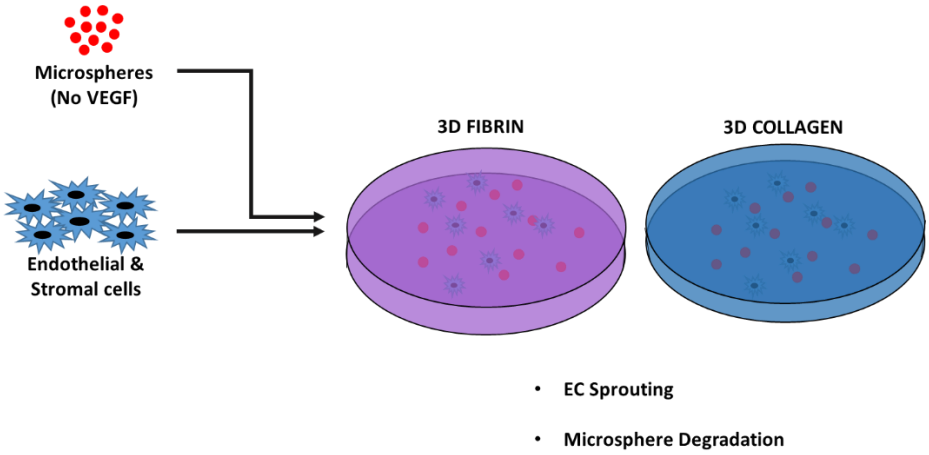

Figure Q-3: Study on effects on EC sprouting and gelatin microsphere degradation when embedding microspheres with stromal cells in three-dimensional fibrin and collagen hydrogels.

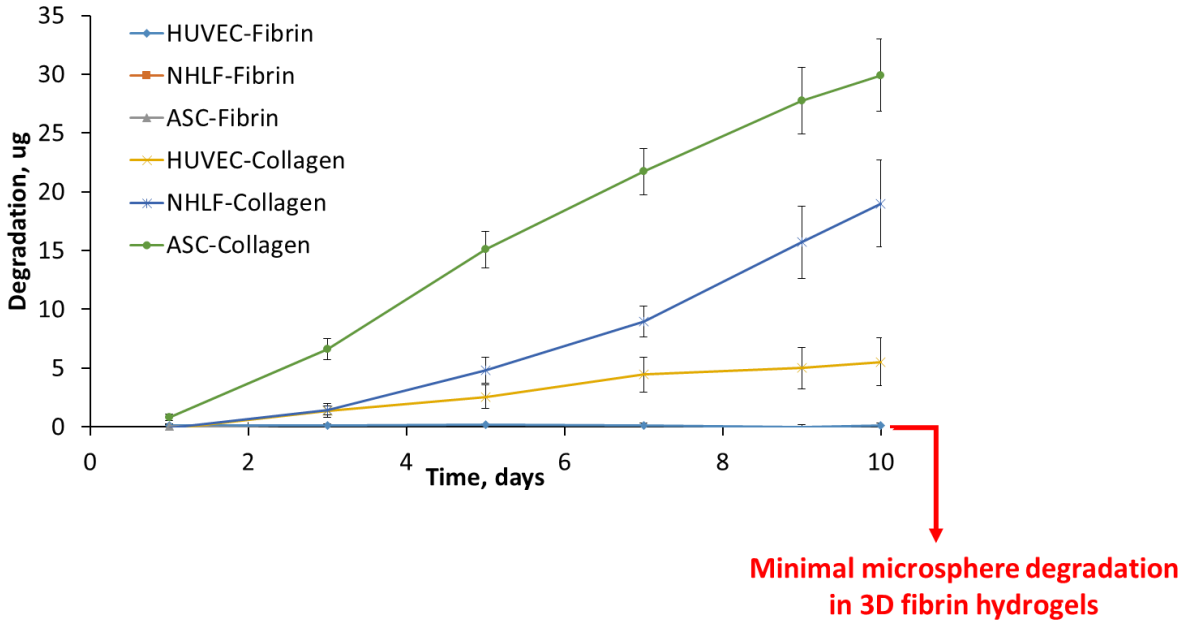

Figure Q-4: Microsphere degradation depends on matrix type.

To determine microsphere degradation on 3D systems; HUVECs, NHLFs, and ASCs were embedded in 2.5 mg/mL fibrin and 2.5 mg/mL collagen hydrogels (Fig. Q-4). The three cells embedded in fibrin hydrogels alone displayed minimal microsphere degradation. ASCs embedded

in collagen degraded microspheres the most, followed by NHLFs, and the least by HUVECs. This was surprising as HUVECs degraded the microspheres the most on the 2D system (Fig. Q-1G).

Vasculogenesis assays require both HUVECs-stromal cell co-cultures for proper vessel formation. For this reason, we embedded HUVECs co-cultured with NHLFs or ASCs. Previous studies done by our lab showed that sprout formation does not occur in collagen hydrogels. Therefore, HUVECs-NHLFs (Fig. Q-5 A-D) and HUVECs-ASCs (Fig. Q-5 E-H) were embedded with (Fig. Q-5 B-D, F-H) and without (Fig. Q-5A, E) microspheres in 2.5 mg/mL fibrin hydrogels only to determine effects of microspheres and stromal cells on sprout formation. HUVECs were stained with UEA-I, nuclei with DAPI, and microspheres (Texas-red)., After 10 days, total sprout length in HUVECs-NHLFs was higher than HUVECs-ASCs condition. However, the addition of microspheres caused a decrease in total sprout length in the HUVECs-NHLFs condition, and an increase in total sprout length in HUVECs-ASCs condition.

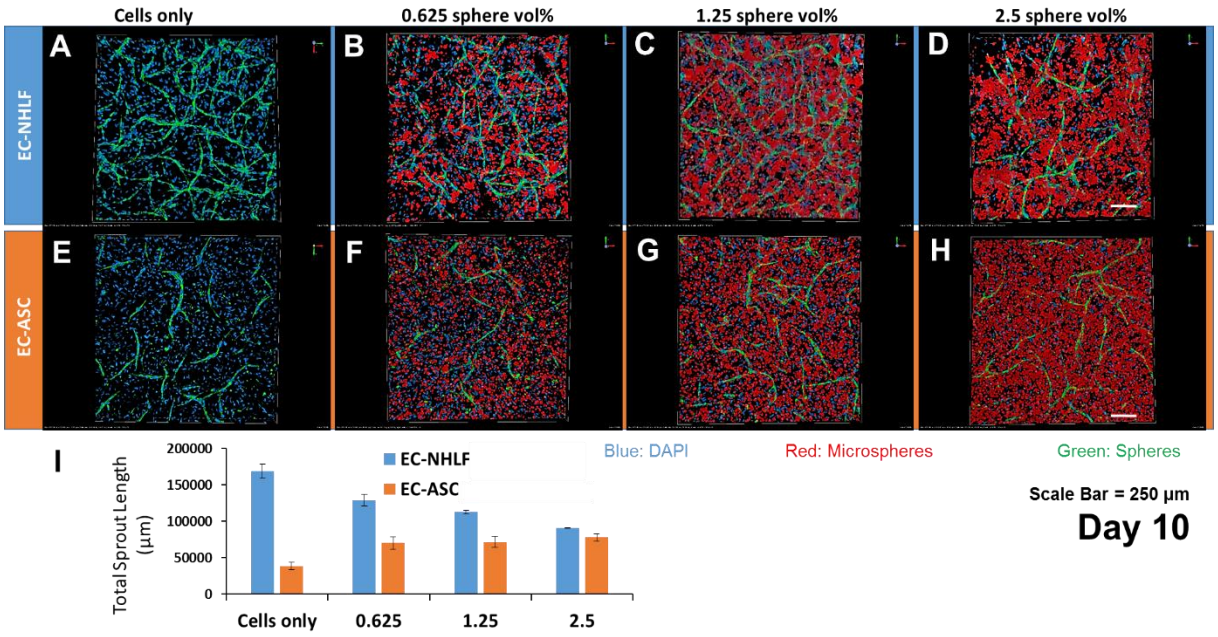

Figure Q-5: Microspheres affect endothelial sprouting in 3D fibrin hydrogels. (A-D) HUVECs-NHLFs or (E-H) HUVECs-ASCs were embedded in fibrin hydrogels (A, E) alone or with (B, F) 0.625, (C, G) 1.25, (D, H) 2.5 vol% of microspheres. (I) Quantification of endothelial sprouting of HUVEC-stromal cell type co-cultures after 10 days. Scale bar – 250 µm.

Since HUVECs and NHLFs formed the highest sprout length when embedded in fibrin, HUVECs-NHLFs fibrin microbeads were developed and pre-cultured for 3 days to allow some

sprout formation to occur (vascular microbeads). In addition, since microspheres were degraded the most by ASCs, then we embedded the pre-cultured microbeads with ASCs and microspheres with or without VEGF in 1.0 mg/mL and 2.5mg/mL collagen (Fig. Q-6).

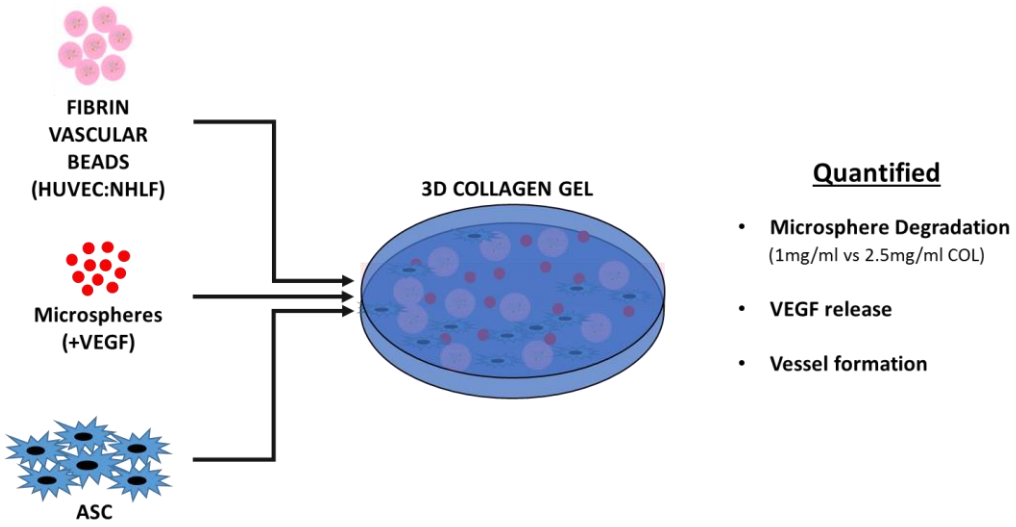

Figure Q-6: Microsphere degradation, VEGF release, and vessel formation studies of fibrin vascular microbeads containing HUVECs-NHLFs embedded with ASCs, and microspheres loaded with and without VEGF in 3D collagen hydrogels.

Loading microsphere with VEGF did not alter microsphere degradation by cells. In addition, an increase in microsphere degradation was found if cells were embedded in lower collagen concentrations (Fig. Q-7). The cumulative VEGF release was low in vascular microbeads embedded with unloaded microspheres in collagen hydrogels (Fig. Q-8) suggesting that VEGF release was due to the ASCs and vascular microbeads (HUVECs-NHLFs) interaction. In addition, the collagen hydrogel concentration (1.0 mg/mL vs. 2.5 mg/mL) did not affect the VEGF release. VEGF-loaded microspheres were embedded without cells in a 2.5 mg/mL collagen hydrogel, and had a higher cumulative VEGF release than cellular constructs with unloaded microspheres. Based on these results, it appears that VEGF-loaded microspheres have an initial burst release and then it reaches steady-state. This release is higher than what's secreted by the cells alone (Fig. Q-8).

Once vascular microbeads were embedded with VEGF-loaded microspheres in collagen hydrogels, the cumulative VEGF release increase even more than the previous conditions. In particular, embedding them in a lower collagen concentration (1.0 mg/mL) resulted in an even higher release of VEGF.

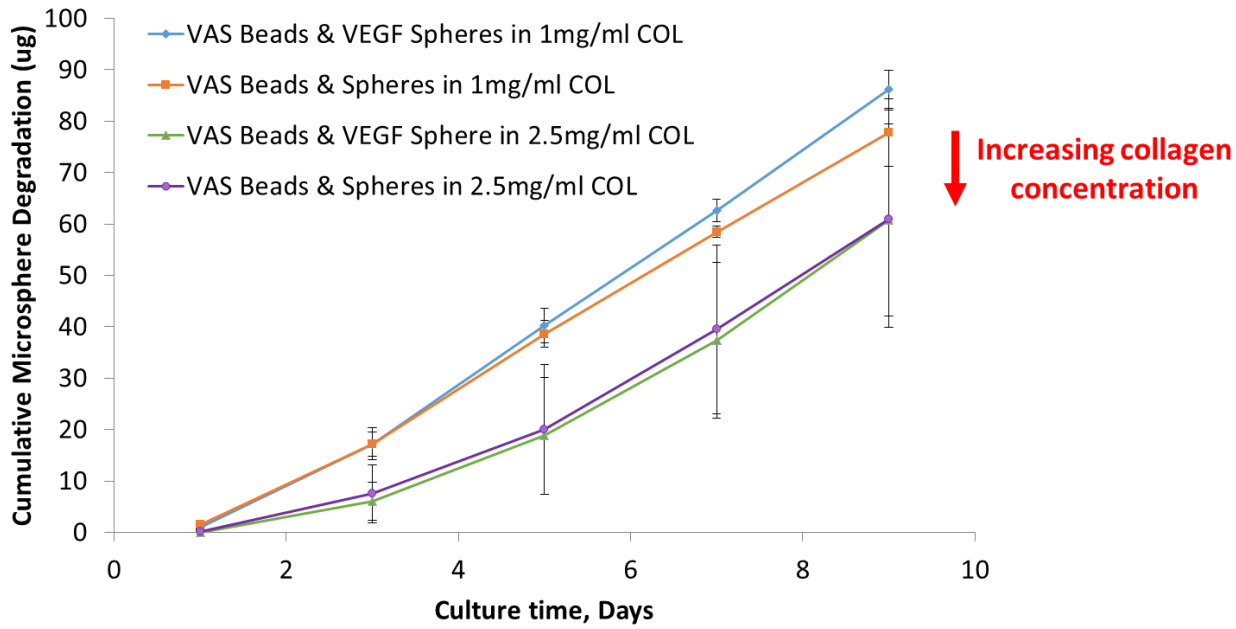

Figure Q-7: Degradation of microspheres decreases with collagen concentrations.

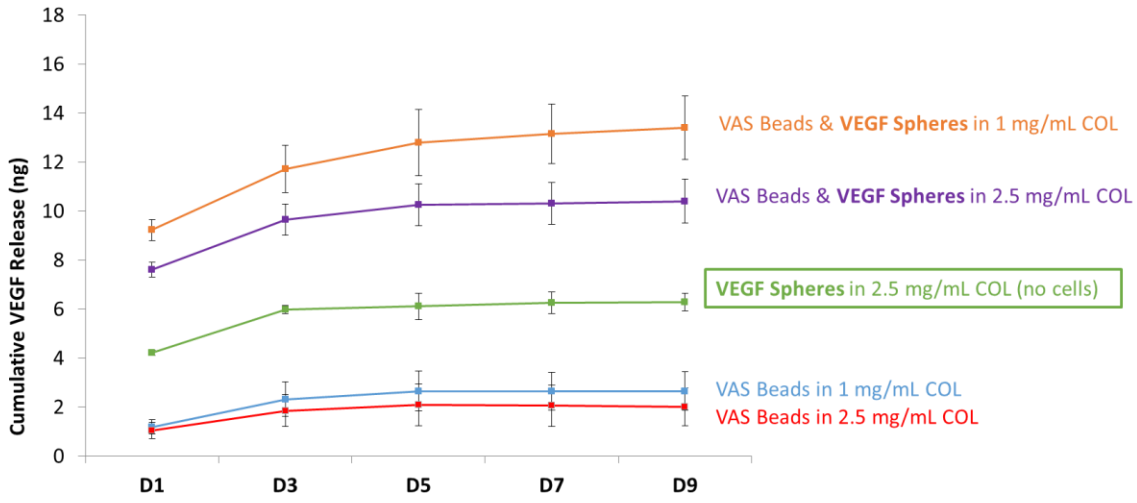

Figure Q-8: Cells degrade microspheres and release VEGF into 3D collagen hydrogels.

Sprout formation did not occur when collagen hydrogels contained no microspheres (see chapter 6). However, the addition of microspheres with (Fig. Q-9) or without VEGF (see chapter 6) resulted in sprout formation in both 1.0 mg/mL (Fig. Q-9A) and 2.5 mg/mL (Fig. Q-9B) collagen hydrogels

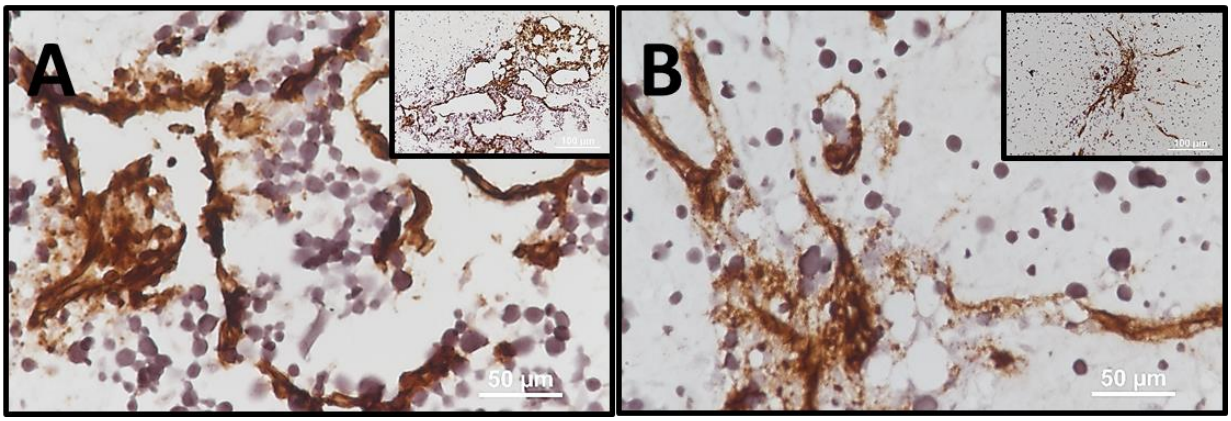

Figure Q-9: Microspheres with VEGF promote EC sprouting in (A) 1 mg/mL collagen hydrogel and (B) 2.5 mg/mL collagen hydrogel. Insets of each image show a wider area containing human endothelial sprouts. Scale bar – 50 µm, 100 µm of insets.

Conclusions:

We found that microsphere degradation is affected by the cells and materials they are interacting with (Fig. Q-10). These cells will degrade the microspheres differently whether they are in 2D or 3D systems. Both NHLFs and MSCs behaved similarly on 2D systems, while ASCs displayed an opposite trend when cultured with HUVECs. This system will continue to be explored to determine whether microspheres loaded with VEGF augment overall vessel formation in 3D collagen hydrogels. It was surprising to find the microspheres alone had an effect on sprout formation.

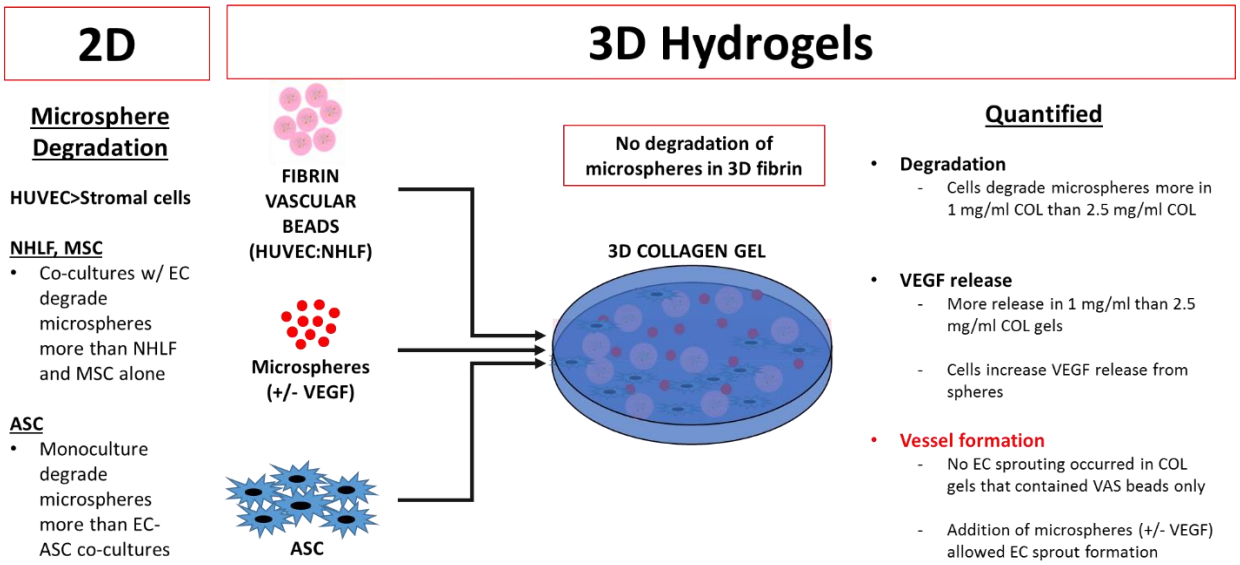

Figure Q-10: Overall summary of preliminary work.